Mission to Investigate Rarefied Aerodynamics on Low Orbiting Satellites

Final Report

July 1, 2014

Delft University of Technology

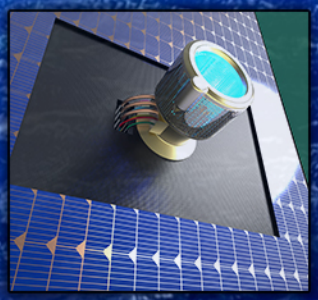

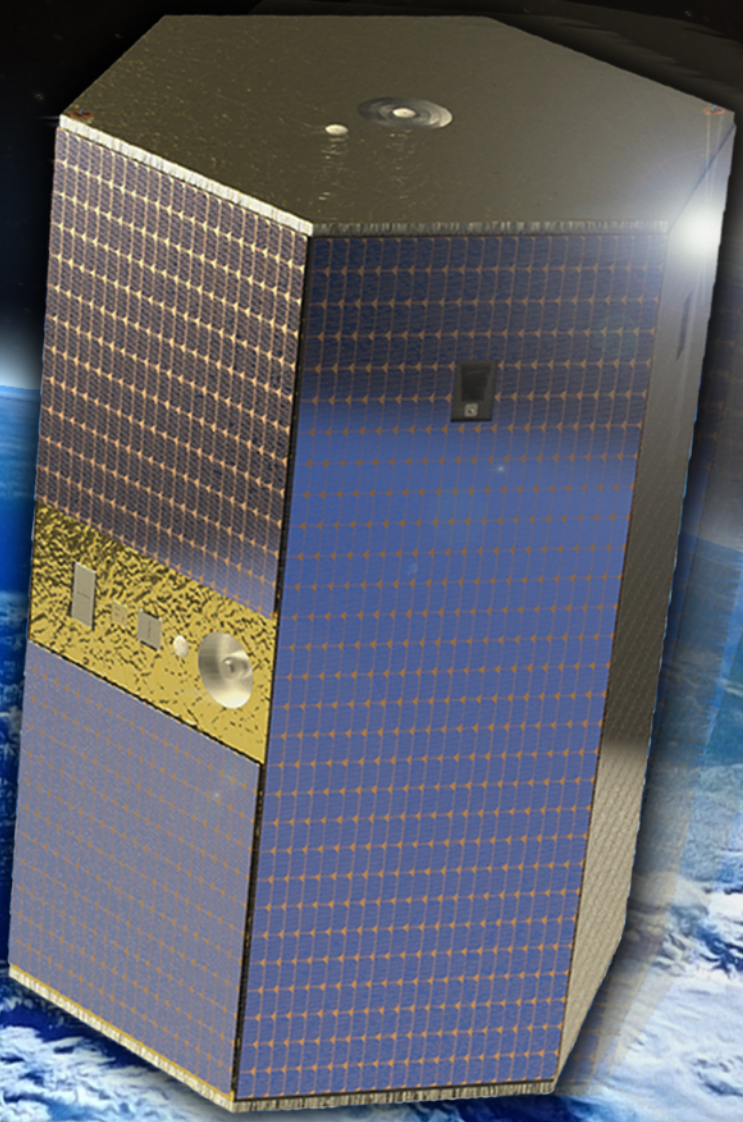

TU Delft Delft University of Technology

Challenge the future

Mission to Investigate Rarefied Aerodynamics on Low Orbiting Satellites

Final Report

Delft University of Technology
Faculty of Aerospace Engineering

July 1, 2014

by

I.A. Argyriou Tsikrikonis,	4126963
R.J. de Boer,	1146068
M.M.H. Van den Broeck,	4152646
B.M. Doekemeijer,	4151968
J. Ehlen,	4158334
J.A. Reichert,	4163605
J. Rijnsdorp,	4140427
P.J.T. van der Stoep,	4101693
N.D.F. Verhaegen,	4175557

Supervisors:
Dr. ir. E. N. Doornbos, Astrodynamics and Space Missions
Ir. A. D. Fernandez Vigo, Aerospace Structures & Materials
Ir. G. Liu, Space Systems Engineering

TU Delft Delft University of Technology

Preface

As a Design Synthesis Exercise (DSE), nine students from the Faculty of Aerospace Engineering at the Delft University of Technology were asked to design a space mission that will investigate the interaction between the atmosphere and the satellite surfaces at low Earth orbit. These students have worked full-time for eleven weeks to provide a conceptual design, that will be presented during a symposium on July 3rd, 2014 at the faculty of Aerospace Engineering. Throughout these eleven weeks, four reports were to be written containing the development of the mission concept and the organisational process leading to this design. This is the fourth and last report in the series, which describes the preliminary conceptual design to a subsystem level. As a group, we want to thank our supervisor Dr. Ir. E.N. Doornbos and our coaches Ir. A.D. Fernandez Vigo and Ir. G. Liu for their guidance during the project. We also would like to thank Ir. J. Bouwmeester and Ir. B.T.C. Zandbergen for their assistance with the design of the communications subystem and the thermal control subsystem, respectively.

I.A. Argyriou Tsikrikonis (4126963)
R.J. De Boer (1146068)
M.M.H. Van den Broeck (4152646)
B.M. Doekemeijer (4151968)
J. Ehlen (4158334)
J.A. Reichert (4163605)
J. Rijnsdorp (4140427)
P.J.T. van der Stoep (4101693)
N.D.F. Verhaegen (4175557)

Delft, June 2014

Contents

Executive Summary

For the past half century, lack of knowledge on interference between gas particles and spacecraft surfaces in the tenuous upper atmosphere have resulted in large discrepancies in important mission properties such as mission lifetime, control ground tracks, and the probability of collisions. Many current drag force estimations rely on a rule of thumb approach introduced in a 1965 paper by Jacchia and Slowey, valid solely for specific shapes and solar conditions.

To cover this scientific gap, a spacecraft mission is designed with primary mission objective to obtain accurate measurements of the interaction of the upper atmosphere with satellite surfaces, operational before 2020. Additionally, the measurements will be used to create a comprehensive model of spacecraft aerodynamics. Several smaller secondary objectives are included such as investigating long-term atmospheric changes, testing non flight-proven equipment and inspecting the temperature and composition of the atmosphere at lower altitudes.

Firstly, the spacecraft orbit profile and the number of satellites is determined based on top-level requirements and a literature study. Secondly, the spacecraft including its subsystems is designed to a conceptual level, including selection of the ground station and launch vehicle. Thirdly, the design is assessed for various topics, such as operational modes, risks and sensitivity to parameter changes. Lastly, recommendations are made for continued mission design.

Literature Research, Concept Design and Concept Analysis

The mission concept, more specifically the type of spacecraft, number of spacecraft and orbit profile, was already previously outlined in the midterm report [1]. To allow reliable satellite drag force modelling, the following parameters are to be measured:

- Linear and angular accelerations
- Total atmospheric density
- Constituent element particle counts
- Gas temperature
- Spacecraft surface temperature
- Particle incidence angle
- Angular distribution of re-emitted particles

An updated atmospheric model based on the NRLMSISE-00 model is developed in order to predict atmospheric conditions throughout the mission lifetime. Several high level mission concepts were looked upon, such as a guest payload mission, a single satellite and multiple satellites missions, including and excluding a propulsion system. A single satellite mission with propulsion system was chosen in for the superior quality of the measurements, the ability to perform secondary missions, high flexibility and robustness. The main disadvantage is of this choice is increased cost.

The orbit profile is as follows. The spacecraft is launched in December 2019 to an altitude of 650 km, where it performs scientific operations from January 2020 until June 2020. Then, the satellite descends to 500 km in July, upon which it performs measurements until December 2020. In January 2021, the satellite descends to 350 km altitude and performs measurements until July 2021. Lastly, the spacecraft ascends back to 500 km and is available for secondary mission objectives starting September 2021. All components are designed for a mission duration of at least six years. 6.0 kg of propellant is implemented to account for all orbit manoeuvres throughout the mission lifetime.

Spacecraft Design and Analysis

The second part of the final report consists of the design of the satellite, including subsystems, system integration and analysis. The following subsystems are considered up until this design phase: payload, propulsion, ADCS, power, thermal control, structures, on-board processing and communications. Next to that, an initial launch vehicle and ground station are selected.

Bus Design

The bus design is strongly related to the electrical power subsystem requirement. In favour of the quality of measurements, no external panels are mounted to the spacecraft bus. This is disadvantageous for the efficiency of energy retrieval using solar cell arrays. To account for this disadvantage, the cross-section of the spacecraft is chosen to be hexagonal. The solar panels mounted radially on this spacecraft have an efficiency between 0.79 and 0.87, depending on the incidence angle of solar rays. Furthermore, a hexagonal bus shape allows for a relatively easy integration of subsystems and components. Lastly, it is beneficial with respect to available launch vehicle payload fairing.

The spacecraft has a length of 3 m and a diameter of 2.2 m. This flows down from back-of-the-envelope calculations on the drag force and from payload fairing properties of feasible launchers. This is one of the first properties to revise, as these values were determined very early in the design.

Payload Subsystem
The scientific operations of the satellite are carried out by the scientific payload. To that end, an adequate mass spectrometer is included in the design, which will provide measurements on composition for both neutral and ionised particles, neutral wind and ion drifts, neutral temperature, and density. The spectrometer uses a combination of magnetic sector and reflectron techniques. A second mass spectrometer is implemented for redundancy.

The accelerometer implemented is similar to the accelerometer used on the GRACE-FO satellite. As part of the mission of the latter, the accelerometer will be flight-proven. Requirements on the positioning of the instrument relate to the center of mass location of the entire spacecraft.

A GPS antenna and laser retroreflector are used for satellite positioning. The choke ring antenna of the GPS system is responsible for precise location and orbit determination. The instrument is also equipped with a helix antenna used for occultation monitoring. Furthermore, two patch antennae are added, for attitude determination and redundancy.

Two configurations of the reflectometer are employed to investigate the gas-surface interactions of a plate, set at an incidence angle with respect to the incoming flow. The first configuration will ionise incoming particles, which will subsequently be detected by a number of micro-channel plate detectors, placed at defined distances around the reflectometer. The second configuration will use an optical scanner to take pictures of the imprint of particles on the silver foil. The contour of the reflectometer is conceptually split in a left and right half. For each half, the foil will be unrolled at the top, and retracted at the bottom, after an image has been taken of the infected segment. The utility of this instrument is limited by the amount of foil implemented.

Propulsion Subsystem
Design of the propulsion system goes hand-in-hand with the concept selection. In the previous design stage, it had been decided to exclude a propulsion system in the spacecraft design [1]. However, this decision is revised; the main reason being to increase the capability and flexibility of the mission. For the MIRALOS propulsion system, multiple different types of systems are considered: cold gas, liquid-bipropellant, liquid-monopropellant, electric ion thrusters and electric hall thrusters. Ion-based thrusters are chosen because of their high flexibility and mass performance. Their main disadvantage is their high power consumption.

A number of available ion thruster systems are considered to be used: the QintyiQ T5 Kaufman ion thruster, the Astrium RIT-10, a radio frequency ion thruster and the Mitsubishi ETS-8 Kaufman ion thruster. The T5 Kaufman thruster is implemented in the MIRALOS satellite design, because of its excellent performance in terms of power consumption, flexibility and efficiency and its good mass performance.

The ion propulsion system does not only consist of the thruster itself. It can be divided into five different components: the thruster package (consisting of the thruster itself and the neutraliser), the propulsion control unit (responsible for control of the thruster, providing power to it and communicating with the spacecraft bus), the Xenon Feedsystem Assembly (regulating pressure and mass-flow of the xenon fuel, and supplying to the different thruster inlets) and finally the tank (for storing the 6 kg of xenon fuel at an initial pressure of 125 bar). The subsystem properties are summarised below:

Main parameters of the MIRALOS ion propulsion system

Total System Mass	28.75 kg (plus 6 kg of xenon)
Thrust Range	1 to 20 mN (more or less is possible)
Power Consumption	55 to 585 W (across given thrust range)
Specific Impulse	500 to 3500 s (across increasing thrust range)

Attitude Determination & Control Subsystem
For the payload operations, highly accurate attitude knowledge and control is desired. The ram surface area is to be pointed in flight direction to minimise uncertainties introduced in aerodynamic calculations related to drag. Furthermore, as moving components would badly influence the performance of the accelerometer, no reaction wheels, momentum wheels or gyroscopes are implemented for attitude control or determination.

For coarse attitude determination, two Honeywell HMR2300r magnetometers are implemented, of which one for redundancy. Additionally, two antennae are added to the current GPS system assembly for redundancy and as a secondary mission objective, providing attitude sensing with an accuracy better than 1°.

For fine attitude determination, two sets of the extremely light-weight TU Denmark's µASC Star Camera Assembly are implemented, each with an accuracy better than $2''$. A total of four optical heads are placed on the spacecraft skin pointing in different directions, implemented such that two optical heads will always be pointed away from the sun and thereby allow operation. Furthermore, for redundancy, a total of four of TNO's Digital Sun Sensors (µDSS) are placed next to the optical units of the µASC, which can operate when star trackers cannot due to sunlight blinding.

For attitude control, two sets of three Zarm Technik's MT70-2 magnetic torque rods are implemented, operated at dipole moments of 20 A·m^2 and 70 A·m^2. The magnetometer is used in support of these rods to accurately determine the magnitude and direction of the Earth's magnetic field. The main advantage of the magnetic torque rods are their lack of propellant, high reliability and

low mass. The disadvantage is their limited operability. However, at the Earth's poles the magnetic field changes direction, which allows for full 3-axis attitude control. Coinciding the centre of pressure with the centre of mass to an accuracy of 0.5 mm (RMS), a maximum attitude drift of 1° is experienced each half orbit.

In order to calibrate the mass-trim assembly, a nodding manoeuvre is performed every two months for a period of 24 hours. This procedure consists of pseudo-random milliNewton-meter torques initiated by 12 cold gas thrusters for full attitude control. A total of 7.2 kg of gaseous N_2 fuel is taken on-board for calibration and additional attitude control in support of the magnetic torque rods.

Electrical Power Subsystem

The electrical power system provides retrieval, storage, regulation and distribution of electrical power to the spacecraft. First, a power source has been selected based on the mission characteristics and orbit profile. A solar photovoltaic-battery system is found optimal for the MIRALOS mission. This system consists of an array of photovoltaic solar cells, a set of batteries and a power regulator unit. The function of a power regulator is to distribute power received from solar cells to the batteries, subsystems and instruments. Efficiency and degradation are decisive in the choice of Triple Junction Gallium Arsenide solar cells. Lithium-ion batteries are selected based on their high capacity and efficiency.
These components are sized based on their maximum required power case, translating to a power requirement of 975 W. This includes a contingency factor of 10% for wiring losses and unexpected power increment.

The battery size is determined accounting for eclipse times, charge/discharge efficiency, depth of discharge and degradation over time. Taking into account the energy needed for battery charging, Earth albedo radiation, temperature degradation, design degradation, assembly inherent degradation and annual degradation due to radiation, the solar array area and mass are calculated. The electrical power system has a total mass of 39 kg, of which 18 kg for the QL075KA batteries, 14 kg for the CI ZTJ PV Cell solar array and 6.5 kg for the Medium Power PCDU. The solar cell arrays cover a total surface area of 17 m^2.

Thermal Control Subsystem

An analysis is performed regarding thermal properties of the spacecraft. A first order estimation is made assuming that the spacecraft is isothermal and completely made out of Aluminium; for the surface properties, the surface properties of the solar cells were used. This leads to a maximum temperature of 27 °C during a non-eclipse orbit with maximum operational waste heat production in the spacecraft. The opposite case, with maximum eclipse orbit and minimum operational waste heat production, yields an average temperature of -23 °C. The extreme minimum occurs during a maximum eclipse orbit under safe mode operations. In this case, the temperature drops to an average of -25 °C, with a minimum of -34 °C. This implies that numerous components require heating.

To get a better insight in the temperature distributions over the spacecraft surfaces, a thermal model is created using a finite-element program called COMSOL. By implementing all radiant heat sources, such as the sun, the Earth, the albedo effect, and the waste heat production of the spacecraft, a fairly accurate model is retrieved. The model shows that the solar panels of the spacecraft can reach temperatures up to 97 °C in direct sunlight, while the opposite side has temperatures as low as -71 °C. The high temperatures greatly affect the efficiency of the solar cells in a negative way.

The most critical temperature requirement is that of thermal stability of the accelerometer. The accelerometer has to remain stable within 10 mK throughout a time period of 200 seconds. This implies that the accelerometer should be highly insulated thermally. The heaters of the accelerometer cannot be placed directly on the instrument itself, since they would compromise the temperature stability requirement instantaneously. Therefore, the direct environment of the accelerometer has to be accurately controlled.

The thermal control system consists of a combination of active and passive control. This is to keep thermal flexibility in good balance with reliability and low complexity. The heated components are controlled by a distributed processor unit, while the excess waste heat is radiated by a passive radiator plate.

Structural Analysis

An initial design is created for the structural components of the satellite. The spacecraft bus will consist of load carrying honeycomb sandwich panels. The panels are fastened together using brackets, without an underlying frame.

The outer panels make use of 1 mm thick carbon fibre reinforced cyanate ester skins on a 10 mm thick aluminium honeycomb core. The central hexagonal floor, on which the accelerometer is mounted, uses a carbon fibre reinforced carbon matrix composite material for both the skins and the honeycomb structure. This material has an extremely low coefficient of thermal expansion, which is required to keep the location of the accelerometer constant.

The dimensions of the structural components are sized to withstand the loads and vibrations experienced by the spacecraft during launch. The eigenfrequencies of the spacecraft have been analysed using finite element analysis software. COMSOL is used for both the structural analysis and thermal analysis. The lowest eigenfrequencies in the lateral and longitudinal directions are 96 Hz and 101 Hz, respectively. This is significantly in excess of the minimum frequencies of 10 Hz and 20 Hz required by the selected launch vehicle.

Buckling analysis of the structure reveals similar over-performance. The maximum allowable normal stress in the critical point, where the spacecraft is connected to the launcher stage, is 48 MPa. The actual worst case stress due to lateral and longitudinal acceleration, including a safety factor of 2, is 8 MPa.

While the performance with regards to buckling and dynamic coupling indicates the structure is overdesigned and could therefore be made lighter, some caution is required. This is because there are a variety of local failure modes that have not been analysed. Furthermore, the skin and honeycomb thicknesses of the panels are already small, and further reduction could lead to difficulties with respect to manufacturing.

The final weight of the structure, including a margin for brackets and fasteners, is 275 kg. This represents 60% of the total dry weight of the spacecraft. This mass fraction is significantly greater than for most other spacecraft, because the MIRALOS satellite is much larger than spacecraft with a similar payload mass.

Command & Data Handling
Three components are implemented on the spacecraft to account for command and data handling between various components and interfaces. These are an on-board computer, a central processing unit (CPU), and a remote terminal unit (RTU). The RTU is usually included in the design of medium to large sized satellites, and has the function of offloading the on-board computer, and providing redundancy.

For all three components, multiple flight-proven products are investigated, upon which a final selection is made. The SCS-750 is chosen as the main on-board computer of MIRALOS satellite. The Motorola PowerPC 603e is found to be the most effective option for the CPU. Finally, the BU-63705 is selected as RTU.

Communications Subsystem
The subsystem not yet touched upon is the communication subsystem. This subsystem was previously designed to a preliminary degree in the midterm report [1]. Firstly, the general system layout is considered, in which the spacecraft transmitter and receiver are treated. The STC-MS01 transceiver is implemented on the spacecraft, after investigating various flight-proven options. Subsequently the link budget is iterated, including all losses and gains related to communication operations. Compared to the analysis presented in the midterm report, some parameters are added, which provide information for the link margin and transmitter power analysis. Comparing various commercially available antennae, the SSTL Patch Antenna is selected. The current design has a minimum link margin of roughly 5 dB, which means that unforeseen losses can be accounted for. Additionally, when these losses grow increase even more in magnitude, the transmitter power can be increased. The communications subsystem is estimated to have a total mass of 1.5 kg, with a maximum power consumption of 38 W.

Ground Station Selection
In the previous report, a preliminary selection of the ground station selection was already considered, as it was required for preliminary communications analysis [1]. Consulting literature concerning the communications subsystem, it becomes clear that the ground station is to be chosen based on antennae properties and location of the station. For the uplink and downlink analysis, a ground station of the ESTRACK network is chosen, as much information is available. This decision can still be revised in a later stage, and does not impact the remaining design significantly. As stated, the location of the ground station is of major importance, as the number of contact periods has to be sufficient for transmitting all data. Because the orbit is determined to be near-polar, a ground station with high latitude is chosen, in order to optimise the number of contact periods per day. Combining this with the available ESTRACK ground stations and taking the station antenna into account, the ground station selected is the one located in Svalbard, Norway.

Launcher Selection
In the previous report, several feasible launch vehicle options were suggested. Incorporating design changes since then, the Ukrainian Dnepr-LV is chosen. This launcher provides sufficient fairing dimensions, it can carry up to approximately 2900 kg of payload mass with a cost of 10 to 20 million dollars.

Resource Allocation
Combining the selected components of all preliminary subsystems, an estimation can be made for the total weight of the spacecraft. This estimation relies both on the selected payload instruments and statistical data. A total spacecraft wet mass of 470 kg is estimated, of which 13 kg is fuel. Furthermore, the maximum power consumption the satellite will experience is estimated at 890 W without contingency. Lastly, the total MIRALOS mission costs is estimated at €121,000,000, including a 10% contingency factor.

System Analysis
The third part of the report contains the system analysis, in which both technical and non-technical aspects of the mission are discussed. First, the spacecraft operational modes are presented. Secondly, verification and validation procedures are touched upon. Thirdly, mission risks are presented and risk mitigation is shortly described.

Firstly, the spacecraft is designed to operate in six different modes. An essential mode for mission success is Safe Mode, triggered in mission-threatening situations. All non-essential operations are turned off, and the focus shifts to communication, thermal control, attitude control and on-board computing. Other modes are Initialisation Mode (triggered after orbit injection), Scientific Mode, Orbit Change Mode, Calibration Mode (for calibration of the mass-trim assembly using the ADCS cold-gas thrusters) and lastly Drag Compensation Mode (required to maintain altitude and orbit at low altitudes).

Secondly, all instruments, subsystems and models used for development require verification and validation, to ensure proper functioning and to minimise the probability of mission failure. Components are assessed on four fronts: inspection, analysis, demonstration and testing. However, as the current design phase is still very conceptual, most verification and validation procedures are not planned in detail and are still open to adjustments.

Thirdly, by analysing all technical risks related to mission and (sub)system design, it was discovered several events exist that significantly affect the probability of mission success. As long as the financial budget allows for it, resources are to be spent with the purpose of reducing the severity of impact of these events and/or their probability of occurrence. The main risks found are related to failure of instruments, failure of the propulsion subsystem, the calibration manoeuvre accounted for by the ADCS, and communication system failure.

Fourthly, a top-level sensitivity analysis investigating the relationships between design changes showed that the current mission design is very robust. Both top- and low-level changes in parameters have no significant effects in the remaining design. The largest design alterations originate from changes in the orbit profile.

Fifthly, a RAMS analysis shows that most spacecraft failures originate from flaws in the communications and propulsion subsystems. The most severe events causing a failure is an internal explosion.

Sixthly, a market analysis shows that the MIRALOS mission is strongly competing with other interesting mission concepts for acceptance and continuation of design at a space agency, such as ESA or NASA. Furthermore, a large financial budget has been assumed early in the design phase, which is disadvantageous for mission acceptance by external agencies.

Seventhly, several considerations are taken with respect to sustainable engineering. International guidelines have been established to ensure fair usage of the space environment, applicable mainly to minimise space debris and maintain usability of frequently used regions in space surrounding the Earth. For this reason, the MIRALOS satellite is designed to burn up in the Earth's atmosphere after its secondary missions have been met. Also, the design relies on electric propulsion, thereby significantly limiting the amount of fuel taken on-board.

Lastly, a Gantt chart is made concerning all future design, operation and termination activities. Until the launch in 2020, the design will be finalised, tested and produced. Throughout operation in 2020 to approximately 2026, the results are inspected for their compliance to the needs of stakeholders, after which it is brought into a burn up orbit and ground activities are stopped. Documentation and interesting results related to both measurements as mission design are published. All activities are ended before January 1st, 2027.

Recommendations

Throughout the entire design process, risk are to be constantly identified, quantified and mitigated. The current design revolves on a single iteration, and many changes are to be made before all subsystems are fully compatible.

The first step is to update all designs based on new estimations of the mass and power consumption. The methods of analysis are to be refined as the design progresses. Furthermore, the spacecraft bus dimensions should be reconsidered based on launcher fairing properties and outdated accelerometer properties. Also, more research is to be performed to available options for instruments, components and flight-proven solutions. Information is still lacking, thereby limiting analysis and conceptual design.

For the ADCS, two main recommendations are made. Firstly, a large risk originates from the lack of information on magnetic interference with on-board instrumentation due to the ADCS torque rods. Using literature and tests, more information on the feasibility of this design decision is to be obtained. Secondly, the calibration procedure is still unknown to a large degree, and thrusters are currently sized using back-of-the-envelope calculations. Due to its high uncertainty and design impact, this will be of high priority.

Lastly, an omni-directional antenna is to be implemented on the spacecraft in order to allow communication with the ground station in case of spacecraft tumbling.

The current design is still very conceptual and is largely based on readily available knowledge and commercially available components. In further development, expected is that top-level design decisions made will not change significantly.

List of Abbreviations

Abbreviation	Definition	First page
µASC	Micro Advanced Stellar Compass	46
µDSS	Micro Digital Sun Sensor	47
ADCS	Attitude Determination and Control System	21
C	Constraint	123
CBS	Cost Break-down Structure	24
CDAE	Command and Data Acquisition Element	87
CDH	Command & Data Handling	75
CERs	Cost Estimation Relations	23
CF	Contingency Factor	23
CFRCE	Carbon Fibre Reinforced Cyanate Ester Composite	71
CHAMP	CHAllenging Minisatellite Payload	45
CM	Calibration Mode	50
CMG	Control Moment Gyro	48
CMT	Center of Mass Trim Assembly	30
CoG	Center of Gravity	21
COM	Communication	123
COPS	Commet Pressure Sensor	27
COPUOS	Committee on the Peaceful Uses of Outer Space	107
CPU	Central Processing Unit	79
CRAF	Comet Rendezvous Asteroid Flyby	27
DFMS	Double Focusing Mass Spectrometer	27
DSE	Design Synthesis Exercise	iii
DSS	Digital Sun Sensor	47
EPS	Electric Power System	57
EU	Electrical Unit	46
EUV	Extreme Ultraviolet Imager	35
FM	Failure Mode	105
FMEA	Failure Modes and Effects Analysis	105
FOS	Flight Operations Segment	87
FOV	Field of View	45
FUV	Far Ultraviolet Imager	35
FY	Fiscal Year	24
GDS	Gas Dynamic Shield	90
GEO	Geostationary Earth Orbit	107
GMAT	General Mission Analysis Tool	15
GN	General	123
GOCE	Gravity field and steady-state Ocean Circulation Explorer	46
GPMS	Galileo Probe Mass spectrometer	27
GPS	Global Positioning System	31
GRACE	Gravity Recovery and Climate Experiment	45
GS	Ground Station	123
GUVI	Global Ultraviolet Imager	20
HV	high voltage	41
ICBM	Intercontinental Ballistic Missile	90
ICON	Ionospheric Connection Explorer	35
ICU	Interface Control Unit	20
IDTS	Ion Drift and temperature Spectrometer	28
IMAGE	Imager for Magnetopause-to-Aurora Global Exploration	35
IMS	Ion Mass Spectrometer	28
INMS	Ion Neutral Mass Spectrometer	27
INTG	System Integration	123
IPCU	Ion Propulsion Control Unit	21
IPEX	Intelligent Payload Experiment	76
ITP	Ion Thruster Package	21
LEO	Low Earth Orbit	1
LN	Launcher	123

Abbreviation	Definition	First page
LRR	Laser Retro-Reflector	20
LST	Local Solar Time	18
LV	low voltage	41
LVA	Launch Vehicle Adapter	90
MAVEN	Mars Atmosphere and Volatile Evolution	27
MCP	Microchannel Plate Detector	35
MEO	Medium Earth Orbit	107
MEOP	Maximum Expected Operating Pressure	59
MiniDSS	Mini Digital Sun Sensor	47
MIPS	Million instructions per second	76
MJD	Modified Julian Date	17
MLI	Multi-Layer Insulation	65
MOI	Moment Of Inertia	21
MTE	Mass Trim Assembly Electronics Unit	21
MTTM	Mean Time To Maintain	105
MTTR	Mean Time To Repair	105
MW	Momentum Wheel	48
NGIMS	Neutral Gas and Ion Mass Spectrometer	27
NMS	Neutral Mass Spectrometer	28
OBC	Onboard Computer	21
OCC	Occultation	21
OH	Optical Head	46
ONMS	Orbiter Neutral Mass Spectrometer	27
PDGS	Payload Data Ground Segment	87
PL	Payload	86
PLF	Payload Fairing	90
POD	Precision Orbit Determination	21
PRISMA	Prototype Research Instruments and Space Mission technology Advancement	76
PROP	Propulsion	123
PRU	Power Regulator Unit	21
PSLV	Polar Satellite Launch Vehicle	90
RAAN	Right Ascension of Ascending Node	16
RF	Radio Frequency	80
RFM	Reflectometer	34
RMS	Root Mean Square	46
ROSINA	Rosetta Orbiter Spectrometer for Ion and Neutral Analysis	27
RTOF	Reflectron Time-of-Flight	27
RTU	Remote Terminal Unit	75
RW	Reaction Wheel	48
SB	Stabilisation Mode	50
SDS-1	Small Demonstration Satellite-1	76
SLR	Satellite Laser Ranging	20
SM	Science Mode	50
SMA	Semi-Major-Axis	16
SMAD	Space Mission Analysis and Design	21
SMART	Small Rocket/Spacecraft Technology	76
SMC	Safe Mode Case	62
SSCM	Small Spacecraft Cost Model	23
SSUSI	Special Sensor Ultraviolet Spectrographic Imager	35
STRC	Structural	123
SUB	Subsystem	123
SUST	Sustainability	123
SWATS	Small Wind and Temperature Spectrometer	20
T	Technical	123
TAI	International Atomic Time	17
TCV	Thruster Control Valve	49
THM	Thermal	123
TIMED	Thermosphere Ionosphere Mesosphere Energetics and Dynamics	35
TT&C	Telemetry, Tracking & Command	86
WCC	Worst Case Cold	62
WCH	Worst Case Hot	62
WTS	Wind Temperature Spectrometer	28
XFA	Xenon Feedsystem Assembly	21

List of Symbols

Symbol	Definition	Unit	First page
A	Surface area	m^2	3
C_D	Drag coefficient	-	3
E	Energy	J	4
E_b	Energy per bit	J	81
F_D	Drag force	N	3
G_{AR}	Receiving antenna gain	-	81
G_{FS}	Free space gain	-	81
J_{mp}	Maximum power point current density	A/m^2	56
L	Length	m	33
L_{ATM}	Atmospheric loss	dB	83
L_{FS}	Free Space loss	dB	83
L_{GSP}	Ground Station Pointing loss	dB	83
L_{ION}	Ionisation loss	dB	83
L_{LTX}	Ground Station Line loss	dB	83
L_{LTX}	Spacecraft Line loss	dB	83
L_{POL}	Polarisation loss	dB	83
L_{SCP}	Spacecraft Pointing loss	dB	83
M	Spacecraft mass	kg	3
M	Molar mass	g/mol	4
M_{link}	Link margin	dB	83
N_0	Noise	dB	81
P_{EIRP}	Equivalent isotropically radiated power	W	81
P_{TX}	Transmitting antenna power	W	83
P_e	Bit error probability	-	82
R	Data rate	bit/s	81
R	Universal gas constant	J/kmol K	4
S	Speed ratio	-	5
T	Temperature	K	4
T_{syst}	System noise temperature	K	81
V	Velocity	m/s	3
V_{mp}	Maximum power point voltage	V	57
α	Accommodation coefficient	-	4
λ	Failure rate	Hz	104
μ	Recovery rate	Hz	104
ρ	Atmospheric density	kg/m^3	3
a_{drag}	Drag acceleration	m/s^2	3
c_{mp}	Most probable thermal velocity	m/s	4
h_{orb}	Orbit altitude	m	85
k	Boltzmann's constant	$m^2 kg\ s^{-2} K^{-1}$	81
v	Gas velocity	m/s	5

1. Introduction

For the past half century, limitations in satellite drag force determination have resulted in large discrepancies in important mission estimations such as mission lifetime, ground track control, and the probability of spacecraft collisions. Many current drag force calculation methods use a rule of thumb approach introduced in a paper by Jacchia and Slowey [2] (1965), which is only applicable to specific satellite shapes and solar conditions.
So far there is an incomplete understanding of the interaction between the tenuous upper atmosphere and satellite surfaces. To date, there has not been a mission that accurately measured both the atmospheric conditions and the resulting accelerations on the spacecraft simultaneously, which is a requirement for creating a comprehensive model. Furthermore, there is limited information available on the way the nature of these interactions varies with the molecular composition of the atmosphere, which in turn varies greatly with altitude and space weather conditions.
The purpose of this report is to provide a conceptual design for a spacecraft mission that resolves this lack of knowledge. The primary mission objective of the design is defined as:

To create a design concept for a space mission to obtain accurate data on the interaction between the tenuous upper atmosphere and satellite surfaces, which can be operational before 2020.

The measurements obtained from the mission will subsequently be used to create a comprehensive model of spacecraft aerodynamics. Furthermore, the spacecraft shall perform research on the thermosphere as a secondary mission objective.
At the conclusion of this project a spacecraft will be designed down to a subsystem level. It will retrieve data on atmospheric properties to allow accurate modelling of force and moment interactions between gas particles and spacecraft surfaces at Low Earth Orbit (LEO) altitude. For this purpose, a systems engineering approach shall be used. This report is the fourth and last report in the series of the project. The contents build upon the conceptual mission analysis presented in the previous report. The requirements, design and instrumentation concepts, resource budgets, and sustainability considerations are all updated.

This report is divided in three parts. The first part of the report presents the theory behind the science objectives, and discusses the high level mission, orbit and spacecraft bus design. These topics are handled in chapters 2 through 5. The second part of the report concerns the detailed design of the scientific payload and the other spacecraft subsystems. These are presented in chapters 6 to 14.

The third part covers the spacecraft system analysis in Chapter 15. This chapter touches upon a number of topics: the functions of the spacecraft including its various operation modi, the internal hardware and software layout, planned verification and verification procedures, risk management, a sensitivity analysis to assess the robustness of the design, a RAMS analysis, a market analysis, the mission approach to sustainability, a compliance check with top-level requirements and lastly a future design and development plan. Finally, the conclusion and recommendations are described in Chapters 16 and 16 respectively.

2. Conceptual Background and Atmospheric Model

This chapter presents an overview of the scientific background for the mission. Section 2.1 discusses the current limitations on the accuracy of satellite aerodynamic analysis. A model for the interaction between rarefied atmospheres and spacecraft surfaces is presented in Section 2.2. Required empirical data that is to be gathered to complete this model is listed in Section 2.3. Finally, the thermospheric model that is used throughout the preliminary design process is presented in Section 2.4.

2.1. Satellite Aerodynamics

The aerodynamic acceleration experienced by a satellite in the direction of the incoming air particles is given by the familiar drag equation displayed in Equation (2.1). Aerodynamic accelerations in perpendicular directions can be obtained from similar equations when substituting the appropriate aerodynamic coefficient.

$$a_{drag} = \frac{F_D}{M} = \frac{1}{2}\rho\frac{AC_D}{M}{V_{inc}}^2 \tag{2.1}$$

Here a_{drag} and F_D are the acceleration and force components in the flight direction, ρ is the atmospheric density, V_{inc} is the speed of the air particles relative to the satellite, and A, M, and C_D correspond to a reference area, the mass, and the drag coefficient of the satellite, respectively.

The mass and physical dimensions of a spacecraft are generally known with high precision. The orbital speed of the satellite combined with the co-rotational speed of the atmosphere is usually taken as an approximation for the relative air particle velocity. The error introduced by neglecting wind speed is usually small, but may be significant during times of high geomagnetic activity [3]. The MIRALOS design includes spectrometers which can determine wind speed, in order to obtain a highly accurate estimate of the incident particle velocity.

Observed values of the drag acceleration have historically been available for a large number of spacecraft, obtained by Earth-based radar tracking of the decay of their altitude over time. Additionally, from the 1960s to the 1980s, there have been a number of satellites which studied the thermosphere and included on-board accelerometers.

In the past, researchers have combined these observed accelerations with an estimated value for the drag coefficient to obtain inferred values for atmospheric density. A constant drag coefficient of 2.2 is a frequently used reference value. Rather than being a fixed value however, Moe et al. (1998) [4] have shown that the drag coefficient varies substantially with altitude, angular distribution of re-emitted particles, and in the case of non-symmetrical satellites, the orientation the spacecraft with respect to the particle bulk velocity.

Attempts to empirically obtain the drag coefficient from spacecraft observations have been complicated by the lack of independent in-situ density measurements. When only accelerations are measured, one can only infer the combined effect of ρC_D. Models are available to predict density and other atmospheric conditions, but the models themselves are partially based on the above discussed assumed drag coefficient values, which introduces substantial inaccuracy. Finally, there is compelling evidence which indicates that increased emissions of carbon dioxide and other greenhouse gasses are causing a downward trend in thermospheric densities [5]. Because current models are based on density observations from several decades ago, they will overestimate the density at LEO altitudes for more recent satellite missions.

Recently, far more precise acceleration data has become available from a number of missions which studied the Earth's gravity field, including the GRACE, CHAMP, and GOCE missions. Unfortunately, these spacecraft were not designed to study the thermosphere, and did not include any instruments to obtain parameters related to gas-surface interaction.

To date, there has not been a single mission which included all necessary instruments to completely characterise the interaction between the tenuous upper atmosphere and satellite surfaces. As a consequence, aerodynamic analysis of satellites is greatly influenced by assumptions about gas-surface interaction, some of which date back to the beginning of the space age. The mission objective of MIRALOS is to finally provide a full quantification of the gas-surface interaction across a wide spectrum of upper atmosphere conditions. In addition to being useful in its own right, the increased understanding gained this way can be applied to obtain new insights from older satellite data.

2.2. Modelling Spacecraft Drag

In this section the method to calculate spacecraft drag coefficients is presented in which the satellite is modelled as a series of flat plates. For each plate, the interaction with the different atmosphere constituents is calculated separately. The total drag coefficient is then obtained by summing the contributions of each constituent on every plate. From this model, a list of atmospheric parameters which should be measured by MIRALOS is derived.

2.2.1. Accommodation Coefficients

An important parameter governing the gas-surface interaction is the thermal accommodation coefficient, given by Equation (2.2).

$$\alpha = \frac{E_i - E_r}{E_i - E_w} = \frac{T_i - T_r}{T_i - T_w} \tag{2.2}$$

Here E_i and E_r are the kinetic energy of the incoming and reflected particles, respectively. E_w is the kinetic energy that the reflected particles would have if they had adjusted to the temperature of the spacecraft surface. The subscripts on the temperatures have identical meaning. The accommodation coefficient can assume values from zero to one. A value of zero indicates that the reflected particles have the same kinetic energy as the incoming particles, and a value of one indicates the particles have fully assumed the surface temperature. Because temperatures in low Earth orbit are significantly higher than spacecraft operating temperatures, an accommodation coefficient higher than zero implies a loss of particle kinetic energy.

When the value of the accommodation coefficient is low, the reflecting particles retain a high amount of kinetic energy, and have thus exchanged a large amount of momentum with the spacecraft. Because the tangential velocity of the reflected particles is in the flight direction of the spacecraft, the spacecraft is accelerated in the opposite direction. Newton's third law indicates that drag increases as the coefficient of accommodation decreases.

Graziano (2007) [6] provides an overview of the factors that influence the accommodation coefficient. Laboratory research has shown that the accommodation coefficient is higher for heavier particles, higher angles of incidence, and a greater degree of surface contamination. In low Earth orbit, the major source of surface contamination is adsorption of atomic oxygen onto spacecraft surfaces. When atomic oxygen and its reaction products are adsorbed onto the spacecraft, incoming particles encounter an irregular surface and tend to reflect diffusely, losing kinetic energy and accommodating to the surface temperature in the process.
The amount of oxygen adsorbed onto the spacecraft surface depends on the density of atomic oxygen at the orbit altitude. For higher altitudes this density is lower, reducing the surface contamination. In addition, as the altitude increases, the fraction of oxygen in the atmosphere becomes lower, making way for the lighter particles of hydrogen and helium. The combined effects of lower surface adsorption and lighter average particle mass should result in a higher degree of specular reflection, and an accommodation coefficient that decreases with altitude.

Moe et al. (1998) [4] investigate the accommodation coefficients of several satellites for which more than one aerodynamic parameter is available, such as orbital decay and rate of spin. They compare the accommodation coefficients that are predicted by Schamberg (1959) [7] under varying assumptions for the angular distribution of re-emitted particles, and find that diffuse re-emission is the best fit for the observed accelerations at altitudes around 200 km.
There has only been one direct measurement of the distribution of re-emitted particles. The Space Shuttle mission STS-8 carried a reflectometer instrument, which measured re-emitted oxygen particles by their impact on a silver film surrounding a flat plate. The results of this experiment showed 97% diffuse re-emission at an altitude of 225 km. While this validated the expectation of diffuse re-emission at low altitudes, it is only a single datapoint, at a single altitude, and for a single set of atmospheric conditions. Measuring the way the distribution of re-emission and therefore the accommodation coefficient varies with altitude and atmospheric composition is one of the main objectives of the MIRALOS mission.

One of the major factors driving changes in the accommodation coefficient is the partial oxygen pressure encountered by the spacecraft. The higher the partial oxygen pressure, the more oxygen is expected to adsorb onto the spacecraft's surfaces.
Pilinski et al. (2010) [8] use fitting parameters on estimated accommodation coefficients for orbits below 300km to model the dependency of the accommodation coefficient on changes in oxygen pressure and predict that accommodation coefficients drop sharply with oxygen pressure. The validity of their model outside of their range of observations is questionable however, and therefore ensuring that a wide range of oxygen partial pressures is encountered during the mission is an important consideration in orbit design.

2.2.2. Drag Coefficients

Figure 2.1 displays a flat plate in a particle flow. The angle between the normal direction of the plate and v_r, the bulk velocity of the gas, is given by angle θ. In addition to their bulk velocity, the particles also have a thermal component of velocity, given as c. The most probable thermal velocity is given by Equation (2.3).

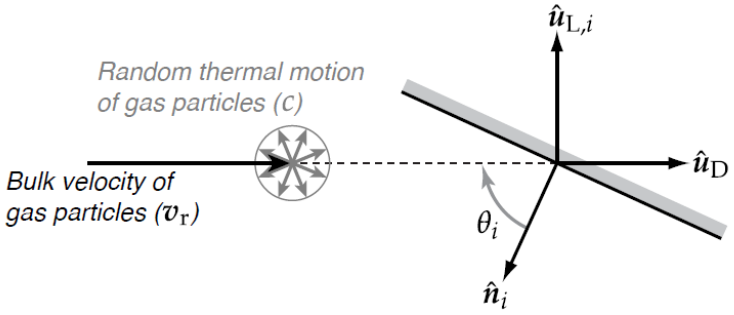

Figure 2.1: Gas particle incident on a flat plate. Image credit: Doornbos (2011) [9]

$$c_{mp,j} = \sqrt{2\frac{R}{M_j}T} \tag{2.3}$$

Here $c_{mp,j}$ is the most probable thermal velocity for particles of constituent gas j, R is the universal gas constant, M_j is the molar mass of gas j, and T is the gas temperature.
The speed ratio S is then defined as the ratio between the bulk velocity and the most probable thermal velocity, as displayed in Equation (2.4).

$$S_j = \frac{v_r}{c_{mp,j}} \tag{2.4}$$

Because thermal velocity decreases with the square root of the molecular mass, the speed ratio differs by a factor of two between helium and oxygen, the two main constituent gasses in the altitude range that will be investigated.
Sentman (1961) [10] proposes a method for calculating the drag coefficient for flat plates in rarefied atmospheres. Using the notation of Moe and Moe (2005) [3], this model is represented by Equations (2.5) and (2.6).

$$C_{D,i,j} = \left[\frac{P_{i,j}}{\sqrt{\pi}} + \gamma_i Q_j Z_{i,j} + \frac{\gamma_i}{2}\frac{v_{re}}{v_{inc}}\left(\gamma_i\sqrt{\pi}Z_{i,j} + P_{i,j}\right)\right]\frac{A_i}{A_{ref}} \tag{2.5}$$

$$G_j = \frac{1}{2{S_j}^2}, \qquad P_{i,j} = \frac{1}{S_j}e^{(-{\gamma_i}^2{S_j}^2)}, \qquad Q_j = 1 + G_j, \qquad Z_{i,j} = 1 + erf(\gamma_i S_j) \tag{2.6}$$

Here, $C_{D,i,j}$ is the drag coefficient contribution of constituent gas j on plate i. The inputs of this model are the speed ratio S_j, the ratio between the panel area A_i and the reference area A_{ref}, γ_i, which is the cosine of the angle between the particle bulk velocity and the normal vector of the panel, and the ratio between the velocity of the re-emitted and incident particles. This later ratio is given by Koppenwallner (2009) [11] as in Equation (2.7).

$$\frac{v_{re}}{v_{inc}} = \sqrt{\frac{1}{2}\left[1 + \alpha\left(\frac{4RT_w}{M_j{v_{inc}}^2} - 1\right)\right]} \tag{2.7}$$

Where v_{re} and v_{inc} are the velocities of the re-emitted and incident particles respectively, R is the universal gas constant, M_j is the molar mass of constituent gas j and T_w is the spacecraft surface temperature.
The total drag acceleration experienced by the spacecraft can now be obtained by combining Equation (2.5) with Equation (2.1), from which Equation (2.8) is found.

$$a_{drag} = \frac{1}{2}\frac{A_{ref}}{M}\rho{V_{inc}}^2\sum_{j=1}^{n}\frac{\rho_j}{\rho}\sum_{i=1}^{m}C_{D,i,j} \tag{2.8}$$

Here, the singular drag coefficient from Equation (2.1) has been replaced by the double summation of the drag coefficient contributions due to each plate and constituent gas. To account for the composition of the atmosphere, the contributions of the individual constituent gasses are weighed by the ratio between that gas' density over that of the total atmosphere.

2.3. Required Measurements to Enable Drag Prediction

As discussed in Section 2.2.1 the accommodation coefficient is one of the most important parameters required to calculate the drag coefficient of orbiting spacecraft. Unfortunately, the accommodation coefficient can not be observed directly. The energy of the incoming particles can be estimated from their thermal and bulk velocities, and the energy that a fully accommodated particle would have can be derived by measuring the spacecraft surface temperature. There is no practical way to measure the energy of the reflected particles however, and therefore the accommodation coefficient has to be inferred by measuring the drag on the spacecraft, together with the atmospheric conditions that are of influence.

For the space mission under consideration, the required parameters to be measured can be derived by working through Equation (2.1) to Equation (2.8) backwards. From Equation (2.1), it can be seen that, to determine the drag coefficient, it is necessary to measure the acceleration and air density encountered by the spacecraft. The accommodation coefficient can then be derived from the drag coefficient model when combined with knowledge about the angular distribution of reflected particles.
As mentioned before, there has as of now not yet been a single mission which has measured all parameters required to fully investigate the nature of gas-surface interactions in rarefied atmospheres. The mission proposed in this report will correct this gap in current understanding, by obtaining contemporaneous measurements of the following parameters:

- Linear and angular accelerations
- Total atmospheric density
- Constituent element particle counts
- Gas temperature
- Wind direction and velocity
- Spacecraft surface temperature
- Particle incidence angle
- Angular distribution of re-emitted particles

These parameters should be measured over as wide a range of values as possible, so that the effect that each has on the resulting drag can be properly evaluated. The actual range that will be measured will be part of the mission concept trade-off, and will be presented in Chapter 4.

2.4. Atmospheric Model

The goal of the MIRALOS mission is to investigate rarefied aerodynamics in LEO. To determine the most interesting locations for measurements in the upper atmosphere, an atmospheric model called the NRLMSISE-00 model was used. This is a semi-empirical model which provides information on temperature, species number densities and total density at altitudes up to 1000 km.

NRLMSISE-00 takes into account various parameters, such as altitude, location, $F_{10.7}$ solar radio flux and the planetary geomagnetic amplitude A_p. However, as no future data is available on these last two parameters, they are to be predicted. Since they are correlated to solar activity to a certain extent (especially the former), the approach used was to exploit the periodicity of solar activity and apply the same periodicity to these parameters.

2.4.1. Longterm Changes

One shortcoming of the NRLMSISE-00 model is that a large part of its database still consists of observations from the 1970s and 1980s. In the meantime, the atmosphere has been undergoing a significant change due to increased concentrations of greenhouse gases such as carbon dioxide and methane. Conditions in the upper atmosphere have changed a lot in recent years: the upper atmosphere has seen a significant density decline, which has an effect on satellite drag [12]. Therefore, the model in its raw form is not representative for current atmospheric conditions.

To refine the model, a density decline of 5% per decade at 400 km altitude is incorporated in the model, as depicted in detail in the previous report [1]. This decline appears to be calibrated around the year 1982, at which the atmospheric properties agree with that of the model. This provides a good estimate under solar minimum conditions, but it is less accurate under solar maximum conditions. However, the assumption should suffice for the primary mission, which is performed under solar minimum conditions. The validity of the model is assessed in Section 15.5.

2.4.2. Model Results

In this section, the results of the model that are relevant to the mission are discussed. These are the atmospheric temperature, helium and oxygen concentrations and density, as these relate directly to the top-level requirements presented in Appendix A.

Temperature

One of the mission requirements is that the measurements include a spread in temperatures of 300 K (MIRALOS-SR-6). Figure 2.2 shows the temperature variations predicted by the atmospheric model as a function of altitude.

The model predicts that, from about 250 km onwards, temperature is almost independent of altitude and equal to the exospheric temperature. However, temperature varies with changes in local solar time and even more with changing solar conditions.

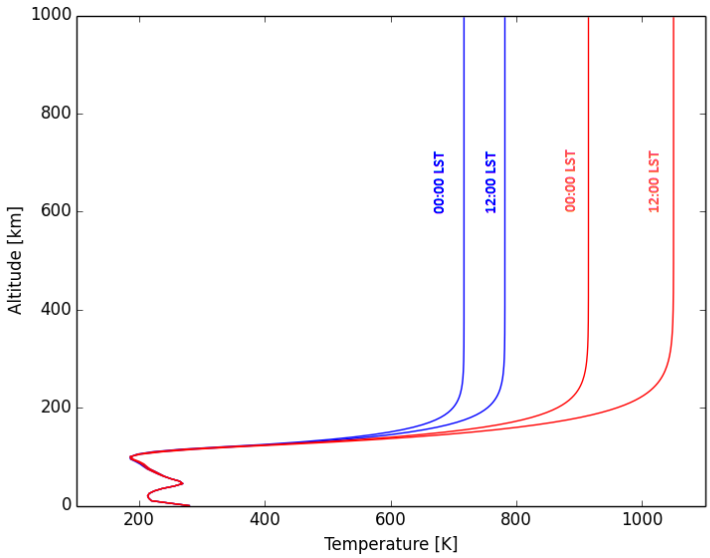

Figure 2.2: Atmospheric temperature for different altitudes, at 50°N and 0°E. The red lines represent the solar maximum conditions and the blue lines represent solar minimum conditions

Therefore, varying the orbital altitude won't help to meet requirement MIRALOS-SR-6. Fortunately, there is no need to do so. Figure 2.3 displays the variations in temperature for different dates at an altitude of 650 km. As can clearly be seen, the temperature differences for different local solar times at a single date can be greater than 300 K. Therefore, the temperature range requirement can be met at any altitude by ensuring coverage of all local solar times throughout the mission.

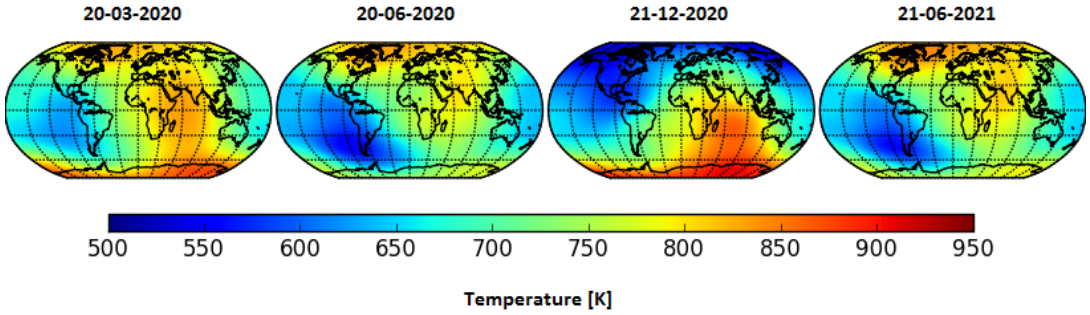

Figure 2.3: Exospheric temperatures for different dates at an altitude of 650 km.

Density

Atmospheric drag is related to the density in the atmosphere, and thus density is an important parameter that had to be considered in the design of the mission. Figure 2.4 shows typical density values that would be encountered according to the model in the upper atmosphere during the three different phases of the primary mission that were chosen in Chapter 4.

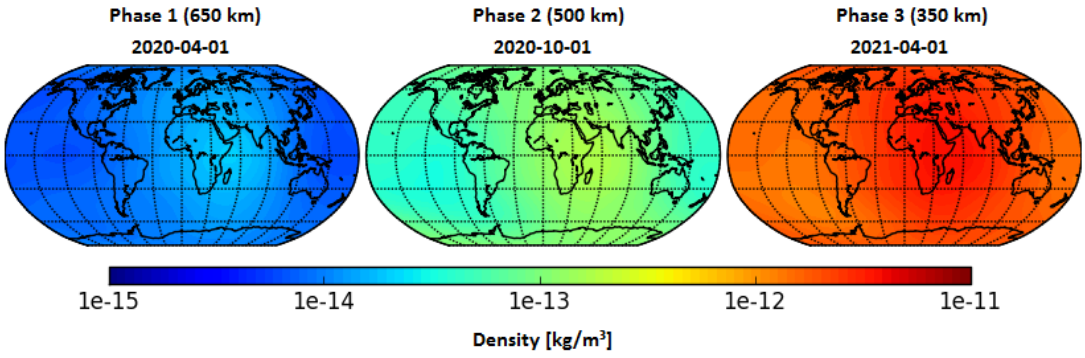

Figure 2.4: Total mass densities during each of the mission phases.

The graphs show that atmospheric density is mainly dependent on altitude and local solar time. In addition to these two factors,

solar and geomagnetic activity also greatly influence atmospheric density.

Helium and Oxygen Concentrations

Another requirement is that measurements should be done under both atomic oxygen and helium dominated conditions (MIRALOS-SR-5). The helium and atomic oyxgen concentrations are shown in Figure 2.5. The top row shows the helium concentrations during each of the mission phases as defined in Chapter 4, while the bottom rows show the atomic oxygen concentrations. The graphs in the top row of the figure show that helium dominated environments could be encountered at altitudes all the way down to 500 km.

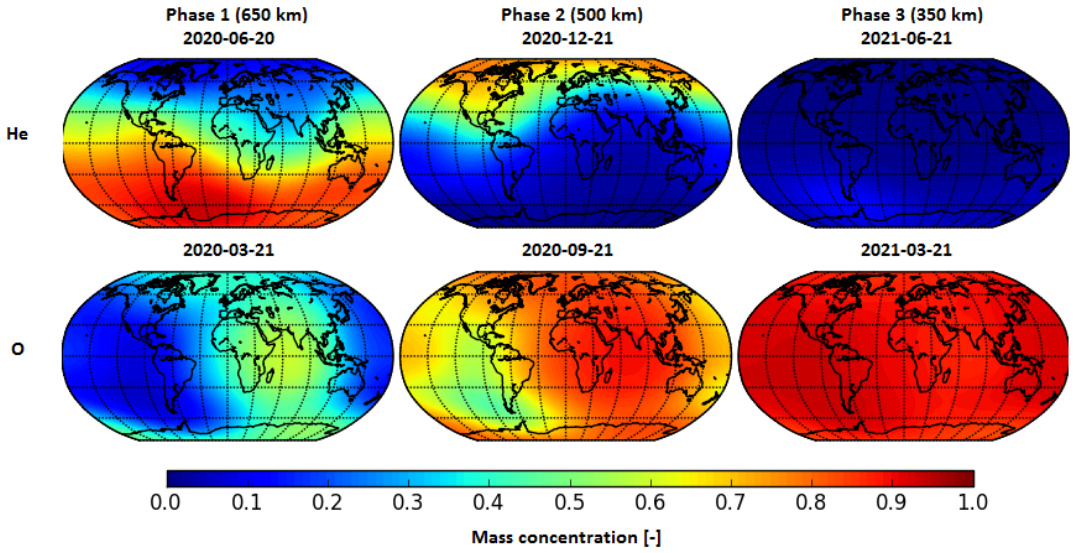

Figure 2.5: Helium (top) and atomic oxygen (bottom) mass concentrations during each of the mission phases. For helium, near optimal dates (solstices) within the various mission phases were chosen.

3. Mission Design

This chapter contains the high level mission design, elaborating on the work done in the Mid-Term Report [1]. Section 3.1 presents a secondary mission objective for the satellite, Section 3.2 contains an updated concept trade-off and Section 3.3 provides an overview of the orbit selection.

3.1. Secondary Mission Objectives

To fulfil the primary mission objective of characterising the gas-surface interaction at satellite altitude, the MIRALOS satellite carries a number of instruments to measure atmospheric properties such as particle density, temperatures, and upper atmospheric winds. This suite of instruments makes the spacecraft a capable platform for thermospheric research. To make use of these capabilities, the spacecraft shall have a secondary mission objective, which it will carry out during and after the primary objectives have been met. The specific research objectives associated with the secondary mission objective are :

- To obtain comprehensive measurements on the atmospheric properties at satellite altitude, for the purpose of creating an up-to-date model of the thermosphere.
- To obtain measurements of the lower atmosphere, in order to obtain a greater understanding of the interaction between the lower atmospheric layers and the thermosphere.
- To obtain long-term measurements of the decrease in thermospheric densities as a consequence of anthropocentric greenhouse gas emissions.

While the spacecraft can obtain highly accurate in-situ atmospheric measurements, it is limited in its altitude coverage. Even when fitted with a propulsion system, the spacecraft can only be at one altitude at a time, and altitudes below 300 km can not be visited for long durations as drag in these lower regions is excessive. Therefore, the spacecraft will include an optical ultraviolet horizon imaging instrument dedicated to the secondary mission objective. This instrument can obtain data on the composition and temperature of the atmosphere at altitudes ranging from 100 km to 300 km, supplementing the in-situ measurements. This instrument is elaborated upon in Chapter 6.

3.2. Concept Development

In the previous report, the mission concept that was selected consisted of a single satellite, using existing flight proven components and featuring no propulsion system. For the final design, the mission concept is revised by means of an updated concept trade-off.

3.2.1. Mission Concepts

For the final design, the following high level mission concepts are considered:

Guest Payload
It might not be necessary to design a dedicated spacecraft mission to meet the stakeholder requirements. Incorporating the required instruments as a secondary payload on a different spacecraft would be significantly cheaper, at the cost of design flexibility.

Multiple Satellites - Single Launch
Using multiple spacecraft significantly increases the flexibility of the mission design, allowing for simultaneous observations at different altitudes. Total mission cost would increase because certain systems have to be duplicated, but the majority of the development costs would be shared.

Multiple Satellites - Separate Launch
Similar to above, but each satellite is launched separately. This allows the spacecraft to be larger, and provides greater flexibility in their orbit design. Costs would significantly increase due to the need for multiple launch vehicles.

Baseline Concept
This is the mission concept that was presented in the midterm report, featuring a single, non-propulsive satellite using existing instruments as much as practicable.

Current Baseline + Propulsion
This concept is similar to the baseline concept, but adds a propulsion system to allow greater flexibility in the orbit design.

Current Baseline + Instrument Development
This concept is similar to the baseline concept, but will include upgraded instruments and subsystems with capabilities tailored for the mission.

Current Baseline + Instrument Development + Propulsion
This concept adds both upgraded instruments as well as a propulsion system to the baseline design.

3.2.2. Trade-off Criteria

The high level mission concepts introduced in Section 3.2.1 will be graded on five different trade-off criteria. These include cost, ballistic coefficient, quality of measurements, ability to fulfil secondary mission objectives, and flexibility. The criteria are discussed below.

Cost
The concepts are scored on their estimated cost relative to the baseline mission concept. Because the cost of the baseline mission was significantly below the mission budget of 350 million Euro, this criterion has a low weight. The scores of the different concepts with respect to this criterion are displayed in Table 3.1.

Table 3.1: Mission concept evaluation with respect to the cost criterion.

Concept	Score	Comment
Guest Payload	Excellent	Costs are greatly reduced, requiring only the development and testing of the instruments and sharing in the launch and operational costs.
Multisat - Single Launch	Marginal	Costs are increased due to duplicated instruments and systems, though development can be shared. Launch costs are unchanged, as launcher candidates have sufficient spare payload capacity.
Multisat - Multi Launch	Poor	Costs are significantly increased due to duplicated instruments and systems and the additional launch.
Current Baseline	Good	Baseline costs are low due to using existing components.
Baseline + Propulsion	Marginal	Development and testing of a propulsion system increases the cost over the baseline reference.
Baseline + Instruments	Marginal	Development and testing of improved instruments increases the cost over the baseline reference.
Baseline + Instruments + Propulsion	Poor	Development and testing costs for the propulsion system and the improved instruments will add significant cost to the mission.

Ballistic Coefficient
The mission concepts are scored on their estimated ballistic coefficient, which is defined as the ratio between the drag area and the mass of the spacecraft. These scores are displayed in Table 3.2. The accuracy of obtained aerodynamic measurements depends on the magnitude of the acceleration, which decreases with mass and increases with spacecraft surface area. In this way, the ballistic coefficient of the spacecraft determines the accuracy with which the acceleration can be measured. This criterion has medium weight.

Table 3.2: Mission concept evaluation with respect to the ballistic coefficient criterion.

Concept	Score	Comment
Guest Payload	Marginal	The ballistic coefficient is determined by the mass and size of the host spacecraft. Since most spacecraft are designed to minimize drag, the ballistic coefficient for this concept will be worse than for a dedicated mission.
Multisat - Single Launch	Poor	Fitting more than one spacecraft in a single fairing will require the individual spacecraft to be smaller, and thus have a worse weight to surface area ratio.
Multisat - Multi Launch	Good	When the spacecraft are launched separately, their ballistic coefficients can remain identical to the baseline.
Current Baseline	Good	The baseline concept has been designed to minimize the ballistic coefficient of the spacecraft.
Baseline + Propulsion	Marginal	The propulsion system and propellant required will increase the mass by 20 - 50 kg.
Baseline + Instruments	Good	The improved instruments are not expected to significantly increase the mass of the spacecraft.
Baseline + Instruments + Propulsion	Marginal	The propulsion system and propellant required will increase the mass by 20 - 50 kg.

Quality of Measurements
The concepts are scored on the quality of measurements they are able to obtain over the course of the mission, as displayed in Table 3.3. While any concept should be able to obtain the measurements required to fulfil the stakeholder objectives, it is not known in advance over what range of atmospheric conditions these measurements should be taken to be able to answer all questions regarding gas-surface interaction at satellite altitude. This criterion is weighted highly.

Table 3.3: Mission concept evaluation with respect to the measurement quality criterion.

Concept	Score	Comment
Guest Payload	Poor	The range of atmospheric conditions encountered depend on the orbit characteristics of the host spacecraft.
Multisat - Single Launch	Marginal	Multiple satellites increase the range of conditions encountered but maximum altitude is still constrained by the instruments.
Multisat - Multi Launch	Marginal	Multiple satellites increase the range of conditions encountered but maximum altitude is still constrained by the instruments.
Current Baseline	Marginal	Range of observed conditions is constrained by the limitations of the instruments and by the single orbital altitude that can be selected.
Baseline + Propulsion	Marginal	Range of measurements is still constrained by the minimum particle count required for the mass spectrometer.
Baseline + Instruments	Good	Improved instruments allow measurements at lower densities ,but lack of propulsion requires an altitude trade-off.
Baseline + Instruments + Propulsion	Excellent	Propulsive capability and improved instruments allow measurements across the widest range of atmospheric conditions.

Secondary Mission
The concepts are scored on their ability to fulfil the secondary mission objective of obtaining long term thermospheric data. This requires measurements of atmospheric conditions over a range as wide as possible, obtaining high spatial and temporal coverage of the thermosphere. The individual concept scores are displayed in Table 3.4. This criterion has medium weight.

Table 3.4: Mission concept evaluation with respect to the secondary mission objectives criterion.

Concept	Score	Comment
Guest Payload	Poor	Little control over orbit characteristics and inclusion of secondary instruments is expected to be problematic.
Multisat - Single Launch	Good	Observations from different orbits contribute to secondary mission objectives.
Multisat - Multi Launch	Good	Observations from different orbits contribute to secondary mission objectives.
Current Baseline	Marginal	Lack of propulsive capability requires a trade-off between longterm secondary mission orbit and low altitude primary mission observations.
Baseline + Propulsion	Good	Observations from different orbits contribute to secondary mission objectives, and propulsive capability allows parking in a longterm secondary mission orbit
Baseline + Instruments	Marginal	Improved instruments contribute to secondary mission objectives, but lack of propulsion requires a trade-off between longterm observations and low-altitude primary mission observations.
Baseline + Instruments + Propulsion	Excellent	Improved instruments contribute to secondary mission objectives and propulsive capability allows for longterm observations at multiple altitudes.

Flexibility and robustness
Finally, concepts are scored on their flexibility and robustness. These scores are displayed in Table 3.5. The primary mission requires observations over a wide range of atmospheric conditions, but it is not known in advance exactly how wide this range should be. Furthermore, the conditions that are experienced by the spacecraft might differ from those anticipated by atmospheric models. Therefore, the mission concept should be robust to these possible deviations from previous expectations, and include the flexibility to adapt to them. This criterion is weighted highly.

Table 3.5: Mission concept evaluation with respect to the flexibility criterion.

Concept	Score	Comment
Guest Payload	Poor	Mission design constrained by primary mission of the host spacecraft. Delays on the part of host spacecraft may compromise solar minimum timeframe observations.
Multisat - Single Launch	Good	Separate spacecraft allow for flexibility in orbit design.
Multisat - Multi Launch	Excellent	Separate launches allow for observations during different parts of the solar cycle. Provides backup capability in the case of launch failure. Second orbit can be modified based on results from first launch.
Current Baseline	Marginal	No capacity to adapt to unexpected conditions due to lack of propulsion. Instruments operating at the limit of their resolution.
Baseline + Propulsion	Good	Propulsion system allows for changes in orbit during the mission.
Baseline + Instruments	Good	Improved instruments are more robust in case atmospheric conditions deviate from expected values.
Baseline + Instruments + Propulsion	Excellent	Propulsion system allows for changes in orbit during the mission, and improved instruments are more robust in case atmopheric conditions deviate from expected values.

3.2.3. Concept Trade-off

The scores of the mission concepts for the various trade-off criteria are summarised in Table 3.6. The width of the column for each criteria is indicative of its relative importance in the trade-off. Based on the trade-off results, it is decided to improve the baseline concept by adding a propulsion system and developing more capable scientific instruments. This concept has excellent scores in the quality of measurements for the primary mission, the capability to perform the secondary mission, and the flexibility to adapt to unforeseen circumstances. It has a slightly worse ballistic coefficient, but this is offset by including a more accurate accelerometer. It will be more expensive than the baseline concept, but the baseline concept was significantly below budget.

Table 3.6: Summary of trade-off scores of the mission concepts for the five trade-off criteria. The relative weight of the criteria is indicated by the width of their column.

	Cost	Ballistic Coefficient	Measurement Quality	Secondary Mission	Flexibility
Guest Payload	Excellent	Poor	Poor	Poor	Poor
MultiSat - Single Launch	Marginal	Poor	Marginal	Good	Good
MultiSat - Separate Launch	Poor	Good	Marginal	Good	Excellent
Current Baseline	Good	Good	Marginal	Marginal	Marginal
Baseline + Propulsion	Marginal	Marginal	Marginal	Good	Good
Baseline + Instrument Development	Marginal	Good	Good	Marginal	Good
Baseline + Instruments + Propulsion	Poor	Marginal	Excellent	Excellent	Excellent

3.3. Orbit Selection

In the previous report, the orbit selection was constrained by the limitations of existing instruments. Furthermore, the lack of propulsion system required a single altitude to be selected. For the updated mission concept, a new orbit selection has to be made.

Table 3.7 displays atmospheric characteristics at a variety of orbital altitudes. These characteristics were simulated for the year 2020 using solar activity in 2008 as a proxy. For the minimum encountered drag acceleration, an accommodation coefficient of 0.5 was assumed.

The improved accelerometer, described in detail in Chapter 6, has an accuracy of 10^{-12} m/s^2. With such an accurate instrument, the minimum drag acceleration encountered is no longer a constraint on the orbit selection. The minimum drag at an altitude of 800 km can still be measured with a relative accuracy of 0.5%, provided that models for the other disturbance forces can be found that are this accurate. The minimum particle density still presents a problem. A more accurate spectrometer is assumed compared to the previous report, but even the most accurate device for which data could be found required a minimum particle count of 1000 per cubic centimeter. This limits the operational altitude of MIRALOS to a maximum of 650 km.

As described in Chapter 2, the accommodation coefficient is one of the most important parameters governing the nature of gas-surface interaction for rarefied atmospheres. This parameter depends on the degree to which atomic oxygen has been adsorbed onto the spacecraft surface, which in turn is a function of the oxygen partial pressure, which is given by:

$$P_O = n_O T k \tag{3.1}$$

Where P_O is the oxygen partial pressure in pascals, n_O is the particle count per cubic meter, T is the gas temperature, and k is Boltzmann's constant. To adequately characterise the variation of the accommodation coefficient for different atmospheric conditions, measurements of oxygen partial pressures across as wide a range as possible are beneficial.

As shown in Table 3.7, obtaining measurements in a helium dominated environment is possible in any orbit above 450 km. Furthermore, as shown in Section 2.4, temperature does not vary with altitude in the thermosphere. Adding a propulsion system to the satellite allows orbit changes during the mission, which allows us to select a series of orbital altitudes in sequence that together provide a wide range of oxygen pressures. The oxygen pressure range is the ratio between the maximum and minimum oxygen pressures encountered during a one year orbit.

Table 3.7: Orbit characteristics during solar minimum, simulated for 2020 based on 2008 solar activity.

Altitude	Min. Helium Concentration	Max. Helium Concentration	Min. Drag [m/s²]	Oxygen Pressure Range	Min. Particle Count [cm⁻³]
800 km	19%	94%	1.84E-10	1761	3.80E+01
750 km	14%	99%	9.16E-10	1171	1.29E+02
700 km	9%	96%	1.33E-09	685	4.90E+02
650 km	5%	96%	2.50E-09	372	2.00E+03
600 km	3%	95%	3.54E-09	137	1.20E+04
550 km	2%	93%	7.98E-09	70	5.80E+04
500 km	1%	84%	2.18E-08	36	2.63E+05
450 km	0%	63%	7.33E-08	19	1.23E+06
400 km	0%	36%	2.73E-07	11	5.50E+06
350 km	0%	16%	1.05E-06	7	2.59E+07
300 km	0%	5%	4.77E-06	4	1.10E+08

Figure 3.1 displays the range of oxygen partial pressures encountered over the course of one year for various orbit altitudes. Values were simulated for the year 2020 using solar activity data from 2008 as a proxy. Based on this variation of oxygen pressures, the orbit profile that is selected consists of three phases: orbit insertion will occur at an altitude of 650 km, after which the spacecraft propulsively drops its altitude to 500 km, and then to 350 km. At the end of the primary mission, the orbit is raised to 500 km again to provide a stable orbit from which to fulfil the secondary mission objectives. Further orbital changes after the primary mission is complete are at the discretion of the mission science team.

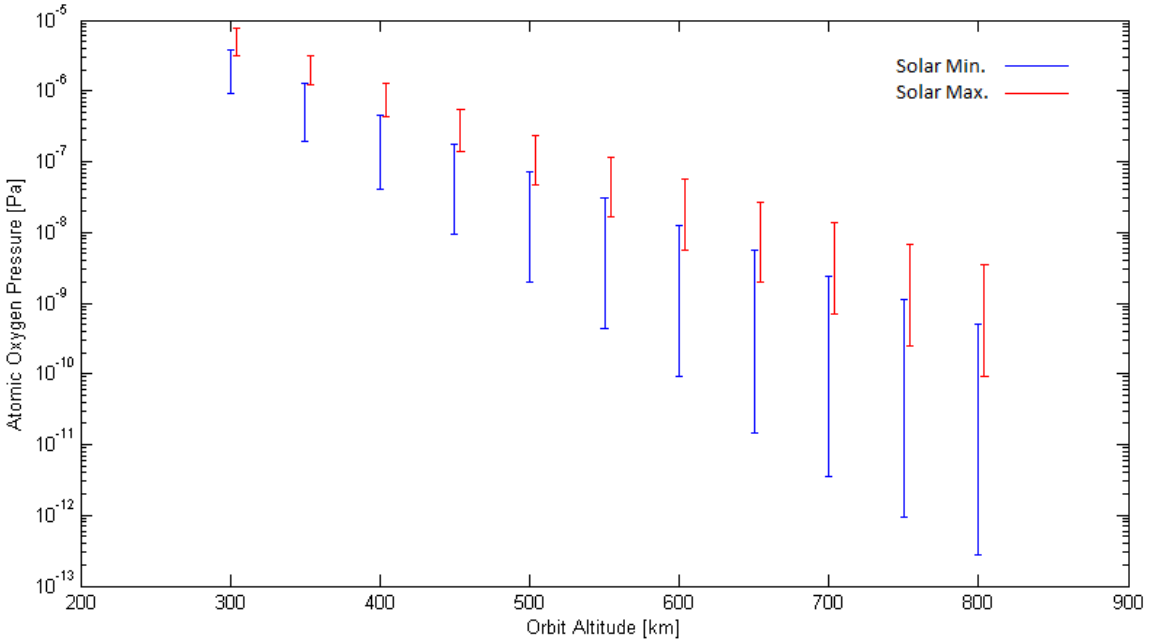

Figure 3.1: Range of oxygen partial pressures encountered during solar minimum and solar maximum conditions for different orbit altitudes.

The final question remaining is the duration of the stay of the spacecraft at each orbit altitude. Analysis of the atmospheric characteristics predicted by the NRLMSISE-00 model shows that the oxygen partial pressure follows a half-yearly pattern, as the planet moves from solstice to equinox and back. This is indicated for an altitude of 550 km in Figure 3.2. The bold line indicates the average oxygen pressure encountered during an orbit, with the other lines indicating the minimum and maximum values.

After six months at a particular altitude the spacecraft has encountered the full range of oxygen pressures that can be encountered. Therefore, the nominal mission design calls for six months of observations each at the altitudes of 600, 500 and 350 km. The spacecraft carries enough propellant to deviate from this mission profile, should the conditions encountered during the mission make this necessary. A full analysis of the orbit profile is presented in Chapter 4.

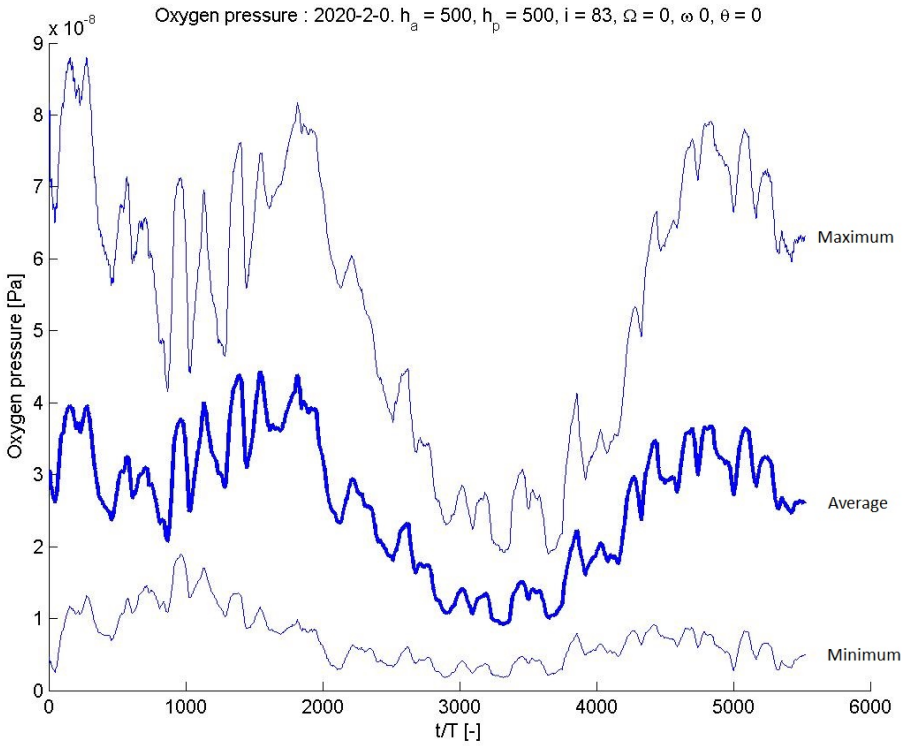

Figure 3.2: Oxygen pressure variation for the year 2020 at an altitude of 500 km. The x-axis displays the number of orbits. The upper curve displays the maximum value encountered on an orbit, the bold line represents the mean encountered value and the bottom curve is the minimum value along an orbit.

4. Astrodynamics

This chapter outlines the analysis of the mission orbits, aerodynamics and manoeuvres involved in the mission. The chapter starts with a general mission profile in Section 4.1, followed by the mission and orbit analysis in Section 4.2 presenting the simulation setup and results.

4.1. Mission and Orbit Profile

This section briefly outlines the mission profile for the primary part of the mission. As any possible secondary mission is not defined in detail up to now, the orbit profile is not defined yet for these missions. Therefore this chapter does not treat that part. A detailed overview of the mission/orbit profile can be found in Figure 4.1 below.

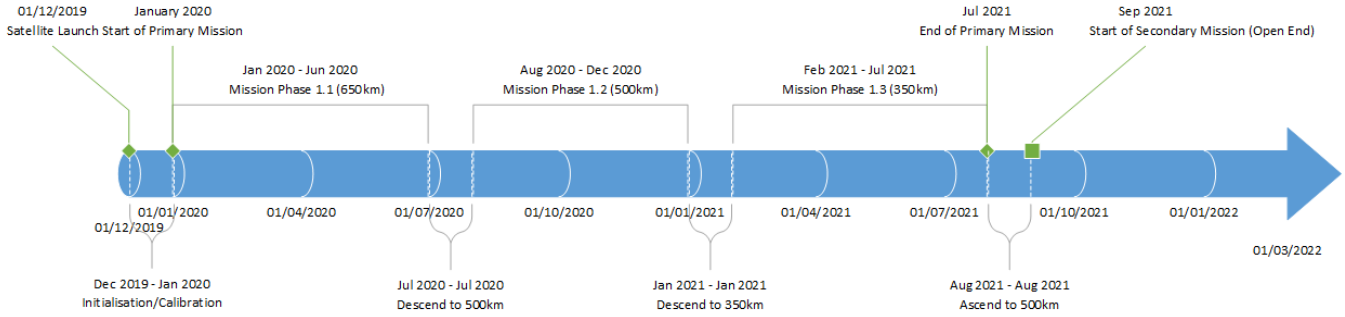

Figure 4.1: Planned Mission Profile/Timeline for the primary mission phase of MIRALOS

The mission profile is generated based upon a number of criteria and requirements: First off all the mission is supposed to be operational by 2020, therefore it was decided to have the launch in December 2019. This is followed by a one month initialisation, calibration and testing phase, after which the actual primary mission is initiated in January 2020. The primary mission is divided into three main phases: one for each measuring altitude at 650 km, 500 km and 350 km. The reasons for these altitudes are explained in Section 3.3. Each phase lasts a bit less than half a year, in order to get measurements for both solstice and one equinox. In between each phase, there is a manoeuvre to change the orbit which is scheduled to last at most one month. At the end of the last part of the primary mission, the satellite is brought back to an altitude of 500 km in order to get out of the high drag region at 350 km. This manoeuvre can however of course be varied, depending on the orbit required for the secondary mission objective. The initial orbit parameters can be found in Table 4.1.

Table 4.1: Initial Spacecraft and Orbit Parameters - Initial Orbit Parameters given in J2000 inertial system

Semi Major Axis:	7028 km
Inclination:	83°
Velocity:	7.53 km/s
Eccentricity:	0.00
Orbital Period:	97.73 min

4.2. Mission and Orbit Analysis

This section presents the analysis of the missions orbits, orbit changes, and manoeuvres. The analysis of the mission was performed in General Mission Analysis Tool (GMAT). The software was developed and is used by NASA for space mission development and analysis. The tool is open-source and available for download [13].

4.2.1. Simulation Setup

The spacecraft parameters used for the simulation can be found in Table 4.2. The actual dry mass used in the simulation is not 457 kg, but 464.2 kg. Such that it includes the fuel mass required for the ADCS thruster, which is not consumed during the simulation as it does not include any active attitude control. Note that the dry mass given here (used in simulation) might be slightly different from the mass budget presented in Section 5.3, which might have been updated after the simulation was completed. Hence the mass given in Section 5.3 is leading. The other parameters in Table 4.2 are based on the initial sizing of the spacecraft bus. The drag coefficient was estimated using the model presented in Section 2.2.2 for a spacecraft with a length

of 3 m, and an hexagonal cross section with sides of 1.1 m. The area of one of the six longitudinal panels was used as the reference area for calculating the drag coefficient.

Table 4.2: Initial pacecraft parameters

Dry Mass:	457 kg
Propellant Mass:	6 kg (Main Engine), 7.2 kg (ADCS)
Drag Coefficient:	4.5
Reflective Coefficient:	1,8
Drag Area:	3.3 m^2
Reflective Area:	6.6 m^2

The GMAT analysis was done using the following model inputs: As a gravity model, the EGM-96 was used with order and precision of both ten. The Moon, the Sun, Saturn, and Jupiter were taken into account for third body perturbation. Solar perturbations are taken into account using the inputs in Table 4.2. The atmosphere model used is MSISE-90 (the most recent available model in GMAT). Only a single $F_{10.7}$ and K_p value can be given as input per year into the simulation, thus the simulation was split up for each year (2019-2026). For each year, an average $F_{10.7}$ and K_p value was predicted using data from the past two solar cycles; these values were then used for the respective year in the simulation. Through the latter procedure, a variation in solar and geomagnetic flux over the solar cycle could be implemented in the simulation.

The orbit decay and life time at a defined altitude is highly dependent on the $F_{10.7}$ and K_p values, and predicting them is rather difficult. Because of this, some margins had to be implemented for the predicted values. The simulation was run once with the nominal predicted values (see Table 4.3) and once using the 50% increased values.

Table 4.3: Nominal Predicted Solar Flux (F10.7) and Geomagnetic Indices (Kp)

Year:	2019	2020	2021	2022	2023	2024	2025	2026
$F_{10.7}$**:**	73.14	69.0	70.6	80.1	113.4	119.9	122.75	180.6
K_p**:**	2.1	2.0	1.0	1.66	2.1	2.33	2.15	3.33

All manoeuvres were performed at a constant thrust level of 18 mN, which for the selected ion thruster (see Section 7.2) corresponds to an specific impulse of $I_{sp} \approx 3200$ s. The fuel used was 6 kg of Xenon, stored under an initial pressure of 125 bar in a blow down tank. All manoeuvres used a single long finite burn with the thrust aligned tangential along track, which is typical for low-thrust manoeuvres. This leaves as the only variable the burn time, which for each manoeuvre was calculated using a forward difference method in a loop. The forward difference method started with an initial guess and the loop was terminated once the desired Semi-Major-Axis (SMA), with an accuracy of ± 1 km, was reached. The orbit maintenance was done using a combined while and if loop, which would raise the orbit everytime the spacecraft doped below a certain altitude.

4.2.2. Simulation Results

The main result of the simulation is the altitude or SMA profile of the spacecraft, which can be seen in Figure 4.2. It is shown both for nominal and high solar activity/spacecraft drag. For the mission phase at 650 km, there is hardly any difference between the two cases. Also, the profiles for the phase at 350 km altitude (Phase 1.3) are almost the same, as the increase in drag is compensated by the additional ΔV required for orbit maintenance (see Table 4.4). However for the the two phases at 500 km altitude a difference is visible, as here no orbit maintenance is performed.

Due to irregularities in the gravity field of the Earth the orbit parameters get disturbed, the Right Ascension of Ascending Node (RAAN) and the argument of perigee shift and inclination, eccentricity and SMA oscillate around there design value. In fact, the eccentricity should first increase up to a certain point due to gravity effects, upon which at some point it will become so big that drag effects become dominant. This reduces the eccentricity again, by which it will slightly oscillate. Its average value lies around 0.00195 and its maximum at 0.0046. The RAAN shifts by about 0.8° to 0.9° westwards every day. The variation in inclination is almost insignificant: it oscillates with less than $\pm 0.15^\circ$ around its design value of 83°. The argument of perigee shifts within the orbital plane against the flight direction and will shift by approximately 360° roughly every 90 days. The main reason for both the shift of the argument of perigee and the right ascension of ascending node is the J2-effect (flattening of the earth).

An orbit analysis usually includes also an analysis of the ground track, which is in this mission only really important for communication with the ground segment and the lay out of the latter. A sample ground track can be found in the chapter dealing with that matter (see Figure 13.4, found in Section 13.4.1).

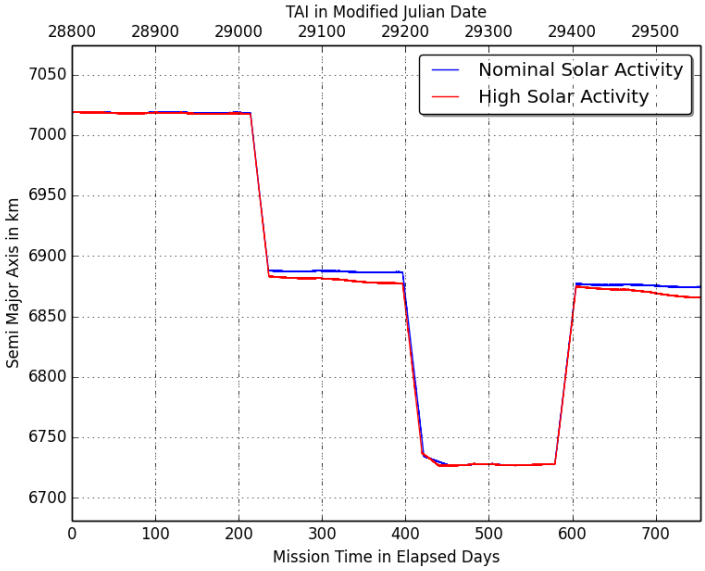

Figure 4.2: Orbit profile of the SMA with respect to mission elapsed days and International Atomic Time (TAI) given in Modified Julian Date (MJD). The blue plot shows the result for the nominal predicted $F_{10.7}$ and K_p values (see Table 4.3) the red plot shows the result with an 50% increase in these values. *MJD = JD- offset, Epoch: 05 Jan 1941 12:00:00.000, offset = 2430000.0 [13]*

Table 4.4: Manoeuvre parameters for nominal predicted $F_{10.7}$ and K_p values (see Table 4.3) and for a 50% increase in these values.

	Normal Solar Activity			High Solar Activity		
Manoeuvre	ΔV	Burn Time	Fuel Used	ΔV	Burn Time	Fuel Used
Descend to 500 km:	71 m/s	514 h	1.06 kg	73 m/s	529 h	1.09 kg
Descend to 350 km:	84 m/s	611 h	1.26 kg	77 m/s	556 h	1.11 kg
Orbit Maintenance:	18 m/s	130 h	0.27 kg	44 m/s	316 h	0.70 kg
Ascend to 500km:	85 m/s	612 h	1.26 kg	85 m/s	611 h	1.25 kg
Total:	258 m/s	1755 h	3.85 kg	279 m/s	2012 h	4.15 kg
Spare:	147 m/s	1042 h	2.15 kg	127 m/s	896 h	1.85 kg

The results of the manoeuvres flown can be found in Table 4.4. As to be expected, the ΔV consumption for the high solar activity/spacecraft drag is slightly higher. Especially the orbit maintenance at 350 km requires more than twice as much ΔV. In both cases, more than 100 m/s ΔV is left after the orbit raise to 500 km and end of primary mission. This leaves sufficient amount of ΔV for most secondary missions. From the table it becomes obvious that also the requirement that a manoeuvre should take no longer than 30 days is fulfilled: the maximum required burn time is around 25 days.

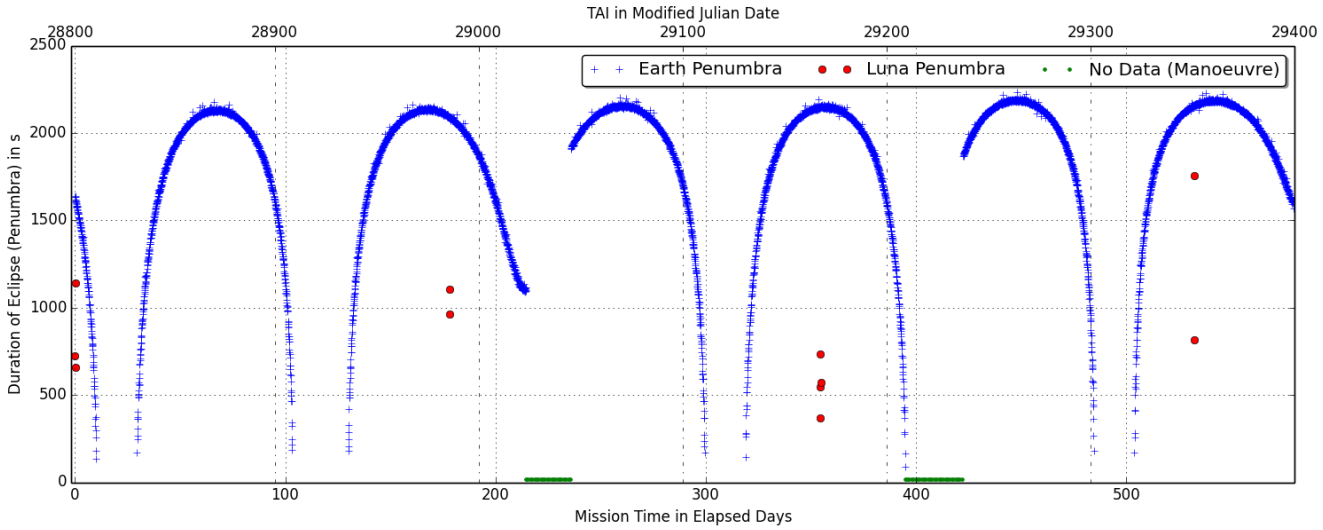

Figure 4.3: Eclipse Profile due to Earth and Luna Penumbra during primary mission with respect to mission elapsed days and TAI given in MJD. Note that eclipse during manoeuvres could not be displayed, the respective time frames are marked with the No Data line

As for this mission both thermal and power control are rather important, one should have a closer look at the lighting conditions the satellite is subjected to. Some instruments, such as the accelerometer, require very accurate and stable thermal control. Furthermore, the ion propulsion system requires a lot of power when operational.

As the chosen orbit has an inclination close to 90° and is of low altitude, the orbit is close to being sun-synchronous (RAAN shifts by about 0.8° to 0.9° per day). A plot of eclipse times and duration can be found in Figure 4.3. Note that during manoeuvres eclipse times could not be calculated, those regions are marked with a dotted green line in the plot. From the plot, one can see that the maximum time the satellite is without sun light is 37 minutes and is at most continuously illuminated for about 27 days.

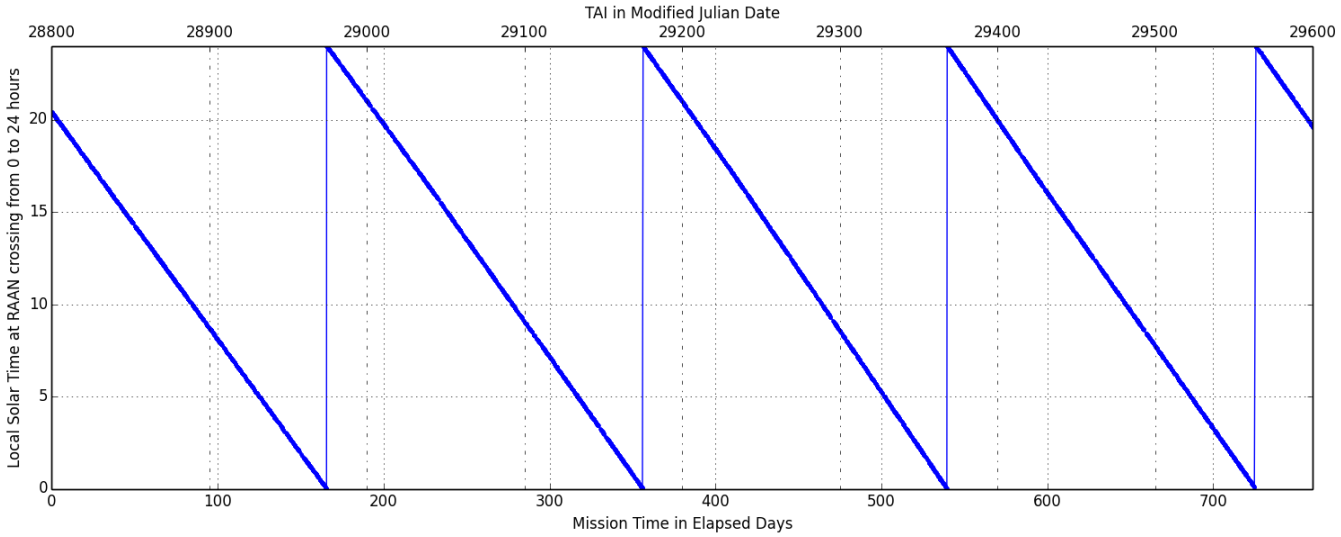

Figure 4.4: LST from 0 to 24 h at ascending node crossing during primary mission with respect to mission elapsed days and TAI given in MJD.

When observing atmospheric compositions and density, also the Local Solar Time (LST) the spacecraft encounters plays an important role. In order to get complete models, it is desired to get a large spread of LST per location and altitude. The LST depends mainly on the spacecraft longitudinal position and the time of the day. A plot of the LST when crossing the ascending node can be found in Figure 4.4. From the plot, it can be deduced that the spacecraft covers all LSTs after approximately every 200 days. This result corresponds to observations in the eclipse plot displayed in Figure 4.3, where the period of full illumination occurs about twice in 200 days, corresponding to a full coverage of all LSTs. When considering that when crossing the descending node the spacecraft sees the same time as at the acending node just with twelve hours different. Therefore the spacecraft actually observes all LSTs in half the time stated above.

5. Spacecraft Design

This chapter describes the spacecraft bus design and system integration. First, the satellite shape is described in Section 5.1. Section 5.2 entails the spacecraft layout and integration of the various instruments. Lastly, the mass, power and cost budgets are assessed in Section 5.3.

5.1. Satellite Shape Design

In Chapter 3 it was decided that the mission shall consist of a single satellite which is to perform measurements at a range of altitudes, with the assistance of a propulsion system. The bus design however has not yet been depicted, and is the subject of this section. First, a decision will be made between a spacecraft with surface-mounted or externally mounted equipment (mainly solar cells). Secondly, a trade-off is made between different bus geometries. Thirdly, the outer spacecraft dimensions are depicted.

5.1.1. Surface-mounted vs. Panel-mounted Equipment

One of the main advantages of external panels is with respect to solar cell efficiency. In Chapter 9 it will be argued why solar panels are implemented for power retrieval throughout the mission. Significant power requirements flow out of the different subsystem designs, which will be depicted in Chapters 6 to 13. To maximise solar cell efficiency, the cells can be mounted on separate surfaces which can be pointed towards the sun. Panel-mounted solar panels are approximately 20% more efficient than surface-mounted solar cells, depending on the satellite shape and orientation. Furthermore, these panels can be used to induce a larger ram area by pointing them in flight direction, from which a larger drag signal is obtained. This allows more accurate accelerometer measurements. However, pointing the panels in flight direction will eliminate the advantage of solar cell efficiency: the panels can only be pointed in one direction at a time. Furthermore, external solar panels have the advantage that it allows components to be mounted further away from the spacecraft bus, which limits electromagnetic interference and simplifies thermal operations.

On the other hand, multiple disadvantages exist for externally mounted panels. First of all, the quality of measurements is reduced as discrepancies are introduced in the satellite ram area. The introduction of concave shapes increases uncertainty in the computation of the drag signal. Additionally, it becomes more difficult to place instruments such as the mass spectrometer or reflectometer, as externally moving panels would influence the inflow of particles. Secondly, the solar panels increase the drag signal, but also induce higher torques on the spacecraft. This puts more strict requirements on the ADCS system. Thirdly, outer panels complicate mounting the spacecraft in the launcher, hence a deployment mechanism would be required. This would further increase uncertainties and complexity of the aerodynamic calculations required to analyse drag. These mechanisms also carry additional risk. Fourthly, outer panels would complicate manufacturing and due to higher stresses on the spacecraft, a heavier structure would be required, which reduces the accuracy of the drag signal. Lastly, these panels increase complexity of the design of internal electronics and the thermal control subsystem.

It becomes evident that the disadvantages of mounting the solar cells on external panels are dominant. The quality of data both benefits and suffers from this decision. As will be presented in Chapter 9, surface-mounted solar cells suffice in power provision, so the increased efficiency of deployable panels is not required. It is decided to mount solar cells on the satellite surface. Furthermore, external panels solely used to increase the ram area are not sensible, as it significantly complicates aerodynamic calculations and will most likely be counterproductive.

5.1.2. Bus Geometry

In the previous subsection, it was decided that the solar cells will be mounted on the bus surface. This translates into a solar cell efficiency of 0.5 to 1.0, depending on the bus geometry and incidence angle. Different bus geometries have different benefits. Six bus shapes are traded off in Table 5.1.

Table 5.1: Summary of bus shape trade-off scores.

Criteria	Weight	Circular Rod	Triangular Beam	Square Beam	Hexagonal Beam	Octagonal Beam	Sphere
Power Efficiency	High	Bad	Bad	Marginal	Good	Marginal	Bad
Ease of Integration	Medium	Bad	Good	Good	Good	Marginal	Bad
Ease of Manufacturing	Low	Bad	Good	Good	Marginal	Marginal	Bad
Launcher Efficiency	Medium	Good	Bad	Bad	Marginal	Marginal	Bad
Quality of Measurements	High	Bad	Marginal	Marginal	Marginal	Marginal	Bad

Six options are assessed: a beam with circular, triangular, square, hexagonal and octagonal shape, and a sphere. These are compared for five criteria, selected for their importance and significant difference between geometries.

Firstly the geometries are compared for their solar cell efficiency. The cell efficiency for optimal and worst case scenarios are estimated, assuming an all-around solar cell coverage on the longer side of the spacecraft. The circular rod and sphere have a constant efficiency of $2/\pi$, independent of orientation. The triangular beam has an efficiency between 0.5 and 1.0, while the square beam has an efficiency between 0.707 and 1.0. The hexagonal and octagonal beam have efficiencies of $0.789 - 0.866$ and $0.765 - 0.819$, respectively. As the demand of power by various subsystems is large, this criteria is assigned a high weight.
Secondly, the ease of instrument and subsystem integration is assessed. On convex surfaces, implementation of solar cells and instruments is troublesome. Additionally, internal subsystem placement requires more attention compared to straight plates. This receives a medium weight due to its effect on the complete spacecraft design.
Thirdly, the ease of manufacturing is assessed. Convex surfaces complicate production and assembly. However, as only a single product is to be produced, low weight is assigned to this criteria.
Fourthly, the launcher efficiency is compared. While shared use of a larger launch vehicle is an option, it is desired to maximise the usage of launcher volume to avoid any reliance on finding an appropriate partner mission. As the launch can attribute significantly to consumption of the financial budget, this criteria is assigned a medium weight.
Fifthly, the impact on the quality of measurements is of utmost importance. Ideally, an infinitesimally thin rectangular plate is flown for data measurements, to minimise uncertainty in aerodynamic calculations. This criteria is assessed similarly to that of power efficiency. The triangular, square and hexagonal beam will have one or two plates pointed in the flight direction. The circular beam, octagonal beam and sphere will have many more (convex shapes will tend be a polygonal shape, due to the limitation in bending of solar panels and instrument apertures). Hence, all geometries but for the circular rod and sphere are assigned marginal scores.

It is concluded that the hexagonal shape is most feasible, as it contains no significant disadvantages and is more efficient than an octagonal beam with respect to power retrieval and spacecraft integration.

5.1.3. Spacecraft Dimensions

The outer spacecraft dimensions were previously sized depending on the available payload volume in existing and feasible launch vehicle options, as described in the Midterm Report [1]. The spacecraft is desired to be as large as possible in order to maximise the drag signal, without requiring large and overpowered launch vehicles (such as the Ariane 5 or Proton).
In the preliminary phase of the design, no launcher was yet selected and outdated information on launchers was used. Because of this, a length of 3 m, with a bus diameter of 2.2 m (i.e. side lengths of 1.1 m) were chosen, which allow for a drag signal that provides the required accuracy, while still fitting in most feasible launch vehicles.

In the next design phase one of the first main steps to take, besides iteration of the mass, power and data budgets, is to critically reconsider this decision. The launcher used, which will be depicted in Section 13.4, allows for a much larger spacecraft. A larger spacecraft would result in a larger drag signal. However, this would also result into a larger structural subsystem, thereby increasing weight and reducing the signal. Alternatively, the implementation of a more accurate accelerometer allows for a smaller, lighter spacecraft to be chosen. These are very important considerations for the remaining design phases. Due to lack of time and resources, this decision is not yet assessed here. All subsystem designs currently are based on the described spacecraft dimensions.

5.2. Satellite Layout Design

The spacecraft layout is based completely on component requirements. As a visual aid for Section 5.2, the location and orientation of each component can be viewed in Figure 5.1.

5.2.1. Payload

The payload location and orientation is fully determined by their measurement location requirement. The reflectometers and the Small Wind and Temperature Spectrometer (SWATS) need to measure the incoming particles, therefore they are located in ram position. The accelerometer coincides with the center of mass of the spacecraft, and is placed on an ultra stable carbon-carbon panel to inhibit the accelerometer from moving with temperature variations. The accelerometer Interface Control Unit (ICU) is placed close to the sensor itself to minimize electromagnetic interference with the connecting harness. The Laser Retro-Reflector (LRR) is placed on the bottom panel, pointing nadir, to enable a line of sight with Satellite Laser Ranging (SLR) stations. The Global Ultraviolet Imager (GUVI) is placed on the bottom panel as well, 90 degrees to the spacecraft orbital velocity, to provide latitudinal scanning of the atmosphere. With the exception of the LRR, all of the payload is either inside the bus, or sunken into the outer panels, in order to simplify the aerodynamic shape of the spacecraft. It might be possible to sunk the LRR in the outer panel with the use of glass cover panels preserving the operational window of the instrument. Further research in next design phases will reveal this possibility.

5.2.2. Antennae

The GPS Precision Orbit Determination (POD) antenna is placed on the top panel, pointing zenith, in order to have a 360 degree hemispherical line of sight, not obstructed by the earth. The GPS satellites orbit much higher, so this location benefits the amount of satellites within contact range greatly. Next to this antenna, a GPS backup antenna is placed. The GPS Occultation (OCC) antenna is situated on the ram panel, so its received signal will pass through the atmosphere, enabling ionospheric occultation measurements. A backup antenna is placed next to this antenna as well. Both backup antennae are merely there to provide the spacecraft a way of attitude determination (as mentioned in Chapter 8), in case one of the two main antennae fail. The GPS ICU is put on the top panel, mainly to counter the GUVI mass. Lastly, two communication patch antennae are put on the bottom panel, pointing nadir, to provide connection with Earth. The transceiver for the communication antennae is placed close to the antennae to minimize line-loss.

5.2.3. Propulsion

Since the spacecraft will both be accelerating and decelerating using the propulsion system, a definite ram or aft position can not be chosen. However, since the thruster will produce a lot of heat, it is placed away as far as possible from temperature sensitive components such as payload, on the outside of the bus. The line of thrust needs to go through the center of mass, and therefore the thruster is placed on the outside of the aft panel, centered. The Xenon Feedsystem Assembly (XFA) and Ion Propulsion Control Unit (IPCU) are placed next to the Ion Thruster Package (ITP), on the inside of the aft panel. The two propellant tanks are placed on the middle panel, close to the center of mass to minimize the increase of center of mass offset during propellant use. They are placed in a configuration countering the center of mass offset caused by each separate tank. The tanks are also placed outward, to increase the eigenfrequency of the carbon-carbon panel, which is required for launch.

5.2.4. Power

The outside of the bus is almost completely covered in solar panels, with the exception of the hexagonal top and bottom panel. Around the ITP a slightly larger cutout is made, to prevent rapid degradation of the surrounding solar panels due to rogue xenon ions. The Power Regulator Unit (PRU) is located next to the batteries on the inside of the top panel, mainly as a counterweight to the GUVI and the two propellant tanks. This location also minimizes thermal interference with payload.

5.2.5. ADCS

The Attitude Determination and Control System (ADCS) consists of sensors and actuators, all of which have requirements enforcing a definite location and orientation within the spacecraft. The two redundant magnetometers are placed on the top panel, far away from sources of electromagnetic interference or ferromagnetic materials, to prevent noise in the measurements. The four Digital Sun Sensors and the four Star Camera Assemblies are put in pairs on the outside panels, so two of each set always point away from the sun, enabling the star cameras to work, and one of the sun sensors always points towards the sun. The star cameras are pointing zenith with an angle of 45 degrees, as to not let the earth albedo interfere with the sensor. The six magnetorquers are put in 90 degree offsets in redundant pairs. The are located far away from the accelerometer, as to not interfere with measurements. The six Mass Trim Mechanisms are located next to the magnetorquers, since these also require three redundant pairs in 90 degree offset, to be able to trim the center of mass on each axis. The Mass Trim Assembly Electronics Unit (MTE) is situated on the bottom panel.

5.2.6. Harness and Electronics

The Onboard Computer (OBC) is put on the top panel to counter the GUVI and propellant weight. However, almost all electronics and interface control units do not require to be at a specific location, the exceptions being thermal and electromagnetic interference requirements. Therefore, the electronics can be used as a means of balancing the spacecraft so the center of mass and the accelerometer coincide.

5.2.7. Balancing

After system integration, the flight model mass properties will be tested, such as total mass, Center of Gravity (CoG) and Moment Of Inertia (MOI). If the center of mass is not within tolerances, small weights can be added to solve the problem. The total weight contingency accounts for this.

5.3. Resource Allocation

In the midterm report an iteration on the preliminary resource allocation was performed, in which the new found mass of the payload instruments played a major role. However, further in the design process it became clear that the Space Mission Analysis and Design (SMAD) estimation numbers do not give accurate results for MIRALOS because it is significantly larger than other spacecraft with similar payload mass. In the midterm report all estimations were based on the payload, which usually works out fine. As a final iteration on the resource allocation a more specific approach is taken, in which only select systems are sized based on payload.

The selected payload instruments including their mass and power contributions are shown in Table 5.2. Further details on the instruments can be found in Chapter 6.

#	Abbreviation	Unit Name
3	**BATT**	Battery
1	**PRU**	Power Regulator Unit
6	**SOL**	Solar Panel
1	**GPS POD**	Precision Orbit Determination Antenna
1	**GPS OCC**	Occultation Antenna
2	**GPS BKUP**	GPS Backup Antenna
1	**GPS ICU**	GPS Interface Control Unit
1	**ANT-T**	Communications Transmitting Antenna
1	**ANT-R**	Communication Receiving Antenna
1	**COMM TRS**	Communication Transceiver
1	**XENON TANK**	Xenon Propellant Tank
1	**XFA**	Xenon Feedsystem Assembly
1	**ITP**	Ion Thruster Package
1	**ICPU**	Ion Propulsion Control Unit
6	**MTM**	Mass Trim Mechanism
1	**MTE**	Mass Trim Assembly Electronics Unit
6	**MTQ**	Magnetorquer
2	**MMR**	Magnetometer
4	**SCA**	Star Camera Assembly
4	**DSS**	Digital Sun Sensor
1	**GUVI**	Global Ultraviolet Imager
2	**GUVI ICU**	GUVI Interface Control Unit
1	**LRR**	Laser Retro-Reflector
1	**ACC**	Accelerometer Sensor Unit
1	**ACC ICU**	Accelerometer Interface Control Unit
1	**SWATS**	Wind & Temperature Spectrometer
1	**RFM 1**	Ionisation Reflectometer
1	**RFM 2**	Foil Scanning Reflectometer
1	**OBC**	On Board Computer

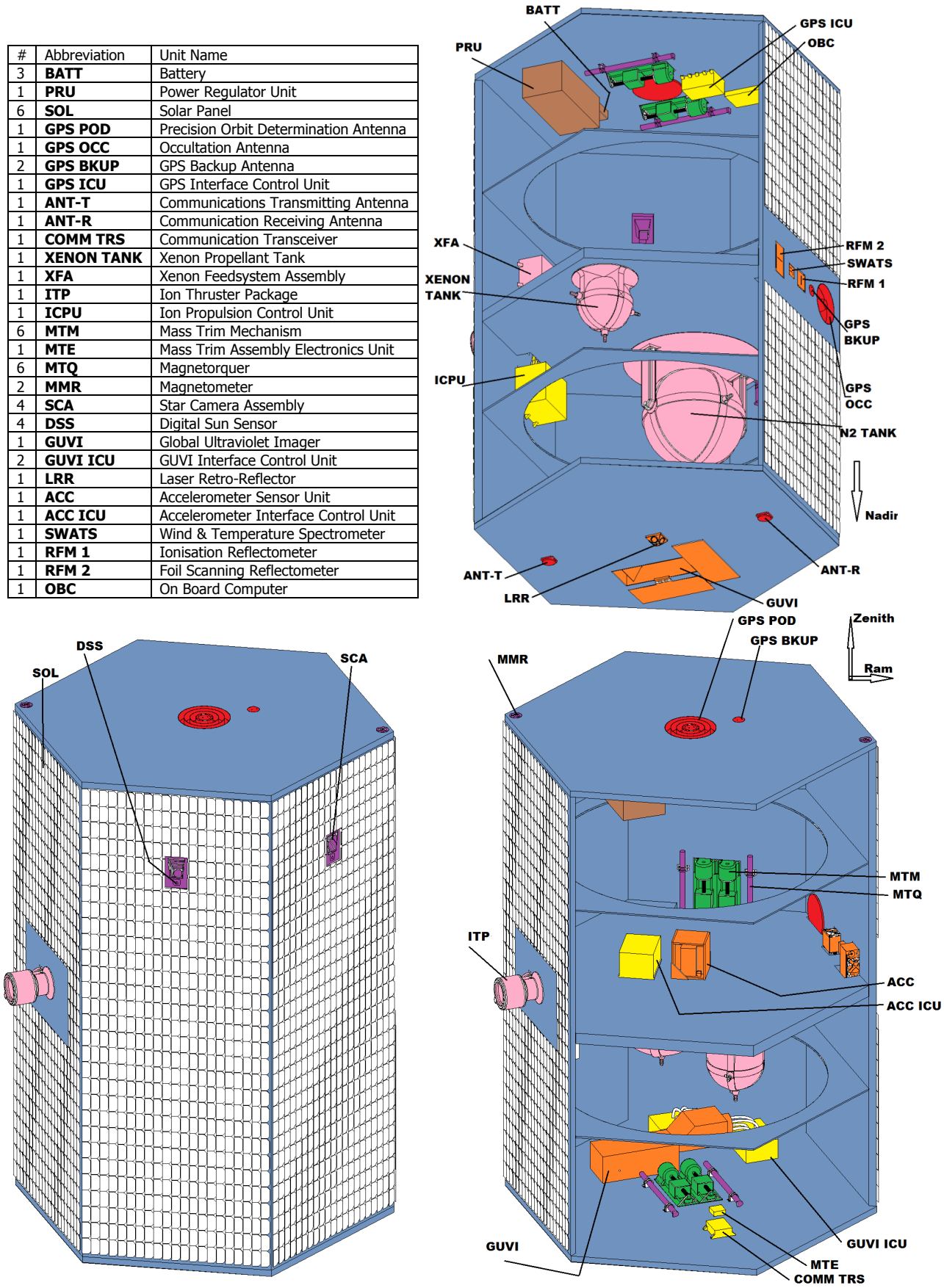

Figure 5.1: Schematic overview of the external geometry and internal subsystem placement. The subsystem categorization of the components is indicated by color.

Table 5.2: Properties of the payload instruments.

Instrument	Product Name	Mass [kg]	Power [W]	Source
Mass, Wind & Temperature Spectrometer	SWATS	0.65	1.3	[14]
Accelerometer	ACC-GRACE-FO	15	25	Section 6.4
Ionisation Reflectometer	RFM 1	0.136	1	[15]
Foil Scanning Reflectometer	RFM 2	0.15	1	[15]
GPS Receiver	TRSR-2	13	17.5	[16]
Laser Retro-Reflector	LRR	1	0	
UV Horizon Sounder	GUVI	19.1	27	
Total		48.9	72.8	
Total (25% CF)		61.1	-	

5.3.1. Mass Allocation

Since MIRALOS is not an ordinary spacecraft, the mass allocation was done differently. The main deviation from standard design is the difference in size and payload mass. To achieve a reasonable drag signal, the spacecraft needs a big frontal area, and needs to be low on mass. Therefore the inside of the bus is quite empty compared to other spacecraft. To cope with this difference, the mass estimation is not solely based on the payload, but also depends on structural mass. It is expected that some systems scale in mass with the structure size, and others mainly depend on payload mass. The following table Table 5.3 shows what the different system mass estimates are, what they are based on, and what their final value is.

Table 5.3: Subsystem Mass Allocation. The second column shows the initial mass estimation, i.e. before there was started with the subsystem design. The final subsystem masses are given in the fourth column.

System	Mass Estimation [kg]	Based on	Final Mass [kg]
Payload	61.11	Sum of Instrument Masses	61.11
Structure	250	Mass Estimate Calculation	275
Thermal	4.21	Payload & SMAD	4.21
Power	31.61	Payload & SMAD	38.99
TT&C	2.11	Payload & SMAD	1.5
C&DH	6.32	Payload & SMAD	7.5
ADCS	34.03	Structure+Payload & SMAD	35.74
Propulsion	38.89	Structure+Payload & SMAD	33.15
Propellant	48.61	Structure+Payload & SMAD	13.21
Total Dry Mass	428.28		457.2
Total Wet Mass	476.89		470.41

The final values in the table are the calculated masses from system design. It can be seen that the deviations from the iterated estimations is only small. Throughout the final design stage all the masses were constantly updated, providing the systems depending on mass the most recent data. The mass estimation of the ADCS and the propulsion system were based on the combined calculated mass of the payload and structure, since these systems fully depend on total system mass. The other system mass estimations such as power, thermal, TT&C and C&DH were only based on payload mass, since it was expected that these only scale with payload.

5.3.2. Power Allocation

The preliminary power allocation in the midterm report was based on ratios from SMAD [17]. In the final design, detailed power requirements were constantly updated, overruling the previously found estimations. The resulting power allocation is depicted in Table 5.4.

In practice, not all systems will be using maximum power at the same time. For instance, the communication system will not be transmitting all the time, and will not be using all antennae on maximum rated power. The sizing of the power system is explained in Chapter 9.

5.3.3. Resource Consumption

In this subsection the initial cost estimation performed for the Midterm Report [1]. The general model used for the cost estimation is the Small Spacecraft Cost Model (SSCM) published by the Aerospace Corporation.

The general cost estimation consists of six main parts, which are stated in the first column in Table 5.5. The satellite bus can be divided into seven elements displayed in italic in the table. The cost estimation is performed using the SSCM, which is based on the data of 53 individual satellites, all with a weight lower than 500 kg. Unfortunately, no information regarding the subsystem cost and payload cost has been found. Therefore, the total satellite, payload and subsystem masses are used to determine the costs by application of Cost Estimation Relations (CERs), which are defined in [18].

Table 5.4: System Power Allocation

System	Max. Power Usage [W]	Note:
Payload	72.8	All Instruments Operating
Structure	0	
Thermal	150	Maximum in Cold Case/Safe Mode
Power	-975	End Of Life Production
TT&C	38	Rare Maximum Case
C&DH	14	
ADCS	14.63	
Propulsion	600	100% Throttle
Propellant	0	
Total	889.43	Sum without Power System

The Launch & Orbital Operations Support cost is estimated using specific information on the Dnepr-LV launcher, which has a launch cost of 20 million USD. Next, the Orbital Operations Support estimated by CERs is added to this cost. The program level cost includes systems engineering, program management, system integration and test, product assurance and labor costs.

The estimated costs for the propulsion system were increased by a factor of 10 to account for the selection of electrical propulsion. Similarly, the estimated program level and payload costs were increased by a factor of 1.5 to reflect the significant amount of instrument development.

Table 5.5 shows the costs per satellite element in thousands of euros for Fiscal Year (FY) 2014.

Table 5.5: Satellite total cost estimation using the SSCM

Element	Cost FY2014 in thousand of euros
Satellite Bus	46744
Structure	23957
Thermal Control	346
ADCS	13315
EPS	6973
Propulsion	2670
TT&C	461
C&DH	1424
Payload	22234
Integration, Assembly & Test	5151
Program Level	12729
Launch & Orbital Operations Support	18116
Ground Support Equipment	2446
SAT TOTAL excl. contingency	109823
SAT TOTAL incl. 10% contingency	120805

As can be seen from Table 5.5, the total satellite cost including a contingency factor of 10% is estimated at 121 million 2014 euros. Without contingency factor this becomes 110 million 2014 euros. This represents an increase of 7.5% of the cost before contingency over the estimate from the Midterm Report.

5.3.4. Cost Break-down Structure

The mission costs are sorted using a Cost Break-down Structure (CBS). This is an AND tree diagram breaking down the total system cost into smaller cost elements. It reflects the costs related to the activities defined in the Project Design & Development logic described in Section 15.12. The CBS is shown in Figure 5.2.

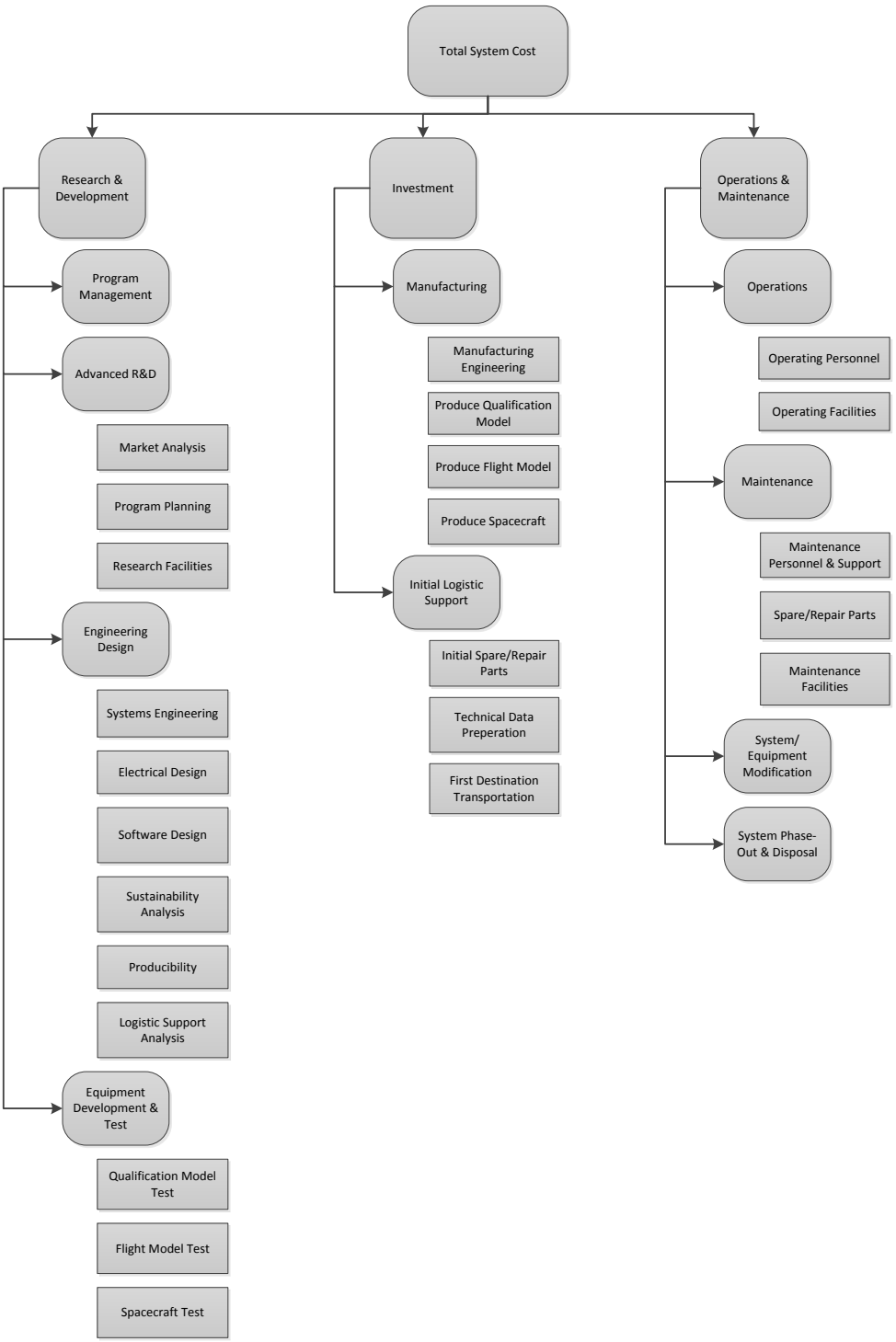

Figure 5.2: Cost Breakdown Structure (CBS) [19]

6. Payload Selection

This chapter entails the selection of the instruments used to measure the atmospheric properties, drag signal, and gas-surface interactions with the assigned accuracy and frequency. The mass spectrometer is discussed in Section 6.1. The wind and temperature spectrometer is briefly touched upon in Section 6.2. The surface temperature sensors are discussed in Section 6.3. The accelerometer instrument is presented in Section 6.4. Regarding positioning, the GPS receiver and laser retro-reflector are discussed in Section 6.5. For the analysis of gas-surface interactions, an overview of the basic reflectometer and its applied modifications are given in Section 6.6. Finally the instrument for the secondary mission is selected in Section 6.7.

6.1. Mass Spectrometer

A mass spectrometer is required to determine the composition and density of the atmosphere segment that the satellite will fly through. In a free molecular flow, atomic oxygen and helium particles impact the surface of the satellite. The mass spectrometer will provide data on the amount of particles that move through the device, including the type of particles and their velocity. One point of concern, applicable to periods of high solar activity, is that ionised particles have a chance to pass undetected through the apparatus if it is not properly configured. Provided that a mass spectrometer first ionises the particles by shooting an electron beam at them, it is probable that already ionised particles will remain unaffected. The energy required to change the composition of ionised particles is much higher than that provided by the electron beam, thus they remain unaffected and mix with the particles that are ionised by the instrument.

Already existing models of the atmosphere show the presence of hydrogen, nitrogen, oxygen, helium, and ionised oxygen. In order to get meaningful results, especially when examining the difference between ionised and non-ionised particles, a more advanced version of the basic mass spectrometer configuration is needed.

6.1.1. Iterative approach

In the previous report (mid-term report) of this project a number of flight-proven instruments were investigated, the goal lying in matching the MIRALOS spectrometry requirements to the specifications of the instrument examined. The approach was iterated for each considered product. These will only be presented here shortly, more information is available in the mid-term report [1].

The Neutral Gas and Ion Mass Spectrometer (NGIMS) is a quadrupole mass spectrometer currently in use by the Mars Atmosphere and Volatile Evolution (MAVEN) space probe. It is based on the Galileo probe mass spectrometer , the Pioneer Venus Orbiter Neutral Mass Spectrometer (ONMS), the Cassini INMS, and the CONTOUR NGIMS. The instrument has two operational modes, one to minimise gas-surface interactions by sampling the gaseous species (open source), and one applying ram density enhancement in an enclosed chamber to provide higher accuracy and sensitivity (closed source) [20]. Considered modifications for the instrument were to tweak the size of the detection plate. By doing this it is possible to allow for the detection of hydrogen (not originally possible) and reduce the top limit of the detection range. The detection can effectively be limited to 32 atomic mass units, corresponding to molecular oxygen.

The Ion Neutral Mass Spectrometer (INMS) originated from the NGIMS used on Comet Rendezvous Asteroid Flyby (CRAF), a (cancelled) mission developed in parallel to the Cassini mission. The INMS also operates in two different modes (open and closed source) [14]. The instrument is found to be able to perform measurements on the atmospheric composition for particle densities of $\geq 5 \cdot 10^4$ cm^{-3} for non-reactive neutrals (like helium) in closed source neutral mode and $\geq 2 \cdot 10^5$ cm^{-3} for reactive neutrals (like atomic oxygen) in open source neutral mode. This limits the altitude at which the satellite can retrieve useful data. Using the NRLMLSISE-00 atmospheric model, corrected for long-term atmosphere changes as described in Section 2.4, the density-altitude relationships were determined [21]. The application of the INMS was thus limited to an altitude of ≤ 600 km for oxygen measurements and ≤ 1000 km for helium measurements at a solar minimum, applicable at the start of the mission in 2020.

The Rosetta Orbiter Spectrometer for Ion and Neutral Analysis (ROSINA) mass spectrometer equipped on the Rosetta orbiter (launched in 2004) is split into three complementary sensors. It includes a Double Focusing Mass Spectrometer (DFMS), a Reflectron Time-of-Flight (RTOF) sensor, and a Commet Pressure Sensor (COPS). The DFMS has a gas mode and an ion mode, which analyse gas and measure ions respectively using a quadrupole mass spectrometer. These two modes also apply to the RTOF, however the latter uses a time-of-flight technique for the mass analysis [22]. Finally, COPS incorporates two sensors that are dedicated to the calculation of the total density and radial flow of particles.

6.1.2. Innovative approach

There are several options when considering innovative undertakings in mass spectrometry. A flight-proven instrument can always be selected, but such an instrument is usually designed for a specific space mission, for specific mission requirements, as presented in the earlier examples. A different approach is to think "outside of the box" and come up with a unique solution to the unique

problem that the MIRALOS satellite has to face. In this section different instrument configurations are presented. A trade-off is carried out to determine the most effective option.

Back to the basics
Mass spectrometry is done through the use of mass analysers. There are several types of analysers, each with their own advantages and limitations, as presented in Table 6.1 [23].

Table 6.1: Mass analysers

Mass Analyser	Mass spectrometer	Advantages	Limitations
Scanning	Magnetic sector	- High reproducibility, resolution, sensitivity, dynamic range - Best quantitative performance	- Cannot use a pulsed ionisation method - Large size, high cost
	Quadrupole	- Good reproducibility - Low-energy collision-induced dissociations - Small size, low cost	- Cannot use a pulsed ionisation method - Limited resolution - Mass discrimination
Time-of-Flight	Reflectron	- Fastest analyser - Can be used with a pulsed ionisation method - Highest mass detection range	- Limited dynamic range - Requires a pulsed ionisation method or ion beam switching
Trapped Ion	Cyclotron	- Highest resolution - Can be used with a pulsed ionisation method - Non-destructive ion detection	- Limited dynamic range - Measurements affected by space charge and ion-molecule reactions - Quality of mass spectrum dependent on excitation, trapping, and detection conditions
	Quadrupole Ion Trap	- High sensitivity - Compact instrument	- Poor quantitation, dynamic range - Measurements affected by space charge and ion-molecule reactions

Examining the information provided in Table 6.1, the limitations of the quadrupole ion trap make it unsuitable for this mission, and its benefits are also provided by other instruments. The cyclotron's non-destructive ion detection property is interesting if for example a second mass spectrometer was to be placed aft to do the same type of measurements. However the fact that the measurements are affected by space charge and ion-molecule reactions, make the instrument ineffective for this mission's environment. The three options left are the magnetic sector, quadrupole, and reflectron mass spectrometer. The limited dynamic range of the reflectron might be a problem; this implying that the resulting mass spectrum is not representative of the particle concentration of the atmosphere. A proper dynamic range may provide useful information on atmospheric properties such as wind vectors and neutral temperature values. The selected mass spectrometer can preferably also be used more effectively than just to determine the composition of the atmosphere.

As a first step, the selected mass spectrometer needs to be capable of providing detection measurements for both neutral and ion particles, with a satisfactory resolving power. Several flight-proven instruments have been found to do this through the use of two different operational modes for the particle source. An open source examines neutral and ionised particles of wall-reactive species (by minimizing gas-surface interactions). A closed source examines non wall reactive neutral species [24].

A point of concern is the aberration experienced by scanning magnetic sectors. The phenomenon is due to the varying energy, thus velocity, of the incoming particles. In order to improve the resolution of such an instrument an electric sector is added prior to the magnetic sector (the segment also referred to as a "velocity selector"). However doing such results in now biased measurements; only selected particles are detected. That is not the case for the reflectron and quadrupole spectrometers, these spectrometers selecting the particles based on their intrinsic property of mass and charge.

Ideally, the selected mass analyser can not only measure the composition of the atmosphere, but also wind and temperature. The reflectron and quadrupole mass spectrometers are not effective for such applications, despite being favorable for composition measurements. Nonetheless it is both theoretically and practically possible to do this type of compiled measurement using an electric and magnetic sector combination, as exemplified by existing flight-proven instruments. By combining applications, a Neutral Mass Spectrometer (NMS) can function as a WTS, as done in the DANDE mission [25]. Similarly, an Ion Mass Spectrometer (IMS) can function as an an Ion Drift and temperature Spectrometer (IDTS). Neutral density is inferred from these measurements.

Result
The compiled instrument should have a measurement capability befitting the atmospheric conditions that MIRALOS operates in. Ideally the instrument should operate well within its operational limits. The range and resolution of the measurements are two important quantities that will define the instrument's technical specifications. The parameters of interest for each component of the sensor are presented in Table 6.2. The parameters are supported by the technical wrap-up of the SWATS sensor, a flight-proven instrument incorporated in several LEO and CubeSat missions. Instrument-wise, the spectrometer of MIRALOS needs to operate in the same way as the SWATS, and also give the same output. The product uses a reflectron with two operating modes for composition measurements, and a energy selector-backed magnetic sector for the neutral wind, ion drift, and temperature measurements [26].

Table 6.2: Wind and Temperature Spectrometer specifications

Instrument	Parameter	Range	Resolution
NMS	Composition	$10^3 - 10^{10}$ cm^{-3}	< 3%
WTS	Density	$10^3 - 10^{10}$ cm^{-3}	< 3%
	Wind	+/- 2000 m/s	16 m/s
	Temperature	1000 – 4000 K	< 1%
IMS	Composition	$10^3 - 10^7$ cm^{-3}	< 3%
IDTS	Density	$10^3 - 10^7$ cm^{-3}	< 3%
	Drift	+/- 2000 m/s	16 m/s
	Temperature	1000 – 4000 K	< 1%

The above values are representative of the values that MIRALOS wants to achieve. By configuring the flight-proven instrument to meet the current mission requirements, a modified version can be employed to carry out the respective measurements in-situ, at the required altitudes.

Interestingly enough, the SWATS sensor is capable of carrying these measurements with minimal mass, power, and volume requirements, thus making it an attractive option to use. However, if modifying this compact sensor is found to be too complex (or even necessary), a combination of two instrument packages can be used. In more detail, the IMS/IMS can stand as a single instrument with two operating modes, and the WTS/IDTS as another. Their technical specifications should still meet the operational range required to be used at the defined operational altitudes, as well as a satisfactory resolution.

The last considered modification concerns the placement of an additional instrument on the opposite side of the spacecraft. In other words, two SWATS-like sensors will be used, one in ram direction, and one at the rear of the spacecraft. In this configuration one of the instruments will always be facing in the flight direction even when the propulsion system is active, and measurements can continue during the several week orbit changing maneuver. The same electronics will be used by both instruments.

6.2. Atmospheric Temperature and Wind Spectrometers

The temperature of the atmosphere is one of the parameters that needs to be determined as accurately as possible to meet the requirements of the mission. In addition to that, gaining insight on the neutral winds experienced by the satellite also allows to improve the measurements in-situ. Both temperature and wind are generally determined by the same instrument, abbreviated as WTS.

6.2.1. WTS Selection

For the selection of a wind and temperature spectrometer, a number of criteria were defined and a trade-off was presented in the Mid-term report [1]. As supported in the discussion for the mass spectrometer selection, an instrument that can carry out both composition and wind and temperature measurements is most effective for this mission. As a result, the SWATS sensor is used as a reference for the type of instrument configuration that will be used on MIRALOS. More information is given in Section 6.1.2.

6.3. Surface Temperature Sensor

The satellite instruments need to incorporate temperature sensors that will measure the temperature at the instrument's heat sink. If the temperature reaches, or possibly surpasses the operational limits of the instrument, a thermal control system will be used to bring the excess (or lack of) heat under control. Temperature sensors are also placed on the surfaces of the satellite. These measurements are important to determine the accommodation coefficient α.

6.4. Accelerometer

The accelerometer is used to measure all non-gravitational forces on the spacecraft. In order to choose an accelerometer for the MIRALOS mission, the required level of accuracy was used as a basis. Typical non-gravitational accelerations on a LEO spacecraft can be found in Table 6.3.

Table 6.3: Expected values of non-gravitational accelerations in LEO [27]

Acceleration origin	**Acceleration magnitude [m/s^2]**
Atmospheric drag	$1 \cdot 10^{-4}$ to $1 \cdot 10^{-9}$
DSRP (Differential Solar Radiation Pressure)	$2.9 \cdot 10^{-8}$
Albedo	$1 \cdot 10^{-8}$ to $1 \cdot 10^{-9}$
Reflected infrared radiation	$4 \cdot 10^{-9}$

Following from the requirements and accuracy of the considered flight-proven instruments presented in the Mid-Term Report [1], the SuperSTAR accelerometer was initially chosen for the mission. STAR stands for "Space Three-axis Accelerometer for Research mission"; it is able to measure the whole range of expected accelerations, and to achieve the precision needed. The SuperSTAR is an upgraded version of the STAR accelerometer, which is itself an upgraded version of the ASTRE. The upgrades are mainly related to the electronics, thus various important characteristics were estimated by looking at ASTRE and STAR. However, after end user input it was decided an even more accurate accelerometer should be used. This removes constraints on other systems and orbit choice, and increases the accuracy of the measurements and the flexibility of the entire mission. Because of the seemingly unusable differential accelerometer of GOCE, the latter using six different accelerometers each of a higher accuracy than the SuperSTAR accelerometer to measure differential accelerations, the option was discarded on the basis of lack of detailed information on the separate accelerometers. Another alternative was considered in this final report. The accelerometer selection was effectively shifted to the dedicated instrument that will be used onboard the GRACE-FO satellite [28], planned for launch in August 2017. Onera predicts the first Proto-Flight models of this nameless accelerometer to be finished by November 2015, and the first engineering model was built in June 2014 [29]. The design of this accelerometer is based heavily on its ASTRE/STAR/SuperSTAR heritage, and will feature the advanced thermal control used in GOCE and will even include core thermal sensors to enable on-ground characterisation of bias and scale-factor. This instrument meets all the accuracy and precision requirements of MIRALOS. Since not all specifications are available at the moment of writing, the missing data is extrapolated from ASTRE and STAR, combined with thermal control.

The GRACE-FO accelerometer poses new requirements on internal temperature (thermal control) and required power. The requirements flowing from the chosen accelerometer design can be found in Appendix A. The mass and size for the total accelerometer package is based on the data of the instrument combined with estimations for the data of the ICU and the thermal control package, including the thermal housing.

Mass Trim Assembly

The GRACE-FO instrument needs to be in the CoG of the spacecraft, with an extrapolated precision of 50 µm in all directions [30]. It is assumed that the CoG and the Center of Mass coincide. Before launch the whole spacecraft will be precisely balanced, as described in Section 5.2.7. During the mission a change in CoG might result from moving parts in instruments, propellant usage and even micrometeorite impacts. To maintain this CoG precision, the deviation from the accelerometer center needs to be measured. Since this is a difficult task to perform in orbit, multiple different approaches are taken. The first approach, a nodding calibration maneuver, is described in Section 8.3.2. A second method is an algorithm based on batch estimation theory, which is described in [31]. Both methods were used on GRACE, and both are depicted in figure Figure 6.1, where the blue line shows the algorithm and the red dots the calibration maneuver. After the CoG shift is determined, a Center of Mass Trim Assembly (CMT)

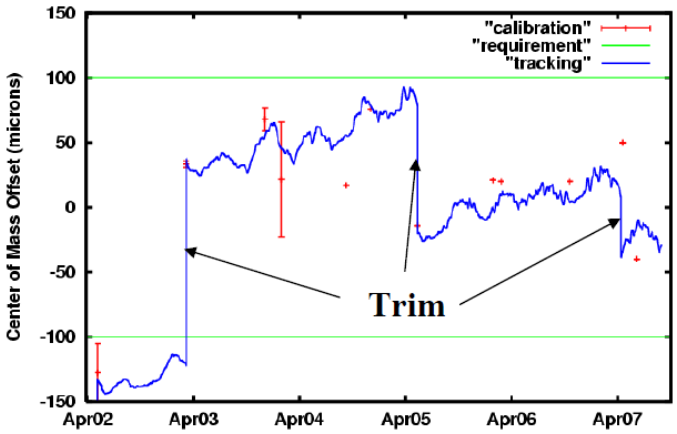

Figure 6.1: GRACE-A Calibration and Tracking [32]

will be used to correct this shift. An adapted version of the original CMT used in the GRACE mission will be used. This trim assembly was custom made for GRACE, with a step size of 10 µm or less over a total range of ± 2 mm in each axis [30]. The effect of a mass trim operation is visible in figure Figure 6.1, denoted by "Trim". For redundancy, six mass trim mechanisms will

be used in MIRALOS, each pair 90 degrees offset from the other.

During the lowest orbit of the mission, there will be multiple drag compensation thruster burns per day, as detailed in Chapter 4. The frequency of these burns inhibits the spacecraft from performing calibration maneuvers during their duration. During each burn, about a gram of xenon propellant will be used. It is calculated using equation Equation (6.1) that the shift in CoG caused by one gram of propellant use will be 0.656 µm, causing calibration need every 76 thruster burns. Between calibrations, the tracking algorithm will provide sufficient CoG data.

$$\frac{\delta mass}{totalmass} \cdot \delta m = \frac{0.001}{457} \cdot 0.3 = 6.56 \cdot 10^{-7} = 0.656\,\mu\text{m} \tag{6.1}$$

6.5. Orbit Determination Instruments

To connect the scientific measurements to a specific location and time in orbit, the location of the spacecraft needs to be known at the time of measurement. This information is also needed for attitude control as presented in Chapter 8. It can also be used to validate the accelerometer data and to determine the accelerometer bias drift. To precisely determine the location of the spacecraft at any given moment, a Global Positioning System (GPS) sensor and a LRR will be incorporated into the spacecraft design.

6.5.1. GPS Receiver

The GPS receiver chosen for this mission is the JPL Turbo Rogue Receiver-2. This receiver is readily available and has flown (in adapted form) in multiple space missions such as CHAMP (TSRS-2/BlackJack) [33], SAC-C (GOLPE) [34], and JASON-2 (GPSP) [35]. The Turbo Rogue has a position accuracy of 2 cm, can receive both L1 and L2 frequencies, and has added features such as measuring the ionospheric electron content, atmospheric soundings permitting the derivation of atmospheric vertical profiles of density, pressure, temperature (of water vapor), and ionospheric electron density profiles (through ”refractive occultation monitoring”) [36]. The choke ring antenna (type of omni-antenna) of the GPS is used for the precise orbit determination, and will be mounted zenith pointing. The GPS is also equipped with a helix antenna used for the occultation monitoring, which points in flight direction. In addition a patch antenna positioned next to the choke ring and helix antenna is included for redundancy and attitude determination, as described in Section 5.2.2.

6.5.2. Laser Retro-Reflector

A LRR will be used to accurately determine the distance between the spacecraft and a laser ranging ground station. The design of the LRR is based on the LRR used in CHAMP [37]. The instrument has also been proven in-flight on GRACE and SWARM [38]. The design requires a flat plate pointing nadir, this is accounted for in the design of MIRALOS Section 5.2.1. The accuracy provided by the LRR is in the $1-2$ cm range for a single laser shot, but accuracy can be dramatically increased (to a millimeter level) by using two-color laser ranging [36]. The latter is an experimental technique, but it is important to point out that it refers to an activity carried out on ground. The technique used changes nothing to the actual design of the instrument. The LRR will be used to calibrate the GPS receiver, and will additionally determine accelerometer bias drift.

6.6. Reflectometer

A requirement for the MIRALOS mission is that it should provide in-situ measurements of the angular distribution of re-emitted and reflected air particles [39]. These measurements combined with measurements regarding the accommodation coefficient have not yet been performed on a satellite mission. Doing so will greatly increase the understanding of the gas-surface interactions regarding satellite aerodynamics.
One example of a mission that operated an instrument to measure the above mentioned angular distribution was the Space Shuttle mission ‘STS-8’ [6]. This instrument, called an Atomic Oxygen Reflectometer, is the only instrument found that conducts angular distribution measurements in-flight.

History and Theory

The reflectometer was used as an experiment on the Space Shuttle mission ‘STS-8’ in 1983. It measured the angular distribution of impacting atomic oxygen atoms on an inclined surface. The lay-out of the instrument is depicted in Figure 6.2. The STS-8 mission lasted for just over 6 days in LEO at approximately 350 km altitude.
The reflectometer is a circular tube encased in an aluminium housing. The tube is coated in a thin layer of silver which reacts with atomic oxygen in the following way:

$$2Ag + O \rightarrow Ag_2O \tag{6.2}$$

The change in optical density of the silver film is then inspected to determine the location of the impact areas and to which degree they have been exposed to the atomic oxygen [40].
An influencing factor to the angular distribution is the adsorption of atomic oxygen on the inclined surface, which changes the accommodation factor, as described in Chapter 2.

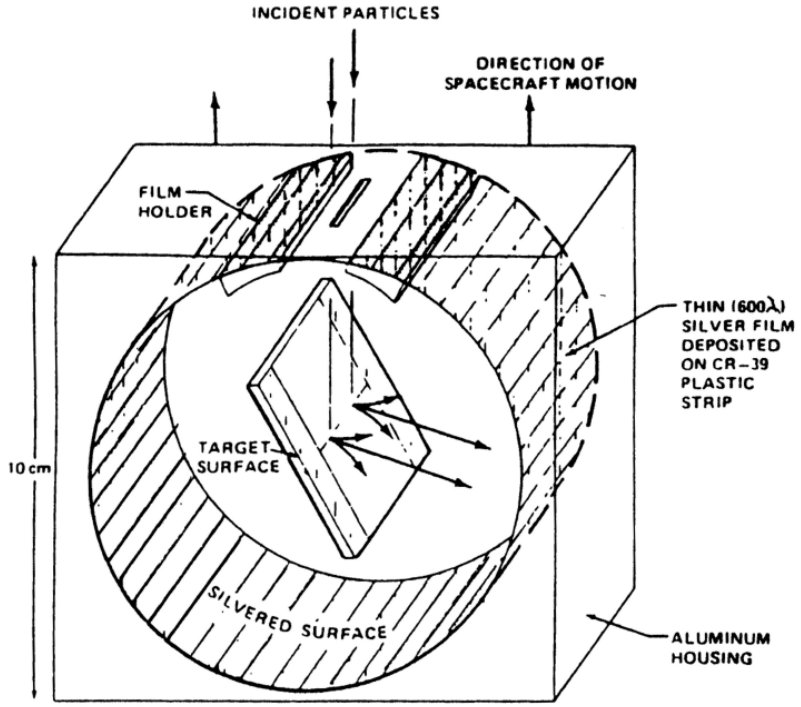

Figure 6.2: Atomic Oxygen Reflectometer as flown on NASA Shuttle Flight 'STS-8' [6]

Compatibility Issues

The layout of the reflectometer is displayed in Figure 6.2. This reflectometer however is designed for a different mission, and therefore not suitable for the MIRALOS mission without making adjustments.

Helium is a noble gas and therefore does not react with most substances. Since the angular distribution determination is also desired for helium atoms this presents a significant problem. Another issue arises with regard to the recovery of the silver film after the experiment. The reflectometer that flew on the Space Shuttle re-entered the atmosphere after the mission; it was therefore possible to examine the film on Earth. Placing a re-entry module on our spacecraft would be very complicated and introduce extra costs. Also, the film is permanently etched by the chemical reaction of the oxygen and silver and will therefore not be reusable for multiple angle measurements.

These issues have to be fixed to make the MIRALOS mission viable. Some adjustments and recommendations for the reflectometer are made in the next section.

Adjustments and Recommendations

In this section some adjusted designs are presented with recommendations regarding the development.

Examining the problem of helium not being reactive, a significant adjustment must be made to the design of the reflectometer to overcome this hurdle. A possible adjustment might be deduced from mass spectrometry theory. Mass spectrometers use metal boxes to detect impacting ionised particles. The impacting particles are positively charged and will therefore pick up an electron from the metal box which generates a small current that can be amplified to detect the impact [41]. This method also implies that the particles entering the reflectometer must be ionised, and a vacuum pump must be installed to remove particles after detection. A schematic representation of this setup is shown in Figure 6.3. To achieve the required range of incident angles, an electric motor would also be required to control the impact surface. There are two main limitations to this redesign. The first stands with respect to the probability that particles that ricochet of the detection plates may interfere with the path of incoming particles. The second, correctable limitation, is that the ionised helium particles might lose their electron to the impacting surface, thus recovering their neutral charge, thus becoming undetectable just prior to detection. Such limitation can be overcome by selecting an adequate non-reactive material for the impact plate.

If helium were to be neglected in the angular distribution measurements, the issue of having to observe the results of the experiment would still be present. Additionally, the permanent chemical reaction prohibits the observation of angular distributions for multiple incidence angles. A solution to this problem could be the use of a silver film roll and a sensor to investigate the film. This setup is illustrated in Figure 6.4. To achieve the required range of incident angles for the impact plate an electric motor would be required to control the impact surface in addition to the motors required to wind and unwind the silver film rolls.

Figure 6.4 shows the concept, but in reality the film system will be needed at both sides of the circle to cover the entire inside surface. This is needed because of the possible diffuse re-emission of particles (see Chapter 2). The requirements state that the angular distribution needs to be measured for incidence angles of 0 to 90 degrees with a minimum resolution of 5 degrees, which

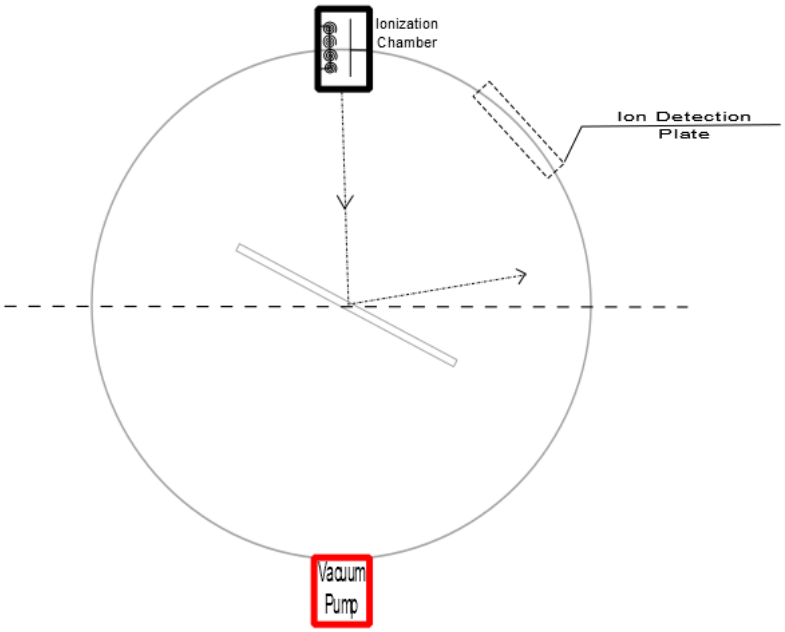

Figure 6.3: Possible Reflectometer concept using Mass Spectrometry elements

means a minimum of 19 measurements. This would require a certain amount of film, calculated as follows :

$$L = 2\pi(0.05) = 0.3142\text{m} \quad \rightarrow \quad L_{tot,min} = 19L = 5.969\text{m} \tag{6.3}$$

Where L is the circumference of the circle, which is the length of film needed for each measurement. And $L_{tot,min}$ is the minimum length of film needed for the entire measurement series, which is already large.
Another issue to keep in mind is that the length of the internal cylinder should be large enough that the diffusely re-emitted particles will still impact on the silver film if re-emitted towards the side.

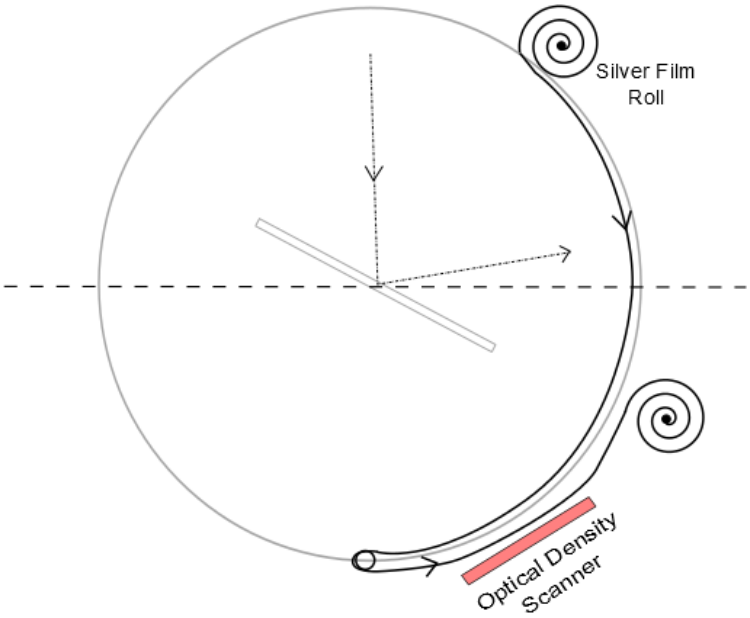

Figure 6.4: Possible Reflectometer concept using a silver film roll

Another recommendation would be to allow the testing of a variety of impact materials. In an area that is heavily dominated by oxygen, the impact plate will most likely be covered entirely by atomic oxygen. However, in higher regions it might be interesting to investigate the dependence of the angular distribution with regard to different materials. Typical spacecraft materials that might be tested are: aluminium, gold, kapton, mylar, composites, and solar cell materials. A setup as depicted in Figure 6.5 will be considered. A version with two or three materials configured in a plate and a triangle respectively might be considered as well.

Another possibility is to use multiple reflectometers. An important issue to consider is whether using different materials does in fact provide insight to the measurements. Specifically, it is known that a layer of atomic oxygen will form on the impacting surface after a defined amount of time, rendering the measurements independent of the underlying material. This might not be the case for higher altitudes where helium is the dominant species. If the material dependence is found to be negligible, this setup might be an unnecessary expense and a single plate of alumina (Al_2O_3) can be used, since it does not react to atomic oxygen. The hypothesis of the presented in this paragraph shall be tested.
Another possible design might use a heated impact plate to investigate the dependence of the surface temperature to the angular distribution.
Research into these design options is required prior to launch. The goal is to raise the technology readiness level (TRL), since none of these concepts have been proven in-flight.

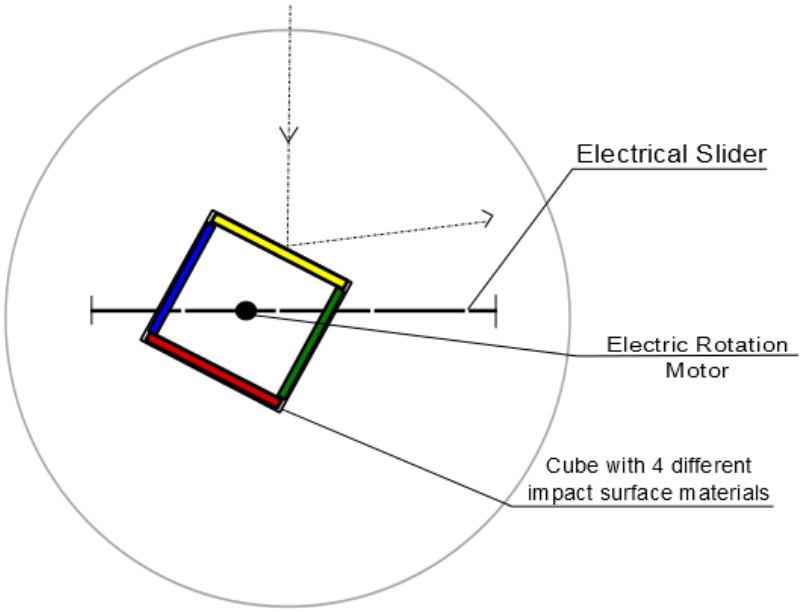

Figure 6.5: Possible Reflectometer concept using multiple impact surfaces with different materials

Trade-Off

The silver-film design has already been proven in-flight, however no re-entry vehicles will be included on MIRALOS, thus the need to redesign the reflectometer instrument. From the above stated design alterations, the Mass Spectrometry-inspired reflectometer is chosen. The reason for this selection is that an angular distribution is desired for helium particles as well. Since helium is not reactive, a reactive film will not yield any data, however ionising the particles before their entry in the instrument chamber allows for proper detection at the sights of impact. Redesigning the instrument to use winding and rewinding film roll presents a number of limitations to the measurements. The most important limitation is that once all the film roll has been used the instrument will become unusable in turn. In case more measurements need to be carried out before ending the mission, such a situation is not desirable.
An important consideration is to incorporate two reflectometers in the final payload, one using the ionising-approach, the other equipped with the film roll. These will be abbreviated as Reflectometer (RFM) 1 and RFM 2 respectively. Such a proposition would allow to account for redundancy, to increase the technology readiness level of the instrument, and to provide insight of the result with respect to the selected design. Two drafts of the design are presented in Appendix B.

Analysis

Having decided upon the reflectometer configuration, its technical performance is defined by its physical properties and the properties of the incoming flow. The material properties of the impacting surface were discussed in the earlier subsections for each redesign respectively. The required length of the film roll presented in Figure 6.4 was measured based on the original reflectometer dimensions. The volume of the entire apparatus was 10 cm x 10 cm x 10 cm, thus a radius of 5 cm for the surrounding foil. It is important however to also consider the size of the orifice from which the particles will enter the instrument. This size is defined in cross-area. For a defined cross-area, an estimate for the incident number of particles is calculated based on an assumed Maxwellian distribution of velocities [42]

$$f = \frac{\rho_\infty}{m(2\pi RT_\infty)^{\frac{3}{2}}} \exp\left(-\frac{(v_{m_1} - Usin(\theta))^2 + (v_{m_2} + Ucos(\theta))^2 + v_{m_3}^2}{2RT}\right) \tag{6.4}$$

The velocity differentials are dependent on the reference frame used, the subscripts (1,2,3) represent components in three perpendicular directions; m_1 is defined normal to the slit opening, m_2 is defined parallel to the opening upwards, m_3 is determined using the right-hand rule. The angle θ is the angle between the gas velocity U and the m_1 axis. All the other parameters are calculated using the available scientific payload. The number of incident particles is defined as

$$N_i = \int_{-\infty}^{\infty}\int_{-\infty}^{\infty}\int_{0}^{\infty} v_{m_1} f dv_{m_1} dv_{m_2} dv_{m_3} dA \tag{6.5}$$

Solving the integrals results in a holistic equation dependent on the area element dA

$$\Rightarrow N_i = \frac{\rho}{m}\sqrt{\frac{RT}{2\pi}}[\exp(-(Ssin(\theta))^2) + \sqrt{\pi}((Ssin(\theta))[1 + erf(Ssin(\theta))]dA \tag{6.6}$$

Using the instrument measurements in concert with a defined cross-area value gives an estimate for N_i. Regarding the detection of the particles reflected and re-emitted by the impacting surface, such discussion is dependent on the design used. For the film-roll-equipped design, the optical density scanner will register pictures of a given length of contaminated segment at a time, such a process is rather straight-forward. Considering the ionised-particle approach however, ion (or microchannel) plate detectors need to be positioned around the impacting surface, replacing the silver foil. Microchannel Plate Detector (MCP)s are constituted of a extensive number of channels that carry out the job of detecting the ions [43]. Configuring a series of channels to serve the purpose of the reflectometer is possible in a manufacturing sense [44]. Given that the original silver foil arcs around the impacting surface, such a shape would be optimal for the assembled MCP. A channel has a typical diameter of 15 micrometers, thus to cover the entire foil would require

$$\frac{w}{d} = \frac{10\text{ cm}}{15\mu m} = 6667\text{ channels} \tag{6.7}$$

$$\frac{L}{d} = \frac{31.4\text{ cm}}{15\mu m} = 20934\text{ channels} \tag{6.8}$$

where w is the width of the foil, L is the length of the perimeter of the foil. The above calculations assume an adjacent positioning of the channels, resulting in maximal accuracy. The accuracy requirement for this instrument is defined to be 2% of 5 degrees, i.e. 0.1 degrees. In other words, an MCP channel should be placed at every

$$\frac{31.4cm}{\frac{360\text{ deg}}{0.1\text{ deg}}} = 0.87\,\mu\text{m} \tag{6.9}$$

for a total of 3600 channels in lengthwise direction. In the width-wise direction, the radius of the instrument is equal to half the width, thus the number of channels has to be doubled to cover the whole width

$$\frac{5cm}{\frac{45\text{ deg}}{0.1\text{ deg}}} = 0.01\,\mu\text{m} \tag{6.10}$$

for a total of $2x450$ channels. Thus to meet the accuracy requirement, the instrument should be equipped with a MCP comprising $3.240.000$ channels.

6.7. UV Horizon Sounder

For the benefit of the secondary mission objectives a UV horizon sounder will be implemented in addition to the primary scientific payload. This instrument looks at the horizon and distills the spectral lines of the thermosphere, getting information on the temperature and composition of a defined range of altitudes. The principle is that these measurements can effectively be combined with the in-situ measurements of MIRALOS. By using the horizon sounder to provide data on the thermosphere altitudes from 100 to 300 km, together with the in-situ measurements at higher altitude, the array of data and deduced information is expanded substantially.

There are a number of exemplary instruments for this type of task. Flight-proven instruments include the GUVI instrument, part of the Thermosphere Ionosphere Mesosphere Energetics and Dynamics (TIMED) satellite, and the Extreme Ultraviolet Imager (EUV) and Far Ultraviolet Imager (FUV) instruments, part of the Ionospheric Connection Explorer (ICON) and Imager for Magnetopause-to-Aurora Global Exploration (IMAGE) satellites. The missions, orbit type, study goals, and dedicated instruments are presented in Table 6.4.

With respect to orbit type, the TIMED and ICON missions stand substantially closer to MIRALOS than IMAGE does. The imaging instrument equipped on TIMED is a modified version of the Special Sensor Ultraviolet Spectrographic Imager (SSUSI) instrument used in a number of meteorological satellite programs; these were placed in sun-synchronous orbit at an altitude of 850km [45].

Table 6.4: Horizon sounder secondary mission instruments

Mission	Orbit type	Study	Dedicated instrument
TIMED	LEO, circular orbit (625km), E=0, i= 74.1°	Global response of the Earth's magneto-sphere to changes in the solar wind	GUVI
ICON	LEO, circular orbit (550km), E=0, i= 27°	Boundary between the atmosphere and space	EUV/FUV
IMAGE	Highly elliptical polar orbit (perigee 1000km), E=0.75	Dynamics of the Mesosphere and Lower Thermosphere	EUV/FUV

With respect to instrument functionality, the three missions aim to obtain similar ranges of measurements, their discrepancy lying at them examining a different range of the mass spectrum.
The actual design and operation of such an instrument is a complex process, hence no re-designs will be examined within the bounds of this exercise. The measurements and orbit of the GUVI instrument and respective TIMED mission match the one of MIRALOS the closest, thus is selected as the best option.

To maintain stability of centre of gravity of the spacecraft, the rotating mirror of GUVI will be configured to remain fixed, in other words no rotation motor will be incorporated in its design. This introduces requirements of pointing accuracy, further discussed in Chapter 8. The instrument will provide information about the inspected thermosphere layer a defined time period before the satellite passes above that segment. The imager's measurements will be combined with the in-situ measurements of MIRALOS, expanding the array of accumulated data on temperature and composition.

7. Propulsion Subsystem

Originally the spacecraft design did not include a propulsion system as it was thought not to be necessary. Later in the design process this decision was re-evaluated and it was found that a propulsion system actually is very beneficial and for some mission objectives even necessary as there is a high risk that the objective requirements cannot be met without. This is described in more detail in Section 3.2.

This chapter deals with the selection and design of a propulsion system, starting with a trade off on the type of propulsion system, followed by a selection of an actual available system. This system is then redesigned to be integrated into the satellite and its properties are described and analysed in further detail.

7.1. Propulsion System Trade-off

This section deals with the selection of the propulsion system type. The type is being outlined into further detail and an available system is selected.

7.1.1. Propulsion Type Trade-off

The main tasks of the propulsion system for MIRALOS are to perform multiple altitude changes in LEO of between $50 - 200$ km per change and to perform orbit maintenance at low Earth orbit altitude (drag compensation). From the initial orbit profile a very initial Delta-V budget of 500 m/s was estimated, which is used throughout this chapter as an initial value for the selection and design of the system. All required manoeuvres require about 250 m/s, this initial value was doubled to take into account reserves, fuel for the secondary mission and controlled reentry. From the mission profile (see Section 4.1, Figure 4.1) it becomes evident that the propulsion system needs to be capable of performing multiple cycles and in between those cycles it has a longer non-operational time. This already rules out multiple concepts such as hybrid and solid rocket propulsion. The time for an orbit change should also be less than a month in order to not unnecessarily increase the mission time. This last requirement rules out very low thrust systems such as solar sails.

For the type of propulsion system in total five types were considered in the trade-off, which are the types that are generally used for satellite propulsion systems (apogee motors): cold gas, liquid (bi- and mono-propellant) and electric propulsion (ion and hall thruster). The five different systems are compared with each other in a trade-off containing five different criteria (mass, flexibility, spacecraft integration, reliability and power required). The weights of the criteria are outlined in the column width (the wider the column the higher the weight). Each criterion is briefly explained in the following list.

- **Mass Performance**: Mass performance includes both the systems estimated dry mass and the propellant mass required for the initially estimated $\Delta V = 500$ m/s. Note that it does not include a possible weight increase of related subsystems due to the specific choice (e.g. the weight increase of the electrical subsystem in case electric propulsion is chosen).
- **Flexibility**: The flexibility includes the number of possible cycles, total burn time and the time it would require to fly a manoeuvre (dependent on the thrust of the system). The mission should measure in different areas of the thermosphere to achieve certain spreads of composition, pressure and density. As those areas are highly dependent on solar and geo-magnetic activity, which are very hard to predict, flexibility is of great importance. It might be required to change the initial orbit profiles during flight, therefore flexibility is given a very high weight in this trade off.
- **Spacecraft Integration**: This criterion deals with the complexity of the integration of the propulsion subsystem into the satellite. Aspects such as additional, large, very complex or dangerous components required to operate the propulsion system are thought of. It is also of importance whether other subsystems will be influenced by the choice of the type of propulsion system.
- **Reliability**: Reliability concerns the fact whether there are very complex and critical components involved such as pumps, valves and power control units. As a temporary or even a permanent failure of the system does not have catastrophic consequences the weight of this criteria is reasonably low.
- **Power Consumption**: As the satellite will only feature body mounted solar cells, which are very limited as the outer surface of the spacecraft is limited, power consumption is an important criterion in this trade-off. Everything above 780 W is said to be not acceptable, because that would require more than 95% of the spacecraft side area to be covered with solar cells leaving not enough space for body-mounted instruments and thruster.

The five systems are compared within the trade-off table (see Table 7.1) considering the five criteria described above. Each of them is given a grade in the form of a colour: Green means excellent, blue reasonable, yellow marginal and red unacceptable. The

Table 7.1: Trade Off table for the propulsion system type (Column width represents importance of the criteria).

Tradeoff Criteria/ System	Mass Performance	Flexibility	Spacecraft Integration	Reliability	Power Consumption
Cold Gas	Unacceptable ($m_{total} \approx 365kg$, $m_{prop} \approx 355kg$) Red	Reasonable (Very high no. of cycles, long lifetime, very low thrust so extremely long burn times) Blue	Marginal(req. very big tank, thermally efficient) Yellow	Very reliable (simple, hardly no moving parts) Green	Negligible ($P_{in} = 0$ - 10W) Green
Liquid - Bipropellant	Reasonable ($m_{total} \approx 75kg$, $m_{prop} \approx 60kg$) Blue	Reasonable (Limited but sufficient no. of cycles and burn time, high thrust so fast maneuvers possible) Blue	Marginal (req. complex feed system, propellant usually toxic, difficult to keep cog. In same position) Yellow	Acceptable (more complex, req. complex feedsystem) Blue	Negligible ($P_{in} = 0$ - 10W) Green
Liquid - Monopropellant	Reasonable ($m_{total} \approx 96kg$, $m_{prop} \approx 86kg$) Yellow	Unacceptable (Too Limited burn time and cycles, medium to high thrust) Red	Reasonable (propellant allways toxic) Blue	Very reliable (simple, hardly no moving parts) Green	Negligible ($P_{in} = 0$ - 10W) Green
Electric – Ion Thruster	Excellent ($m_{total} \approx 30kg$, $m_{prop} \approx 6kg$) Green	Excellent (Good Life time, very high number of cycles and low but reasonable thrust) Green	Marginal (produces quite some heat, req. complex feed system and extra solar cells) Yellow	Less reliable (new technology, little higher failure rates, backup req. if mission critical) Blue	High ($P_{in} \geq 0.4kW$) Blue
Electric – Hall Thruster	Excellent ($m_{total} \approx 34kg$, $m_{prop} \approx 10kg$) Green	Excellent (Good Life time, very high number of cycles and low but reasonable thrust) Green	Marginal (produces quite some heat, req. complex feed system and extra solar cells) Yellow	Less reliable (new technology, higher failure rates, backup req. if mission critical) Yellow	Unacceptable High ($P_{in} \geq 1.5kW$) Red

reason for the grade is briefly explained in the table. The values and facts given in the table originate from first order estimates and facts that can be found in literature or from data sheets for representative existing systems [18, 46–49].

From the table it becomes immediately visible that three of the five systems are not feasible: The cold gas system would require enormous amounts of propellant. A mono-propulsion system has the problem that it uses a catalyst grid for ignition which degrades each time upon ignition, limiting such a system to approximately ten duty cycles. Hall thrusters with a reasonable thrust range would require too much power.

The only two systems left to choose are liquid bi-propellant and ion thrusters. Both of them score quite high in most criteria apart from spacecraft integration where they only score marginal. The results for both systems are roughly equal; however, ion thrusters perform excellent in flexibility, which has a very high weight in this trade off, therefore they are chosen for the MIRALOS propulsion system.

7.1.2. Basic Principles of Ion Thrusters

Before continuing with a selection of an available ion thruster one should have a closer look at the working principles of such thruster types. This is done in the following section. Note that the facts stated in this section mainly originate from Martinez-Sanchez [48] and Goebel [49].

All ion thrusters have a similar general working principle and can be divided into three sections.

The propellant, nowadays xenon (historically also mercury and caesium) gets ionised in a plasma generator. The ions then get accelerated by an acceleration grid and afterwards the electrons are resupplied to the ion to neutralise it and to keep the spacecraft and thruster from getting a net charge (see Figure 7.1). The way the propellant gets ionised is however substantially different for each type. For the DC discharge and Kaufman type ion thruster (the latter is actually a subclass of the first one), a small constant amount of xenon is injected through the hollow cathode where the electrons get extracted. Those electrons then flow into the discharge chamber, in which the main flow of xenon gets injected. The electrons in the chamber then try to flow from the cathode to the anode and on their way hit and ionise the Xe in the discharge chamber. The ionised Xe^+ gets accelerated by the acceleration grid outwards of the thruster producing thrust. The anode in the discharge chamber is usually protected by a magnetic field; that way the electrons are kept in the discharge chamber for a longer time. This is illustrated in Figure 7.1. The Kaufman type thrusters do not use a fixed magnetic field but a variable one which is generated by solenoids. This way the fast electrons that did not ionise any neutral xenon yet cannot reach the anode. This increases the overall efficiency of the thruster. Varying the magnetic field strength also allows to throttle the thruster over a wide thrust range. A schematic layout of a Kaufman type ion thruster can be found in Figure 7.3b.

In a radio-frequency thruster the propellant gets directly injected into the main chamber. The electrons are extracted by means of radio-frequency waves (typically around 10 MHz), which are produced by a set of antennas mounted to the side of the cylindrical

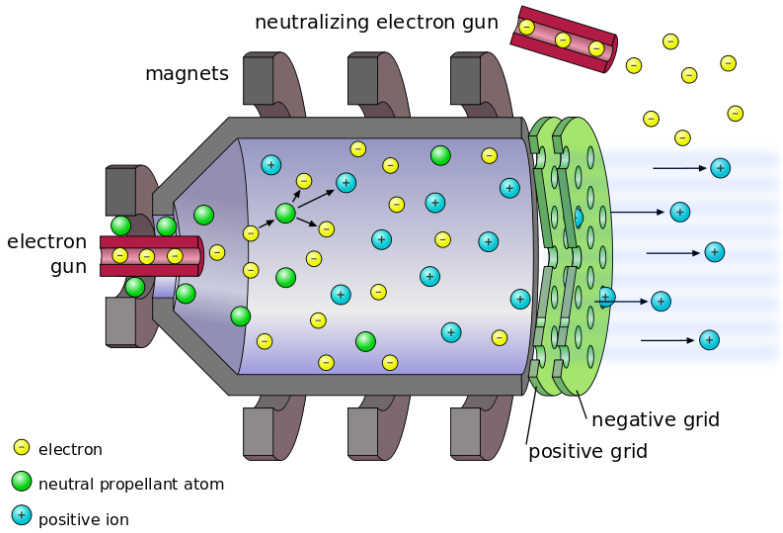

Figure 7.1: Basic working principle of a DC-discharge (electron bombardment) ion thruster. Image-credit: O. Räisänen [50]

or conical chamber (those antennas have to be protected by the means of an insulator). The electrons extracted in that way then ionise the main part of the propellant, like in a DC discharge thruster. Furthermore, acceleration of the Xe^+ ions and later neutralisation is also similar and is illustrated in Figure 7.1. Those type of thrusters have the advantage that they require a less complex power supply (less weight and less power consumption); the main reason for that is that they do not require very high DC voltages. This effect can also be seen in the later trade-off (see Table 7.2). One disadvantage however is that the antennas that produce the radio frequencies waves need to be shielded off and insulated from the rest of the chamber and this insulation degrades which limits the life time of such thrusters.

Next to the two classes described above (DC-discharge and radio-frequency) there also exists a third class, the microwave ion thrusters. This class is not described in further detail in this report as this class does not play a role in the trade-off below.

7.1.3. Ion Propulsion System Trade-off

Now that ion propulsion has been chosen as a general concept for the MIRALOS mission, the propulsion system is now worked out in further detail: an available propulsion system is chosen in an additional trade off.

Based on initial estimation it was found that in order to meet the requirement that the spacecraft should be able to perform a orbit change in max. a month around 15 to 20 mN of thrust are required. This restriction together with the absolute maximum power consumption of 780 W limits the selection to four available ion thrusters [49]: The Hughes-L3 13 cm XIPS DC-discharge ion thruster, the QinetiQ T5 Kaufman ion thruster [51–54], the Astrium RIT-10 radio frequency ion thruster [55] and the Mitsubishi ETS-8 Kaufman Ion Thruster [56]. The first thruster (Hughes-L3 13 cm XIPS) is not included in the trade-off as there is a substantial lack of available information compared to the other three systems. All thrusters considered in the trade-off are flight proven hardware: The T5 has flown on ARTEMIS and GOCE, the RIT-10 has flown on EURECA and ARTEMIS and the ETS-8 has flown on a Japanese built experimental communication satellite carrying the same name.

The actual trade-off is performed in vary similar manner as above in Section 7.1.1. The only major difference is the criteria are slightly different. The criterion Spacecraft Integration was excluded as all three systems do not differ in that, so it would add nothing to the trade-off. In addition, the reliability criterion was excluded as more specific reliability statistics are available and all three thrusters are flight proven hardware. Furthermore, an efficiency criterion was added to compare both fuel efficiency (Isp) and electric efficiency (how much heat is generated). The trade-off can be found in Table 7.2.

From the table (Table 7.2) it becomes clear that the Mitsubishi ETS-8 is not an option as its power consumption is way too high to be even marginally, already dismissing one of the three options. The winner of the the trade-off is the QintyiQ T5 Kaufman ion thruster. It scores excellent in three out of the four criteria and performs reasonable in the fourth criterion. It has an excellent power consumption, can be throttled over a very wide thrust range, is extremely accurate and allows for a very high number of cycles. It is only outperformed in terms of mass performance, where the Astrium RIT-10 is more than 10 kg lighter due to the reason that the radio-frequency thrusters are lighter in general (see Section 7.1.2).

7.2. MIRALOS Ion Propulsion System

In the previous section the QintyiQ T5 Kaufman ion thruster was chosen for the MIRALOS propulsion system. This section describes not only the thruster itself but the propulsion system as a whole, followed by a performance analysis. The MIRALOS

Table 7.2: Trade-off table for the ion propulsion system (column width represents importance). All relevant information can be found in [49, 51–56]

Tradeoff Criteria/ System	Mass Performance	Specific Power Consumption	Flexibility	Efficency
Quinetiq T5 Kaufman Thruster	Total: 28.75kg (Thruster 2.95kg, ECU 16.7kg, XFS 7.5kg, Tank 1.6kg) Blue	585W at nominal Thrust of 20mN Green	>8500 Cycles, Thrust Range 1 to 20mN (more or less Thrust is possible, but not certified), highly accurate Green	ISP of 3500s @ 20mN, Electric Efficiency 76.6% Green
EADS-Astrium RIT-10 Radiofrequency Thruster	Total: 17kg (Thruster 2.2kg, ECU 10.15kg, XFS 3.05kg, Tank 1.6kg) Green	570W at nominal Thrust of 15mN Blue	>6000 Cycles, Thrust Range N/A , Accuracy +/- 0.9% Blue	ISP of 3400s @ 15mN, Electric Efficiency 76.5% Green
Mitsubishi ETS-8 Kaufman Thruster	Estimated total: 50kg Yellow	880W at nominal Thrust of 20mN Red	>3000 Cycles, Thrust Range 20 to 25mN Yellow	ISP of 3200s @ 20mN, Electric Efficiency 78.9% Blue

ion propulsion system is a derived version of the propulsion system used on ESA's GOCE mission. More information about that can be found in [51–54].

7.2.1. System Description

The ion thruster itself is not the only component of the propulsion system. It requires additional support equipment such as power and control electronics, a xenon tank plus feed and flow regulating system. The system has an estimated weight of approx. 28.75 kg. A schematic layout of the whole system can be found below in Figure 7.2.

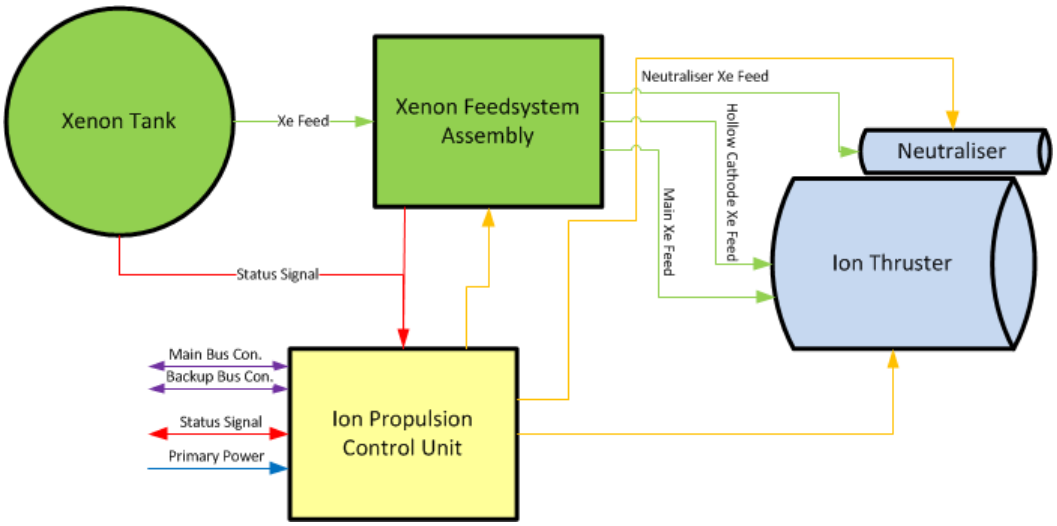

Figure 7.2: Layout of the MIRALOS Ion Propulsion System

The propulsion system consists of four major components: The ITP (the thruster including neutraliser and support/mounting equipment), the IPCU, which provides power to all the elements and controls the thruster, the XFA regulating the pressure and xenon flow rates to the different thruster elements. The last element is the xenon tank. Each component is described in further detail below.

Ion Thruster Package (ITP)

The main component of the ITP is the the actual QintyiQ T5 Kaufman ion thruster (see Figure 7.3a). The thruster weighs 2.95 kg and has the following dimensions: Ø190 mm x 242 mm (including mounting). The grid has a diameter of Ø100 mm [51]. The working principle of a Kaufman type ion thruster was already touched upon in Section 7.1.2, but can be nicely illustrated using Figure 7.3b.

A small component of the propellant gets fed through the hollow cathode where the electrons then get extracted and emitted into

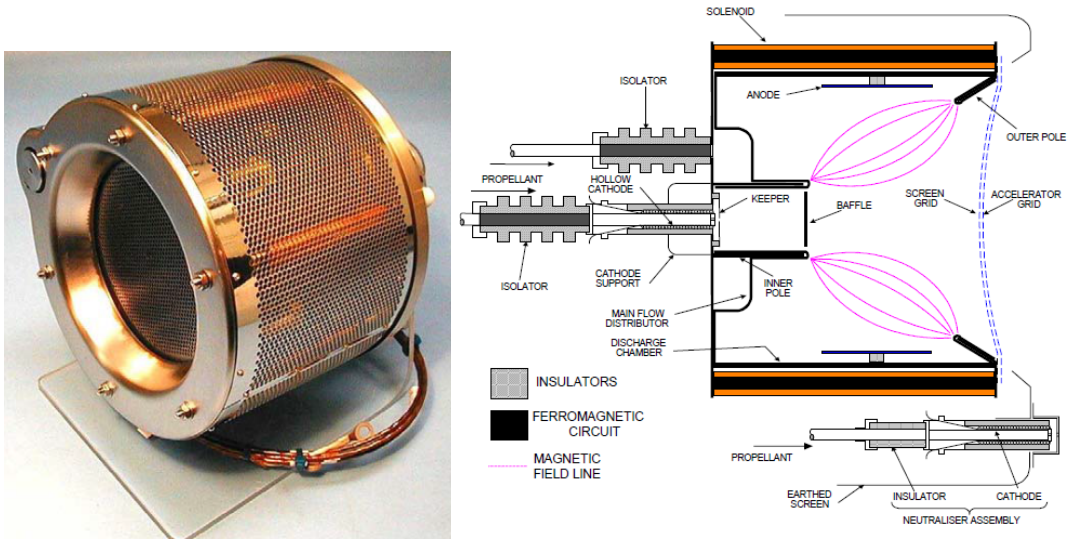

(a) Picture (b) Schematic Section View

Figure 7.3: The QinetiQ Ltd T5 Kaufman Type Ion Thruster [51]

the chamber; here they are accelerated towards the ring anode. On their way to the anode they hit the xenon and ionise it into Xe^+. The electrons, if at high speed (hence they have not hit/ionised anything), get diverted from the anode by the magnetic field (pink field lines), created by the solenoids. The Xe^+ gets repelled by the anode, is accelerated out of the thruster and through the acceleration grid. The adjustable magnetic field allows to decrease or increase the amount of xenon that gets ionised and thus produces any thrust. This allows to widely adjust the thrust range; however, using this method to decrease the thrust also leads to a decrease in Isp as part of the xenon will just be wasted since it is not ionised; hence this part does not produce thrust. Once there the Xe^+ gets resupplied with the electrons which were extracted earlier and emitted by another cathode (see bottom right of Figure 7.3b.
Performance characteristics of the system (the thruster in specific) can be be found in Section 7.2.2

Ion Propulsion Control Unit (IPCU)
The IPCU is responsible for supplying power in the correct form and magnitude to each component. It controls all functions of the ITP and XFA and communicates with central CDH systems. The electronics are all housed in one box (300 mm x 250 mm x 200 mm) weighing 16.7 kg [51]. The system has an electrical efficiency of at least 92%. It contains the following modules/functions:

- Control Electronics: provide control and interface with the bus and the XFA
- AC Inverter: converts spacecraft DC power to AC used for low voltage (LV) and high voltage (HV) supply
- Ion Beam Converter: converts spacecraft DC into HV DC for the hollow cathode
- LV Control and Supply: supplies LV to ITP and provides link to HV Control (auxiliary DC/DC LV supply for IPCU)
- HV Control and Supply: supplies HV to ITP and provides link to LV Control (auxiliary DC/DC HV supply for IPCU)

Xenon Feedsystem Assembly (XFA)
The task of the XFA is to convert, regulate and control pressure and mass flow from the tank at 125 - 5 bar to the operational pressure of the ITP, which is 2.5 bar. As seen from Figure 7.3b the ITP requires three different inputs, which are all at different mass flow rates. The hollow cathode and neutraliser cathode operate at a constant mass flow of 0.11 and 0.041 mg/s. The main supply operates at a variable flow rate, varying with thrust/power settings ranging from 0.01 to 0.63 mg/s [51]. This is done by a sequence of pressure regulators (PR) ,pressure transducers (LPT), gas purifier (GP), flow restrictor (FR), sensors(FS) and control valves (FCV) and isolation valves (IV). The schematics can be found below in Figure 7.4. The system weighs approximatly 7.5 kg and has the following dimensions: 150 mm x 200 mm x 350 mm.

Xenon Tank
Based on the initial estimations made above, 6 kg of xenon fuel is required. The initial tank pressure is 125 bar. As there was no available tank with those specifications a custom tank is designed.

The tank is assumed to be spherical and made from Aluminium 7075-T6 (σ_{yield} = 360 MPa and ρ = 2800 kg/m^3) and using a safety factor of 1.5. Xenon is usually stored in spacecraft in super-critical state reaching a high density of ρ = 1500 kg/m^3 at about room temperature [48]. From this, one can deduce the propellant and tank volume; 20% of the propellant volume should be added to the tank volume to account for sloshing and possible expansion [18]. This results in a effective volume of 27.3 l and a total volume of 32.7 l. Using the formula for thin-walled stress in a spherical pressure vessel $\sigma = \frac{pr}{2t}$, one can find a required

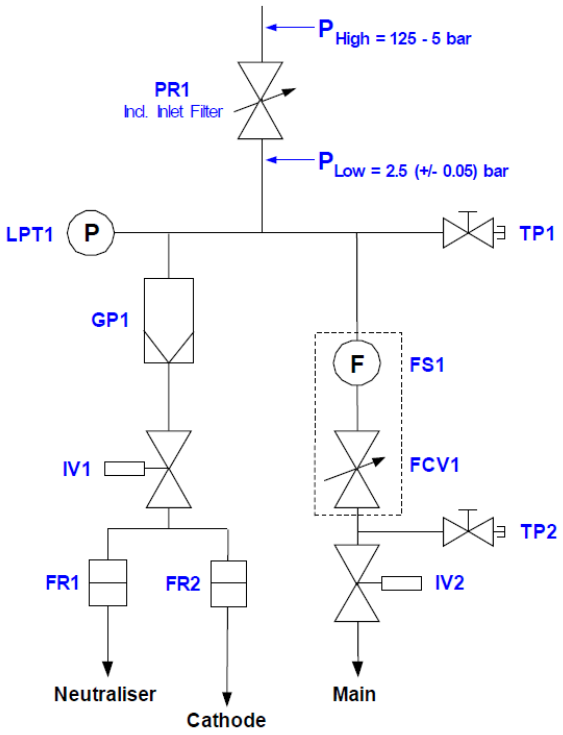

Figure 7.4: Layout of the Xenon Feedsystem Assembly [51]

wall thickness of 4 mm. When adding another 50% (to account for mounting, support, valves etc.) this results in a tank empty mass of 1.62 kg.

Considerations on Reliability

Previous missions using ion propulsion have almost always been using multiple ion thrusters. This was either because the ion propulsion was used for North-South station keeping of GEO satellites or because a propulsion system was absolutely mission critical as in the case of JAXA's Hayabusa or ESA's GOCE mission. For the latter reason, including multiple thrusters was mainly done because ion thruster were not considered as reliable as a chemical propulsion system.

So one could ask the question why this mission uses only one ion thruster. First of all, in the case of MIRALOS the propulsion is not absolutely mission critical; a failure would still allow us to fulfill large parts of the primary mission objectives. The only point in the mission where it is quite critical is during the primary mission phase at 350 km as there it is needed for extensive drag compensation. Would the propulsion system fail at that altitude during the scheduled time one would have approximately two to three months to restart the ion propulsion system otherwise the satellite will have decayed and burned up in the atmosphere. However, at that time already the major part of the primary mission phase would be completed, therefore for now it is assumed that a second system for redundancy is not required. If analysis at a later stage of the project shows that a redundant system is required, all components (ITP, ICPU and XFA) can be duplicated to form a redundant system (as done in ESA,s GOCE mission). Apart from additional cost, this would only result in marginal weight increase of approximately 28 kg.

7.2.2. System Performance

The final section of this chapter briefly describes the performance of mainly the T5 ion thruster, but also of the ion propulsion system in general. The system is capable of producing producing 0 - 20 mN of thrust with a power input ranging from 55-585 W (see Figure 7.5a). As already explained earlier the system is capable of producing more thrust. Experiments described in [53, 54] have shown that thrust levels of more than 30 mN are possible. However, operating at such high thrust ranges results in a faster degradation of the acceleration grid, hence a faster loss of performance over lifetime and a shorter lifetime in general.

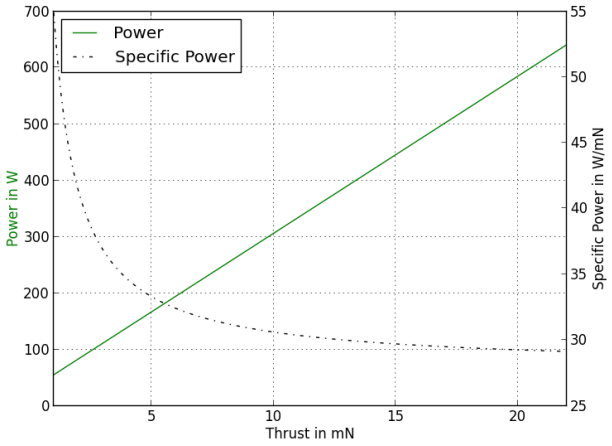

(a) Power Consumption

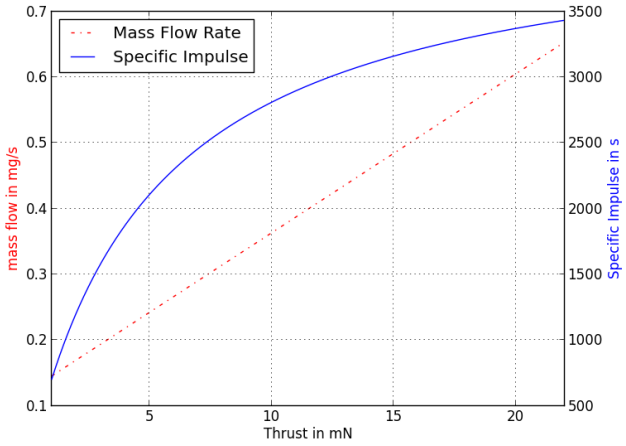

(b) Fuel Consumption

Figure 7.5: Performance estimation of the T5 Kaufman Ion Thruster (based on [52–54])

As seen in Figure 7.5b the xenon mass flow rate also varies linearly with thrust/power input resulting in a logarithmic increase in specific impulse with respect to thrust. Hence the flying at higher thrust levels is more efficient in terms of fuel, but not in terms of power usage. When looking at the performance values shown in Figures 7.5a and 7.5b one should keep in mind that those decrease over the lifetime of such a thruster due to degradation of the acceleration grid.

8. Attitude Determination & Control

This chapter outlines the design for the ADCS. This subsystem's purpose is to control and retrieve the orientation of the spacecraft. It is an essential subsystem for payload operations, ground station communication, and orbit control. First the ADCS requirements will be introduced in Section 8.1. Secondly, the sensor selection is done in Section 8.2. Thirdly, an actuator assembly is designed in Section 8.3. An overview of the final ADCS design is provided in Section 8.4.

8.1. ADCS Requirements

There are multiple requirements and restrictions that the ADCS design must comply to. These originate both from top-level requirements and from the requirements imposed by the other subsystems. These restrictions are displayed in Table A.1.

8.2. Attitude Determination

Based on the requirements introduced in Section 8.1, several options exist for orientation sensing. These are displayed in Table 8.1.

In this table, the different sensing options are assessed for criteria in which they differ significantly and which are of importance to the design process. The options that differ significantly and/or conflict with the mission success have a high weight. Properties that vary significantly dependent on the sensor design have a low weight. Mass and power consumption have large effects on the remaining design process, but can be accounted for, and hence receive a medium weight.
It can be concluded that no single option exists to account for attitude sensing. External sensors are required for calibration of internal sensors, if applied. Furthermore, external sensors either do not meet the accuracy requirements (magnetometers, GPS) or have a limited operating range (earth, star and sun sensors). Additionally, sensors that meet the accuracy requirement have a limited FOV and require knowledge on the approximate orientation. Hence, two sets of sensors are implemented: coarse sensors are selected in Section 8.2.1 and fine attitude sensors are selected in Section 8.2.2.

8.2.1. Coarse Attitude Sensing

For coarse attitude sensing, the accuracy restriction of Table 8.1 is eliminated and both magnetometers and GPS appear feasible options. Also Earth sensors or coarse sun sensors can be applied.

Table 8.1: ADCS Sensor Trade Off (Green: exceeds requirements. Yellow: meets requirements. Orange: may or may not meet requirements. Red: does not meet requirements.)

Criteria (Weight)	**Magneto-meter**	**Earth Sensor**	**Star Sensor**	**Sun Sensor**	**GPS**	**Gyroscope**
Source	[18, 57, 58]	[18, 59–61]	[18, 36, 62–74]	[18, 75–78]	[18, 64, 79, 80]	[18, 81, 82]
Sensor Type (-)	External	External	External	External	External	Internal
Impact on Measurements (High)	Requires calibration	Outer geometry affected	Outer geometry affected	Outer geometry affected	Outer geometry affected	Moving parts
Time to Settle (Medium)	Low	Medium	Medium	Medium	Low	Low
Accuracy (High)	$0.1 - 3^\circ$	$0.05 - 1^\circ$	$0.0003 - 0.01^\circ$	$0.005 - 3^\circ$	$0.25 - 0.50^\circ$	0.001° (excl. drift)
Mass (Medium)	$0.1 - 1.2$ kg	$0.5 - 4$ kg	$1 - 5$ kg	$0.1 - 2.0$ kg	< 0.5 kg	$0.1 - 15$ kg
Output Frequency (Medium)	$1 - 150$ Hz	$1 - 20$ Hz	$5 - 10$ Hz	$5 - 10$ Hz	50 Hz	400 Hz
Operating Range (High)	Always	In shadow	In shadow	In sun	Always	If calibrated
Lifetime (Low)	> 6 years	$5 - 7$ years	$7 - 10$ years	> 10 years	> 8 years	Critical
Power (Medium)	< 1 W	$0.3 - 10$ W	$5 - 20$ W	$0 - 3$ W	< 2 W	$1 - 200$ W

Earth Sensors

From Table 8.1 it can be seen that Earth sensors perform worse than other coarse sensors in most aspects. Furthermore, it is found that CHAllenging Minisatellite Payload (CHAMP) and Gravity Recovery and Climate Experiment (GRACE) use coarse Earth and Sun sensors, however, very limited information has been found on the ADCS sensors that are carried by these missions. As these sensors rely on the viewing of light sources, disadvantages exist related to blockage of view and operation under spin. As coarse attitude sensors are relatively small contributors to the spacecraft design, a limited amount of resources are spent on

research. Furthermore, Earth sensors are not required by other subsystems and are in conclusion not chosen for coarse attitude sensing [18, 59–61, 83–86].

Magnetometer

Magnetorquers will be applied for attitude control, as will be explained in Section 8.3. For this, the magnitude and direction of the Earth's magnetic field is required. While this can be obtained by combining GPS data with a model, it is usually more accurate to measure it in-situ using magnetometers. Additionally, magnetometers have proven to be reliable light-weight coarse attitude sensors and consume little power [18]. For attitude sensing, the magnetometer measures the magnetic field and compares it to a model of the electromagnetic field of the Earth. However, due to internal magnetic interference of components, the magnetometer is often mounted away from the satellite on a connecting boom [36, 87]. As the design process is still preliminary, it is very difficult to obtain a reliable estimation of the internal dipole moment of the spacecraft.

To measure the internal dipole moment in-situ, components can be disabled one-by-one and the changes in the magnetic field should be measured. However, several components such as the power system and the onboard computer are always required to run for spacecraft operation, and hence this procedure has limited success. Therefore attitude knowledge using GPS signals can additionally be used for comparison and validation, as explained in the next paragraph. The Gravity field and steady-state Ocean Circulation Explorer (GOCE) mission however has proven to be able to coarsely determine spacecraft orientation using a surface-mounted magnetometer [88].
Two 3-axis sensing magnetometers are implemented into the spacecraft, of which one is used for redundancy. Magnetometers have low weight and power consumption, thus no extensive trade-off is performed. The Honeywell HMR2300r is selected for its lack of moving parts, high accuracy, renowned manufacturer, and high reliability [57]. The properties of the magnetometer are displayed in Table 8.2.

GPS

For additional coarse attitude sensing, GPS signals can be used, yielding results with RMS errors smaller than 1° [18, 80]. As GPS antennae are already implemented and applied for location determination, it is weight and cost efficient to also use the instrument for attitude sensing by adding additional antennae [80].
Two GPS antennae are added, of which one is for redundancy. This adds additional redundancy to the GPS system used to determine the satellite's location. Lastly, since the concept of attitude sensing using GPS signals is still not widely applied, proving the concept is an interesting secondary mission objective.

8.2.2. Fine Attitude Sensing

Looking at Table 8.1, star sensors, sun sensors, and gyroscopes, meet the accuracy desired for fine attitude sensing. However, all of these are limited in operation.

Gyroscopes

The main advantage of gyroscopes is that, when calibrated, it is always able to provide attitude knowledge with a very high frequency. The great disadvantage with gyroscopes is the introduction of vibrations in the satellite, which introduces uncertainty in the measurements of the accelerometer. Furthermore, gyroscopes are limited in the sense of operation due to their need for calibration, thereby still requiring sun or star sensors. The high-accuracy gyroscopes have a high power consumption (approximately 30 W) and a weight contribution that is several times higher than more accurate star sensors. [18, 81, 82, 89–93]. Concluding, no gyroscopes are implemented.

Star Sensors

Star sensors currently provide the most accurate attitude sensing available with low usage of resources. Many flight-proven designs exist with varying performance. While most star trackers meet the accuracy requirement, more accurate sensing is beneficial to the quality of data. While researching literature, one sensor assembly stood out: the Micro Advanced Stellar Compass (μASC) developed by the Technical University of Denmark [73], containing 2 Optical Heads (OH) and 2 Electrical Units (EU). Its properties are displayed in Table 8.3.

Table 8.2: Honeywell HMR2300r Specifications [57]

Criteria	Value
Accuracy	$0.12 - 0.50$ %
Range	$2 \cdot 10^{-4}$ G
Mass	40.0 g
Power	0.45 W
Operating Temperature	-40 to $+50^\circ$ C
Lifetime	6 yrs

Table 8.3: μASC Specifications [73, 74, 94]

Criteria	Value
Accuracy	$2''$ (RMS)
FOV	N.A.
Mass	425 g
Power	3.70 W
Operating Temperature	-70 to $+20^\circ$ C
Lifetime	> 30 yrs

The µASC is an updated version of the original ASC, applied in missions such as CHAMP, GRACE, and GOCE [94]. More accurate solutions exist such as the Ball Aerospace's HAST, but these have a much higher weight and power consumption [95].
The main limitation of a star tracker is sun blinding. For this reason, two sets of µASC are implemented. Additionally, requirements are put on the thermal control subsystem due its limited operation conditions.

Sun Sensors
The main attitude sensing will be done by star trackers, which are always available due to the presence of 4 OHs. However, sun sensors are added for redundancy to allow operation during blinding if OHs fail. Due to their high accuracy, low weight and power consumption sun sensors are often applied as redundant attitude sensors in current spacecraft design [18]. The limitation to these sensors is that the sun is required to be in view, which is exactly when the sun sensors are put into operation, replacing the star tracker OHs temporarily. Hence, 4 sun sensors are placed each next to an OH of the µASC.
Many options are available. However, two lightweight sun sensors stand out with an accuracy close to the state of the art, developed by TNO [18, 75–78]. These two sensors are updated versions of the Digital Sun Sensor (DSS) applied in the GOCE mission [88]. Their properties are displayed in Table 8.4 and traded-off. Accuracy is important as this sensor backs up the highly accurate µASC during operation. The allowed operating temperature is important since the sensor will always operate in sunlight. Lifetime is considered essential, as the sun sensors are meant for redundancy. FOV is not essential as coarse sensors are available, and mass and power do not differ significantly.

Table 8.4: Digital Sun Sensor (DSS) Revision Specifications (Green: exceeds requirements. Yellow: meets requirements. Orange: may or may not meet requirements.)

Criteria	**Weight**	**MiniDSS** [76]	**µDSS** [77]
Accuracy	Medium	$0.007°$ (RMS)	$0.010°$ (RMS)
FOV	Low	$102°$x$102°$	$50°$x$50°$
Mass	Low	72 g	N.A. (< 100 g)
Power	Low	0.065 W	0.021 W
Operating Temperature	Medium	-15 to $+50°$ C	-40 to $+80°$ C
Lifetime	High	N.A.	N.A.

Both are very similar in specifications and it is unclear to what degree they are related. Due to the larger allowed temperature range the µDSS is selected. Expected is that the mass does not significantly deviate from that of the mini-DSS. The lifetime is expected to be similar to other sun sensors, which is in the order of 10 years [18]. This will be verified by consulting TNO in a later stage.

8.3. Attitude Control

For actuator design, first an estimation is made of the disturbance torques in Section 8.3.1. Secondly, a decision is made on the actuator system in Section 8.3.2.

8.3.1. Estimation of Disturbance Torques

The spacecraft undergoes several disturbance torques throughout its orbit. Furthermore, due to a minimalistic eccentricity there are slight changes in attitude which are to be initiated through torques. These torques are sized for an extreme case at 300 km orbital altitude with eccentricity 0.01.

Gravity Gradient
The gravity gradient is the first disturbance torque on the spacecraft. With the extreme case of a difference in moment of inertia of $2 \cdot 10^2$ kg·m^2 and a $5°$ misalignment angle, a disturbance torque of $4 \cdot 10^{-5}$ N·m is experienced [18]. This difference in moment of inertia is an arbitrary large value, since very little information on the spacecraft properties are known at this point of the design. Hence, this disturbance torque will typically be several orders of magnitude smaller than predicted.

Internal Dipole Moment
Most satellites have an internal dipole moment due to electronics interference within the structure. This dipole moment interferes with the Earth's magnetic field lines in a similar way as magnetic torque rods do, and thereby create an undesired disturbance torque. This internal dipole moment is usually less than 20 A·m^2. This disturbance in the worst case scenario will be approximately $1 \cdot 10^{-3}$ N·m [18].

Atmospheric Drag
The maximum atmospheric drag experienced is measured using the atmospheric model tool described in Section 2.4 to be $2 \cdot 10^{-2}$ N at solar maximum over the winter pole. By allowing a maximum separation of the centre of pressure and centre of mass of 0.5 cm, and assuming a spacecraft mass of $3.5 \cdot 10^2$ kg, this yields a maximum drag disturbance torque of $1 \cdot 10^{-4}$ N·m [18]. The atmospheric drag signal will typically be multiple times smaller than predicted in this extreme case.

Varying Slew Rate

The spacecraft will rotate 360° every orbit. However, due to its very slight eccentric orbit, the slew rate slowly varies. The maximum angular rate to maintain the orbit pointing is $2 \cdot 10^{-8}$ rad/s^2. Even with a very high moment of inertia, the torque required will be several magnitudes smaller than the torques caused by other disturbances.

In the case all torques are applied under the same angle, a worst-case total disturbance torque of approximately $1 \cdot 10^{-3}$ N·m is experienced. However, if magnetorquers are used for attitude control, the internal dipole moment can be countered and this disturbance can be minimised. Hence, the total disturbance force is of the size of $1 \cdot 10^{-4}$ N·m. With a moment of inertia of approximately 500 kg·m^2, it would take $3 \cdot 10^3$ seconds (over half an orbit) for the attitude to drift more than 1° from its initial orientation. As the direction of the magnetic field changes depending on the location of the satellite, there is a 3-axis attitude control at least each half orbit. Thus, the maximum attitude drift will be 1°, and typically even several times smaller. Because of this, the ram surface area of the satellite will differ 0.1% from its initial value. If constant 3-axis attitude control is applied, a pointing accuracy of several orders of magnitude smaller can be achieved.

8.3.2. Actuator Selection

The different options for attitude control are displayed in Table 8.5. Firstly, the criteria consists of parameters that have important contributions to the design or performance of the ADCS. Also, properties that are significantly different between actuators are traded-off, such as momentum buildup. The significantly differing parameters heavily influencing the actuator performance have been given a high weight. The design complexity has been given a low weight, as it does not affect the final performance of the ADCS. The remaining criteria have been given a medium weight. An option for attitude control that is left out is to use Earth's gravity gradient, as the magnitude of force is too small to be considered.

Looking at the table, not a single option stands out. The requirement MIRALOS-SYS-T-SO-ADCS-8 readily eliminates the option

Table 8.5: ADCS Actuator Trade Off (Green: exceeds requirements. Yellow: meets requirements. Orange: may or may not meet requirements. Red: does not meet requirements.) [18, 82]

Criteria	Weight	CMG	Magnetic torquer	RW/MW	Cold Gas Thruster	Electric Thruster
Actuator Type	-	Internal	Internal	Internal	External	External
Performance Range	High	$25 - 500$ N·m	$1 - 4000$ A·m^2	$0.01 - 1$ N·m	< 5 N·m	< 5 N·m
Impact on Measurements	High	Vibrations, resonance	Magnetic interference	Vibrations, resonance	Disturbance force, mass flow	Disturbance force, mass flow
Momentum Buildup	Medium	Yes	No	Yes	No	No
Operating Range	High	Always	Orthogonal to Magnetic Field	Always	Always	Always
Operating limit	Medium	Actuator Lifetime	Actuator Lifetime	Actuator Lifetime	Amount of fuel	Power System/Actuator Lifetime
Mass	Medium	> 10 kg	$0.4 - 50$ kg	$2 - 20$ kg	$0.01 - 1$ kg (excl. fuel)	< 1 kg (excl. fuel)
Power	Medium	$90 - 150$ W	$0.6 - 16$ W	$10 - 100$ W	< 3 W	$14 - 300$ W
Complexity	Low	Moderate	Easy	Moderate	Moderate	Difficult

of Control Moment Gyroscopes (CMGs), Reaction Wheels (RWs), and Momentum Wheels (MWs). Additionally, these actuators build up momentum and therefore will require additional actuators. Furthermore, the torques introduced are larger than desired, and are therefore infeasible. From this, the following realistic options remain for attitude control:

- Constant 3-axis control using thrusters
- Constant 3-axis control using magnetometers and thrusters
- Periodic 3-axis control using magnetometers and allowing attitude drift

Thrusters

Examining the option that only (cold gas) thrusters are applied, a total required fuel mass larger than $1 \cdot 10^2$ kg is found ($I_{sp} = 70$ s) to be needed, sizing for solely the constant magnetic disturbance force. After consulting with the stakeholders, it was concluded that the maximum attitude drift of 1° predicted in Section 8.3.1 is sufficient. Therefore for the scientific operations magnetorquers suffice, and are more feasible than cold gas thrusters. Furthermore, electric thrusters put large requirements on the electrical power system and introduce significant complexity and reliability issues to the design, as was previously discussed in Chapter 7. No thrusters are used during the scientific operations of the mission.

However, thrusters are applied in order to meet the T-SO-ADCS-13 requirement for calibration of the mass-trim assembly as is done in the GRACE mission [87]. It is still unclear why GOCE does not use its magnetic torque rods for calibration, but it is

expected that similar problems would be encountered with the mission at hand. Possible reasons are the need for high angular rate for short duration, undesirable accelerometer behaviour due to the induced magnetic field or, alternatively, uncertainty in the torques induced by the magnetorquers. Due to a lack of information, it is assumed that a similar calibration procedure will be used for this satellite. Cold gas thrusters are used for their ease of spacecraft integration, cost, power consumption, reliability, and sustainability. The main disadvantage to not apply cold gas thrusters for permanent orbit control is the high fuel weight, as by Chapter 7. This disadvantage is minimal for calibration considerations, since little fuel is used in total as will be shown in the next paragraph.

Calibration occurs every two months throughout a 24 hours period, and consist of thrusters firing pseudo-random pulses of 10^{-3} N magnitude, similar to GOCE [96]. A total of 12 thrusters are implemented for complete attitude control without redundancy, as a single thruster failure has no severe consequences on performance [96, 97]. The accelerometer measures the linear acceleration due to changes in attitude and a misalignment between the centre of gravity and the centre of mass. The maximum misalignment is 50 µm as found in Section 6.4. The accuracy of the accelerometer is $1 \cdot 10^{-10}$. Thus, with a moment of inertia of 500 kg·m², a torque of $1 \cdot 10^{-3}$ N·m is required for the nodding manoeuvre. Placing thrusters at the outer ends of the satellite, this yields a required thrust of $0.67 - 0.91$ mN, depending on the axis ($I_{sp} = 60$ s). For calibration every 2 months a total maximum fuel mass of 4.8 kg is required. Taking into account 50% contingency for additional attitude control and more frequent calibration, a fuel mass of 7.2 kg is estimated.

Several options exist for the thruster. However as this design is still open for changes in the type of thrust employed, a conservative choice is taken. Properties of the Thruster Control Valve (TCV) are displayed in Table 8.6, which has a large range of operating thrust values [98, 99]. This component is also applied in GOCE. GN_2 is used for propellant due to its reliability, low cost, and storage tank requirements [100]. Benefits of other propellants with respect to weight are not significant, as the fuel mass is already low. *Note: the G in the chemical notations stands for Gaseous*

Table 8.6: MOOG Bradford TCV Specifications [98]

Criteria	Value
Thrust	100 µN-500mN
Propellant	GHe, GN_2, GXe, Dry Air
Mass	< 200 g
Operating Temperature	-40 to $+70^\circ$ C
Lifetime	N.A.

Table 8.7: ZARM MT70-2 Specifications [101]

Criteria	Value
No. Coils	1
Range	$0 - 70.0$ A·m^2
Mass	2.2 kg
Power	2.6 W
Operating Temperature	N.A.
Lifetime	> 10 yrs

The fuel tank is sized in a similar manner as for the orbit control system described in Chapter 7. Filling the tank up to 80% with GN_2, a spherical fuel tank with an inner radius of 0.291 m and a thickness of 0.013 m is found. The fuel has a density of 264 kg/m³ and is stored at a pressure of 280 bars. The tank is made from woven carbon fibre fabric with a yield strength of 450 MPa and a density of 1610 kg/m³. The tank weighs 11.4 kg.

Magnetic Torque Rods

Magnetic torque rods are theoretically able to operate for a very long time span, as it does not rely on an limited source of fuel. Furthermore, magnetorquers can be operated at different currents and thereby can induce torques of varying magnitude. Their power consumption is relatively low and their weight significantly less than the cold gas actuators. Furthermore, magnetic torque rods have a high reliability and are easy to implement in the design. GOCE has proven that highly accurate 3-axis attitude control is possible using solely magnetorquers [88]. However, due to internal magnetic interference, the magnetic actuators operate with limited accuracy.

Two operation modes are considered for the magnetorquer. One operation mode uses a current that induces a dipole moment of approximately the size of the internal dipole moment of 20 A·m² and in opposite direction. Furthermore, a coarser mode should be available that allows for coarse attitude control and quick attitude changes.

Not much information was found on space-proven magnetorquers. However, one renowned manufacturer of magnetic torque rods is ZARM Technik, which has also produced the magnetorquers for GOCE and GRACE [101]. Multiple models are available. Depending on the size of the internal dipole moment, the size of the rods should be decided. Due to its low power and mass requirements, the MT70-2 magnetic torque rod is selected. Its specifications are displayed in Table 8.7. The cold gas system will be used for detumbling as well, although the magnetorquers are mainly used.

Lighter or less power consuming magnetorquers have dipole moments of 30 A·m² or less, which may or may not be sufficient to compensate for the internal dipole moment. Furthermore, magnetorquers with higher dipole moments attribute to higher power consumption or mass and are not by definition more beneficial. For the maximum disturbance case, after each half orbit the attitude correction using magnetorquers will take less than $2 \cdot 10^2$ seconds. Furthermore, 90° attitude changes can take up to a quarter of an orbit from a non-drifting mode. As no additional requirements exist on the rate at which attitude changes should occur, the magnetometer configuration is sufficient.

A total of two sets of 3 magnetorquers each is implemented on the spacecraft for 3-axis attitude control, of which one set for redundancy. The sets of magnetorquers are positioned next to the mass-trim assembly separated from other important electric components. This is to minimise the electromagnetic interference occurring by the induced magnetic field.

8.4. Final Configuration

The final ADCS configuration is displayed in Table 8.8. The following operation modes are available: Science Mode (SM) for the instrument operations, Calibration Mode (CM) for the mass-trim assembly positioning and Stabilisation Mode (SB) mode for coarse attitude control after deployment or orbit changes. The explanation of the different modes is provided in Section 15.3.

Table 8.8: ADCS Configuration Summary ([1]Standard, [2]Backup)

Manufacturer	Product	Amount (+red.)	Mass [kg]	Power [W]	Operation Modes
TU Denmark	μASC	1 (+1)	0.85	3.70	SM[1], CM[1]
TNO	μDSS	2 (+2)	< 0.4	0.043	SM[2]
Honeywell	HMR2300r	1 (+1)	0.080	0.45	SB[1], SM[1]
JPL	TSRS-2 Antenna	1 (+1)	< 0.2	< 0.25	SB[2]
Zarm Technik	MT70-2	3 (+3)	13.2	$2.6 - 7.8$	SB[2], SM[1]
MOOG	TCV	12 (+0)	< 2.4	< 6	CM[1], SM[1]
-	GN_2 Fuel	(+50%)	7.2	0	CM[1], SM[1]
-	Fuel Tank	1 (+0)	11.4	0	All
Total	-	-	35.7	$6.8 - 14.6$	-

A few notes are made with respect to the ADCS design. First, the fuel required for the calibration of the mass-trim assembly is a very rough estimation. Since little information about this exact procedure is known, it is important to perform more research on this topic and decide on the frequency and protocol of these calibrations. This can be resolved by coming in contact with the designers of the ADCS for GOCE.
Secondly, research is to be performed regarding the magnetic interference between components within the satellite and its influence on attitude determination using the magnetometer. Also, the impact of the usage of magnetorquers must be assessed.
Thirdly, it is important to determine the reliability of the magnetorquers. Failure of these actuators will severely impact the mission success and result in preliminary mission termination.
Lastly, the design lifetime and reliability of the sun sensors should be assessed by consulting TNO.

9. Electrical Power Subsystem

The Electrical Power System (EPS) provides, stores, regulates and distributes electrical power to the payload instruments and spacecraft subsystems. The design of the EPS should maximise efficiency, safety, reliability while minimising mass, volume, thermal requirements and costs. This chapter will describe the design process of the EPS. First, in section Section 9.1 the general power requirements set by the spacecraft will be presented. In the second section a power source will be selected. The selected power source will be a solar photovoltaic system. For this system a solar cell trade-off will be performed in the third section, which is followed by a solar cell trade-off in Section 9.3. Section 9.4 will handle the battery trade-off. Finally, the selected EPS will be sized for the required spacecraft total power in Section 9.5.

9.1. General Spacecraft Power Requirements

Before starting with choosing a particular power source, requirements for the EPS have to be discovered. To do that, one first looks at the mission profile of the MIRALOS-mission.

During parts of its lifetime, the MIRALOS-satellite will be covered in the shadow of the Earth. Therefore the EPS should be able to provide power even when the only natural power source is not available: solar radiation. This consideration will have no effect on the solar independent power sources (e.g. RTG, nuclear reactor and fuel cells), for the solar dependent power sources (e.g. solar photovoltaic, solar thermal dynamic) this will create a need for a battery system. Orbital analysis pointed out that the maximum eclipse time during the mission lifetime will be 2220 seconds (see Figure 4.4 in Section 4.2.2). At that moment the altitude will be 350 km and the orbital period will be 5484 seconds. Also the possibility of a solar eclipse due to the moon was investigated, which happens rarely and has to be accounted for. This will be further elaborated on in Section 9.5.

The MIRALOS-mission has a design lifetime of six years. This is important for the degradation of the power system, because the required spacecraft power must be provided at all times, including at end of life. Therefore, the EPS must be sized for End-of-Life conditions. The degradation will be further elaborated on in Section 9.5.

Another important requirement can be set by the spacecraft propulsion system. In order to be able to perform a trade-off between the different power systems a coarse estimate of the required power has to be made. The choice for an electrical propulsion system can induce a large restriction on the power source. In fact, this choice actually has been made as is documented in Chapter 7. The electrical propulsion system needs 600 W of power on its own. Based on the power estimation from Section 5.3, the power of the other spacecraft subsystems sum up to a maximum value of 290 W. This is a conservative value, though the resulting power range of 660-980 W, i.e. including 10% contingency, will exclude already most of the power sources, as will be explained in the next section. A more detailed power budget will be used later in this chapter in Section 9.5.

9.2. Power Source Trade-off

With the basic constraints being set up in the previous section, it is now possible to perform a power source trade-off. Six different power sources are considered [102]:

- **Primary Battery** - A primary battery is a battery which cannot be recharged. The battery is used as the only power source and can only last for a couple of weeks. As this power source can only be used for missions with a short mission lifetime, it will not be further considered in this chapter, as the MIRALOS mission lifetime of six years will be a killer requirement.
- **Fuel Cell** - A fuel cell converts chemical energy into electricity. The difference with batteries is that fuel (e.g. hydrogen and oxygen) is used to constantly refill the fuel cell. The fuel cell capacity can be easily increased by providing more fuel. The fuel cell converts the chemical energy directly into electricity and therefore surpasses the low efficiency thermal-to-mechanical conversion resulting in a high efficiency of up to 80%. For space qualified fuel cells this efficiency drops to 10%. A disadvantage of a fuel cell is its limited lifetime. For long duration missions the amount of fuel that has to be taken aboard will be too high to be a mass efficient power source.
- **Solar Photovoltaic** - In our case a photovoltaic system requires batteries as previously explained. Therefore it will be further referred to as a solar photovoltaic-battery system. Photovoltaic conversion of solar radiation is the most common used power source for spacecraft. It is especially used by Earth orbiting satellites as at the distance of 1 AU, the solar constant of 1368 W/m^2 is sufficient for the existing solar cells to cover most spacecraft power requirements. The batteries have to be charged during sunlight in order to power the load during eclipse. This system will also require a power regulator unit to distribute the power to the payload and subsystems.
- **Solar Thermal Dynamic** - Solar radiation can also be used to heat up a liquid producing gas. The increase in volume drives a rotating turbo-generator or a reciprocating alternator producing electricity. The efficiency of such a system is twice

as high as that of the photovoltaic system [102]. It is usually used for spacecraft requiring higher energy rates of 5-50 kW. A disadvantage of this power source is the solar radiation concentrator. This is a large parabolic panel used to concentrate the solar radiation onto a small area. An advantage of this component is the increase in drag, which would increase the drag signal observed by the accelerometer. A disadvantage of the concentrator is that it introduces concave shapes in the design, yielding a more complex and less accurate drag estimation.

- **RTG** - RTG stands for Radioisotope Thermoelectric Generator. It is used by deep space and outer planetary missions for which the solar radiation is insufficient to deliver the required power. As the name suggests, it uses an on-board nuclear energy source or a radioactive isotope to generate electrical power. Disadvantages of an RTG are the high costs and high radiation affecting payload instruments.
- **Nuclear Reactor** - A nuclear reactor can provide power for a spacecraft independently of distance to the Sun. It is also used by spacecraft requiring a high degree of radiation hardness under nuclear threat. However, a nuclear reactor powering a satellite severely affects the satellite properties, just like the previously discussed RTG.

The trade-off between these power sources is performed using Table 9.1. In this table, each column represents a trade-off criterion. Six criteria have been considered. The weight of each criteria is stated between curved brackets. The weights vary from low over medium to high. A high weight stands for a criterion immediately crossing out one or more options. A criterion with a low weight can only be the decisive factor when all other criteria are equal. For each criterion the degree of fulfilment of this criterion with respect to the MIRALOS-mission is illustrated by a red-orange-green color range. Red means low fulfilment, orange means medium fulfilment and green meaning high fulfilment.

The first criterion is power. This is the power range the power source can deliver. This criterion is given a high weight because if the MIRALOS required power range is outside the power range of a power source, it is simply not an option anymore. The power range of the MIRALOS-satellite has been determined and equals 660-980 W, eliminating the solar thermal dynamic and nuclear reactor options because they become efficient from 5 kW onwards. Therefore these power sources are marked with a red color.

The second criterion is specific power. This criterion is important for the mass of the satellite. The higher this value, the lower the mass will be. This criteria has been given a medium weight.
The specific cost is a criteria with a low weight. As can be seen from previous cost estimations in Chapter 5, the costs are still significantly lower than the EUR 350 million budget. Therefore it can only be decisive when the other criteria are indecisive.
Degradation is a criterion accounting for losses in performance over time. Power sources requiring photovoltaic cells will always lose performance over time due to interaction with solar radiation. The other power sources are much less influenced by radiation. The degradation criterion is given a low weight because a high degradation can be compensated with a high specific power, therefore the specific power criterion is way more decisive.

Table 9.1: Power source trade-off. The first row shows the criteria with the corresponding weight between brackets. An asterisk (*) means that a value depends on mission lifetime). Sources: [18], [102]

Power Source	**Power (high) [kW]**	**Specific power (medium) [W/kg]**	**Specific cost (low) [$/W]**	**Degra-dation (low)**	**Attitude obstruction (medium)**	**Thermal constraints (medium)**
Solar Photovoltaic	<300 green	<200 green	low green	medium orange	medium orange	low green
Solar thermal dynamic	5-300 red	<15 red	low green	medium orange	medium orange	medium orange
RTG	<10 green	<20* red	medium orange	low green	low green	medium orange
Nuclear reactor	5-300 red	<40* red	high red	low green	medium orange	high red
Fuel cell	<50 green	<275* orange	medium orange	low green	none green	medium orange

Attitude is a criterion used to address the attitude requirements set by the power sources. Although solar radiation dependent power sources might give a high attitude obstruction, in the case of the MIRALOS-satellite for which the hypothetical solar panels would be body mounted, the attitude obstruction can be compensated by distributing the solar arrays such that for every useful attitude enough power can be created. Sizing for attitude obstruction will increase the power source mass, though it is given a medium weight.

The last criterion is the constraints a certain power source sets on the thermal control subsystem. The higher the thermal requirements, the more power the thermal control subsystem will need. This will increase the mass of the electrical power system. This criterion is given a medium weight.

As can be seen from Table 9.1 the row corresponding to the solar photovoltaic power source contains the most green boxes. Therefore, a solar photovoltaic battery system is selected. In the following sections, trade-offs will be performed on solar cells and battery types.

9.3. Solar Cell Trade-off

The solar photovoltaic battery system consists of photovoltaic array of solar cells, a set of batteries, a power regulator and control circuits. The function of a power regulator is to distribute the power received from the solar cell arrays to the batteries and spacecraft subsystems and payload. Control circuits is the cabling needed for this electricity distribution.
In this section a solar cell will be selected out of four solar cells; silicon, gallium-arsenide, indium-phosphide and triple junction gallium-arsenide.

A solar cell is selected by performing a trade-off with the following criteria. Weights are assigned to the criteria with the same scale as used for the power source trade-off.

- **Product efficiency** - This is ratio of the electric power produced by the solar cells to the incident solar radiation power. [medium]
- **Degradation** - Degradation is the loss in performance during lifetime. Causes of this degradation are radiation and impacts of micro debris particles. The degradation is expressed in percent loss in performance per year. [medium]
- **Cost** - The costs for each solar cell are expressed in USD per Watt. [low]
- **Mass** - The specific mass is expressed in kilograms per square meters. [medium]

Table 9.2 shows the solar cells trade-off. The color scale is similar to the one used for the power source trade-off.

Table 9.2: Solar cell trade-off. The first row shows the criteria with the assigned weights between brackets. Sources: [18], [103], [104], [105]

Type	**Product efficiency (medium) [%]**	**Degradation (low)**	**Cost (low) [$/W]**	**Mass (medium) [kg/m^2]**
Silicon	22 orange	3.75 red	378 green	0.32 green
GaAs	18.5 red	2.75 orange	852 red	0.81 red
InP	18 red	0.18 green	na	0.73 red
TJ GaAs	30 green	1 green	617 orange	0.84 red

From the table it can be seen triple junction gallium-arsenide solar cells are the most favourable ones to use for the MIRALOS-mission. Therefore the gallium arsenide triple junction solar cells are selected. Nowadays, this type of solar cells are being increasingly used in space industry seeking high efficiency and good manufacturability [102].

An example layout of a typical triple junction gallium-arsenide solar cell is depicted in Figure 9.1. As can be seen from the figure the cell can also consist of elements other than Ga and As. Each of the layers has its highest absorption efficiency for a different portion of the solar spectrum as can be seen on the graph.

9.4. Battery Trade-off

As previously explained, a solar photovoltaic power source needs batteries if used on a satellite experiencing eclipses during its lifetime, which will be the case for the MIRALOS-satellite. Different types of batteries do exist. Batteries differ in the material that has been used as electrodes. The four main types used for space applications are NiCd, NiH_2, Li-ion and Li-polymer. These are being traded off in Table 9.3. Again, the same weight scale (see brackets) and fulfilment scale has been used. The criteria used to perform the trade-off are discussed below:

- **Capacity** - This is the maximum storable energy per kilogram of battery. This criterion has been given a heigh weight since this mainly drives the mass of the spacecraft. [high]
- **Energy efficiency** - This is a measure for the energy loss during charge and discharge of the battery. [medium]

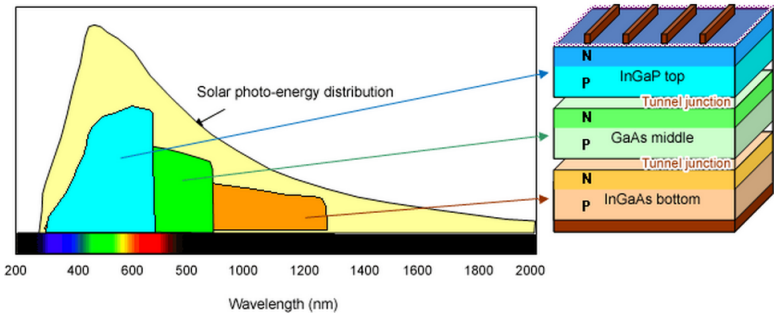

Figure 9.1: Triple junction gallium arsenide solar cell layout and absorption ranges of the solar radiated spectrum [106]

- **Operation life** - The operation life is based on the decrease in Depth-of-Discharge (DOD) with increasing charge-discharge cycles. [medium]
- **Thermal requirements** - This criterion represents the combined effect of operating temperature range and thermal power. The lower the temperature range and the higher the thermal power, the higher the thermal requirements. [medium]
- **Risk** - Lots of information from previous missions is already known for the NiCd and NiH_2 batteries. The amount of information for Li-ion batteries starts to increase as more and more spacecraft are being equipped with these types of batteries. The risk criterion is of low weight. This is because the available risk information has not been updated for three years, which means that decisions based on this criterion cannot be seen as important as for the other criteria. [low]

Table 9.3: Battery trade-off. The first row shows the criteria with the assigned weights between brackets. Sources: [18] [107], [108]

Type	**Capacity (high) [Whr/kg)**	**Energy efficiency (medium) [%]**	**Operation life (medium)**	**Thermal req. (medium)**	**Risk (low)**
NiCd	30 red	72 orange	medium orange	44 green	low green
NiH2	60 orange	70 orange	high green	50 green	low green
Li-ion	125 green	98 green	medium orange	33 orange	medium orange
Li-polymer	150 green	99.8 green	low red	60 green	high red

The table shows that the NiH_2 and Li-polymer battery rows have the most green boxes. Unfortunately, the operation life of the Li-polymer battery is insufficient for the MIRALOS-mission. Current batteries of this type only operate for 30000 charge/discharge cycles. Assuming a maximum altitude of 650 km the MIRALOS-satellite will at least comprise 32000 cycles. Hopefully, developers will soon increase the maximum charge/discharge cycles. The Li-polymer battery will probably become the number one battery used in space within several years. Excluding the lithium polymer battery, at first sight the NiH_2 seems to be the best option. However, as the Li-Ion battery has double the energy capacity of the NiH_2 one, which is of high weight, it compensates for the higher thermal requirements and higher risks, which are of lower weight. Therefore, the Li-ion batteries are selected for the photovoltaic-battery power system.

9.5. EPS Sizing

In a next step the solar photovoltaic-battery system has to be sized, i.e. the mass, power and dimensions have to be calculated. First, the maximum required power case has to be identified as well as some general EPS parameters. Section 9.5.1 will explain the dimensioning of the batteries. It is followed by the solar array sizing, discussed in section Section 9.5.2.

The electrical power system has to be dimensioned for the case the satellite requires its maximum power. The spacecraft subsystem maximum power requirements have been listed in Table 5.4. However, the spacecraft components will not require their maximum power at the same moment in time. Therefore, it is needed to determine what realistic combination of operating instruments and subsystems to expect. A discussion with the responsible subsystem engineers resulted in a list of satellite components for which the simultaneous operation accumulates maximum required power. This list is shown in Table 9.4. Also, the eclipse time should be taken into account when identifying the highest required power scenario. The highest power load

case occurs when the satellite will have its longest eclipse time. This is due to the need for more batteries which also have to be charged during the illumination period, resulting in both an increase in battery mass and an increase in solar array area. Longest eclipse times occur at minimum altitude. As stated in Chapter 4, the minimum altitude that will be reached within the MIRALOS-mission lifetime is 350 km.

Table 9.4: Subsystem power allocation in the Orbit Change Mode, i.e. the maximum required power case

Satellite component	Required power [W]
Payload	70.8
Thermal	150
TT&C	18
On-board Processing	20
ADCS	26.7
Propulsion	600
TOTAL (excl. cont.)	886
TOTAL (incl. 10% cont.)	975

Some general parameters had to be determined in order to continue with the EPS sizing. Those are shown in Table 9.5. It has to be noted the solar constant depends on the solar activity. However because of the difference of only 0.1% in the solar constant between solar maximum and solar minimum the solar constant is assumed to remain constant with solar activity. [109]

Table 9.5: General parameters used for sizing of the EPS

Parameter	Value	Source
Solar constant	1368 W/m^2	[18]
S/C power consumption incl. contingency	975 W	Chapter 5
S/C minimum altitude	350 km	Chapter 4
Operating lifetime	6 years	Chapter 4
Battery type	Li-ion	Section 9.4
Solar cell	Triple junction GaAs	Section 9.3
Earth albedo	0.25	[110]
Sat single side width	1.1 m	Chapter 5
Sat single side length	3 m	Chapter 5

9.5.1. Battery Sizing

The Li-ion batteries will be the first component of the EPS that will be sized. This is because the required energy for charging the batteries is an important parameter for the solar array sizing. Table 9.6 shows several important Li-ion battery parameters.

Table 9.6: Li-ion battery parameters used for sizing

Parameter	Value	Source
Energy density	533 kJ/kg	[108] [18]
Charge/discharge efficiency	0.98	[18]
Depth-Of-Discharge (DOD)	0.30	[18]
Specific cost	N/A $/W	N/A

First, the battery energy required per orbit is calculated using the total required power as listed in Table 9.5 and the longest possible eclipse time at 350 km. Dividing this value by the battery efficiency results the energy needed to charge the battery, i.e. 2.17 MJ. This value will also be used later on when sizing for the solar array. The battery mass needed for this energy capacity equals 4.1 kg at BOL conditions. Next, the degradation has to be taken into account. At EOL conditions, the DOD will only be 30%. This means that every battery can only be discharged for 30% of its capacity. Therefore, the battery mass should be 13.6 kg in order to have sufficient energy capacity at EOL.

The battery dimensions are very dependent on the manufacturer of the battery. Gathering of information on manufacturers such as Quallion [108] and Clyde Space [107] resulted in the QL075KA battery to be the best candidate for the MIRALOS mission. Mass and dimensions for this battery are given in Table 9.7. As can be seen from the table, the amount of batteries is not an integer. Further consultation with Quallion will reveal whether a smaller version of the QL075KA or another low capacity battery is available. It has also been considered to include three batteries which results in battery redundancy, reducing the severity of the battery failure risk. This option is selected for now. The values corresponding to the QL075KA three-battery-case are given within brackets.

Table 9.7: QL075KA battery characteristics for the MIRALOS satellite [111]

Parameter	Value
Specific power	148 Whr
Single battery mass	1.82 kg
Single battery volume	7.89E−4 m^3
Total battery mass	13.57 kg (18.17 kg)
Total battery volume	$1.77E-3$ m^3 ($2.37E-3$ m^3)
Amount of batteries	2.24 (3 incl.)
Battery cycle life	>100000

9.5.2. Solar Array Sizing

Table 9.8 shows the parameters used to determine the solar array dimensions, mass, power and costs. Note that the design and assembly inherent degradation factor of 0.87 also accounts for effective cell area loss due to interconnects between cells, usually made of kovar.

Table 9.8: Solar cell parameters used for sizing

Parameter	Value	Source
Cell mass	0.84 kg/m^2	[103] [104] [105]
Cell cost	617 $/W	[18]
J_{mp}	165 A/m^2	[112]
V_{mp}	2.41 V	[112]
$\frac{dJ_{mp}}{dT}$	0.091 A/($m^2 \cdot K$)	[112]
$\frac{dV_{mp}}{dT}$	−7 mV/K	[112]
Nominal solar cell temperature	301 K	[18]
Solar cell temperature	370 K	Thermal Analysis, Section 10.1.5
Design and assembly inherent degradation	0.87	[18], [88]
Annual degradation factor	0.99	[18]
Illuminated satellite surface	5.71 m^2	Chapter 5

As mentioned before in Table 9.5, the energy rate or power of the satellite is 977 W. This power will be generated by solar arrays distributed over the side panels of the hexagonal spacecraft. The flat top and bottom panels of the MIRALOS-satellite will be left free for instruments, e.g. antennae. Also, as a high satellite drag is preferred, the spacecraft will propagate with the bottom area facing the Earth and the bottom panel facing away from the Earth. Therefore, it is inefficient placing solar cells on this panels as it would not be possible to let them always face the Sun. Figure 9.2 shows the illuminated areas for two power sources. The main power source will of course be the Sun. At least two sides of the hexagonal satellite will be illuminated by the Sun as can be seen in Figure 9.2. The second considered power source is the albedo of the Earth. On average, the Earth reflects 25% of the incoming radiation. Taking into account eclipses, on average half of the satellite side areas will be receiving albedo radiation, see Figure 9.2. Also, the low incident angle of radiation coming from the Earth results in a lower array efficiency compared to the case for which the radiation would have an incident angle of 90°. This reduction in efficiency depends on altitude, equalling 0.30 at 350 km.

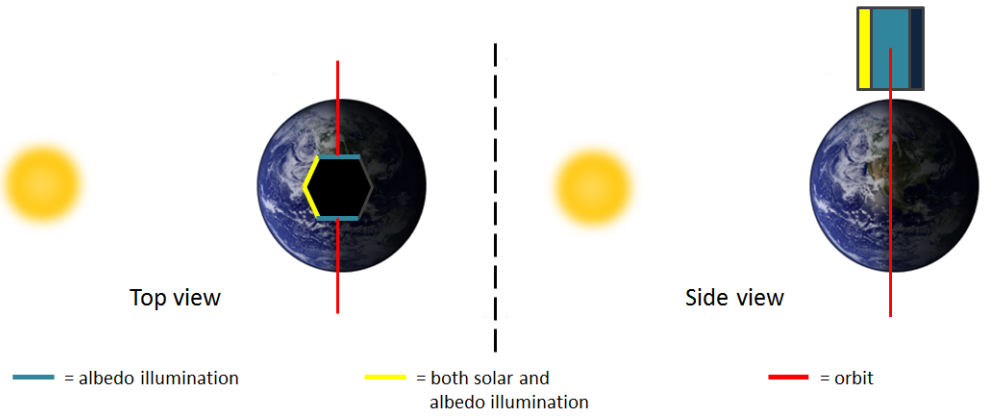

Figure 9.2: Spacecraft illumination conditions. A yellow color indicates illumination by both the Sun and Earth albedo radiation. An electric blue color stands for illumination by Earth albedo radiation only. The red line represents the satellite's orbit.

The cell efficiency is calculated by multiplying the maximum power point current density J_{mp} with the maximum power point

voltage V_{mp} and dividing by the solar constant. The nominal operating temperature of the solar cells is 301 K at which the cell efficiency equals 0.29. If the temperature of the solar cell exceeds nominal temperature, the J_{mp} increases with 0.091 A/m² per Kelvin and the V_{mp} decreases with −7 mV per Kelvin. Therefore, the solar cell efficiency drops for higher than normal temperatures. Thermal analysis indicated that the highest expected temperature of the solar cell would be 370 K, for which the cell efficiency drops to 0.24. This temperature is reached by the solar cells after several orbits of constant illumination in combination with operating ion thrusters. Orbit analysis has demonstrated that this extreme case occurs during the MIRALOS mission.
Having discussed the power sources and efficiencies, the required solar array area can be calculated using the required solar energy per orbit of 5.40 MJ. The calculation takes into account the solar cell efficiency, design and assembly degradation factor, annual degradation and radiation incident angles. This results in a total solar array area of 17.05 m², having a mass of 14.32 kg and a cost of EUR 0.48 million.

Triple junction GaAs based solar cells with nominal efficiencies close to 30% are manufactured by many different aerospace companies. Those include Spectrolab, Emcore, Clyde Space and Azurspace. Most of these companies offer covered interconnected cell (CIC) configurations. These CICs consist of kovar interconnects and a coverglass with a thickness of around 100 µm both protecting the cells from harmful radiation and reducing reflectivity with the use of a special coating. The CIC selection procedure should also account for ferromagnetic materials as their magnetic field can disturb the measurements of the magnetometers. The interconnections between solar cells contribute most to the magnetic field induced by the solar array. These interconnects are typically made out of kovar [113]. According to T.G. Stern and S. DeLapp [113], the kovar interconnects induce a magnetic field of at most 14 nT at a distance of 10 cm. Molybdenum interconnects can be used as a substitute for the kovar ones, as their induced magnetic field at 10 cm stays below 1 nT.

The covered interconnected ZTJ Photovoltaic Cell by Emcore, of which the characteristics are given in Table 9.9, would be a good candidate for the MIRALOS satellite. The cell consists of four layers: InGaP junction, InGaAs junction, Ge junction and Ge substrate.

Table 9.9: ZTJ Photovoltaic Cell characteristics for the MIRALOS satellite [112]

Parameter	Value
BOL Nominal efficiency	29.5%
Specific mass	0.84 kg/m²
Total array mass	14.32 kg
Total array area	17.05 m²
Percentage of S/C side area	86.1

Table 9.10: Medium Power PCDU characteristics [114]

Parameter	Value
Reliability	0.99975
Mass	6.5 kg
Volume	546 x 260 x 200 mm²
Life time in LEO	6 yr
Power	0.5 - 3 kW

9.5.3. Power Regulator Unit
The PRU collects the power produced by the solar arrays and distributes it to the payload and subsystems. It also acts as a transformer, i.e. adapting the voltage to the bus voltage or payload voltage. The characteristics of a suitable PRU (Medium Power PCDU by Astrium) are shown in Table 9.10. The Medium Power PCDU also includes the necessary control circuits.

9.5.4. Summary
Table 9.11 shows a summary of the characteristics of the selected electrical power system.

Table 9.11: Summary of EPS design

Parameter	Value
Battery type	QL075KA
Battery mass	18.17 kg
Solar array type	CI ZTJ PV Cell
Solar array area	17.05 m²
Solar array mass	14.32 kg
PRU type	Medium Power PCDU
PRU mass	6.5 kg
Total EPS mass	38.99 kg

The electrical block diagram is shown in Figure 9.3. It illustrates the power provision and power break-down as well as the relations between the electrical power subsystem components and the spacecraft components. The numbers in the diagram accompanying the branches represent the amount of power provided by the power source to the particular spacecraft component(s). The power values followed by an asterisk can deviate a lot from the given value depending on the spacecraft mode. Transformers are used to change the voltage level from the Electric Power System (EPS) unit to the subsystems and instrument voltage levels.

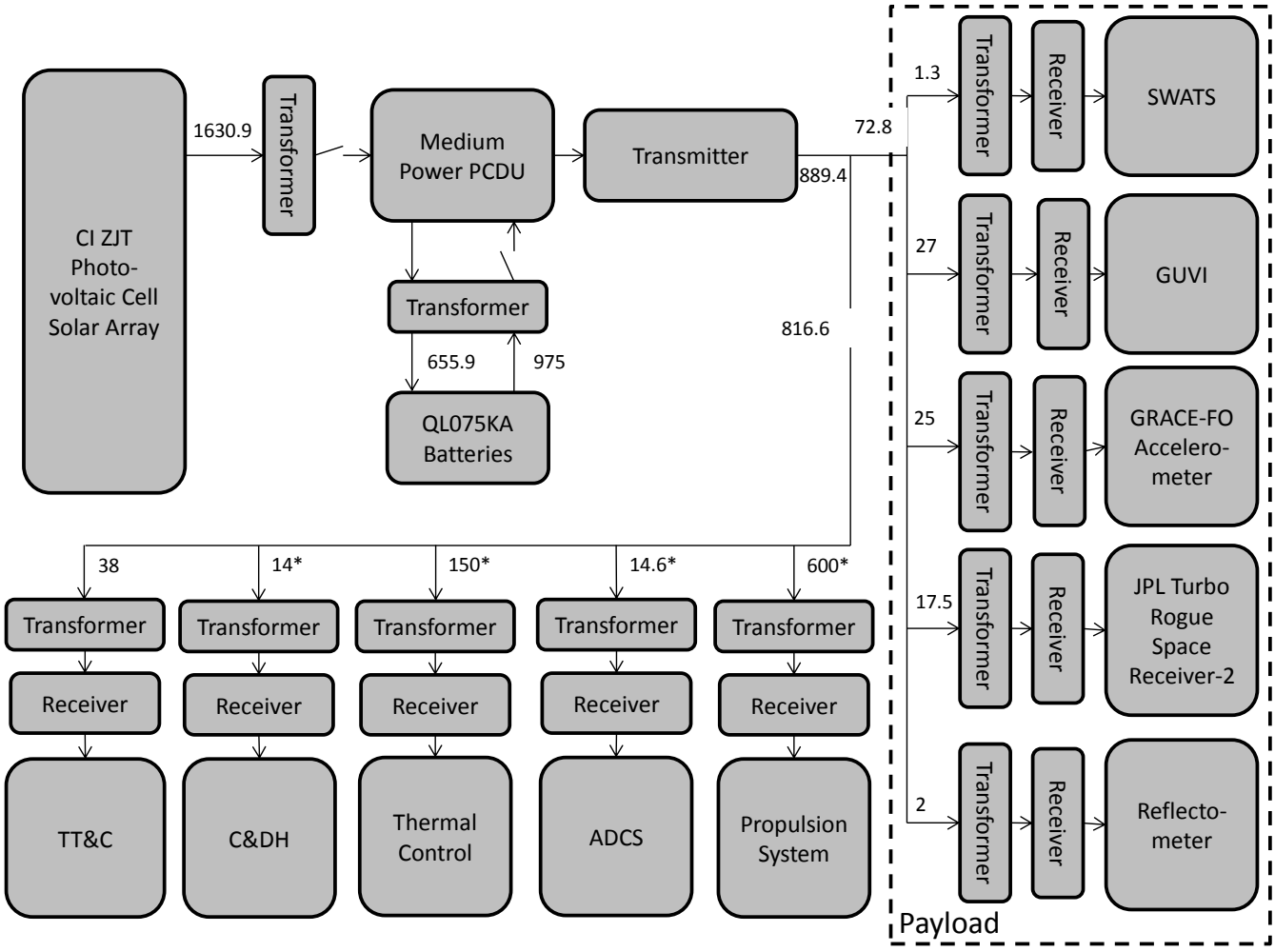

Figure 9.3: Electrical Block Diagram. The numbers accompanying the arrows represent the power flow in Watts.

10. Thermal Control

This chapter presents the analysis and design of the thermal control subsystem of the MIRALOS spacecraft. The thermal analysis is depicted in Section 10.1 and contains the thermal requirements, the worst-case scenarios, a first order estimation using a simple isothermal model and an analysis using finite-element method software. Section 10.2 presents the selection of radiators and thermal blankets as well as a design of the individual thermal control of certain instruments.

10.1. Thermal Analysis

In this section, the thermal analysis results and the methods with which they were acquired will be elaborated on.

10.1.1. Requirements

The instruments that are used on the MIRALOS spacecraft have requirements with respect to temperature. The main type of temperature requirements are the operational and survival temperature ranges. The ranges used are depicted in Table 10.1.

Table 10.1: Temperature ranges of individual spacecraft components

Part	Operational Range [°C]	Survival Range [°C]
Star Sensor	-70 to 20	-70 to 80
Magnetometer	-40 to 85	-40 to 85*
Sun Sensor	-15 to 50	-15 to 50*
Cold-gas thruster	-40 to 70	-40 to 70*
Lithium-Ion battery	10 to 25	0 to 35**
Power Regulator Unit	-35 to 70	-35 to 70*
Antennae	-20 to 50	-30 to 60
Transceiver	-20 to 60	-20 to 60*
Solar Panels	-180 to 95	-180 to 95*
CPU	-55 to 125	-55 to 125*
Onboard Computer	-20 to 50	-20 to 50*
Accelerometer	0 to 50***	-20 to 70***
Ion Thrusters	-80 to 270	-80 to 270*
ECU Thrusters	-20 to 50	-20 to 50*
Thruster Feedsystem	-10 to 60	-10 to 60*
Xenon fuel tank	20 to 46	20 to 46*
Cold gas tank	-70 to 108	-70 to 108*
GUVI	-24 to 55	-29 to 60

*Same range as operational due to unavailable information

**Range taken from literature[115]

***Assumption for electronics. Stability more important than range.

The table shows that the lithium-ion battery has the most critical temperature range requirement, since its operational range is quite narrow. However, the used accelerometer has the most strict requirements. It requires a temperature stability of 10 millikelvin per 200 seconds [88]. Therefore it requires a accurately controlled thermal environment. The methods used to design for the critical thermal requirements will be further elaborated on in Section 10.2.3.

Since xenon is stored in a supercritical state and the critical temperature of xenon is 289.733 K [116], this means that the fuel temperature cannot drop below 289.733 K. The maximum temperature is determined by the fuel tank's Maximum Expected Operating Pressure (MEOP), which is 125 bar. The density of the full tank is 1.5 g/cm^3, and from the MEOP and density the maximum operating temperature can be obtained. This temperature was estimated to be 323 K from thermodynamic tables. Taking a safety margin of about 3 K, the tank operational temperature requirement was set to be between 293 K and 319 K (20 °C to 46 °C). For the fuel pipes, the same requirement is taken.

For the cold gas tank, the lowest temperature is determined using the material minimum service temperature [117]. The maximum temperature is again determined by the MEOP, which is 280 bar, as defined in Section 8.3.2. For this, the ideal gas law was used with a compressibility factor of 1.1. For both temperatures, a 3°C margin was used, giving a minimum operating temperature of -70°C and a maximum operating temperature of 108°C.

10.1.2. Theoretical Background

At the basis of thermal analysis lies the heat equation, which for the satellite thermal analysis is the following (ignoring convection terms):

$$\rho c_p \frac{dT}{dt} = -\nabla \cdot (k \nabla T) + Q \tag{10.1}$$

where Q is a local heat source term given in W/m³. This equation can be used to locally calculate the temperature, or it can be integrated with respect to volume to get a first-order estimate of the entire system. Setting the term $\frac{dT}{dt}$ equal to zero leads to the equation to solve for steady state behavior, and setting the conduction term $(-\nabla \cdot (k \nabla T))$ equal to zero makes the system isothermal. Solving the PDE requires that the initial conditions (i.e, the temperature at each point of the satellite in the initial state) and boundary conditions (heat sources) are defined. For the satellite, these heat sources are explained further below.

Radiation

A large portion of the heat sources on a spacecraft are radiative heat sources. In order to better understand the following discussion, two important formulas are given. For any surface and any wavelength λ, the relative amounts of radiation that are reflected (ρ), transmitted (τ) or absorbed (α) are related:

$$\alpha(\lambda) + \rho(\lambda) + \tau(\lambda) = 1 \tag{10.2}$$

Furthermore, the absorptivity is equal to the emissivity for any wavelength:

$$\alpha(\lambda) = \epsilon(\lambda) \tag{10.3}$$

Because of this last relation, α and ϵ can be used interchangeably, although some authors in the field of space engineering reserve the former for the solar spectrum only and the latter for the infrared spectrum.

Heat sources

An important part of thermal analysis is defining the heat sources. The heat sources considered for the MIRALOS satellite are presented here.

Solar radiation

The sun was modelled as a black body at a temperature of 5777 K [118]. Using Planck's law, the spectral radiance could be obtained. The figure below shows that the obtained spectrum agrees very well with the solar spectrum obtained from the ASTM E-490-00a model, which is a standard air mass zero (AM0) model used for solar irradiance [119]. Both the calculated spectrum and the spectrum from the ASTM E-490-00a are shown below in a normalised form.

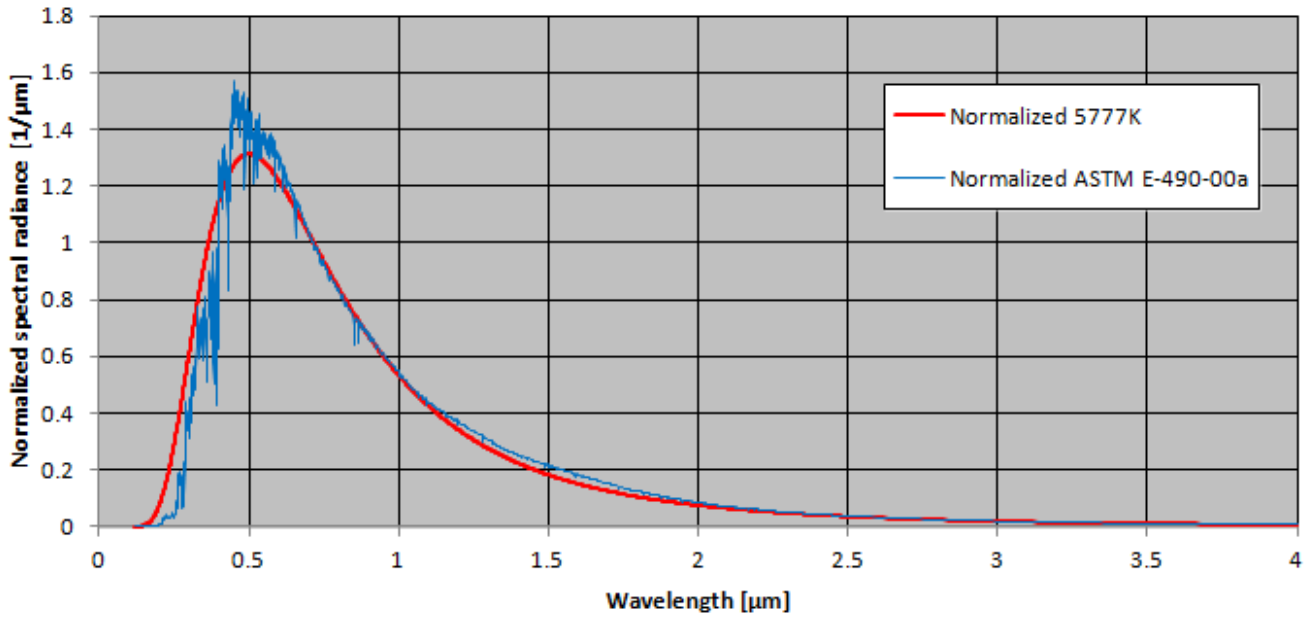

Figure 10.1: Normalised spectral radiance of the ASTM E-490-00a model (blue) and a black body at 5777 K (red).

The graph shows that the assumption to model the sun as a black body at 5777 K is reasonable. The solar radiative power was taken to be $3.844 \cdot 10^{26}$ W.

Calculation of the spectral radiance from the sun shows that the sun emits emits about 96.7% of its radiation in the form of short wave radiation and 3.3% of its radiation in the form of long wave radiation. Therefore, the reported solar absorptivity for various materials was used for the irradiance in the above defined short wave range, whilst the reported IR emissivity for materials was used for the long wave range. The solar irradiance can then be calculated as:

$$G_s = \frac{P}{4\pi d_s^2} \tag{10.4}$$

where d_s represents the distance from the sun. This gives a solar irradiance of 1322 W/m² at aphelion and a solar irradiance of 1414 W/m² at perihelion.

Earth albedo

The normalised spectral radiance of Earth's albedo was assumed to be the same as that of the sun (although it is not exactly identical [82]), as seen in Figure 10.1. The albedo irradiance on a surface of the satellite can be determined as:

$$Q_{alb} = G_s \cdot a \cdot VF\alpha_s \cdot A \tag{10.5}$$

In this formula, a is the albedo factor (which can vary greatly depending on cloud cover, local solar time, etc.) and VF is the earth view factor for the spacecraft surface on which the albedo irradiance is calculated.

Earth IR radiation

For the IR irradiance from Earth, the Earth was assumed to be a black body at 255 K. For this temperature, the spectral radiance at wavelengths shorter than 2500 nm is negligible, and thus only the material IR absorptivity (which is equal to its IR emissivity) was used for calculating the Earth IR irradiance on the spacecraft surfaces using Equation (10.6), where G_{IR} varies between 216 W/m² and 258 W/m² [17]:

$$q_{IR} = G_{IR} VF \alpha_{IR} A \tag{10.6}$$

Free molecular heating

Another contributing factor is the effect of free molecular heating. Free molecular heating is defined as:

$$Q_{FMH} = \alpha \frac{1}{2} \rho V^3 \tag{10.7}$$

At a minimum orbital altitude of 350 km, the predicted density from the atmospheric model is at the most on the order of 10^{-11} kg/m³. Using an orbital velocity of 7700 m/s and a conservative accommodation coefficient of 1, this gives about 2 W/m² heat flux at the lowest orbit altitude in the mission. As a result, this effect was ignored for the in-orbit thermal analysis.

Internal heat dissipation

The last type of heat source used in the analysis is the heat that is generated internally inside the spacecraft, mainly due to Joule heating. The heat generated by a component is given as:

$$Q_{comp} = (1 - \eta_e)P \tag{10.8}$$

where η_e is the electrical efficiency of the component, and P the power used by the component. These last heat sources are highly dependent on operating mode, and the total internal heat generation can vary greatly during the mission.

Earth view factors

The Earth view factors in equations Equation (10.5) and Equation (10.6) are determined in the manner described by Rickman [120]. The Earth view factor for surfaces whose normal has an angle of 0° with the nadir vector is calculated with:

$$VF_{0^\circ} = \left(\frac{R_e}{R_e + h} \right)^2 \tag{10.9}$$

For surfaces with a normal deflected 90° angle from the nadir vector, the following equation is used:

$$VF_{90^\circ} = \frac{1}{2\pi} \left[\pi - 2sin^{-1} \left(\sqrt{1 - \left(\frac{R_e}{R_e + h} \right)^2} \right) - sin \left(2sin^{-1} \left(\sqrt{1 - \left(\frac{R_e}{R_e + h} \right)^2} \right) \right) \right] \tag{10.10}$$

For surfaces with a normal to zenith, the Earth view factor is equal to zero.

Solar cell absorption

The solar cells used have an external efficiency of 29.5% under nominal operating temperatures, which means that, for an irradiance of 1367 W/m^2, about 403 W/m^2 is converted into electrical energy. Since 96.7% of the solar irradiance is taken to be in the short-wave spectrum as discussed in Section 10.1.2, the external efficiency of the solar cell in that particular spectral range of the solar irradiance is equal to 0.305, as by Equation (10.11).

$$\eta_s = \frac{403}{0.967 \cdot 1367} = 0.305 \tag{10.11}$$

Since the solar cell has a reported absorptivity α_s of 0.9 [121] and can be seen as opaque (τ = 0), it means that for thermal design purposes the short wave absorptivity should be taken to be 0.9 - 0.305 = 0.595, as the rest of the energy is converted into electricity rather than heat.

10.1.3. Worst Hot, Worst Cold & Safe Mode Case

The design of the thermal system should provide for the worst-case scenarios. In thermal design these are the Worst Case Hot (WCH), Worst Case Cold (WCC) and Safe Mode Case (SMC). The thermal system should provide the necessary heating and cooling to accommodate for these extremes. The separate cases are analysed and depicted in this section.

The orbits of the hot and cold cases are shown in Figure 10.2. In the hot case, the spacecraft is assumed to be in continuous sunlight and thus has an orbit beta angle of 90°. This situation will occur and lasts a significant amount of time (up to 27 days, as mentioned in Section 4.2.2), as the orbit will still be quite close to sun-synchronous. For the cold and safe mode cases, the spacecraft is an orbit with a beta angle of 0°, where the maximum eclipse time occurs.

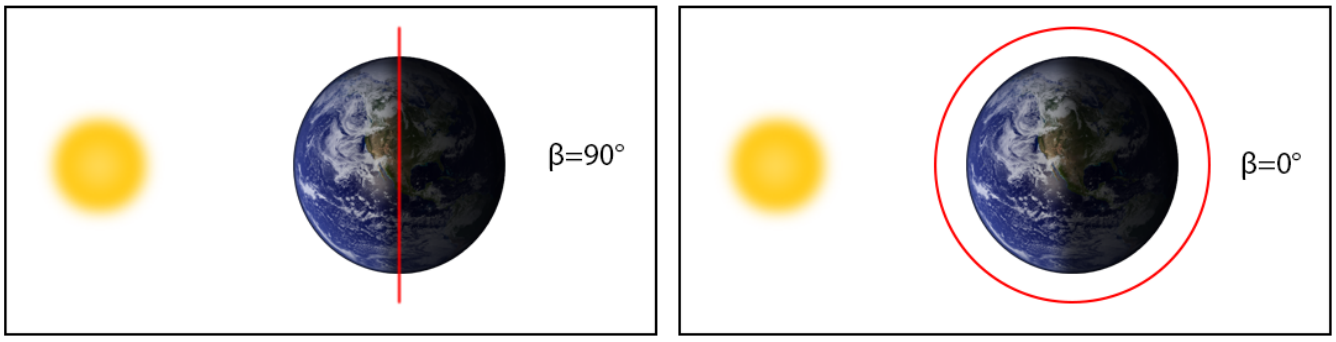

Figure 10.2: Orbits considered for the hot (left) and cold and safe mode cases (right).

Furthermore, for the hot and cold case, the extreme values of the heat sources described in Section 10.1.2 were considered. The values for these are given in Table 10.2.

Table 10.2: Parameters for the hot, cold and safe cases.

	Hot Case	**Cold Case**	**Safe Mode**	**Unit**
Solar irradiance G_s	1414	1322	1322	W/m^2
Earth IR irradiance G_{IR} [17]	258	216	216	W/m^2
Orbit altitude h	350	350	350	km
Eclipse fraction	0	39.7%	39.7%	-
24-h 3.3σ Albedo factor a [115]	0.55	0.22	0.22	-

The WCH, WCC, and SMC are described below. Here, also the heat generation due to electronics and other components inside the spacecraft in each of the cases is presented.

Worst Case Hot (WCH)

The WCH situation takes into account the highest possible values of all heat sources combined. During WCH analysis it is assumed that all instruments and subsystem components are running at full power; the values are presented in Table 10.3. Other relevant heat source values are depicted in Table 10.2.

Table 10.3: Heat dissipation with regard to sub-system components (Hot-Case)

Component	Power Input	Efficiency	Heat Dissipation
UV Horizon Sensor (incl. heater)	27 [W]	0.15	23 [W]
On-board Processing	14 [W]	0.20*	11.2 [W]
Accelerometer	25 [W]	0.20*	20 [W]
Mass/Wind Spectrometer	1.3 [W]	0.20*	1.04 [W]
Reflectometer	2 [W]	0.20*	1.6 [W]
GPS Receiver	17.5 [W]	0.20*	14 [W]
TT&C	38 [W]	0.20*	30.4 [W]
ADCS	14.63 [W]	0.20*	11.7 [W]
Thruster IPCU	585 [W]	0.92	46.8 [W]
Total:	724.43 [W]	0.7795	159.74 [W]

*Efficiency of 20% is assumed since no information is available [122]

Worst Case Cold (WCC)

The WCC situation occurs when the spacecraft is in maximum eclipse (at 350 km altitude) with its payload and sub-systems functioning at lowest power and the thruster turned off. Furthermore, the lowest possible values of the other contributing heat sources are taken into account as depicted in Table 10.2. The values of the heat dissipation of the instruments and sub-system components can be found in Table 10.4.

Table 10.4: Heat dissipation with regard to sub-system components (Cold-Case)

Component	Power Input	Efficiency	Heat Dissipation
UV Horizon Sensor	27 [W]	0.20*	23 [W]
On-board Processing	9.5 [W]	0.20*	7.6 [W]
Accelerometer	25 [W]	0.20*	20 [W]
Mass/Wind Spectrometer	1.3 [W]	0.20*	1.04 [W]
Reflectometer	2 [W]	0.20*	1.6 [W]
GPS Receiver	17.5 [W]	0.20*	14 [W]
TT&C	18 [W]	0.20*	14.4 [W]
ADCS	14.63 [W]	0.20*	11.7 [W]
Total:	114.93 [W]	0.1879	93.34 [W]

*Efficiency of 20% is assumed since no information is available [122]

Safe Mode Case (SMC)

The SMC takes into account the lowest possible values of the heat sources when the spacecraft is in a maximum eclipse orbit at 350 km altitude. The lowest possible values of the contributing heat sources are taken into account as shown in Table 10.2. During the SMC scenario it is assumed that the subsystems are running at minimum power and the scientific instruments are shut off, as well as the ion thruster as described in Section 15.3. The used values are presented in Table 10.5.

Table 10.5: Heat dissipation with regard to sub-system components (Safe-Mode)

Component	Power Input	Efficiency	Heat Dissipation
On-board Processing	9.5 [W]	0.20*	7.6 [W]
GPS Receiver	17.5 [W]	0.20*	14 [W]
TT&C	18 [W]	0.20*	14.4 [W]
ADCS	14.63 [W]	0.20*	11.7 [W]
Total:	59.63 [W]	0.20	47.7 [W]

*Efficiency of 20% is assumed since no information is available [122]

10.1.4. First Order Estimation

When starting the thermal analysis of a spacecraft, it is very useful to get a grasp at the order of magnitude of certain parameters such as the worst-hot case, worst-cold case, required radiator area, and so on. Therefore a first order estimation was made assuming an isothermal, rectangular cuboid spacecraft. This allowed for simple first order calculations.

First a surface material had to be chosen to establish emissivity and absorption values. The surface property values of a triple junction gallium-arsenide solar cell were used since a large part of the MIRALOS spacecraft is covered in solar cells. This surface has an emissivity of $\epsilon_{IR} = 0.87$ and an absorptivity of $\alpha_s = 0.595$ [121].

To model the spacecraft as a rectangular cuboid, the spacecraft dimensions had to be translated to this geometry. The two square

top and bottom plates will have the same area as the two hexagonal top and bottom plates as used on the spacecraft (3.1 m^2). For the four side plates, the area is calculated by taking the total area of the side plates of the spacecraft and dividing it by 4.
The first step in the calculations is to establish worst-case hot, worst-case cold, and safe-mode temperatures. To be able to perform these calculations, certain heat fluxes must be determined along with view factors regarding the rectangular side plates and square top/bottom plates. The following subsections present the calculations regarding these values.

Hot Case Analysis
Now that the heat source values are known, it is possible to calculate an equilibrium temperature for the cases. It is assumed that uniform energy dissipation occurs over the surface of the spacecraft. The calculation is done as follows for the hot-case (where σ is the Stefan-Boltzmann constant):

$$T_{max} = \left(\frac{Q_{sun} + Q_{albedo,sides} + Q_{albedo,bottom} + Q_{IR,sides} + Q_{IR,bottom} + Q_w}{\sigma \cdot \epsilon_{IR} \cdot A_{total}} \right)^{1/4} = 27°\text{C}/300\text{K} \tag{10.12}$$

This is the equilibrium temperature in constant sunlight. The used formulas for the individual components can be found in Section 10.1.2. Q_w is the collective term for all the combined waste heat sources.

Cold Case Analysis
Calculating the cold case is very much similar to that of the hot case. However since an eclipse occurs, the heat sources are not constant throughout the orbit. Therefore, as a first estimate, an average is taken for the varying heat sources. The varying sources are the solar radiation and the albedo effect. It is assumed that no penumbra region occurs. Since the highest eclipse time occurs at an altitude of 350 km, this value is taken for the analysis of the cold-case.
Using the values found in Tables 10.2 and 10.4 and multiplying the solar radiation and albedo effect by 0.60 (the percentage of the orbit that lies in the sun), the following temperature are yielded:

$$T_{min} = \left(\frac{0.603 \cdot \left(Q_{sun} + Q_{albedo,sides} + Q_{albedo,bottom}\right) + Q_{IR,sides} + Q_{IR,bottom} + Q_{w,min}}{\sigma \cdot \epsilon_{IR} \cdot A_{total}} \right)^{1/4} = -23°\text{C}/250\text{K} \tag{10.13}$$

This is a decent first order approach to get the order of magnitude. However, the variations along-track are not taken into account, while this effect might be very significant. Therefore a MATLAB script was written to simulate the orbit for a period of 10 orbits to estimate the maximum, minimum and mean temperature. This was performed while taking the previously found minimum temperature as an initial temperature. Furthermore, the specific heat constant (C_p) of aluminium has been taken to represent the bulk material of the spacecraft, since a large fraction of the spacecraft mass consists of the structure which has an aluminium honeycomb core. The following differential equation was used to calculate the temperatures along-track:

$$\frac{dT}{dt} = \frac{Q - A \cdot \sigma \cdot \epsilon \cdot \left(T^4 - T_{amb}^4\right)}{C_p \cdot M_{S/C}} \tag{10.14}$$

The MATLAB script uses a backward difference method to estimate the temperature at each point with a timestep Δt of 60 s. The results can be observed in Table 10.6 and fig. 10.3a. The previous spacecraft temperature (T_{min}) turned out to be a very good estimate for the mean temperature. It can be observed from Figure 10.3a that the temperature graph quickly converges to a steady, recurring pattern.

Table 10.6: Observed temperatures in orbit simulation

T_{mean}	T_{max}	T_{min}
-23[°C]/250[K]	-15[°C]/258[K]	-33[°C]/240[K]

Safe Mode Analysis
The calculation for the SMC is done in the same way as the cold case. The used values are depicted in Tables 10.2 and 10.5. The orbit-average temperature (T_{SM}) is found to be 248 K using Equation (10.13). Additional MATLAB results are depicted in Table 10.7 and fig. 10.3b.

T_{mean}	T_{max}	T_{min}
-25[°C]/248[K]	-17[°C]/256[K]	-34[°C]/239[K]

Table 10.7: Spacecraft temperature variation during safe mode

These temperature evolutions seem to match the ones presented in literature qualitatively [82, p. 347].

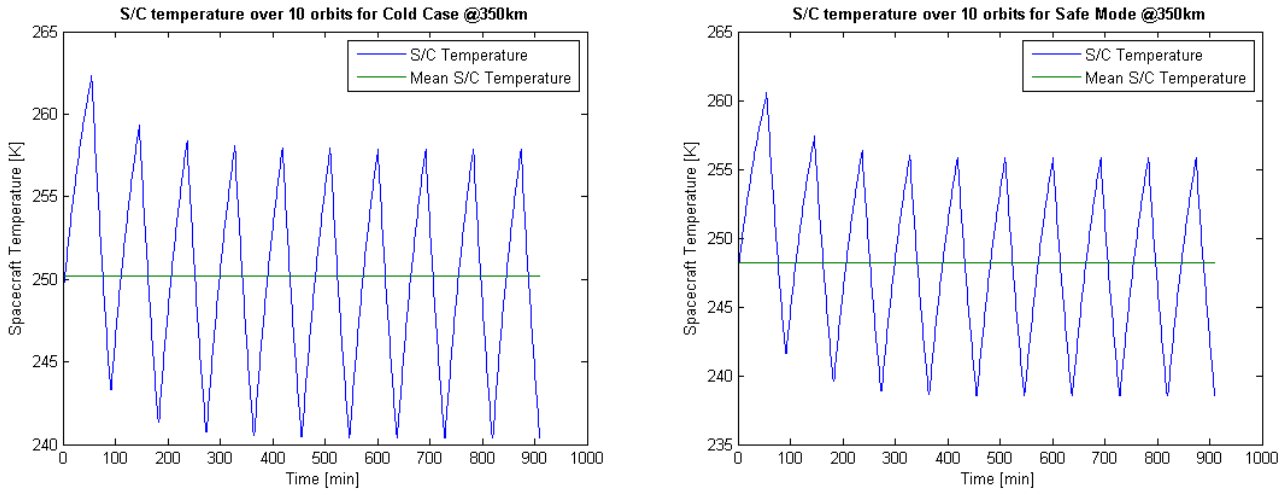

(a) Spacecraft temperature variation during cold case

(b) Temperature variation during safe mode case

Figure 10.3: Spacecraft temperature variations over 10 orbits

Sensitivity Analysis

To check whether the calculations are of any value, it has to be checked that the used program is not overly-sensitive to certain inputs. Since similar code has been used to get values for the hot, cold, and safe mode case, the parameter sensitivity is only described for the worst hot case. The results are displayed in Table 10.8.

The table shows that the temperatures are all reasonable and within the same order of magnitude. No big fluctuations occur when changing certain key parameters. This gives assurance about the proper functioning of the MATLAB code, and robustness of the design.

Table 10.8: Sensitivity analysis results. Values are varied by $\pm$ 20%

Parameter	T @ -20% [K]/Value	T [K]/Value	T @ +20% [K]/Value
Albedo factor (a) [-]	293.67 / 0.44	299.67 / 0.55	305.34 / 0.66
Earth IR (G_{IR}) [W/m^2]	296.83 / 206.4	299.67 / 258	302.46 / 309.6
Heat dissipation (Q_w) [W]	299.47 / 127.8	299.67 / 159.74	299.90 / 191.69
Surface area (A_{tot}) [m^2]	316.88 / 22.05	299.67 / 27.56	286.33 / 33.08

10.1.5. COMSOL Analysis

In addition to the analysis which has been done with the isothermal model that was created, a thermal analysis was done using COMSOL. Even though COMSOL is generally not the program used for satellite thermal analysis (other programs like for example ESATAN are more established in the space community), it has been used before for this purpose [123, 124].

Model parameters

For the COMSOL analysis, a detailed model of the spacecraft was made, which can be seen in Figure 10.4. The model contains the general structure of the spacecraft, the solar panels and the components that dissipate most heat. Other (smaller) heat sources were not added, but their heat contribution was distributed over the inside of the structure. Lastly, a few selected components (fuel tanks, accelerometer, XPFA) were added as well. Two radiators were placed in the model, one zenith radiator of 0.03 m^2 and one nadir radiator of 0.04 m^2. Without these radiators, the internal temperatures in a fully insulated model with Multi-Layer Insulation (MLI) would become very high.

Except for the free molecular heating, all heat sources discussed in Section 10.1.2 were added to the model. Material properties were determined as good as possible, but not all materials have been defined yet or sometimes data for thermal properties just was not available.

For the modeled structure, a lot of different surface finishes were used. Most of the exterior is covered by solar cells with an MLI blanket below, and the zenith and nadir faces of the spacecraft are also covered in an MLI blanket. The external radiator surface was assumed to be quartz mirror. Finally, on the interior all surfaces were assumed to be coated with a black paint to reduce internal temperature gradients.

The properties shown here have not been corrected for surface degradation due to atomic oxygen, UV radiation or contamination. Also, the temperature dependence of solar cell efficiency has not been taken into account. This implies that as time passes, the model error is expected to become larger. Aside from surface properties, the material densities, thermal conductivities and specific

Table 10.9: Properties of used surfaces in the COMSOL model.

	ZTJ Emcore Solar cell	MLI blanket	Quartz mirror	Black paint
Solar absorptivity	0.595*	0.005	0.05	0.95
IR emissivity	0.87	0.005	0.88	0.90

heat at constant pressure had to be determined. Unfortunately, it was not possible to obtain this data for all materials used in the model, and approximations had to be made. For the solar panels, for example, the properties of Germanium were used, since most of the solar cell is the Germanium substrate. These approximations lead to further inaccuracies in the model.

Results

For the WCH temperatures, the temperature distribution in the spacecraft is shown in Figure 10.4. This figure shows the temperature distribution in the spaceraft after one month in an orbit with a 90° orbit beta angle, starting from an initial isothermal state at 273.15 K. As such, it can be taken as a good approximation of steady-state behavior.

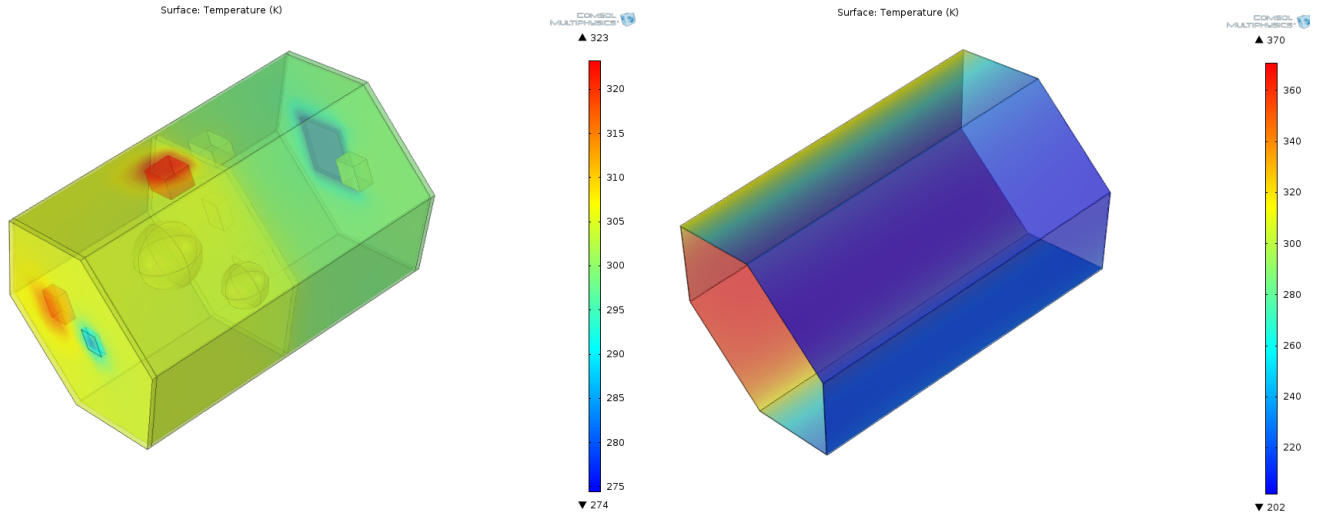

Figure 10.4: Worst case hot steady state temperatures for the satellite structure (left) and solar panels (right). The position of the sun can be deduced from the hot surfaces in the picture on the right.

What can be seen is that the solar panel temperatures can reach up to 370 K at the hottest points. This greatly reduces their efficiency. The average temperature on the sunlit surfaces is 356 K in this state. These numbers agree with hand calculations where the solar panels were seen as completely insulated on all sides except for the sunlit side.

The temperature distribution in the structure shows a temperature difference between the zenith side, where a large 0.5 m^2 radiator was chosen, and the nadir side, where a 0.04 m^2 radiator surface was chosen, with zenith-side temperatures at around 300 K and nadir-side temperatures at around 305 K in the hot case. Lastly, it can be seen that the IPCU and GUVI instrument generate a lot of heat during operation.

The temperatures in this model differ a bit from the isothermal model presented in Section 10.1.4. The main reason for this is that the isothermal model did not consider the spacecraft structure to be well-insulated. Because of the insulation, the solar panels experience much larger temperature variations than predicted in the first-order estimation and the insulated structure does not conduct the heat away as easily, although radiators were added to provide an outlet for the heat.

For the WCC temperatures, the temperature distribution in the spacecraft after 2 years in a maximum-eclipse orbit is shown in Figure 10.5, again starting from an initial isothermal temperature distribution of 273.15 K.

Because of the chosen orientation of the WCC orbit as shown in Figure 10.2, the top and bottom side solar panels shown in the figure (the bottom one is in the flight direction) have the smallest angles with respect to the sun-spacecraft vector, and thus experience a greater radiative heat flux due to solar radiation than the other solar panels. On average (over an orbit), the heat flux on these two panels is the same, and hence they have the same temperature. It can be seen that the temperature of the solar panels is significantly lower than in worst hot case scenario, being about 90 K less (compared to WCH surface average of the sunlit panels).

For the structure, the average temperatures are around 280 K for the nadir-side and 275 K for the zenith facing side, which is about 25 K less than in the hot case. Also, the GUVI reaches about 295 K in this case.

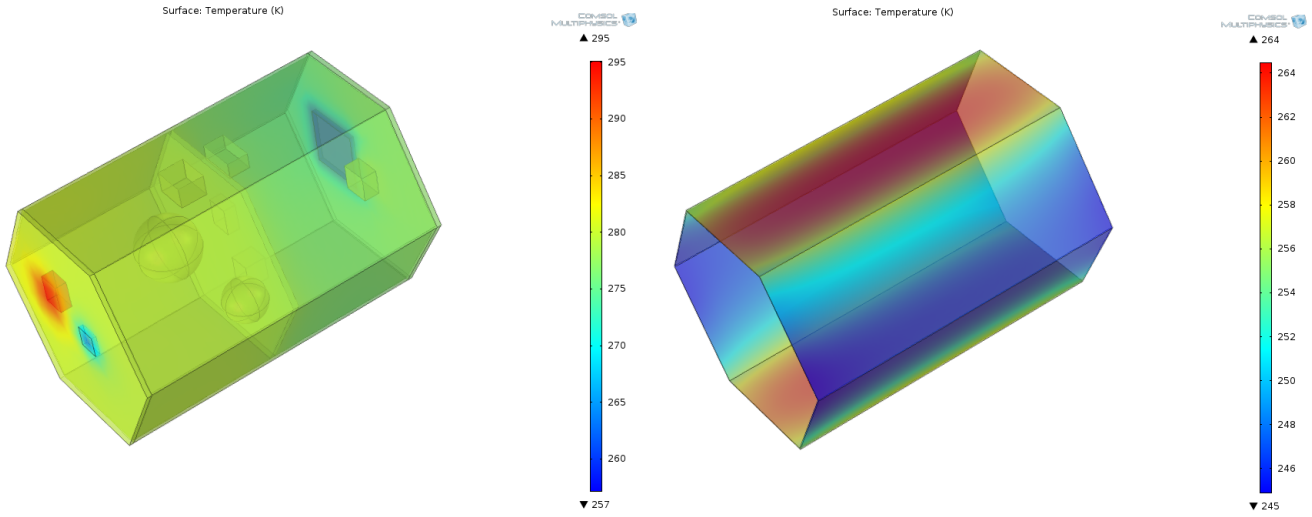

Figure 10.5: Orbit-average worst case cold temperatures for the satellite structure (left) and solar panels (right).

For the WCC, the temperatures also differ quite a bit with the first-order estimation. Once again, insulation is the reason for the difference.

Table 10.10 lists the WCH and WCC temperatures for some of the modelled components. All components listed were mounted to the spacecraft structure, except for the Xenon fuel tank, as this would have required the design of a mounting structure rather than the sphere it was modelled as. As a result, the Xenon fuel tank does not include the effect of conductive heat transfer, even though the panel on which it was mounted is a highly conductive panel.

Table 10.10: WCH and WCC temperatures for a number of satellite components that were modelled

	Accelerometer	IPCU	GPS	GUVI	Xenon	Cold Gas
WCH Temp	303 K	322 K	301 K	317 K	304 K	304 K
WCC Temp	279 K	279 K	280 K	294 K	279 K	279 K

10.2. Thermal Design

In general, it is more desirable to control the spacecraft temperature with passive thermal control rather than active thermal control if feasible (when there are no huge weight penalties, for example). For the MIRALOS mission, power consumption has to be limited since the choice of an ion propulsion system along with the fact that the solar panels cannot be easily oriented (because they are body mounted) means that the power budget needs to be carefully controlled. Furthermore, the satellite has a large volume with a lot of space inside for components, so careful component placement should be able to solve most of the thermal problems. For these reasons, the design of the thermal control subsystem for the MIRALOS mission should focus on passive methods.

This section describes the thermal control system on hardware level based on the results obtained from Section 10.1.

10.2.1. Radiator Selection

Based on the isothermal WCH analysis seen in Section 10.1.4, a preliminary estimate can be made regarding the required radiator area [17]. This calculation assumes no environmental heat input at T_{max} with maximum heat dissipation by the spacecraft components. Since the lithium-ion battery needs to be below 25 °C this is taken as the desired T_{max}. This leads to Equation (10.15) where A_r is the radiator area and ϵ_r is the emissivity of the radiator surface finish.

$$\frac{Q_w}{A_r} = \sigma \cdot \epsilon_r \cdot T_{max}^4 \tag{10.15}$$

The radiator surface finish should be a material with high IR emissivity over solar absorption ratio. A very good candidate material would be quartz-mirror which has an emissivity of 0.88 and an absorptivity of 0.05. Using these values yields a radiator area of 0.4 m^2.

To be most effective, the radiator should be placed facing zenith direction. This is due to the fact that the Earth radiates a large amount of IR radiation, which gets absorbed by the radiator, while the IR radiation received from the Sun is only 3.3% of its total radiated power (see Section 10.1.2); this is about 90% less than the IR radiation received from the Earth. On the other hand, the COMSOL model shows that the carbon-carbon panel inside the spacecraft effectively divides the spacecraft into two

separate thermal environments, although the conduction through this plate is high so the temperature difference between the compartments is limited. This may create the need for a nadir radiator surface in addition to a zenith radiator. For compensation, the zenith radiator surface should be reduced accordingly, to keep the overall thermal balance intact.

Since the spacecraft structure is an Aluminium honeycomb core with CFRP face sheets with a low thermal conductivity, a conductive path from the spacecraft interior wall towards the spacecraft exterior wall is required. The conduction through the sandwich panel is done in the following way: on the structure inside, a thermal doubler is placed. From the thermal doubler, heat pipes go through the structure towards the radiator on the outside of the structure. Another possibility would be to see if a more conductive (especially in the plane direction, to spread out the heat) material can be used for the top and bottom panels of the structure, so that the spacecraft structure may be used as a radiator.

10.2.2. Thermal Blanket Selection

The temperature of the spacecraft can vary significantly throughout the orbit. Even when no eclipse occurs, the spacecraft has significant temperature differences between the shadow and sun sides. This is not favourable for maintaining the functioning of the spacecraft's internal components. The spacecraft also carries an accelerometer with a temperature stability requirement of 10 mK in 200 s. It is therefore required to protect the internal structure against temperature variation. This is accomplished through insulation.

The common method of insulating a spacecraft is through the use of MLI. The typical composition of a MLI blanket is depicted in Figure 10.6. The reflector/spacer layers are usually sheets of metalised kapton. kapton is a very good insulator material because of its low conductivity of 0.12 W/m·K [125]. As an illustrative comparison, this is 0.059% of the conductivity of aluminium.

Gilmore [115] provides Equation (10.16) to calculate the effective emittance of a MLI blanket of N noncontacting layers of emissivities ϵ_1 and ϵ_2 on opposite sides. If the desired emissivity is known, the number of required layers is computable using Equation (10.16). Using a minimum design temperature of 20 °C because of the Xenon fuel tank and minimum spacecraft waste heat production (see Table 10.5), a required emissivity of $4.375 \cdot 10^{-3}$ is obtained from Equation (10.17). The layers are taken to be aluminised kapton with emissivities of 0.57 and 0.02 for kapton and aluminium, respectively [126]. Applying Equation (10.16), it is concluded that at least 4 layers of aluminised kapton are required.

However, the driving requirement for the MLI blanket is degradation due to atomic oxygen. This is especially critical for the areas that are not covered by solar panels. The worst-case scenario would occur at the lowest altitude, where the atomic oxygen density is highest. At 350 km altitude, the oxygen density is about 10^9 atoms/cm^3. Multiplying this value with the orbital speed and orbital period yields a flux of $4.223 \cdot 10^{18}$ atoms/cm^2 per orbit. With a lifetime of 6 years and a degradation of kapton of $2.6 \cdot 10^{-24}$ cm^3/atom, the total degradation accommodates to 3.8 mm in the spacecraft lifetime. Therefore, to be on the safe side, around 4 mm of kapton should be used. However, more research by materials-science specialists should be performed in a later stage to get a more precise estimation.

$$\epsilon = \frac{1}{\frac{1}{\epsilon_1} + \frac{1}{\epsilon_2} - 1} \cdot \left(\frac{1}{N+1} \right) \tag{10.16}$$

$$\epsilon_{req} = \frac{Q_{w,min}}{\sigma \cdot A_{total} \cdot T^4_{max,design}} \tag{10.17}$$

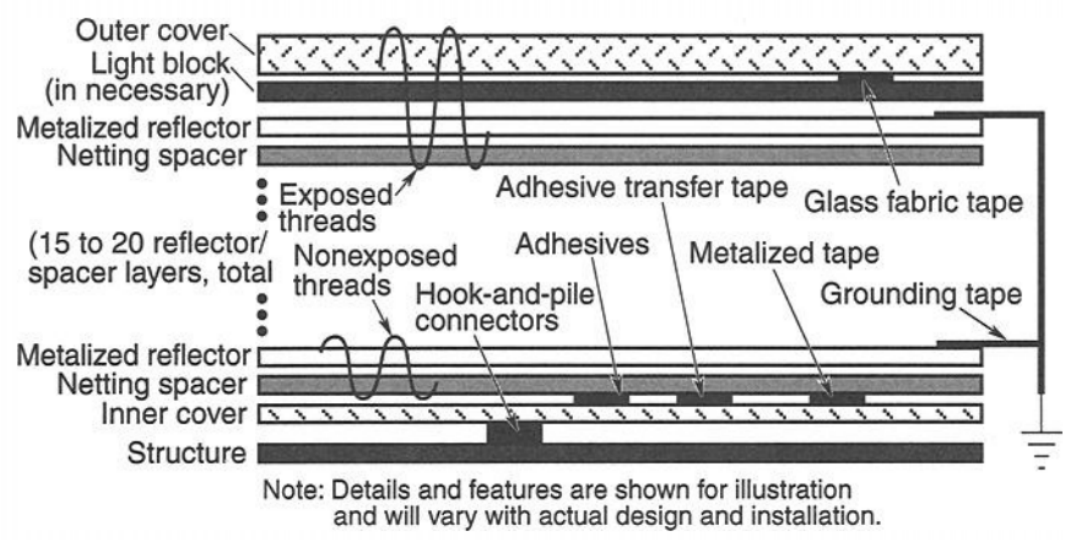

Figure 10.6: Composition of a typical MLI blanket [115]

10.2.3. Thermal Control of Instrumentation

The sole purpose of thermal control is to keep all the spacecraft components at their designed operating or survival temperatures, depending on the active spacecraft mode. Figures 10.7 and 10.8 show the the minimum temperatures of a selection of the spacecraft subsystems in the coldest operating mode and survival mode, respectively. This provides the insight that most components need heating. Table 10.11 shows an overview of the components with known temperature ranges and whether or not they need heating. Since the table is the same for Operating Mode (OM) and Survival Mode (SM), the two tables are merged.

The most critical component regarding temperature stability is the accelerometer. Since it requires a very stable temperature the accelerometer unit has to be insulated. This will most likely be done using MLI. To keep the accelerometer at operating temperature, some heating is necessary. However, the slightest addition of heat to the accelerometer will compromise its stability requirement. Therefore the environment around the accelerometer shall be heated instead of the accelerometer itself. More extensive research should be done in the future to ensure a stable environment for the accelerometer and minimise the effect of fluctuations in waste heat of the surrounding components.

Table 10.11: Heating required when components are marked with X

Part	OM/SM
Star Sensor	
Magnetometer	
Sun Sensor	X
Cold-gas thruster	
Lithium-Ion battery	X
Power Regulator Unit	

Part	OM/SM
Antennae	X
Transceiver	X
Solar Panels	
CPU	
Onboard Computer	X
Accelerometer	X

Part	OM/SM
Ion Thrusters	
ECU Thrusters	X
Thruster Feedsystem	X
Xenon fuel tank	X
GUVI	X
Cold gas tank	

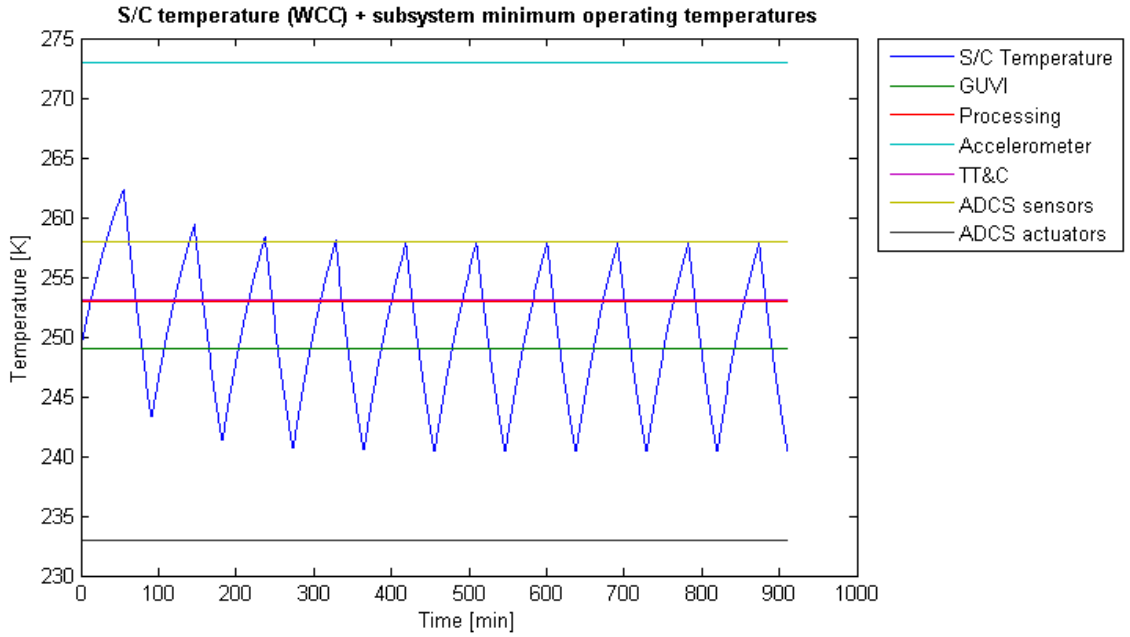

Figure 10.7: Spacecraft temperature and minimum temperature of selected components - Cold Case (minimum operating temperatures)

10.2.4. Thermal Management Hardware

At this stage in the design, it is still too soon to commit to either passive or active thermal control. Active thermal control is more expensive and complex than passive control, but it does have some very significant advantages. In multiple occasions satellite missions have been saved by active thermal control, since it is possible to update the thermal management from ground. However, since active thermal control is more complex it is also more prone to failure. Therefore redundancy has to be built in. An example of a typical layout of the heater system is depicted in Figure 10.9. Even though passive control might be used for the gross of the thermal management, some form of active control will most likely be implemented to control the components with strict temperature requirements, such as the accelerometer.

10.2.5. Power Requirement

Because many parameters are yet unknown for the thermal subsystem design, a rough estimation has to be made regarding the power usage.The temperature of the spacecraft is around the operational temperature range during worst-hot case. The low end of the spacecraft temperatures is during maximum eclipse safe mode. The order of magnitude of the difference between

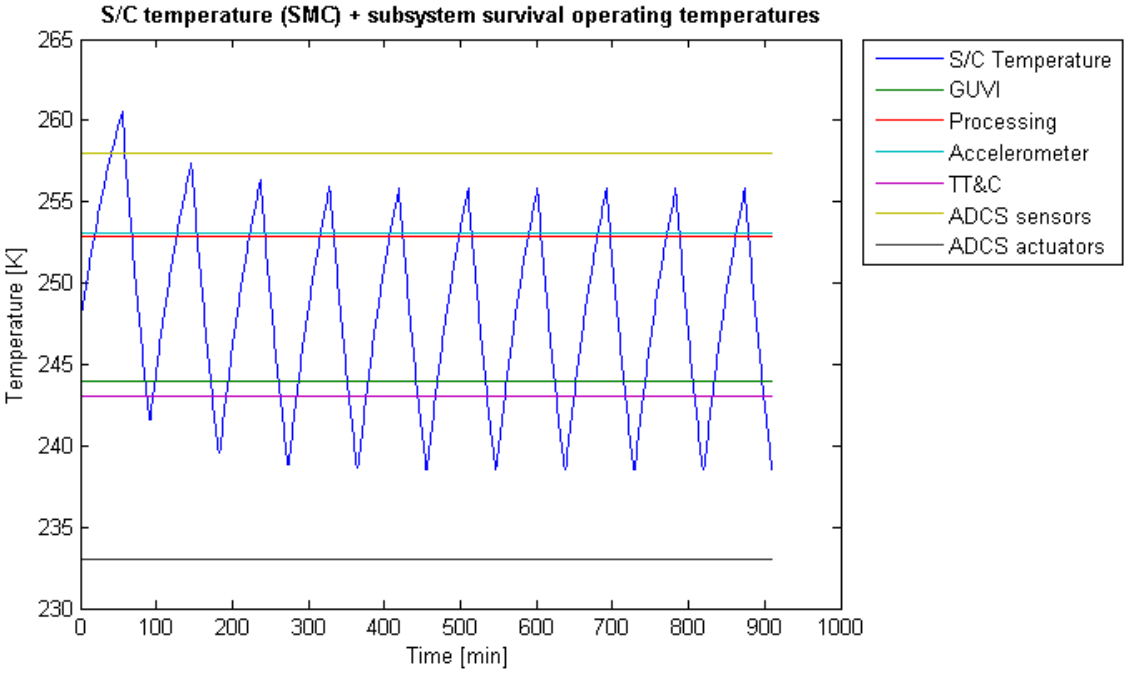

Figure 10.8: Spacecraft temperature and minimum temperature of selected components - Safe Mode Case (minimum survival temperatures)

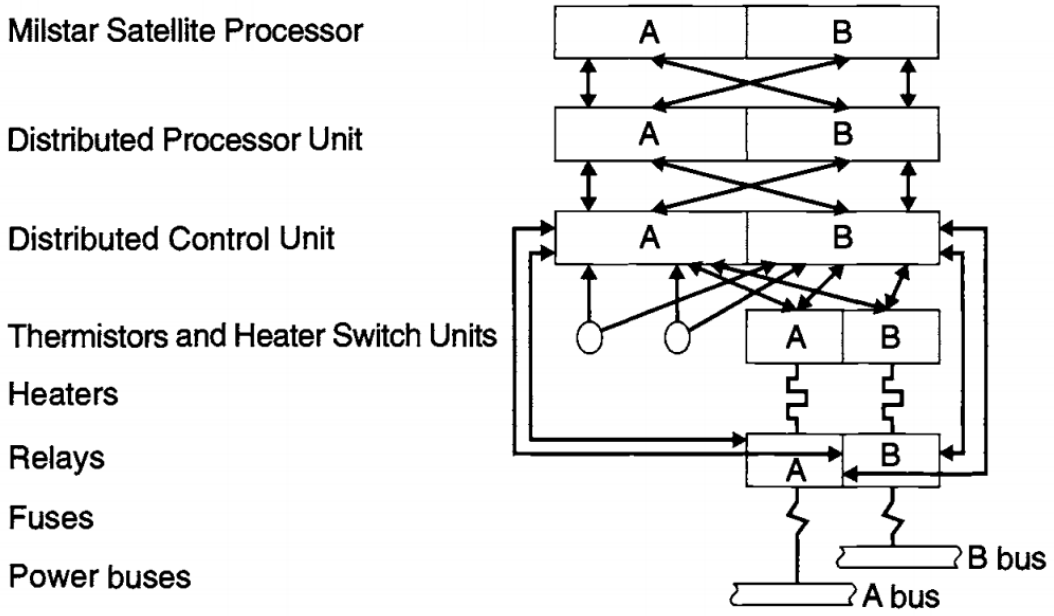

Figure 10.9: Heater-system redundancy example [115]

these cases, 100 W, was chosen as a preliminary power estimation. However, since the spacecraft has a number of strict thermal requirements, a contingency of 50% was chosen for this stage of the design, resulting in a power budget of 150 W. At a later stage in the design, the internal components might be placed in strategic locations for optimal thermal management which would most likely significantly decrease the required power consumption.

11. Structural Analysis

This chapter presents the structural design of the spacecraft bus. Section 11.1 lists the requirements the structure must meet. The design process and selected geometry are presented in Section 11.2. The eigenmodes of the spacecraft are analysed in Section 11.3. Buckling performance is analysed in Section 11.4. An overview of the results and recommendations for further design are presented in Section 11.5.

11.1. Structural Requirements

The spacecraft bus structure must be strong and stiff enough to withstand the loads experienced during launch, as well as to provide a stable platform for mission operations once in space.

Among the various considerations influencing structural design are:

Launch loads - During launch, the spacecraft will experience high g loads, in both longitudinal and lateral direction. The structural elements must be strong enough to prevent failure in compression and buckling. The magnitude of these loads depend on the launch vehicle and the flight profile. For the Dnepr launch vehicle, the maximum loads experienced during launch are 8 g and 1 g in the longitudinal and lateral directions, respectively [127]. Accelerations for other launch vehicles are below these values.

Vibration - During launch, the spacecraft will be subjected to vibration loads by the launch vehicle. In order to prevent vibrational coupling, the lowest eigenfrequency of the spacecraft must be higher than the frequency of launch vehicle vibrations. For the Dnepr launch vehicle the eigenfrequencies of the spacecraft should be higher than 20 Hz in the longitudinal direction and higher than 10 Hz in the lateral direction. To maintain flexibility in launch vehicle selection, a safety margin of 2 will be applied.

Thermal stability - In order to obtain acceleration measurements with the required accuracy, the location of the accelerometer needs to be very precisely controlled. This requires the accelerometer mounting bench to exhibit low thermal expansion, and preferably the rest of the spacecraft structure as well.

Weight - To obtain accurate acceleration measurements, the weight of the spacecraft should be as low as possible. Because MIRALOS is significantly larger than other spacecraft of the same weight class, the weight of the structural components represent a large percentage of dry mass.

Manufacturability - While the level of detail in the structural design remains limited in this design phase, some consideration has to be given to the constraints imposed by manufacturing concerns. Among other things, this influences the minimum thickness of the various components.

11.2. Structural Design

The structural elements of the spacecraft are comprised of honeycomb sandwich panels, with the outer skin panels forming a load carrying structure. For the central hexagonal floor supporting the accelerometer, both the skin and the honeycomb structure are made from a quasi-isentropic Carbon Fibre Reinforced Carbon Matrix (Carbon-Carbon) composite. A similar design was used for the accelerometer bench for GOCE, because of the extremely low coefficient of thermal expansion exhibited by this material. All other structural panels use quasi-isentropic Carbon Fibre Reinforced Cyanate Ester Composite (CFRCE) skin panels and aluminium 7076 T6 honeycomb structures. Material properties for these materials are given in Table 11.1.

Table 11.1: Structural component material properties

Material	**Youngs Modulus** [GPa]	**Density** [kg/m3]	**Coefficient of thermal expansion** [μstrain/mK]
Carbon-Carbon	100	1700	-0.15
CFRCE	110	1650	13.6
Al 7076 T6	69	2800	22.9

Figure 11.1 displays the arrangement of the major structural components of the spacecraft bus. Stacked in longitudinal direction (relative to the launch vehicle) are three hexagonal floors and 2 hexagonal stiffeners. The middle hexagonal floor is the carbon-carbon mounting bench for the accelerometer. Each hexagonal floor is supported by a rectangular stiffener. The purpose of these and the hexagonal stiffeners is increase the eigenfrequencies of the panels they are mounted on. The outer surfaces of the spacecraft are formed by the upper and lower hexagonal floors and six rectangular panels.

Table 11.2 provides a breakdown of the spacecraft structure and lists the size and weights of each panel.For both the carbon-carbon and the aluminium honeycomb structures, a honeycomb side length of 5 mm and a wall thickness of 0.5 mm are assumed. The resulting honeycomb has a volume density of 11.5%. A 10% weight margin is added to the sum of the panel weights to account for brackets, bolts and local reinforcement of the honeycomb panels at mounting locations.

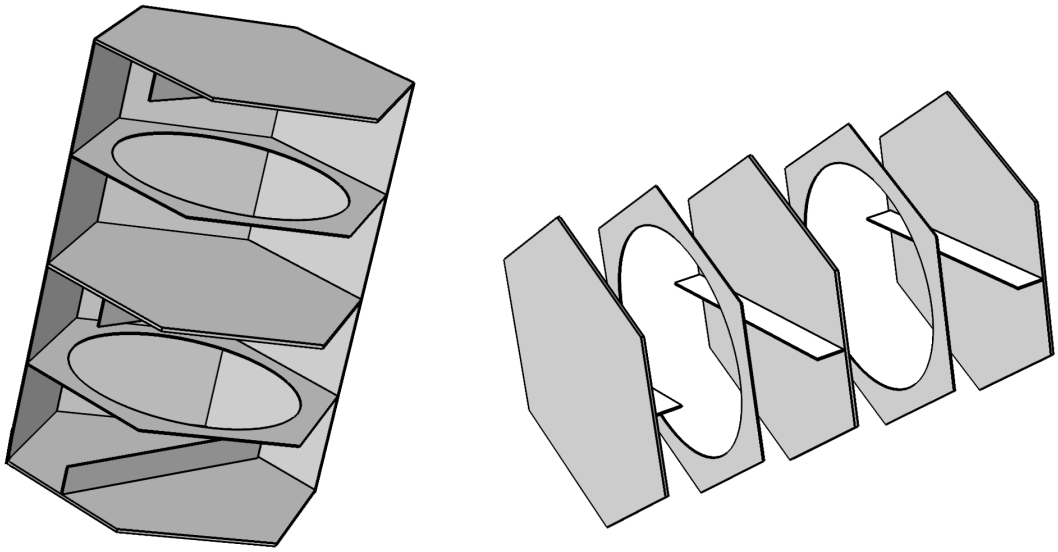

Figure 11.1: Schematic representation of the major structural elements of the spacecraft bus

Table 11.2: Spacecraft structural breakdown

Component	**#**	**HC height** [mm]	**Skin thickness** [mm]	**Weight** [kg]	**Total weight** [kg]
Hexagonal Panel (CFRCE / Alu core)	2	40	1	40.9	81.8
Rectangular Panel (CFRCE / Alu core)	6	10	1	18.9	113.4
Accelerometer Bench (Carbon-Carbon)	1	50	1	33.8	33.8
Hexagonal Stiffener (CFRCE / Alu core)	2	10	1	6.5	13.0
Rectangular Stiffener (CFRCE / Alu core)	3	15	1	2.6	7.8
				Total Weight	249.8
				10% margin	25.0
				Final Weight	274.8

11.3. Finite Element Analysis

Accurately estimating the structural properties of a honeycomb sandwich structure is computationally intensive. Therefore, a number of simplifications have been made to analyse the eigenfrequencies of the spacecraft structure.
First, it is assumed that normal stresses are only carried by the skin. Under this assumption, the moment of inertia of the panel used for the purposes of buckling and vibration analysis is provided solely by the steiner terms of the moment of inertia due to the panel skin:

$$I = 2bt_s(\frac{h}{2})^2 \tag{11.1}$$

Where b is the panel width, t_s is the skin thickness and h is the thickness of the honeycomb structure. Neglecting any contribution from the honeycomb structure is conservative. If the honeycomb is assumed to have a contribution that is equal to a solid section weighted by the honeycomb volume density, it would contribute between 10% and 50% of the total moment of inertia, depending on panel geometry.

To analyse the vibrational eigenmodes of the structure, the finite element analysis tool COMSOL is used. analysing the actual honeycomb geometry would be very intensive computationally, which is why the honeycomb sandwich panels are modelled as solid plates with equivalent properties. The natural frequency of a structure is a function of its mass and stiffness. The thickness of an equivalent solid plate is determined by equalizing its moment of inertia:

$$\frac{1}{12}bt_e{}^3 = I = 2bt_s(\frac{h}{2})^2 \tag{11.2}$$

$$t_e = \sqrt[3]{6t_s h^2} \tag{11.3}$$

Where t_e is the equivalent solid panel thickness. The weight of the panel is then divided by length, width and equivalent thickness to obtain an equivalent panel density.

A model of equivalent solid plates has been constructed with proof masses attached to the appropriate panels, to simulate the weight of the attached instruments and systems. The side edges of the lower hexagonal plate were constrained to be fixed to simulate the connection to the launcher stage.

The vibrational response of the model was analysed in COMSOL. The resulting eigenfrequencies are listed in Table 11.3 for the first six modes. The lowest eigenmode of the spacecraft is the lateral vibration of the skin panel where the thruster assembly is attached, with a frequency of 96 Hz. The lowest longitudinal mode occurs at the upper hexagonal panel at 101 Hz. These lowest lateral and longitudinal eigenmodes are displayed in Figure 11.2. The finite element software finds the eigenmodes by solving for an amplitude response that tends to infinity, so the absolute values of the displacements it finds are nonsensical. For that reason, no scale is given in the figures.

Table 11.3: Eigenmodes and frequencies of the spacecraft

Direction	Location	Frequency
Lateral	Thruster panel	96 Hz
Longitudinal	Upper hexagonal panel	101 Hz
Lateral	Instrument panel	114 Hz
Longitudinal	Lower hexagonal panel	120 Hz
Longitudinal	Accelerometer bench	135 Hz
Longitudinal	Upper hexagonal panel	145 Hz

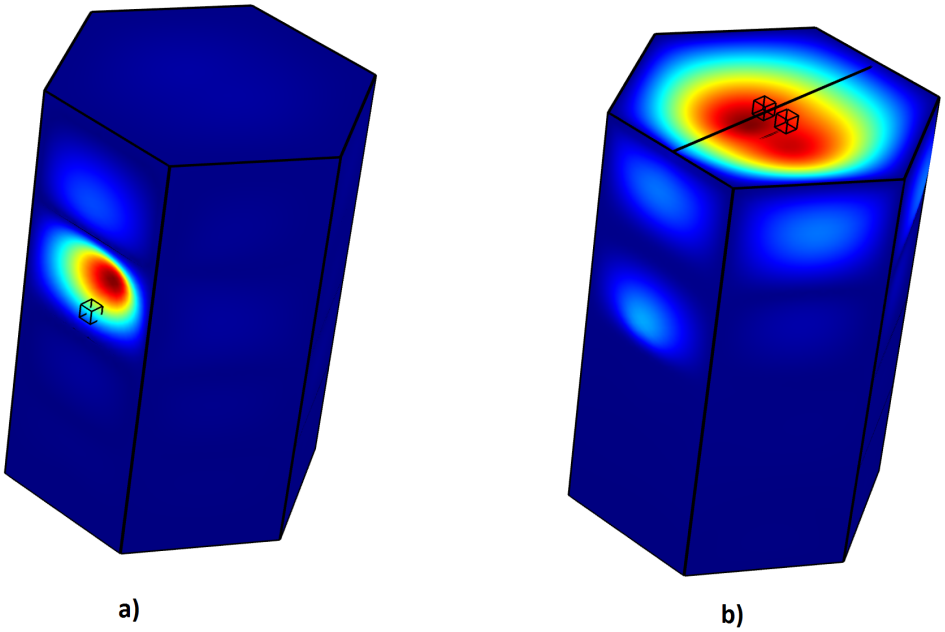

Figure 11.2: Lowest vibrational eigenmodes of the spacecraft. Panel a displays the lowest lateral eigenmode with a frequency of 96 Hz. Panel b displays the lowest longitudinal eigenmode, with a frequency of 101 Hz.

11.4. Buckling Analysis

To analyse the critical buckling load of the spacecraft, again the assumption is made that only the panel skins carry direct stresses. The panel moment of inertia is then given by Equation (11.1). The critical buckling stress is given by:

$$\sigma_{cr} = \frac{P_{cr}}{A} = \frac{\pi^2 EI}{L^2} \frac{1}{2t_s b} \tag{11.4}$$

Where A is the cross-sectional area of the panel and L is the length between supports. The critical buckling stress for one of the six outer panels at the base where the spacecraft is connected to the launcher stage is given by Equation (11.4) as 48.2 MPa.

In Equation (11.4) it is assumed that the panel can be treated as a column clamped at one end and simply supported at the other. In reality, the panels are fastened together at all edges, but only at discrete points. The resistance of the structural panels to column buckling will therefore be better than predicted by Equation (11.4), but it is not straightforward to estimate by how much.

The maximum accelerations experienced during launch are 8 g in the longitudinal direction and 1 g in the lateral direction. The maximum normal stress induced by these loads occurs in one of the six outer panels at the location where the spacecraft is connected to the launcher. At this critical point, the combination of the stress due to the axial load and the stress due to the bending moment induced by the lateral acceleration is maximum.

Assuming the axial load is evenly distributed over the six outer panels, the stress in the critical point, after applying a safety factor of 2, is given by:

$$\sigma_{axial} = \frac{2 \cdot 8gW}{6 \cdot 2t_s b} \tag{11.5}$$

Where W is the weight of the spacecraft. The resulting stress due to axial loads at the critical point is 5.4 MPa.

To estimate the normal stress due the bending moment introduced by the lateral acceleration, the spacecraft is modelled as a hexagonal shell with thickness $2t_s$. The lateral acceleration is modelled as a load equal to the spacecraft's weight, applied at the centre of gravity. The normal stress, after applying a safety factor of two, is then given by:

$$\sigma_{lateral} = \frac{My}{I} = \frac{2 \cdot gW\frac{L}{2}}{\frac{5\sqrt{3}}{16}(b^4 - (b - (2t_s)^4)} \tag{11.6}$$

The resulting normal stress due to the bending moment is 2.2 MPa. The total normal stress at the critical point is then 7.6 MPa.

11.5. Structural Optimisation

Table 11.4 displays a summary of the structural performance of the spacecraft. The required performance values include a safety margin of 2, so the margin factor reports overperformance in excess of this margin. In the case of both the minimal eigenfrequencies as well as the maximum experienced stresses, there is a large margin of safety. This implies that the structure is overdesigned, and could be made lighter while still maintaining sufficient performance.

In the case of the buckling analysis, the critical stress relation used assumes the panel can be represented as a column clamped at both ends. In reality, the skin panels are fastened to each other by brackets and bolts at all edges, but only at discrete points. This will force the panel to buckle in a more complex mode than simple column buckling, and the actual critical buckling stress will therefore be higher.

It should be noted that the analysis in this chapter has been done on a much simplified representation of the structural design. In particular, the honeycomb sandwich structures have been replaced by equivalent solid skin panels, and it is not known what degree of inaccuracy this introduces. Furthermore, there are a number of failure modes which have not been investigated. These failure modes include local skin buckling, detachment of the skin from the honeycomb structure, failure of the honeycomb structure in shear or compression, and failures at the locations where the components are fastened together.

It is our recommendation that a much more detailed structural analysis is performed at the next stage of the design, which takes into the account the concerns discussed in this section. At present, the structural design is a rough initial estimate which is likely to be heavier than a more optimized design could be.

Table 11.4: Structural performance of the spacecraft

Requirement	Required value	Actual Value	Margin factor
Lateral eigenfrequency	20 Hz	96 Hz	4.8
Longitudinal eigenfrequency	40 Hz	101 Hz	2.5
Normal stress	< 48.3 MPa	7.6 MPa	6.4

12. Command & Data Handling

The Command & Data Handling (CDH) subsystem is the 'brains' of the satellite. It carries out commands and commanded manoeuvres, and manages the flow of data collecting and processing all information from the subsystems and payload. It also keeps and distributes the spacecraft's time. The requirements for the C&DH mainly flow from the communications subsystem. They will be discussed in Section 12.1. The C&DH is carried out by the OBC discussed in Section 12.2. The OBC is responsible for carrying out the function of attitude and orbit control, telecommand implementation, housekeeping telemetry processing, on board time synchronisation and distribution, failure detection, and more [128]. For the scope of this exercise, only flight-proven instances of onboard computers and processors are examined. The CPU is selected in Section 12.3. The Remote Terminal Unit (RTU) is considered in Section 12.4. A few exemplar functions of the latter include the gathering of telemetry from temperature and pressure sensors, and control of the AOCS actuators and sensors.The C&DH functions are displayed in Figure 12.1.

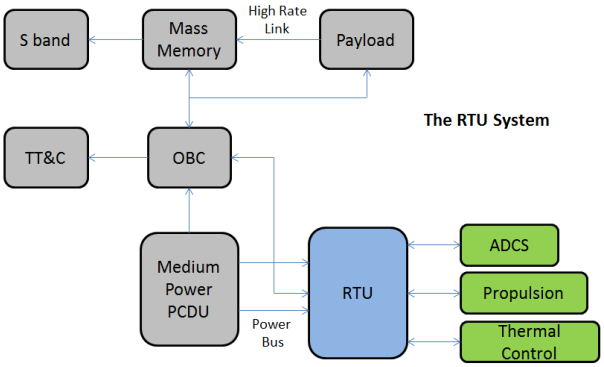

Figure 12.1: Diagram of the spacecraft's avionics. The OBC, Medium Power PCDU and RTU together form the C&DH.

12.1. Requirements

The design of the command and data handling system is driven by requirements following from the communication subsystem. As already mentioned, the data collection and processing is one of the main functions of the C&DH. Therefore, most of the requirements will be driven by the data rate.

As can be seen from Table 13.3, the total data rate of the satellite equals 36 kbit/s. The satellite will make contact with a ground station at least once every 12 hours for the transmission of the data. Under the assumption the satellite sends all of its data down during communication with the ground station, the data storage of the C&DH can be calculated as shown in Equation (12.1), resulting in a minimum computer memory of 219 MB. During the mission lifetime of six years, the amount of transmitted data will have accumulated to a value of 937 GB.

$$Memory = 41.5 \frac{\text{kbit}}{\text{s}} \cdot 12 \cdot 3600\,\text{s} = 1792800\,\text{kbit} = 224100\,\text{kB} = 218.84\,\text{MB} \approx 219\,\text{MB} \tag{12.1}$$

An additional requirement can be set up by analysing the CPU clock speed. Unfortunately no information about the required computing power has been found yet. Some logical limits however can be set to the CPU clock speed. For example the purpose of the mission can reveal its computational power. The CPUs for computationnaly intensive missions, like communication satellites and imaging missions, typically require clock speeds of over 200 MHz. Therefore an upper limit for the clock speed of the CPU used for the MIRALOS mission has been set to 200 MHz.

12.2. On Board Computer

A number of satellite OBCs are reviewed, however the limited amount of available information for the subsystem impedes a detailed analysis. The uncovered specifications of each product are presented in Table 12.1. For each, relevant satellite missions that made use of the particular product are cited.

The SCS750 produced by Maxwell Technologies is a single board computer (configurable for dual redundancy) with an IBM PowerPC processor [129]. The SCS750 was used on board the Glory satellite, an Earth-climate and atmospheric monitoring mission launched in 2005 [130]. Similar to the SCS750, the OBC750 is used onboard LEO satellites. This OBC is included mainly on imaging missions such as the KazEOSat-2, designed for wide-swath multispectral imagery, launched in 2009 [131]. Another

computer used in imaging missions is the OSCAR computer. It is produced by Airbus Defence and Space. The computer was implemented on the Spot-6 and 7 commercial imaging satellites, and the Spanish optical high-resolution imaging mission SEOSat [132] [133]. Lastly, information was retrieved on the OBC of GOCE, however information was mingled between the properties of the computer and that of the CPU [88].
The values presented with an asterisk in Table 12.1 are estimated values. The selected criteria for the trade-off are mass, power, Million instructions per second (MIPS) at a specified frequency, ram memory size, included redundancy, and temperature range.

Table 12.1: List of the on board computers to be compared

Computer	Mass [kg]	Power [W]	MIPS [@ MHz]	Memory [Mbyte]	Redundancy	Temperature Range [°C]
SCS750	1.5	7.5	1800 @ 800 200 @ 400	256	Included	-30 to +65 (op.) -40 to +70 (non-op.)
OBC750	2.5	20	1333	16	Included	-20 to +50 (op.) -30 to +60 (non-op.)
OSCAR	5.2	15	26 @ 32	256	Included	-40 to +85 (op.)
GOCE	5*	10* (CPU 1W)	17 @ 24	2x500	Included	-40 to +80* (CPU -55 to +125 op.)

Based on the above specifications and provided mission profiles, the SCS750 is selected as the better alternative to be used as the on board computer of MIRALOS. The SCS750 requires the least power and mass, while meeting the memory requirement of 219 MB. Although the mentioned OBCs are provided with their own CPU, it might be of interest to examine these individually. The SCS750 built-in CPU is oversized with its 400 or 800 MHz. Therefore the CPU unit will be replaced by a more suitable one, aiming to increase the flexibility of the design. This investigation is done in the next section.

12.3. CPU

Assuming that the processor unit of the previously mentioned OBCs can be interchanged, this section looks at the different products which could stand as good competitors of the already incorporated processing unit inside the SCS750. The specifications of each CPU are presented in Table 12.2; the values followed by an asterisk show estimated quantities. Note that Table 12.2 only contains CPUs with a clock speed smaller or equal to 200 MHz.
Starting off, the Motorola PowerPC 603e CPU was a processor used on the Gravity Recovery and Climate Experiment mission [134]. Next, the PowerPC 750 was used in the three (cancelled) TechSat-21 missions, designed for a 560 km altitude orbit formation-flying mission [135]. Looking into older designs, the Dynex MAS31750 was incorporated into the computer design of Rosetta, a satellite designed to carry comet composition measurements [136]. It was also used on the Double Star satellite, studying the Earth's magnetosphere, and the EnviSat, designed to carry out Earth observation activities including in-situ composition measurements.
Based on the PowerPC 750, the RAD 750 processor (successor of the RAD 6000) is used on several missions such as WorldView-2, a commercial satellite designed for high-resolution imagery, but also on technology-demonstrating satellites such as the XSS-series designed by the US Air Force Research Laboratory. The RAD 5500, successor of the RAD 750, will provide a tenfold improvement on performance by integrating new technology advancements. This product however will not be used in this trade-off due to its low technology readiness.
Another processor, used in flight and technology-demonstrating satellites, is the Leon3-FT. A mission that made use of the processor was the Prototype Research Instruments and Space Mission technology Advancement (PRISMA) mission, flying in a sun-synchronous orbit of 720 km altitude. The last processor examined is the Spacecube 2.0, an autonomous hybrid processor/computer system able to provide up to 25 times the processing power of the RAD 750 [137]. The technology readiness level of this system was raised through the Small Demonstration Satellite-1 (SDS-1), Small Rocket/Spacecraft Technology (SMART), and Intelligent Payload Experiment (IPEX) missions. The SDS-1 and IPEX satellites were introduced in a sun-synchronous orbit at 666 km and 1080 km respectively, while the SMART satellite flew in a circular orbit of 400 km altitude.

Table 12.2: Characteristics of the compared processors

CPU	CPU [MHz]	Power [W]	MIPS [@MHz]	Memory [Mbyte]	Cross-area [mm^2]	Temperature range (op.) [°C]
Motorola PowerPC 603e	200	4.5	283 @ 133	8	81	−55 to +125 *
PowerPC 750	500	6	175 @ 133	128	40	−55 to +125
Dynex MAS31750	25	15	3.5 @ 25	256	80 *	−55 to +125
RAD 750	200	3.5*	400 @ 200	128 *	130	−55 to +125
Leon3-FT	33	7 *	100 @ 33	64	80 *	−55 to +125 *
Spacecube 2.0	200	15	4400 @ 200	16 x 512	127×127×178 mm [Volume]	−40 and 100 *

In terms of performance, the Motorola PowerPC 603e, the RAD 750, and the Spacecube 2.0 are the more attractive options. However Spacecube 2.0 provides a much higher MIPS value, this traded-off for power consumption. Based on the initial power distribution requirement per subsystem, defined in the early stages of the report, a power of 15 W lies beyond the set upper bound for the quantity. From the two remaining options, the RAD 750 consumes less power, and has comparative values to Motorola's PowerPC. Nevertheless, it is important to note that the value for power and memory for the RAD 750 are estimates. To minimize uncertainties in the design, the Motorola PowerPC 603e is finally selected.

12.4. RTU

Remote Terminal Units are usually found on medium to large-size satellites. An investigation and pre-selection of an RTU will be carried out in this section. Detailed information could only be extracted from two products, thus the preliminary trade-off will be set up solely based on these. The two considered RTUs are the ASP55, manufactured by Airbus Defence and Space, and the BU-63705, produced by Data Device Corporation. The specifications of these can be found in Table 12.3.

Table 12.3: Properties of the compared Remote Terminal Units

RTU	Mass [g]	Power [W]	RTU [MHz]	Cross-area [mm]	Temp. Range (op.)
ASP55	9	0.25	10	30 x 30	−55 to 150 °C
BU-63705	48.2	2	16	45.7 x 53.3	−55 to 125 °C

The ASP55 appears to be a better option than the BU-63705, yet the latter provides a better performance in terms of MHz. The mass, power, size, and temperature range are acceptable for both, the BU-63705 is selected based on performance.

13. Telemetry, Tracking & Command

This chapter contains the design of the communication subsystems and some of its components. In the Mid-Term Report [1] some preliminary design work concerning this subsystem was already done, in which a preliminary link budget was considered. Using the book of Couch [138] the main parameters of the link budget were considered and some preliminary values were computed. Five antennas were considered to be possible options for the MIRALOS mission. As an iteration on the work that was done in the Mid-Term Report, this chapter handles the second iteration of the communications subsystem. The subsystem is strongly influenced by the on-board processing system described in Chapter 12.

In Section 13.1 the general system layout is considered, in which a diagram is shown concerning the flow of the data from spacecraft transmitter to ground station receiver. This is not shown for the uplink, as it is similar to the flow diagram of the downlink (Figure 13.2). As part of the general system layout the spacecraft transmitter (for downlink) and the spacecraft receiver (for uplink) are considered and a device is chosen using a trade-off. Section 13.2 contains the link budget analysis, in which the preliminary design from the Mid-Term Report with its most important values is shown. Subsequently the link budget iteration is performed, where all changes in parameter values are shown and in which some new parameters are introduced. In Section 13.3 the results from this iteration are shown, an antenna is selected and the link budget is completed. Finally the ground segment is discussed, as this is a major part in the communications subsystem. The ground station selection is discussed in Section 13.4, whereas the operations and logistics are handled in Section 13.4.2

13.1. General System Layout

The preliminary design phase concluded, some detailed design can now be done. In the Mid-Term Report the communication system was briefly described and an overview from spacecraft sensors to ground segment data processors was given in the form of a flow block diagram, which is shown in Figure 13.1. In this diagram it can be seen that the CPU is the component which connects all sensors and actuators.

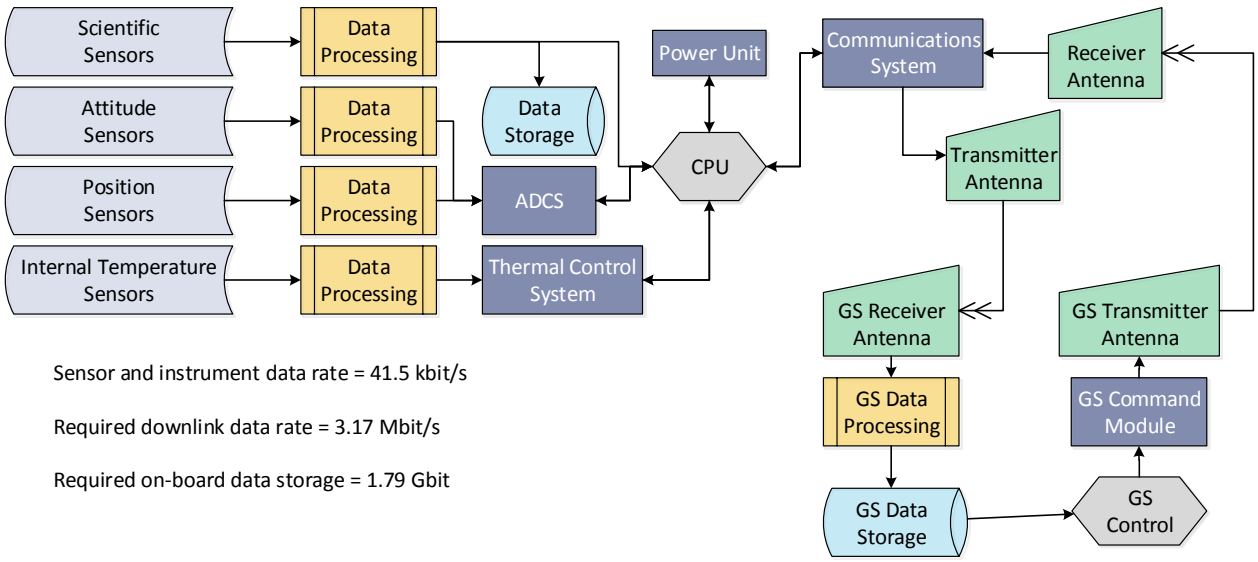

Figure 13.1: Data handling and communication flow diagram

The final design phase initiated, this overview can be expanded and divided into several different parts. The actual transmission and receival segment of the subsystem can be split into three important parts, which can be seen in Figure 13.2.

As depicted, the transmitter receives the input which consists of digital data sent by the Central Processing Unit (CPU). Because the data is already digital, no sampler, hold device, nor quantiser have to be used (these are only required for analog signals). This means that the input signal can directly be encoded (if necessary) and be sent to the transmitter circuit. When the signal is sent down to the ground segment, the free space in between the spacecraft and the ground station is denoted as the channel.

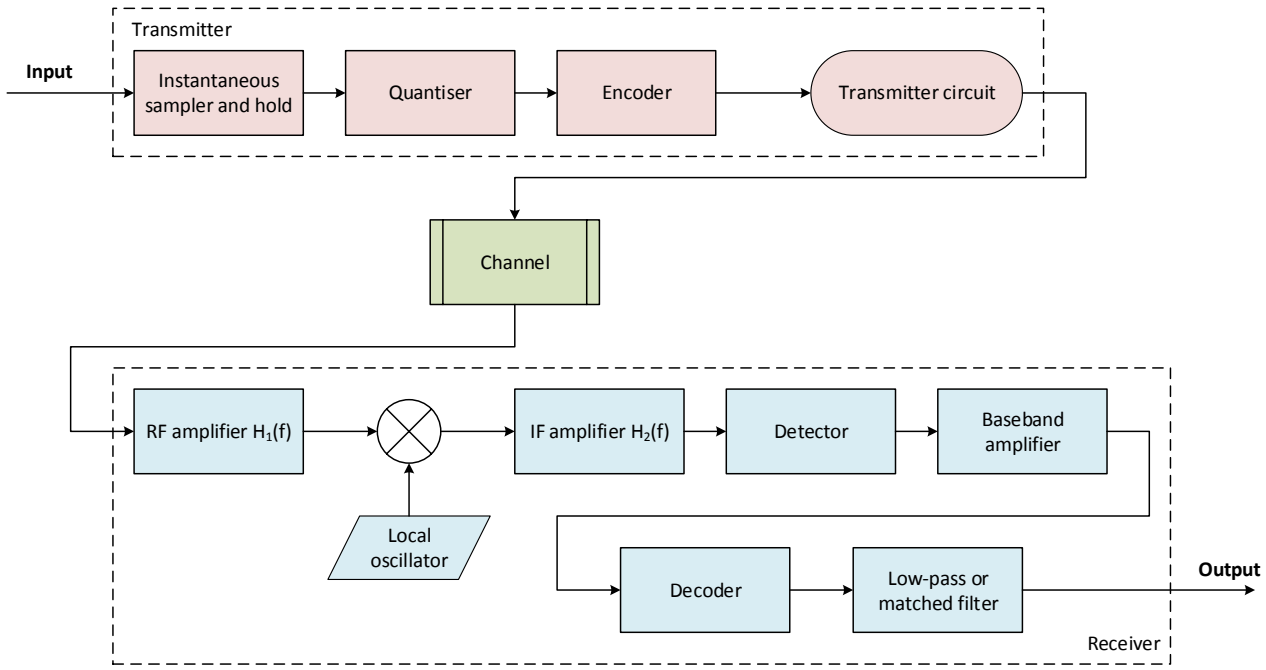

Figure 13.2: General overview of the transmission and receival segment [138]

After the signal is received it can be decoded if it was encoded at the spacecraft. A possible low-pass or matched filter can be used if necessary. The signal coming out of the receiver can be used for analysis.

Transmitter

In this paragraph the transmitter trade-off is done, in which five different transmitters are considered. The table that was made during this trade-off is shown in Table 13.1.

Table 13.1: Summary of the transmitter trade-off

Transmitter	SSTL	CS-CPUT-STX-01	ISIS TXS	T-711	STC-MS01
Company	Surrey Satellite Technology	Clyde Space	ISIS Space	L-3 Cincinnati Electronics	COM DEV Europe
Data Rate (high)	9.6 kbit/s - 8.0 Mbit/s	up to 2.0 Mbit/s	up to 100 kbit/s	up to 4.0 Mbit/s	up to 6.25 Mbit/s
Modulation Technique (low)	BPSK/QPSK	QPSK/OQPSK	BPSK/GMSK	BPSK	QPSK/OQPSK
Frequency Range (high)	2200 MHz - 2290 MHz	2400 MHz - 2450 MHz	2100 MHz - 2500 MHz	2200 MHz - 2300 MHz	2200 MHz - 2300 MHz
Consumption Power and RF Output Power (medium)	Consumption: 38.0 W RF Output: 4.0 W	Consumption: 6.0 W RF Output: 1.0 W	Consumption: 4.0 W RF Output: 0.63 W	Consumption: 192 W RF Output: 30 W	Consumption: 18 W RF Output: 2.2 W
Mass (medium)	1800 g	100 g	62.0 g	6600 g	780 g
Dimensions [mm] (low)	200x191x80	96x90.2x17	90x96x15	193x193x122	145x110x50
Temperature Range (medium)	253 K - 323 K	248 K - 334 K	N/A	239 K - 355 K	253 K - 333 K
Source	[139]	[140]	[141]	[142]	[143]

On the first row five different transmitters are listed, produced by the companies defined in the second row. The other rows contain trade-off criteria and the values per transmitter. The following colour coding is used: green = good, yellow = neutral, red = bad. The N/A (grey) means that the value for a specific parameter could not be found for a particular transmitter. Behind the trade-off criteria stated in the first column the weight of that particular criterion is placed between brackets (...). As can be seen, the data rate and the available frequency range are the most important criteria, because they are critical for the communications subsystem design. By summing all criteria it can be seen that one transmitter is more suitable than the others, which is the STC-MS01.

Receiver
In the previous paragraph the transmitter trade-off was done, in which the STC-MS01 was chosen to be the transmitter on the spacecraft. However, only the downlink process was considered. Next to the scientific data that are sent to the ground station, the ground station has to provide the spacecraft with for example commands and software updates. For this an uplink is required, in which a receiver has to be incorporated in the spacecraft design.

The chosen transmitter is a transceiver, which means that it can both transmit as receive signals. This means that no trade-off regarding the receivers has to be done.

STC-MS01
The transceiver that is used for the MIRALOS mission is the STC-MS01, produced by COM DEV Europe. It has the S-band receiving and transmission frequency range, which complies with the ESTRACK requirements [144]. The receiver has a 4.0 W power consumption, whereas the transmitter has a 14.0 W power consumption. It can provide an output power of maximum 2.2 W, using QPSK modulation. The data rate can be increased to 6.25 Mbit/s without any transmission problems. Its operation temperature range lies between -20 °C and 60 °C. Concerning the placing of the transceiver in the spacecraft, the line length has to be minimised in order to make the spacecraft line loss (as described in Section 13.2) as small as possible.

13.2. Link Budget Analysis
In this section the link budget calculations are elaborated on and the communications subsystem is designed in more detail. Section 13.2.1 contains a short recap of the preliminary design done in the Mid-Term Report [1]. In Section 13.2.2 the link budget iteration is performed, in which the link budget equation is considered again. Section 13.3 contains the results of all the work done in this section.

13.2.1. Preliminary Design
Before the more detailed design of the communications subsystem can be done, the results of the preliminary design are shortly discussed. First, a flow diagram of the subsystem was created, which has already been discussed in Section 13.1. Then the downlink and uplink budget were considered, in which several ground stations were discussed and the different parameters from the link budget equation were explained. Finally the visiting frequency and the memory size were computed, which completed the preliminary design of the communication subsystem. The results are revised in Table 13.2, in which the Kiruna Ground Station (KIR-1), FSK modulation and a bit error probability of 10^{-12} were assumed.

Table 13.2: Results of the Preliminary Link Budget Design

Parameter	Preliminary Value	Unit
f_c	2300	MHz
λ_c	0.130	m
d_{max}	1000	km
R_{instr}	27.6	kbit/s
G_{AR}/T_{syst}	27.7	dB/K
P_e	10^{-12}	-
G_{FS}	-171.1	dB
SNR	13.9	dB
T_{vis}	$5.4 \cdot 10^3$	s
R_{vis}	$2.3 \cdot 10^3$	kbit/s
M	1.2	Gbit

In the preliminary link budget the instrument data rate was used for calculations, because the orbit was not determined yet. After the orbit was determined the visibility time and data rate could be computed. However, there was not any time left for iterating the link budget calculations.

13.2.2. Link Budget Iteration
In the previous subsection a short recap of the link budget analysis was provided. In this subsection the second link budget iteration is done. First, the link budget equation is considered again [138]:

$$\left(\frac{E_b}{N_0}\right)_{dB} = (P_{EIRP})_{dB} + (G_{FS})_{dB} + \left(\frac{G_{AR}}{T_{syst}}\right)_{dB} - k_{dB} - R_{dB} \tag{13.1}$$

For every parameter the possible changes with respect to the first iteration are described. However, this first iteration only contained the parameters that were described in the book of Couch [138], which considered the preliminary link budget design. For the second iteration several additive losses were added in order to create a more precise link budget design.

Receiving antenna gain to system noise temperature

Considering the G/T values there is a change with respect to the preliminary link budget analysis. After the first iteration the Kiruna-1 Ground Station was used for an example calculation, however, the Svalbard Ground Station (SG-3) is selected for the mission. The reason for this is that the SG-3 has a higher latitude than the KIR-1, which enables more frequent contact periods. It is possible to use more than one ground station, but for the second iteration and the communication subsystem design it is assumed that only the SG-3 station is used and that the satellite contacts this ground station at least twice a day. The G/T value that is associated with the SG-3 station is 23.0 dB/K, which is divided into a ground station antenna gain of 49.9 dB and a system noise temperature of 491 K.

Data Rate

In the first calculations of the the link budget, the first instrument data rate estimate was used, which had a value of 27.6 kbit/s. However, after considering the visibility of the satellite, it appeared that this value was by far not critical for the communication subsystem design. For the lowest orbit height at which measurements will be done, the visibility angle was calculated to be 34.5°, which resulted in a minimum visibility time of approximately $5.4 \cdot 10^3$ s. As the minimum orbit height did not change, the visibility time did not change either.

Table 13.3: Instrument data rate division of the MIRALOS spacecraft

Instrument	**Data rate [kbit/s]**
Mass Spectrometer	1.50
Accelerometer	NA
Temperature Spectrometer	NA
Reflectometer	1.50
GPS Receiver	17.0
GUVI	8.40
Subtotal (+25% CF)	*35.5*
Housekeeping (+25% CF)	*6.04*
Total	41.5

Because the GUVI instrument was added, the instrument data rate has increased. In Table 13.3 the different instruments (described in Chapter 6) and data rate values are shown. In the bottom of the table the housekeeping data rate is presented, which is derived from the CHAMP reference mission [36]. From this mission, the housekeeping data rate was defined to be 17% of the total instrument data rate.

The total data rate of all instruments plus 25% contingency was found to be 35.5 kbit/s, which then provides a housekeeping data rate of 6.04 kbit/s. The data rate that was to be used for the downlink budget analysis was computed by adding the total instrument data rate and the housekeeping data rate , which is 41.5 kbit/s. For the lowest orbit (350 km) the downlink data rate was found to be 3.17 Mbit/s, using the calculations that were stated in the Mid-Term Report [1]. This downlink data rate will decrease with increasing altitude, as the visibility time is larger for higher orbits.

Free Space Gain

The free space gain is, as described in the Mid-Term Report [1] related to the wavelength of the transmitted signal and the distance between the satellite and the ground station. After the first iteration the carrier frequency was set to 2300 MHz, which corresponds to a wavelength of 0.13 m. The maximum orbit altitude was set to 1000 km.

For the second iteration the maximum orbit altitude can be reduced to 650 km, because the orbit is known. As a certain carrier frequency will most likely be assigned to our mission, the worst case scenario is used for the communication subsystem design. This scenario was also handled in the first iteration, thus the frequency remains 2300 MHz.

As the degradation of the signal power is influenced by the orbit height, a worst case scenario can be defined. For higher altitudes the signal will lose more of its original power as it has to travel longer through the free space. Therefore this worst case scenario can be set for the highest orbit altitude.

Signal to Noise Ratio

For the signal to noise ratio, one parameter appeared to be very important. The bit error probability, in combination with the used modulation technique would define the value of the signal to noise ratio for the communications subsystems. According to the book of Couch [138] this relation is:

$$P_e = Q\left(\sqrt{2\frac{E_b}{N_0}}\right) = \frac{1}{2}\,\mathrm{erfc}\left(\frac{\sqrt{2\frac{E_b}{N_0}}}{\sqrt{2}}\right) \tag{13.2}$$

in which the $\frac{E_b}{N_0}$ is the signal to noise ratio. The erfc function is the complementary form of the error function. However, using the AMSAT/IARU Annotated Link Model System [145] and the fact that QPSK modulation is used, a signal to noise ratio of 10.5 dB is determined for the link budget analysis.

Second Iteration Losses
As described earlier in this section, the second iteration of the link budget contained some additional parameters, which were not considered in the preliminary design. These parameters only consist of losses and are described in this paragraph. From the AMSAT/IARU Annotated Link Model System [145] some values for these parameters could be estimated.

- **Spacecraft Line Loss** - The data are not directly sent from the CPU to the antenna, but they pass through several other components in the subsystem. For example, the signal that is to be transmitted has to be modulated before it can be sent. All connection lines between these components induce small power losses, dependent on the length of the lines. The connection points of the lines and their respective components also induce some small losses. The total spacecraft line loss is assumed to be 1.6 dB [145], as the connection wires are very short within the spacecraft [146].
- **Spacecraft Antenna Pointing Loss** - The ideal situation would be when the spacecraft antenna and the ground station antenna are aligned exactly on the same line. However, this is not always the case; therefore a spacecraft antenna pointing loss is included, which is dependent on the angle between the spacecraft antenna symmetry axis and the vector from the spacecraft to the ground station antenna. The pointing loss of the spacecraft antenna is assumed to be 0.6 dB [145].
- **Spacecraft to Ground Station Antenna Polarisation Loss** - The difference in vibrating orientation of the signals that are transmitted from spacecraft to ground station induces a very small loss. This loss is assumed to be 0.2 dB [145].
- **Atmospheric, Ionospheric and Rain Losses** - As the signals travel a large distance through the atmosphere, a small part of the transmitted waves are absorbed by molecules in the atmosphere, which causes a power loss. With a spacecraft elevation angle of 5 degrees and using table 3.3 of the book of Ippolito [147] the atmospheric loss is determined to be 2.1 dB [145]. The same effect occurs in the ionosphere; a small part of the waves is absorbed by the ionised particles in the ionosphere. A loss of 0.5 dB is assumed [145]. Finally, when there is rain somewhere in the path of the signals, a small part of the waves is absorbed by the rain. However, this will not be accounted for in this iteration of the link budget.
- **Ground Station Line Loss** - Similar to the line loss on the spacecraft, the ground station line loss is dependent on the type of cable, the length of the cables, the type of connectors and in-line devices. Again, taking the cable length from [146], a total line loss of 2.3 dB is determined for this link budget [145].
- **Ground Station Pointing Loss** - For the ground station a parabolic dish antenna is used, which also has a pointing loss with respect to the spacecraft. However, because this antenna is a lot larger than the spacecraft antenna, and because it is not only used for the MIRALOS mission, the pointing loss will be higher than for the spacecraft. Using the AMSAT/IARU sheet, a pointing loss of 0.2 dB [145] is estimated for a pointing error of 80 millidegrees (from the ESTRACK ground station manual) [148].

Equivalent Isotropically Radiated Power
The only parameter of the link budget equation that is left is the P_{EIRP}, which is the equivalent isotropically radiated power. On this parameter the antenna design is based, as it includes the transmission antenna power and gain. In the following section the link budget calculations are done again and an antenna trade-off will be done. The chosen antenna, resulting from this trade-off, has a certain gain, which can then be used to compute the transmission power P_{TX}.

13.3. Link Budget Analysis Results

As a result of the previous subsection the link budget equation can be adjusted to the second iteration. The newly discovered losses have to be included to come to a proper link budget calculation. The revised equation is shown in Equation (13.3). *Note that all values are in decibels.*

$$M_{link} = P_{TX} - L_{LTX} + G_{AT} - L_{SCP} - L_{POL} - L_{FS} - L_{ATM} - L_{ION} - L_{GSP} - k + \left(\frac{G}{T}\right) - L_{LRX} - R - \left(\frac{E_b}{N_0}\right) \tag{13.3}$$

All defined values are listed in Table 13.4. Next to each parameter a short description is given. The parameter that was not described in the previous subsection is the link margin M_{link}, which provides a 'buffer' for losses that were not accounted for.

From Table 13.4 it can be seen that the spacecraft antenna gain and transmitter power are not yet known. These two variables have to be determined using an antenna selection procedure. When these parameters are known the link margin can be computed, which has to have a value of 0.0 or higher. The value that is stated in the spacecraft antenna gain row (denoted with *) is determined in the following paragraph.

13.3.1. Antenna Trade-off

As stated in the previous paragraph, an antenna trade-off has to be done in order to compute the link margin. For this trade-off seven different antennas are selected, which include five different types of antennas. The turnstile antenna, half-wave dipole and

Table 13.4: Second link budget iteration for h_{orb} = 650 km

Parameter	Description	Value
L_{LTX}	Spacecraft line loss	1.6 dB
L_{SCP}	Spacecraft pointing loss	0.6 dB
L_{POL}	Polarisation loss	0.2 dB
L_{FS}	Free space loss	−167.4 dB
L_{ATM}	Atmospheric loss	2.1 dB
L_{ION}	Ionospheric loss	0.5 dB
L_{GSP}	Ground station pointing loss	0.2 dB
k	Boltzmann's constant	−228.6 dB
$\left(\frac{G}{T}\right)$	Receiving gain over system temperature	23.0 dB
L_{LRX}	Ground station line loss	2.3 dB
R	Downlink data rate	62.8 dB
$\left(\frac{E_b}{N_0}\right)$	Signal to noise ratio	10.5 dB
G_{AT}	Spacecraft antenna gain	7.0 dB*
P_{TX}	Spacecraft transmitter power	– dB
M_{link}	Link margin	– dB

loop antenna are not considered, as these are not used for satellite missions. The trade-off is shown in Table 13.5, where the left column defines all trade-off criteria, with their weight given between brackets.

The following colour coding is used: green = good, yellow = neutral, red = bad, grey = N/A.

Table 13.5: Summary of the antenna trade-off. The first column shows the criteria with the assigned weights between brackets.

Antenna	SSTL Helix	HG Helix	SSTL Patch	CS Patch	SECT-A0022	GRID-A0006	1321-LYRM
Type	Helix	Helix	Patch	Patch	Mast	Dish	Yagi
Frequency Range [MHz] (high)	2200 - 2290	2200 - 2300	2000 - 2500	2200 - 2300	2300 - 2700	1350 - 2700	2280 - 2350
Maximum Power Handling [W] (medium)	10.0	N/A	10.0	6.0	20.0	50.0	400
Gain [-] (high)	N/A	15.4	7.0	8.0	12.0	23.0	17.5
Weight [kg] (medium)	0.500	1.270	0.080	0.080	1.000	15.00	0.907
Volume [m³] (low)	$3.89{\cdot}10^{-3}$	N/A	$1.34{\cdot}10^{-4}$	$1.38{\cdot}10^{-4}$	$1.40{\cdot}10^{-3}$	$7.02{\cdot}10^{-1}$	$1.04{\cdot}10^{-3}$
Temperature Range [K] (medium)	253 - 323	218 - 358	253 - 323	248 - 358	242 - 324	233 - 363	N/A
Bandwidth Sufficient (medium)	No	No	No	No	Yes	Yes	No
Compatibility with Spacecraft (high)	Neutral	Neutral	Good	Good	Neutral	Bad	Bad
Source	[149]	[150]	[151]	[152]	[153]	[154]	[155]

As seen in Table 13.5 the patch antennas score higher than the other antennas. As all N/A cells are directly coloured grey and thus are not chosen, both helix antennas and the yagi antenna can be discarded. The mast antenna can be discarded because it does not fit within the frequency requirements (2200 - 2300). The dish antenna has good power handling, frequency range (and thus bandwidth sufficiency) and gain. However, because it has a huge weight, volume and because it induces concave shapes on the spacecraft it is chosen not to use the dish antenna.

For both patch antennas there is only one disadvantage with respect to the larger antennas. Because the bandwidth is not sufficient for both uplink and downlink, two antennas have to be installed, which doubles the power usage and the weight. Because the SSTL patch antenna has a higher power handling and a larger frequency range (with which both uplink and downlink frequencies can be reached) this one will be selected for the MIRALOS mission.

SSTL Patch Antenna

As described in the previous section the SSTL patch antenna came out of the trade-off. It is a really low weight antenna, weighing only 80 grams, and has a gain of 7.0 dB. It can handle a maximum total RF power of 10 W. This is sufficient, as the transceiver that is used can only produce 2.2 W of RF output power. The antenna has an operating temperature range between −20°C and 50°C at an approximated lifetime of 7 years. On the Surrey Satellite Technology Ltd. source [151] it is stated to be a flight-proven design, inter alia on the GRACE and CHAMP satellites. Concerning the placement of the patch antennas, they have to be mounted on the surface that is pointing nadir in order to minimise the pointing loss of the spacecraft.

Redundancy
As described earlier in this chapter, two antennas are incorporated in the spacecraft design; one for the uplink and one for the downlink. It was decided that the SSTL Patch Antenna was to be used for both the link budgets. However, some redundancy has to be included to prevent mission failure when one of these antennas fail. Next to that, one antenna should be included which can account for when the spacecraft attitude has deflected with respect to its desired attitude. In such a case it still has to be possible to contact the satellite from the ground station, in order to send commands to restore the possible subsystem failures on the spacecraft. For this an omni-directional antenna is to be used, as it has to send data in every direction in order to contact the ground station at every spacecraft attitude deflection. It only has to be able to send some housekeeping data of the spacecraft and to receive commands from the ground station; for this antenna a different link budget analysis should be considered. The design of the omni-directional antenna is not done in this report.

13.3.2. Link Budget Completion
With the antenna selected in the previous paragraph the link budget can be completed. As described in Table 13.5 the gain of the SSTL S-band Patch Antenna is 7.0 dB. With this value the link margin can be plotted against the two other varying parameters: the orbit altitude and the transmission power.

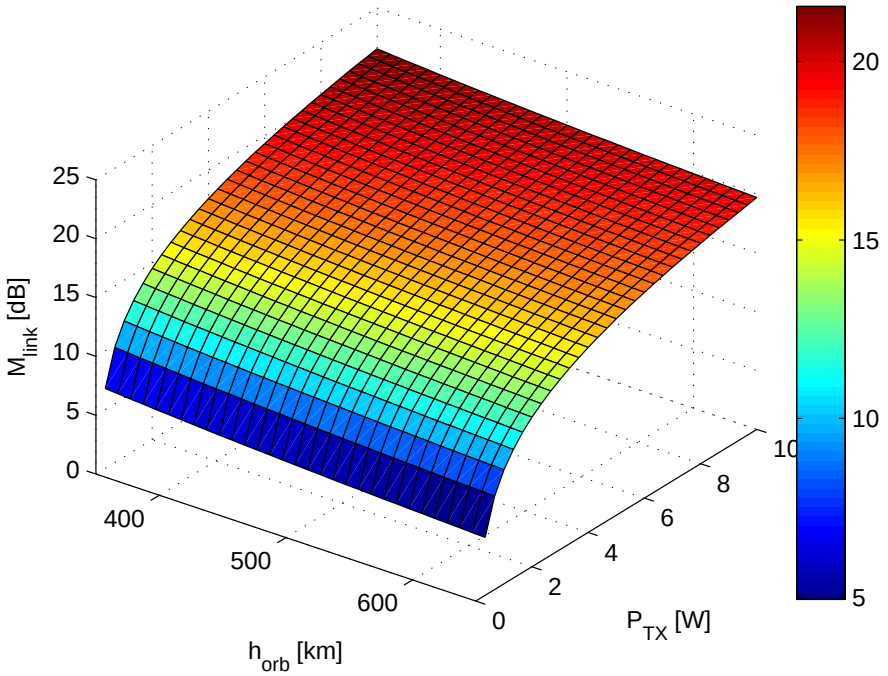

Figure 13.3: Transmission power and orbit altitude versus the link margin (coloured bar represents the value of the link margin in dB)

This figure shows three parameters plotted against each other; the orbit altitude, the transmission power and the link margin. It can be seen that the link margin increases slightly with decreasing altitude, which means that the highest orbit altitude induces the lowest margin for non-accounted losses. Relating the transmission power to the link margin it can be said that the link margin increases a lot with increasing transmission power. This causes the critical design point to be at the lowest corner, which is at the front, close to the crossing of the P_{TX}- and the h_{orb} axis. The maximum altitude is fixed; it was chosen during the design process and its value is 650 km. The transmission power however can be varied, and can be increased if for example a higher data rate is required or if the path loss is higher due to rain.

13.4. Ground Segment and Operations
This chapter describes the ground station and launcher selection. In Section 13.4.1 the ground station selection is discussed, in which the ground track is shown and in which a final ground station is chosen for the mission. Ground station operations and logistics are described in Section 13.4.2.

13.4.1. Ground Station Selection
In this section the ground station selection is described, which was already handled in the Mid-Term Report [1]. This is an important aspect of the communication subsystem design, as the ground station influences the link budget analysis. The main parameters for the ground station selection are the orbital parameters, which were discussed in Chapter 3. The inclination of the

orbit is defined to be 83 °, which means that the spacecraft will be in a near-polar orbit. This is an advantage for ground station selection. For polar orbits the ground track of the spacecraft shifts per orbit, depending on the orbital period and the rotation speed of the Earth. This longitudinal shift has the same value in degrees for every latitude, however, the exact distance (in unit of length) is the largest at the equator and the smallest at the poles. Therefore, when choosing a ground station with a high latitude the number of contact periods per day can be larger.

Using a ground station from the ESTRACK network the number of possible ground stations decreases. This is done as there is much information available concerning these ground segments. A similar ground station from another network can also be used for this mission.
From the ESTRACK ground station manual [148] it can be seen that the ground station with the highest latitude is the Svalbard Ground Station (SG-3), which lies at approximately 78 ° N. In Figure 13.4 it can be seen that the exact shift in longitude is smaller at the poles, where the Svalbard Ground Station is denoted.

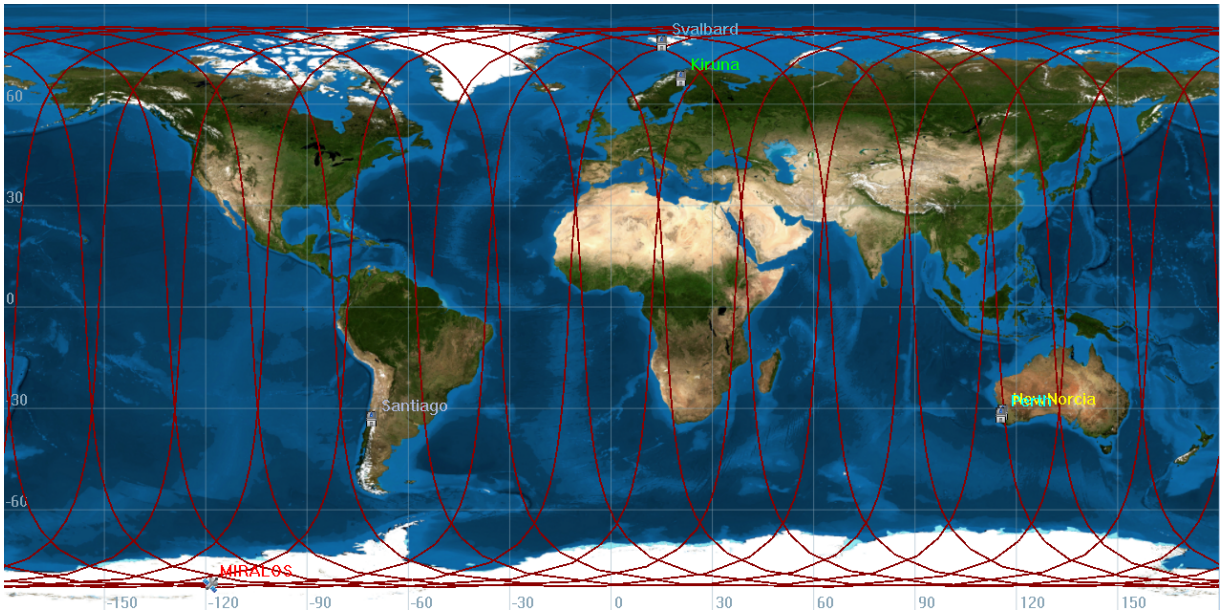

Figure 13.4: MIRALOS ground track at 650km for one day with several ESTRACK ground stations

As described in Chapter 13 the communications subsystem design is based on the SG-3 station, at it is determined that the ground station fully complies with the up- and downlink requirements. An assumption was made during the TT&C design, which included that the SG-3 station is contacted at least twice a day, which means that all data that are obtained within twelve hours have to be sent in one contact period. This is the worst-case scenario for the mission and it will not happen often; most days the spacecraft can have more than two contact periods a day, which decreases the required data rate and thus increases the link margin of the spacecraft. Additionally, also other ground stations, such as Kiruna, New Norcia, Perth and Santiago (which are denoted on the map in Figure 13.4) can be used, thus again decreasing the downlink data rate.

As for the uplink, in the communications subsystem design (Chapter 13) a specific antenna is incorporated for receiving signals from the ground stations. These signals basically contain commands and infrequent software updates. As the uplink budget was not considered in Chapter 13 because it was determined not to be critical over the downlink budget, this can be done in further design, taking the main parameters of the SG-3 station into account.

13.4.2. Ground Operations and Logistics

An important aspect of spacecraft missions are ground station activities. This section displays the operations and logistics that take place on Earth in order to control the spacecraft and to retrieve data that are transmitted by the spacecraft. The main purposes of the ground station were introduced concisely in Section 13.4.1. The operations are displayed using a flow diagram in Figure 13.5.

After mission initiation, the satellite will consequently transmit data to the ground station. The Payload (PL) data will be processed, stored and distributed to the scientific community. Furthermore, information on the subsystems such as provided power and internal temperature are transmitted to the ground station. Using these data, subsystem faults can be detected and corrected in an early phase in order to avoid preliminary mission failure. Thirdly, data of the spacecraft orientation and position is transmitted to the ground for trajectory prediction and avoidance of collisions. Furthermore, orbit control is necessary to maintain the operating conditions for PL. Once the mission is finished or has failed, the EOL procedure is initiated, taking sustainability into account. The mission-specific ground activities are displayed in Table 13.6.

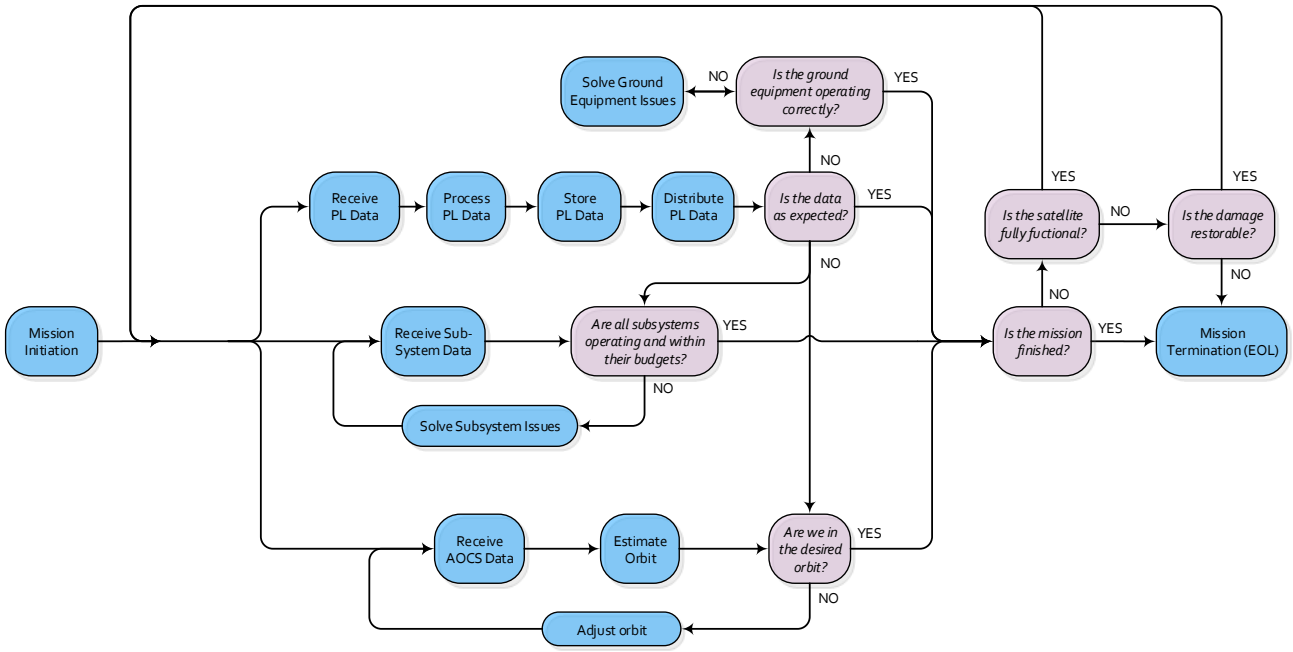

Figure 13.5: Flow Diagram of Ground Station Operations

Table 13.6: Mission Related Ground Operations [156, 157]

Operation	**Elaboration**
Mission Initiation	The ground operations include the initiation of the mission. This means the complete development process including verification and validation. Also, this includes launcher operations and the commands, if applicable, for the spacecraft to change to PL configuration.
Mission Termination	When the spacecraft has fulfilled its purpose, it can be discarded. Alternatively, if the spacecraft failure is definite, it should also be discarded. For this, a protocol is developed and it's EOL procedure is initiated. This protocol is set into motion by a command from the ground station.
Data Retrieval	The ground station is to retrieve the data transmitted by the spacecraft. This includes PL data, orientation, location and subsystem data such as component temperature, power supply and power usage.
Data Processing	The retrieved data is organised and structured. From this data, predictions are made to the current orbit and determined is whether this orbit will have negative consequences for the mission. If necessary, the required action for orbit modification is determined.
Command Transmission	If after data processing it is concluded that orbit modifications are necessary due to PL considerations or to avoid a collision with an object, commands are transmitted to the satellite for these modifications to happen.
Data Management	After data processing, the data is stored in a safe environment and spread to the scientific community for research purposes.
Documentation Management	For the current and future missions, it may be valuable to document the mission from early development activities to late- and post-mission activities such as mission termination and data research.
Equipment Upkeep	On a timely basis the ground station equipment is to be maintained in order to ensure correct functioning and avoid equipment failure.
Energy Control	Both ground station and spacecraft should spend resources in a durable sense. For spacecraft operations, this can be related to standby modes for components and subsystems. For ground operations, this can be related to use of green equipment (i.e. with low power consumption).
Waste Control	Waste exerted to the environment should be kept to a minimum. This can be done by replacing paper documentation with digital software, for example.

In Table 13.6 some operations are mentioned which can be listed under the Command and Data Acquisition Element (CDAE). This part of the ground segment is responsible for the acquisition of all data that are retrieved from the spacecraft and all commands that are to be send to the spacecraft. Next to this part, two other ground segment elements can be defined [27]: the Flight Operations Segment (FOS) and the Payload Data Ground Segment (PDGS). The former element uses the analysed data for the production of commands. It also provides software updates, it ensures that the spacecraft flight is performed as planned and

it restores the spacecraft flight if necessary. The latter element provides verification and validation of the data and handles the data so that they can be used for the modelling of the atmosphere. All three ground segment elements are strongly interrelated and in Chapter 16 the main recommendations with respect to the ground segment are discussed.

Besides the spacecraft-ground specific operations, the ground station takes into account additional logistic affairs. These are summarised in Table 13.7. It is to be expected that an existing ground station will be used for these operations, rendering the particular analysis diminituve throughout the mission design.

Table 13.7: Non-Mission Related Ground Operations [156, 157]

Operation	**Elaboration**
Personnel Management	Employees are to be hired, managed, motivated and kept content throughout their working experience.
Office Supplies Management	For office related activities within the ground station, tools such as pen, paper and staplers are to be available.
Office Equipment Management	Office equipment such as computers and printers are to be available. Furthermore, these should be maintained and kept up-to-date.
Furniture Maintenance	Office furniture is to be available and maintained for personnel. Think of chairs and desks.
Real-estate Management	Activities related to the electricity, gas and water networks are to be maintained in order to avoid problems in operation and dangerous scenarios.
Cleaning Services	The offices are to be cleaned on a periodical basis.
Other	There are many other tasks the ground station has to take into account, but these are not treated in further detail. Think of activities such as mail management, communication with media, safety implementations (smoke detector, fire extinguisher, exit routes, first aid).

14. Launcher Selection

In the Mid-Term Report [1] some launcher selection was done, which will be summarised in this section. As described in Section 13.4.1 the spacecraft will be in near-polar orbit, which limits the number of available launch sites. However, the launcher is of more importance, so the launch site selection will be done based on the to be used launcher, which is selected using the trade-off in the following paragraph. In Table 14.1 the actual launch vehicle trade off is performed. The results are shortly discussed in Section 14.2.

14.1. Launch Vehicle Trade-off

In Table 14.1 the trade-off of a selection of relevant launchers is depicted. The candidate launchers are selected by looking at dimensions, launch cost and maximum payload mass for LEO injection.

Table 14.1: Launch Vehicle Trade-off (Colours are discribed below)

Launcher	Payload (LEO) [kg]	Launch Sites	Inclination Range [deg]	Usable Fairing Dimensions [m]	Launch Cost
Russia and/or Ukraine					
EuRockot	1950	Baikonur/ Plesetsk	~ 65-100	L: 3.66, D: 2.52	36 M$ (2013)
Soyuz-2.1v	3050	Baikonur/ Plesetsk	~ 55-100	L: 5.07, D: 3.80	N/A
Start-1	532	Plesetsk/ Svobodny	~ 76-98	L: 2.25, D: 0.66	3.5 - 7 M$ (1994)
Dnepr-LV	2900	Baikonur/ Yasny	~ 55 - 100	L: 5.4, D: 2.27	~ 10 - 20 M$ (2003)
India					
PSLV-CA	2100	Satish Dhawan	~ 20 - 99	L: 3.01, D: 2.90	N/A
PSLV	3250	Satish Dhawan	~ 0 - 99	L: 3.01, D: 2.90	20 M$ (1999)
United States					
Minotaur IV	1735	Vandenberg/ Wallops/ Kodiak/ Cape Canaveral	~ 28 - 116	L: 2.87, D: 2.05	50 M$ (2014)
Minotaur I	580	Vandenberg/ Wallops/ Kodiak/ Cape Canaveral	~ 28 - 116	L: 3.39, D: 0.90	~ 13 M$ (2001)
Antares	> 5000	Kodiak/ Wallops	~ 28 - 116	N/A	N/A
Japan					
Epsilon	1200	Uchinoura	N/A	N/A	~ 38 M$ (2013)
Europe					
Vega	1500	Kourou	~ 5.2 - 100.5	L: 3.52, D: 2.38	~ 42 M$ (2012)

- **Green:** This means that the property is acceptable for the MIRALOS mission.
- **Yellow:** This means that the property is not ideal but no requirement is violated. The launcher might still be a viable option.
- **Red:** This means that the property is unacceptable for the MIRALOS mission, and the launcher is therefore discarded as a viable option.
- **Grey:** This means that the property is not available. Too many unavailable properties means the launcher is not a viable option for the trade-off.
- **White:** This means that the property is not important for the trade-off.

As stated in the summation above, the launchers which have yellow-coloured cells in the trade-off table might still be a viable option. The EuRockot and Vega launchers are slightly more expensive than for example the PSLV, but this might be due to the fact the launch prices are given in different years and inflation is not taken into account. The launchers can also possibly be shared with third parties which lowers the cost for the MIRALOS mission as well. The dimensions that are needed for the fairing

are a length of 3 m and a diameter of 2.2 m as stated in the Mid-Term Report [1]. This eliminates a few launchers in the trade-off table (Table 14.1). The most viable options are shortly described below.

PSLV and PSLV-CA: The Polar Satellite Launch Vehicle (PSLV) is an Indian launcher capable of injecting spacecraft in a polar orbit. It is an affordable option with a large payload capability. The PSLV-CA is a modified version of the PSLV. The PSLV-CA (Core Alone) is essentially the PSLV without the 6 strap-on boosters. This limits the allowable payload mass while conserving the payload dimensions. This is a very good property for the MIRALOS mission, since the spacecraft has a relatively large volume-to-mass ratio. The launch cost is not available, but will most likely be lower than the cost of the PSLV, because less mass is launched into space.

Dnepr-1: The Dnepr-1 is an Ukrainian launcher constructed as a converted Intercontinental Ballistic Missile (ICBM). It is capable of injecting a relatively high mass into a polar low-Earth orbit with a low launch cost. This low cost is mainly because the ICBMs are already available and can be modified relatively easy. The low launch cost and good payload volume make this launcher a very good option for the MIRALOS mission.

14.2. Trade-off Discussion

In the Mid-Term Report no decision was made on the launcher that is to be used. Using Table 14.1 and the previous paragraph it can be seen that the to be used launcher is either the PSLV, the PSLV-CA or the Dnepr-LV. For the PSLV-CA the launch costs are not available and thus this option will discarded. For the comparison of the PSLV and the Dnepr-LV, it can be stated that the PSLV can carry somewhat more payload. However, because the satellite weight is approximately 475 kg, the maximum payload weight of the launchers will not be exceeded, so this trade-off criterion can be ignored. Then, both launchers can reach the inclination of the orbit, so this criterion can be neglected as well. Comparing the final two criteria, it can be said that the fairing volume of the Dnepr-LV is a lot larger than for the PSLV, which means that the satellite dimensions can be increased if necessary. Next to that the price of the Dnepr-LV lies between 10 and 20 million dollars (based on the Dnepr-I from the Launch Vehicle Catalog [158] whereas the PSLV will already cost 20 million dollars. From this it can be concluded that the Dnepr-LV is the most feasible option, looking at cost and fairing dimensions, and thus the Dnepr-LV will be used for the MIRALOS mission.

14.3. Spacecraft Launch Vehicle Integration

Originally the Dnepr Launch Vehicle had two types of Payload Fairing (PLF) one standard and one extended type [127]. For the launch of TerraSAR-X a third type has been developed, which can accommodate even larger spacecraft. This Type-3 PLF will also be used to launch the MIRALOS spacecraft [159]. A schematic integration sketch of the spacecraft integrated into Launch Vehicle Adapter (LVA) and fairing can be found below in Figure 14.1.

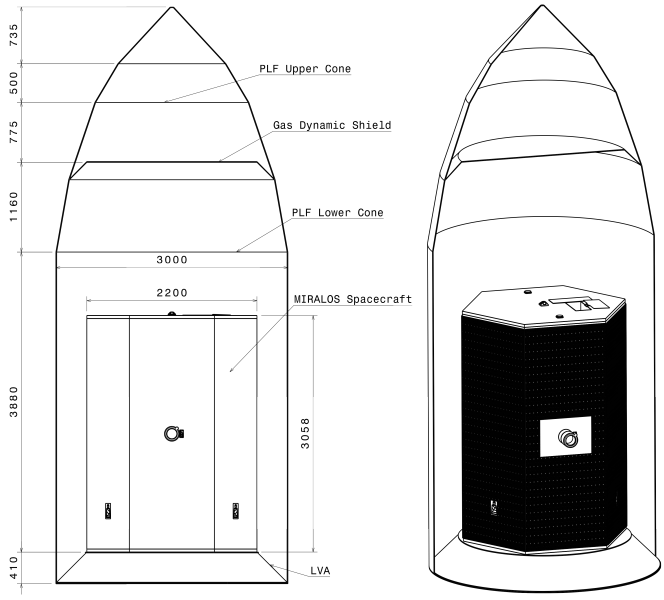

Figure 14.1: Spacecraft integrated into the Launch Vehicle (PLV dimensions are approximated based on [159])

The PLF is divided into two sections the upper and lower cone, the two sections are being divided by the Gas Dynamic Shield (GDS), which protects the spacecraft. The GDS can be customised, thus it can be moved up or lower to allow more useful space in the lower cone. From Figure 14.1 it becomes clear there is quite a lot of empty space above the spacecraft and technically the GDS can be moved upwards even further to allow for more usable room. Therefore, it is advisable to modify the fairing to fit another big or multiple small satellites on top. This was already done for PLF Type-2 and most likely can also be implemented for PLF Type-3. This option of sharing the launcher would reduce the launch cost.

15. Spacecraft System Analysis

This chapter assesses the performance of the satellite including subsystems. The spacecraft functions are depicted in Sections 15.1 and 15.2. The different modi in which the spacecraft operates are elaborated on in Section 15.3. The hardware and software are presented in diagrams in Section 15.4. Verification and validation procedures are described in Section 15.5. The mission and design risks are assessed in Section 15.6. The design properties are analysed for their sensitivity to changes in Section 15.7. The RAMS analysis is displayed in Section 15.8. The market analysis is shortly described in Section 15.9, upon which general sustainability considerations are presented in Section 15.10. A requirement compliance matrix in presented in Section 15.11. Finally, a project planning is presented in Section 15.12, entailing the remainder of the mission, including continuation of the design process, operation and termination.

15.1. Functional Breakdown Structure

The functional breakdown structure represents the functions the MIRALOS satellite has to perform. It is shown in Figure 15.1. The functions are arranged in an AND format. In this diagram the functions are ordered hierarchically, whereas a chronological overview of the functions is given in Section 15.2.

Figure 15.1: Functional Breakdown Structure

15.2. Functional Flow Block Diagram

In the baseline report [15] a functional flow diagram was created to visualise the logical operations within the spacecraft mission. This section contains the updated and extended version of this block diagram and it can be split in several parts.

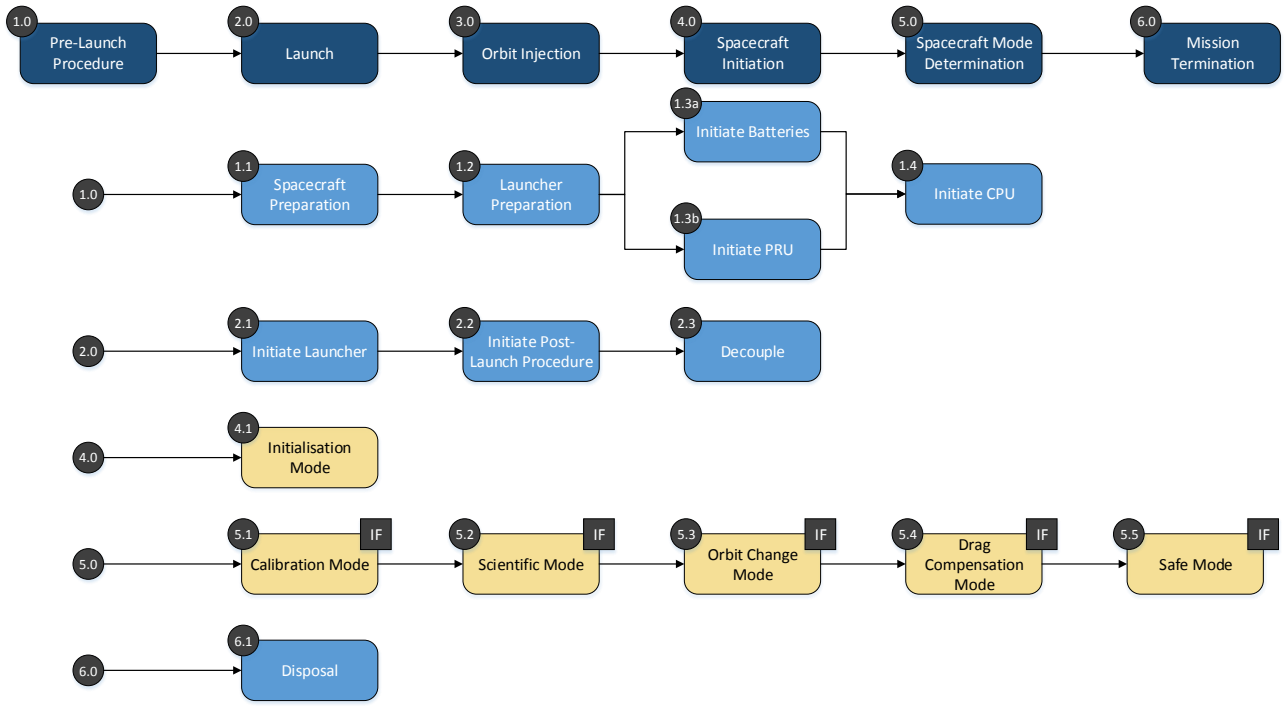

Figure 15.2: Top Level Functional Flow Diagram

The top level of the FFBD is shown in Figure 15.2, in which the six top level operations are described to be: pre-launch procedure, launch, orbit injection, spacecraft initiation, spacecraft mode determination and mission termination. It can be seen that the CPU, the batteries and the PRU are already initiated before the spacecraft is launched. In the fourth and fifth block the different spacecraft modi are stated, where the 'IF'-block denotes that only one of the five modes is initiated (so no modes can be initiated simultaneously). These modes are described in Section 15.3.

Figure 15.3 then shows the initialisation mode, which is part of the spacecraft initialisation. It can be seen that five subsystems are activated during this mode, and the sequence that is stated in this figure does not necessarily have to be the actual sequence of initiation. The subsystems are in no case initiated simultaneously.

Finally, in Figure 15.4 the other five spacecraft modes are shown, and for every mode it is stated which subsystems are either switched on or off. For some modes it is denoted which mode will follow after it is finished.

15.3. Spacecraft Modes

In Chapters 6 to 13 and section 13.4 the spacecraft subsystems were described. Next to that, the full lay-out of the satellite was considered in Chapter 5. Now that all subsystems within the satellite are determined several different spacecraft modes can be defined, which describe a certain 'setting' of the spacecraft. This section contains six modes which are of importance for the MIRALOS mission. For every mode the importance is described as well as the subsystems that have to be functioning while in this mode, as can be seen in Figures 15.3 and 15.4.

Safe Mode

One of the most important modes of actually any spacecraft is the safe mode, in which only the essential subsystems are kept switched on. The mode is designed to prevent damage or complete failure of the spacecraft in some particular situations. Such situations are defined beforehand, and for the MIRALOS mission the following triggering situations are defined:

- **Temperature out of range** - when the internal temperature of the spacecraft exceeds either the upper or the lower limit of the beforehand defined temperature range the safe mode will be initiated.
- **Spinning rate** - when the rotation rate of the spacecraft exceeds the beforehand determined limit the safe mode will be initiated.

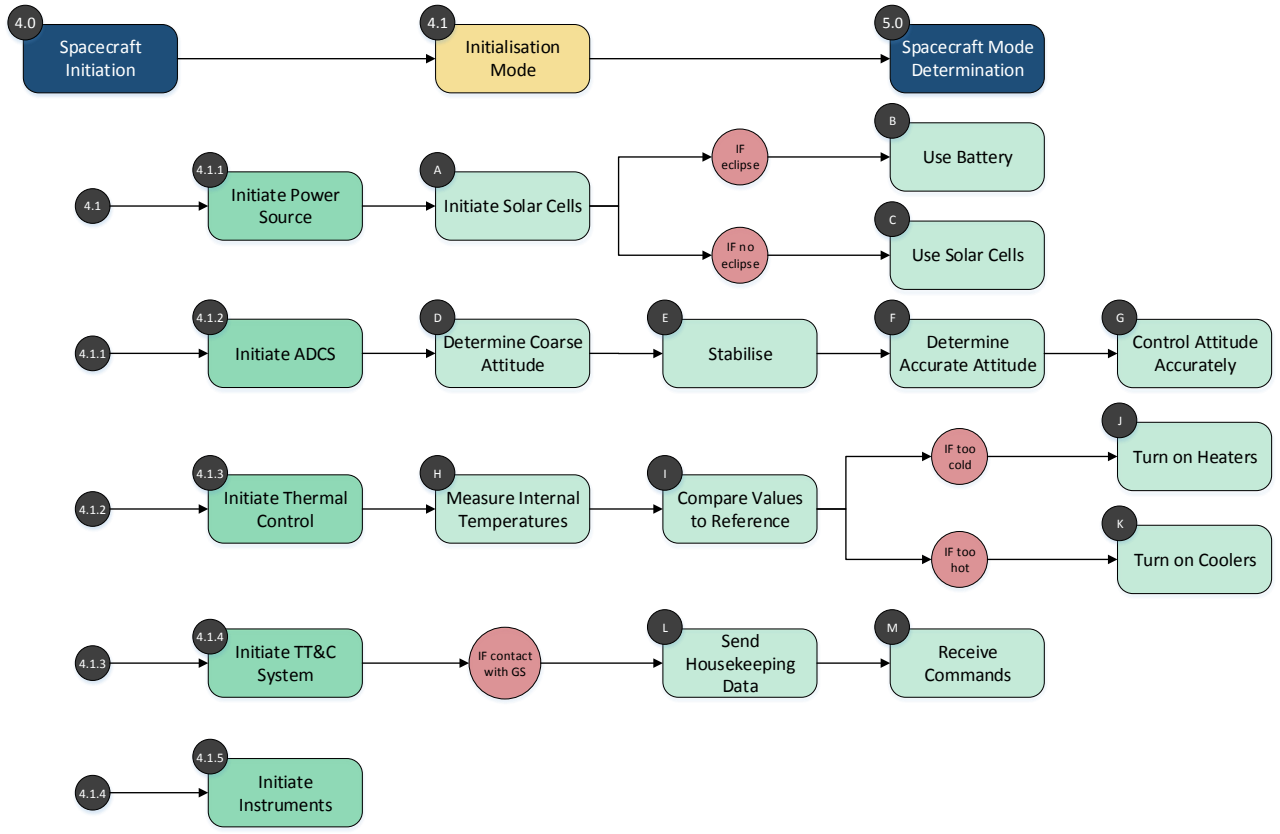

Figure 15.3: Initialisation Mode Functional Flow Diagram

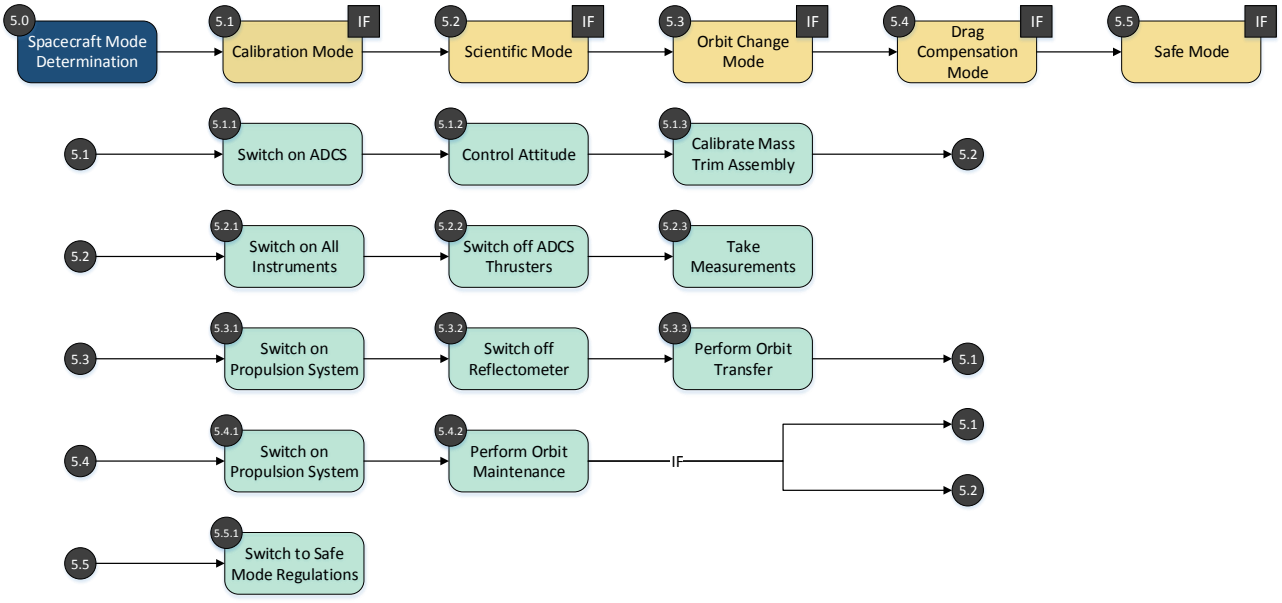

Figure 15.4: Spacecraft Modes Functional Flow Diagram

- **Sudden pressure change** - when the pressure sensors determine a sudden pressure change that exceeds the beforehand determined value the safe mode will be initiated.
- **Sudden power change** - when the spacecraft suddenly starts generating much less power, or when one of the subsystems starts consuming much more power, the safe mode will be initiated.

- **Attitude failure** - when the attitude of the spacecraft is such that the instruments are facing the sun or are not directed in flight direction, the safe mode will be initiated.
- **Unrealistic instrument data** - when one of the instruments starts generating unrealistic data the safe mode will be initiated.
- **Unrealistic component/sensor data** - when one of the components or sensors starts generating unrealistic data the safe mode will be initiated.

In the case one these events happens a predefined sequence will be followed, after which the spacecraft actually is in safe mode. For the MIRALOS mission, the most important part is that the power supply to the payload, the propulsion subsystem and the cold gas system of the attitude control is shut down immediately. The desired attitude then has to be regained using the magnetic torquers. This is required for the thermal control subsystem to balance the internal temperature to a steady value, which lies in the predefined temperature range. Next to the ADCS and the thermal control subsystem the communications system will be kept switched on, as the housekeeping data have to be sent to the ground station for analysis. The ground station also has to be able to send commands to the spacecraft if necessary.

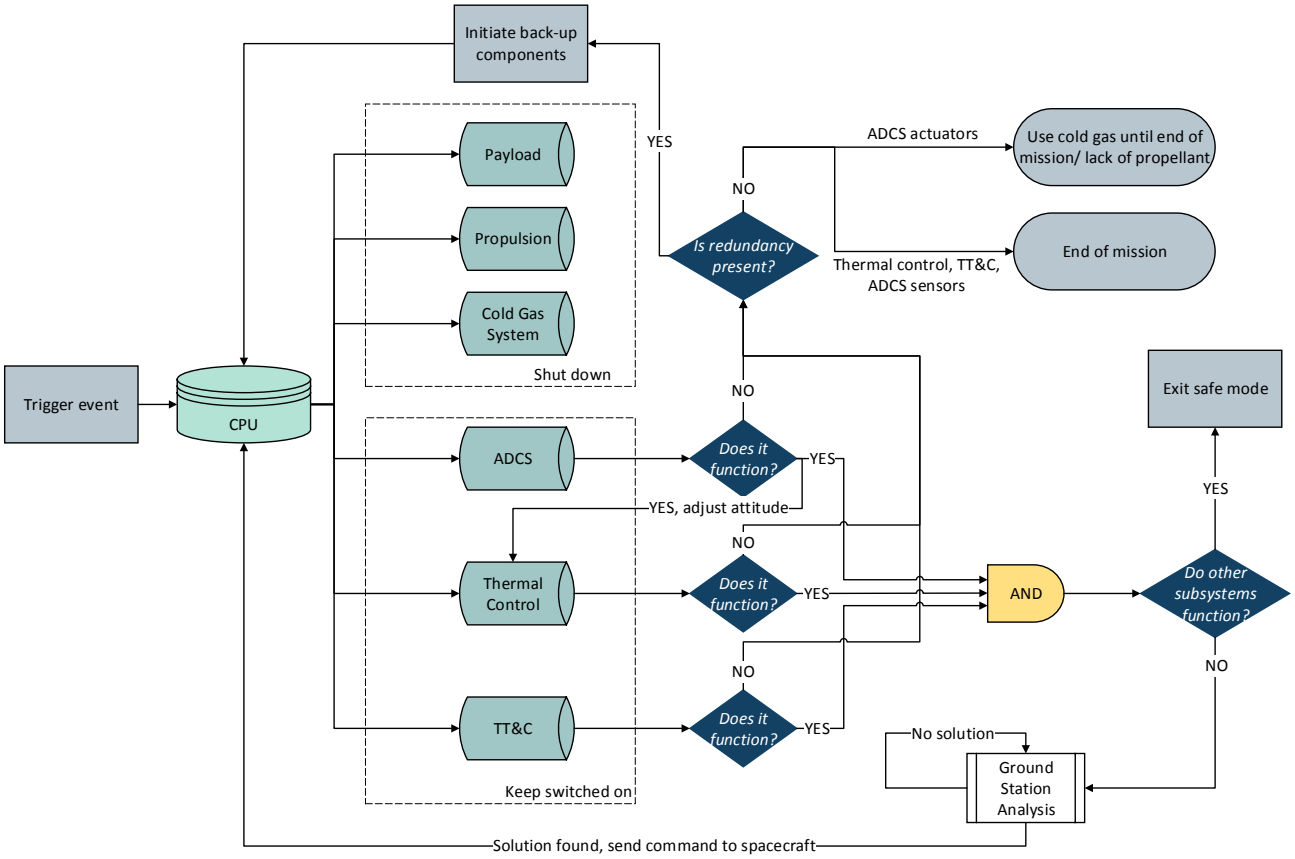

Figure 15.5: Safe Mode Flow Diagram

Figure 15.5 provides a flow diagram of the safe mode, in which the first block is the trigger event, which initiates the safe mode. Through the CPU the power supply to the payload, propulsion and cold gas system is shut down, while the ADCS, the thermal control and the TT&C subsystem are kept switched on. The next step is to find the subsystem in which the error occurred. Firstly, for the essential subsystems (which are still working) this is checked. As described earlier in this section the ADCS has to adjust the attitude in order for the thermal control subsystem to maintain a constant internal temperature. When an error occurs in the essential subsystems the redundancy is checked. In the case back-up components are still available on the spacecraft, these will be initiated; in the case these components are not available any more the mission is either terminated in the case of the ADCS sensors, TT&C and the thermal control or cold gas thrusters are used for the rest of the mission in the case of failure in ADCS actuators.

It is also possible that there is no error in the essential subsystems. In this case it is checked whether there is an error in the other subsystems. If not, the safe mode is terminated. If so, data of these subsystems is sent to the ground station, where a thorough analysis is done in order to find a solution for this error. Such a solution is then sent to the spacecraft, after which the whole cycle is passed again.

Initialisation Mode
After the spacecraft is deployed in its orbit only a few subsystems are (partly) functioning. The CPU is switched on in orbit in order to control all other subsystems. It gains its power from the battery until the spacecraft is deployed in its orbit and the solar cells can be used. Finally, part of the thermal control subsystem is already running during launch, as the spacecraft and all its instruments have to survive all thermal loads that are present during the launching process. The initialisation mode then is started when the spacecraft is in orbit, and the main factor is that all subsystems are initiated subsequently. They can not be switched on simultaneously, as possible subsystem failures can not be detected then.

Scientific Mode
When the scientific part of the mission is initiated the spacecraft will have to go into the scientific mode, in which all instruments are switched on in order to take measurements. The only subsystems that are switched off are the propulsion system and the cold gas thrusters of the ADCS system, as they are not required. They also induce disturbances on the spacecraft, and when they are switched on, but not used, they consume power unnecessarily.

Orbit Change Mode
In case an orbit change is required a specific mode has to be entered, in which the propulsion subsystem has to be initiated. All instruments can be kept switched on, however, only the reflectometer has to be shut down, as it does not generate any relevant data during orbit transfer.

Calibration Mode
After an orbit change is made, the spacecraft has to be calibrated, which means that the attitude has to be adjusted to the desired setting. Therefore the ADCS has to be switched on in the calibration mode. When the spacecraft attitude is controlled the particular instruments and the mass-trim assembly have to be calibrated before the spacecraft can return to the scientific mode.

Drag Compensation Mode
The last mode that is described is the drag compensation mode, in which the orbit is maintained. This mode is initiated two to five times a day with a duration of 2060 seconds for nominal solar activity. Because the spacecraft is orbiting at a low altitude it experiences such a significant amount of drag that it will slow down a small bit and thus really slightly drop altitude. In order to compensate for this, at a certain frequency the satellite will have to go into drag compensation mode, in which the propulsion system is switched on and maintains the orbit by providing low thrust.

15.4. Hardware and Software Block Diagrams
The hardware block diagram illustrates the components of the MIRALOS satellite and their mutual relations and interactions. It is shown in Figure 15.6. Figure 15.7 contains the software block diagram. In this diagram the MIRALOS components are represented in a simplified way in order to allow for a detailed view on the interconnections that should be presented in the software.

15.5. Verification & Validation
A significant part of the mission depends on the reliability of subsystems. This procedure ensures that obvious design and manufacturing flaws are filtered out in an early stage, which greatly increases the probability of mission success. This section depicts the verification and validation procedure for the models, instruments, and subsystems used in the MIRALOS mission.

15.5.1. General Verification and Validation Methods
Some of the methods used apply to most, if not all, of the instruments and subsystems (referred to as 'units' in this subsection). These will be listed hereafter.

1. Inspection:
    - Dimensions of the unit will be inspected to make sure that they comply to the technical drawings. This is to filter out any manufacturing errors.
    - Assembly of the unit is inspected. This way it is made sure no parts have been forgotten.
    - The unit will be inspected for structural compatibility with the spacecraft bus to ensure that mounting is possible.
    - The unit will be inspected for obstructions of its moving parts and sensors when mounted and deployed on the spacecraft bus.
2. Analysis:
    - The thermal properties of the spacecraft will be simulated with a theoretical model to ensure that the unit under analysis stays within its operating temperature range. This model will be verified and validated with existing theory and thermal tests on simple shapes.
    - All the individual components of the unit will be analysed with respect to their lifetime probabilities to ensure that all individual components match (or exceed) the required lifetime of the system it belongs to.
    - Using an artificial set of data, the desired atmospheric parameters are determined. This is to make sure the design is compliant to what is needed by the stakeholders and no atmospheric properties are forgotten during the design.

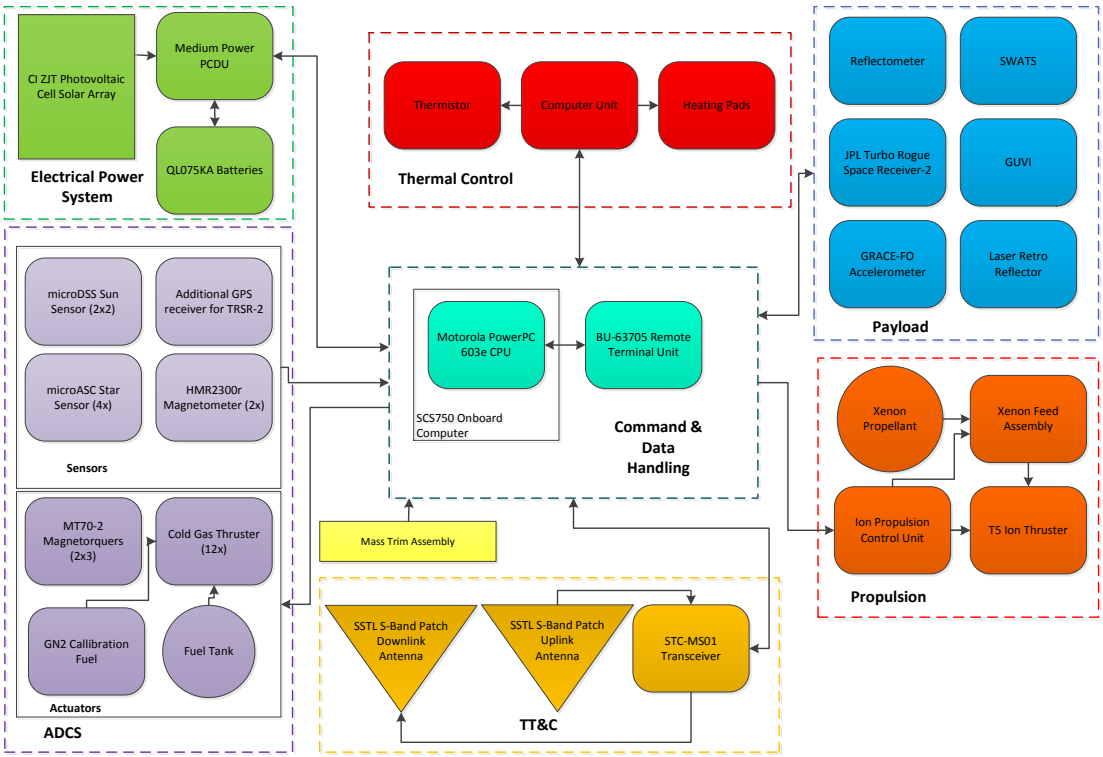

Figure 15.6: Hardware Block Diagram

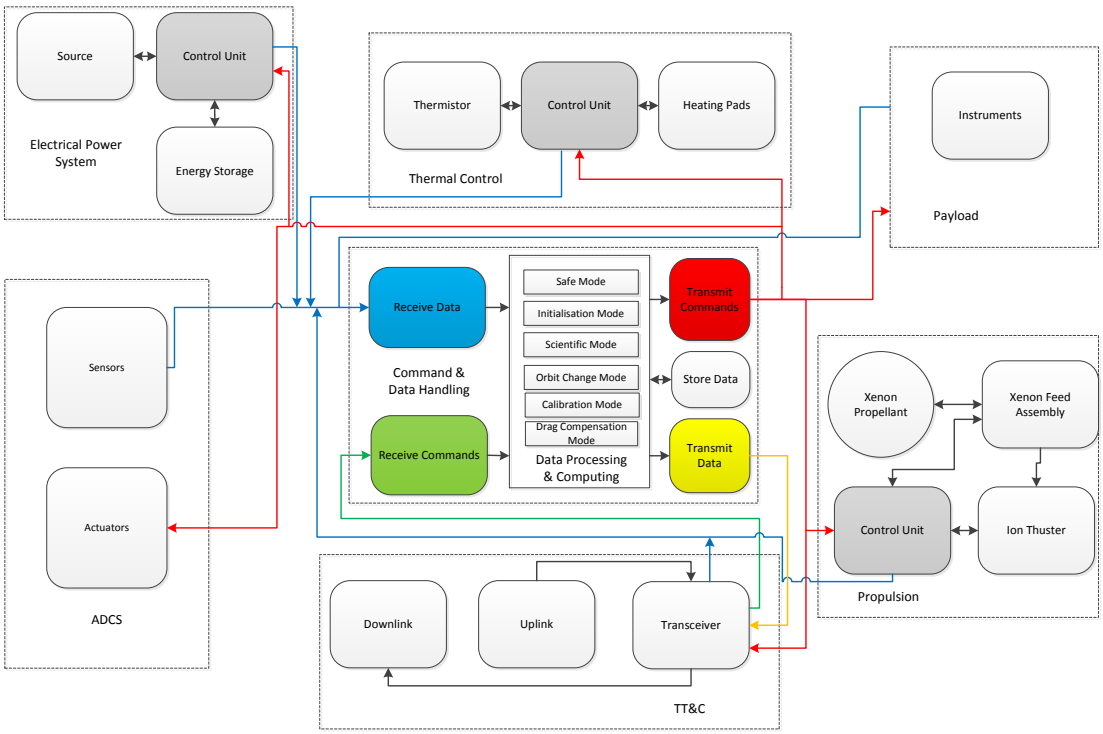

Figure 15.7: Software Block Diagram

3. Demonstration:
    - If applicable, the unit will be turned on to demonstrate the compliance to its respective power budget.
    - The generated output of the unit will be demonstrated and checked for correct format. This goes hand-in-hand with inspection of the documentation of the used equipment.
    - It will be demonstrated whether the unit digital interface is compatible with the on-board computer interface. To this extent, receiving and distributing data is tested.
    - When applicable, it will be demonstrated that the moving parts of the unit are free to move within the desired range and are fully functional.
4. Testing:
    - The unit will be exposed to at least an upper boundary of the amount of radiation that it is expected to resist during its lifetime.
    - The unit will be tested for the fluctuating thermal and low vacuum conditions experienced during it's lifetime. The changing conditions may furthermore influence the power consumption.
    - The unit will undergo a shaker test to ensure that it will withstand the vibrations encountered during launch.
    - The unit will undergo an operation test exceeding its lifetime limits, if considered a crucial component to spacecraft operations.

If a component or unit seems to be functioning incorrectly, its sub-components will be evaluated and more verification and validation procedures will be planned. However these actions are not planned or elaborated on in this report.

15.5.2. Instruments

A crucial part of the spacecraft which requires verification and validation relates to the payload instruments. The quality of the data retrieved by these instruments define the quality and success of the mission. Hence, verification and validation is described for each instrument.

GPS Receiver

The GPS antenna and receiver will be verified using a simulation. The device has already been proven to be space compatible over the given mission lifetime. Hence, only the assembly and the integration in the spacecraft is tested.

Using a hardware model, the GPS signal is simulated for multiple orbit conditions encountered during the mission life. The flight model receives this model and the on-board computer should return its (virtual) location. Since the signal is simulated, it can be controlled, and the location that should be returned by the on-board computer can be determined.

In orbit, the GPS signal can be verified by a LRR, if implemented on the satellite. If a laser is pointed from Earth on the satellite, a mirror will reflect this laser signal and return it to Earth. Hereby the exact location of the satellite can be determined.

Mass Spectrometer

The mass spectrometer measures the concentration of different constituents in the upper atmosphere. Furthermore, the instrument is set to measure ion drift, neutral wind, and neutral temperature. This device is an flight-proven product, therefore does not need to be tested separately. However the production, assembly, and integration, is tested during the design process and post-launch.

Before launch, the mass spectrometer is tested by on-ground tests in high-vacuum test facilities (for example the IV10 Vacuum Chamber at the University of Pisa, Italy). Its accuracy after calibration and the system integration in a structural and data interface sense will be assessed in this way.
After launch existing measurements on the upper atmosphere will be used to validate the instrument's measurement. Another available approach would be to compare the resulting data with the density predicted by the modified NRLMSISE-00 model. However this model will require validation too, as described in Section 15.5.4.

Temperature Measuring Equipment

The temperature is one of the important properties measured in-situ by the spacecraft. It has to be ensured that this device functions correctly before and after launch.

During post-launch operation, the model can be verified in multiple ways. The NRLMSISE-00 model gives an initial prediction of the atmospheric temperature based on location and solar conditions. Due to uncertainties and assumptions in the model, the temperature will not exactly match the measured temperature. However, the measured temperature should not deviate significantly from the value predicted by the model. Furthermore, the measurements on the local neutral temperature should coincide with measurements of previous missions such as DANDE [25] and STP-H4-SWATS [160]. Additionally, an old article from Spencer [161] may also be used for validation. However measurements from this article are outdated and are limited to an altitude of approximately 400 km. Hence, long-term atmosphere changes should be taken into account, as described in Section 2.4.1.
Furthermore, pre-launch on-ground tests can be performed to pinpoint faults by design or manufacturing. By on-ground tests, a

flight model is put into a testing environment with extremely low density and particles at a known temperature. The response of the device is looked upon and should coincide with the known value.

Since this is an off-the-shelf device, it need not be tested separately. Only the implementation, calibration and assembly are validated.

Laser Retro Reflectometer

The reflectometer instrument is used to measure angular distribution of re-emitted/reflected air particles. As seen in Section 6.6, multiple re-designs of the reflectometer used on the 'STS-8' Shuttle mission have been proposed. Since no final design decision has been made, the verification and validation methods for this instrument will be quite general.

At first, a check will take place whether the reflectometer complies to the general instrument requirements and the reflectometer requirements themselves. The requirements imply that a number of verification and validation methods need to take place. In addition to the steps to be taken as described in Section 15.5.1 a few additional processes need to take place.

The reflectometer needs an incoming flux of particles to take its measurements. This depends on the local density and the area of the intake-slit at the top of the reflectometer. Both these parameters can be investigated using a numerical model. The area of the slit might be adjusted to allow for the desired incoming flux of particles. In-flight tests will be conduced to determine whether the reflectometer is working correctly. The in-flight output data should make sense if compared to the a-priori simulations.

Since the conditions encountered by the MIRALOS mission are not reproducible on Earth no actual tests can be conducted before deployment. However, since a comparable design (the reflectometer from the 'STS-8' Shuttle mission) has been tested in orbit some features can be considered as proven.

Verification of the data acquired from the reflectometer will be conducted using the available models for the angular distribution of re-emitted and reflected air particles in combination with the acquired values for the accommodation coefficient.

Accelerometer

The SuperSTAR accelerometer is used to measure accelerations of the satellite, which are used for the calculation of the drag, in order to be able to derive the accommodation coefficient. It is a very sensitive instrument which needs to be mounted and secured with extreme precision. The accelerometer has already been used on previous missions (GRACE) and is therefore a proven flight model. However it is still necessary to verify it in combination with the MIRALOS spacecraft, both on Earth and in-flight.

Besides the procedures which are described in Section 15.5.1 a few calibration procedures have to be completed. These calibration procedures are pre-flight, internal and external calibration, possibly supplemented by satellite-to-satellite tracking observations [162].

Pre-flight calibrations consist of orientation and temperature calibrations and a pendulum bench test. A multi-parameter calibration can be conducted which can account for gain and offset in each channel of the accelerometer, as well as induced thermal stresses, cross-axis interference, package rotation, cubic non-linearities and temperature dependence [163]. The allignment of the accelerometer will also be tested on the test bench for further confirmation. However, the 1 g environment will pose difficulties since the accelerometer is designed for 0 g use. A drop-tower test might be conducted to simulate the 0 g environment as experienced in-flight.

Internal calibration is conducted in-flight. In this procedure the possible thrusters are calibrated first, using the un-calibrated accelerometer. After the possible thruster calibration the thrusters are fired in a controlled manner to calibrate the accelerometer. This procedure provides information on relative scale factors, and misalignments of accelerometer pairs.

The external calibration is a validation method that is conducted to establish that the gradients of the gravitational observations match the values of gravitational models and ground data. This procedure filters out remaining unsolved errors.

Finally, satellite-to-satellite tracking observations can be used to further calibrate the accelerometer. This method uses the GPS receiver and SLR data to obtain an even higher calibration accuracy.

Laser Retro-Reflector

A retro-reflector is incorporated in the MIRALOS spacecraft to allow for very accurate altitude measurements, using SLR, for the spacecraft. This can be used to validate accelerometer data and determine the accelerometer bias drift (as described in Section 6.5.2).

The SLR itself is a very simple concept and therefore only the general verification and validation methods as described in Section 15.5.1 are used. An in-flight test is in reality already a scientific measurement and will only verify that the mirror of the SLR is indeed pointing towards the Earth and is not obstructed.

UV horizon sounder

Designed to carry out the secondary mission of further studying the dynamics of thermosphere, this instrument has been flight-proven on board the TIMED satellite [164]. Regarding the validation of the instrument, information can be compared to the measurements carried out by the TIMED mission, and insight can be gained by composition and temperature measurements of other satellites in the examined altitude segment.

15.5.3. Subsystems

The separate subsystems are assessed in this subsection. As these subsystems have been designed in more detail compared to the mid term report, a more extensive discussion of the verification and validation for these subsystems is given below. The verification and validation actions should be planned properly. For each task the objective, the way to achieve the objective (e.g. inspection, analysis, ...), the facilities, people and money, the description of the activiy, the execution and documenting should be properly planned.

Attitude Determination and Control System

The subsystem concerned with attitude determination and control should be tested by analysis, simulation and on-ground tests. Firstly, the satellite including ADCS should be simulated throughout its orbits to determine whether the star and sun sensors will always be available for attitude retrieval. Additionally, the magnetic field of the Earth throughout the orbits should be looked upon to ensure the magnetic torques will suffice for attitude control and to what accuracy. Also, the performance of sensors under spinning should be considered for spacecraft stabilisation.

For sensor verification, all sensors must be assessed individually and in different configurations. The spacecraft should be illuminated from different angles and performance of the star and sun sensors under blinding should be analysed. In a similar sense as the verification for the GPS system, the attitude determination using GPS antennae should be looked upon. Lastly, the magnetometer can be tested by simulating the spacecraft's internal instruments and the Earth's magnetic field. Furthermore, real life tests should be performed additional to simulation and analysis to all these sensors.

For actuator verification, a simplified spacecraft dummy can be developed including predetermined disturbances of which all properties are known, upon which its attitude is controlled using the actuators. Secondly, a computer model should be developed that accurately predicts the torques on the spacecraft and the Earth's magnetic field. For this disturbances, the centre of pressure and the centre of gravity are to be determined accurately. These values depend on the fuel distribution and the mass-trim assembly, different configurations are possible that influence the magnitude of the torque. Realistic worst case scenarios must be considered. Furthermore, the effect of the magnetic torque rods on the internal spacecraft electronics should be analysed by tests and analysis. The calibration procedure should be verified by computer simulation and the thrusters will be tested by operation in excess of their designed lifetime at least twice.

Orbit Determination and Control System

This subsystem accounts for orbit determination and orbit control. It will be tested by simulation using an analytical model, as it closely depends on GPS measurements and the ADCS. The verification and validation procedures are described in Sections 15.5.2 and 15.5.3 respectively.

Electrical Power System

The EPS uses covered interconnected photovoltaic cells in combination with lithium-ion batteries and a power regulator unit which are manufactured by the companies Emcore, Quallion and Airbus Space and Defense respectively. Therefore, both the verification and validation for these individual components has already been performed by the corresponding companies. Inspection of these verification and validation processes is needed, especially for the degradation factors which have played a very important role in the sizing of the EPS. Errors can also occur for the connections between these EPS components. Verification and validation of the interconnected components has to be assured. The interconnected EPS can be verified using a test model on Earth. The test model should meet every specified power requirement. Also, as temperature is an important parameter for the efficiency of the EPS, the test model should be tested under extreme temperature conditions and analysis should point out whether the efficiency decreases as expected and whether the power requirements are met. The system should also be inspected for its magnetic field strength and thermal radiation. The EPS can be validated by demonstrating the correct operation for each of the spacecraft modes which are discussed in Section 15.3.

Thermal Control System

During the preliminary design of the thermal control subsystem a large amount of simple first order estimates are made. MATLAB codes were written to perform these calculations. Since requirements constantly change slightly during the design of the spacecraft these scripts significantly speed up the process. These small scripts all had to be verified using simple calculations by hand to see whether the orders of magnitude make sense.

It is very challenging and computationally expensive to perfectly model the spacecraft's thermal control system. Therefore it is more time and cost-efficient to perform tests using a preliminary thermal design as a starting point and fine-tuning it accordingly.

The thermal control subsystem is designed specifically for the MIRALOS mission. It therefore requires testing both before and after integration, and before and after launch. Before assembly, the thermal control system is put into a simulation environment where it will be exposed to a high-vacuum and heating with a power flux of at least $1.4 \cdot 10^3$ W for the duration of at least one orbital period. Furthermore, it will be exposed to vacuum conditions and zero power flux at the predicted minimum temperature experienced during orbit for the duration of at least one orbit. The thermal control system test is done to ensure that the system maintains a temperature within the operating conditions of the instruments. This test will be repeated after assembly and integration with the spacecraft bus and subsystems. These test will not only ensure the correct functioning of the thermal system, but will also validate the results obtained from finite-element software such as COMSOL.

After launch the separate subsystems and instruments containing internal temperature measurement units will be checked periodically to make sure that the systems operate within their allowed temperature range.

Structures
The spacecraft structures will be supporting the loads of every subsystem and protect the spacecraft from harmful vibrations and loads during launch. The spacecraft resistance against vibrations will be tested with the use of a shaker test. Another test should simulate the launch loads and verify the spacecraft rigidity. Furthermore, the spacecraft structures should withstand the thermal loads and the structures thermal deflections should be inspected. The spacecraft structures can be validated by showing the correct compatibility of the subsystems with the structural frame. The subsystems should be mounted correctly onto the spacecraft frame. The frame has to consist of appropriately positioned connectors for the subsystem to be located at the designed spot within the spacecraft.

C&DH
The system that will be processing all commands and providing the interfaces between different spacecraft components requires verification and validation. Verification is achieved by running on-ground tests with simulated input and output signals to the on-board computer and the system is checked for CPU clock speed and its output of thermal radiation. Furthermore, the computer and interfaces are exposed to radiation and electromagnetic fields as experienced during orbit to assure no large biases are introduced to the system over the mission lifetime. The computer software program has to be thoroughly verified. A proper compiler can already check for code language errors. This can be done by splitting the program into parts and checking each part for its output when simple inputs are used.

Regarding validation, all the subsystem functions are checked. Any deviations found during the validation of subsystems can be related back to an erroneous OBC, as it processes all data and commands both internally and of external origin. However, since all data retrieved shows deviations, it is much more likely that the OBC system is failing rather than all other subsystems simultaneously. Validation is also performed by component inspection for compatibility.

Instrument Package
The instrument package comprises all the scientific instruments which are used on the MIRALOS mission. These include the mass spectrometer, accelerometer, reflectometer, temperature measuring equipment, GPS receiver, and laser retroreflector. The individual verification and validation methods for these instruments are described in Section 15.5.2. The individual instruments are not only verified themselves, but are also used to verify the other instruments. Since most instruments are very delicate and precise, this process is very important for the success probability of the mission.

Propulsion System
The propulsion system picked to fly on the MIRALOS mission has been flown multiple times (GOCE, ARTEMIS) and is therefore very well characterised. It has been extensively tested both in flight and on ground. Nevertheless it is advisable to conduct ground testing of the system, both of the separate components, the propulsion system as a whole and the whole system integrated into the spacecraft.

During orbit, the accuracy of the propulsion system can be evaluated. Knowing both all drag forces on the spacecraft, its attitude, orientation and the amount of thrust provided by the thrusters during a manoeuvre, the change in orbit can be predicted analytically. Since all forces and torques are well defined by the multiple payload instruments, the orbit can be predicted very accurately. Large deviations in the predicted and experienced orbit indicate errors in the propulsion system, ADCS or the orbit control system.

Communication System
The communication system will be verified on ground using a physical simulation, similar to the test for the GPS device discussed in Section 15.5.2. The signal received at the spacecraft will be simulated and the spacecraft response is measured. Similarly, the signal transmitted by the spacecraft is received and analysed.
In flight, the resulting data will be verified by comparing it to expected data of models and existing missions. Furthermore, the response to commands transmitted to the spacecraft can be validated by looking at the consecutive changes in location and orientation. This requires a validated AOCS and ADCS, as depicted earlier in this subsection.

Ground Station and Launcher Selection
The to be used ground station and launcher are aspects of the mission that are not controlled by the spacecraft design group. The verification and validation that can be done for these parts of the mission are done by the ground station and launcher groups themselves.

15.5.4. Models
Several models are applied throughout the design process to simplify iterations and calculations. These models are verified and validated to ensure no errors are introduced by these tools. For models the verification process is the determination of whether

a simulation model accurately represents the chosen physical model. The validation process is the determination of whether the simulation results accurately represent the physical problem.

NRLMSISE-00
The NRLMSISE-00 model has been verified and proven to predict the atmospheric properties up to 1000 km altitude with acceptable accuracy [21]. However, modifications have been made to the model in order to account for long-term atmospheric changes. These atmospheric changes are still not well-defined and there is no accurate correction factor found up to this point. Rather, the goal of this mission can be defined to further refine and improve the NRLMSISE-00 model.
As far as the validation of these models is concerned, drag estimations can be done using recent LEO missions and then compared to what is predicted by the model. Furthermore, when the MIRALOS spacecraft is in orbit and gathering data, the updated model will be validated with true measurements.

Development Tools
Many tools have been designed in order to allow quick design iterations and budget estimations. These tools are not treated each in detail, as their goal and importance varies significantly. It is not sensible to discuss all of them separately. Rather, a general procedure is subsequently described for verification and validation procedures.
For verification procedures, simple inputs of which the output is known are inserted into the software. If the results agree with what is expected by theory, the model is assumed verified. To the extent of model validation, existing validated models and results from real-life tests are used, if validation is deemed necessary. For simple, back-of-the-envelope calculations, no extensive validation is performed.

General Mission Analysis Tool
The General Mission Analysis Tool has been developed mainly by NASA for real-world engineering studies, education, and analysis for real space missions. The tool passed its final acceptance testing in September 2013 and it can be therefore safely assumed to be verified and validated [13]. Nevertheless the outcome of the simulation should be verified and validated as it is still possible that the tool is improperly used or errors are made in the input. This was done by checking the output with expected reference values from literature. For example, based on the ballistic coefficient and altitude of the spacecraft, it can be found in the SMAD [18] that the spacecraft should decay in less than one solar cycle. This could also be seen in the simulation. Also low-thrust maneuver behaviour was checked by simple calculations and comparison with expected behaviour from literature. Further simple sanity checks were performed; a results match up with the basic theory of orbital mechanics was checked. While performing this check it was found for instance that the spacecraft initial altitude would increase way above its insertion altitude, which is physically not possible. The reason for that was the usage of a wrong coordinate system.
After having completed the verification and validation of the GMAT tool it can be said that the results are adequately verified and validated for this stage of the project.

15.6. Risk Assessment

In order to minimise the risk of preliminary mission termination, risks that influence satellite performance are quantified, qualified and assessed. The risks are displayed in Table C.1. These risks are identified on their probability and severity of occurrence. Risks for the overall mission and for the different subsystems are identified. The risk map falling from this table is displayed in Table 15.1.

Table 15.1: Risk map for the mission. Risks are categorized in terms of probability of occurrence and impact.

	Impact			
Occurrence	Negligible	Marginal	Critical	Catastrophic
High		M16	M09-1	
Medium		M09-5, M11-3	M08-4, M09-4, M11, M11-1, M11-2, M18	
Low		M04-1, M04-2, M09-2, M18	M05, M06, M07, M08, M08-2, M08-3, M09, M14, M17, M19	M04, M12, M12-1
Very low	M01, M02, M03	M12-2	M04-3, M08-1, M09-3, M10, M13, M15	

From this table, it can be concluded that most resources should be spent on risk M09-1, followed by risks M06, M08-4, M09-4, M11, M11-1, M11-2, and M18. Further design should aim on reducing these risks and reducing either probability of occurrence or severity of occurrence. These risks are to be updated constantly. New risks should be qualified, quantified and mitigated. Old risks should be mitigated and eliminated.
Furthermore, risks related to development and design of the mission are depicted in the sensitivity analysis which can be found in Section 15.7.

15.7. Sensitivity Analysis

A sensitivity analysis is performed to assess the influence of fluctuations and modifications on major system design parameters. For this reason, a N^2-chart is made that displays and relates important design parameters. This tool is used to determine the robustness of the mission design.

The sensitivity chart is displayed in Figure 15.8. The main design parameters are listed diagonally and related to each other in the remaining cells. The effects of changes in major parameters displayed in square blocks are described in the chart in the elliptical elements. The colour scheme applied is defined as follows: green cells mean there is little to no correlation between the parameters, or/and the chance of changes in parameters due to other changes are negligible. Yellow cells indicate the probability of change is present, but is very small. Alternatively, also the change itself could be not very significant and hence is of no real importance. Red cells mean that the chance of change is clearly present and any iterations must keep these relationships into perspective.

This N^2-chart could be made significantly larger to include more subsystems. However, as these are currently being designed and limited information is available, this may be done in a later stage in the design. Currently only top-level design decisions are considered.
From this figure it is readily seen that no critical risks on lower levels exist that would require a top-level redesign of the spacecraft. The most important relationship originates from the performance of scientific payload. Namely, if the scientific payload does not suffice to all requirements with the orbit depicted, the orbit profile might require change. Furthermore, changes in the satellite shape is strongly correlated to the quality of measurements. However, both of these changes have a very small probability of occurrence.

Changes on a high level such as orbit profile and mission duration do have consequences for the spacecraft mass, size and subsystem designs. However, most subsystem designs at the current stage still allow fluctuations in the mission profile and are sized for extreme conditions, including safety factors. Changes in orbit profile and duration are very improbable, and the current design is flexible to account for this. It can be concluded that the current mission design is very robust to parameter changes.

15.8. Reliability, Availability, Maintainability, and Safety Characteristics (RAMS)

The discipline of reliability engineering is a sub-discipline within systems engineering and is analysed in this section. It is made up of four characteristics, and although these will be examined separately henceforth, it is important to remember that they are interrelated.

15.8.1. Reliability

Reliability translates to the probability that a system will perform as specified for the whole length of a mission, under the specified operating conditions. Selecting a redundancy approach for the MIRALOS mission, three options are considered. These are: a single system redundancy, a system redundancy, or a partitioned redundancy [18].

On a general level reliability can be expressed in terms of a Weibull distribution as shown by Equation (15.1).

$$R = e^{-(\alpha t)^{\beta}} \tag{15.1}$$

When examining the spacecraft subsystems, the reliability of the overall system is expressed as the product of the reliabilities of the subsystems. This is displayed in Equation (15.2).

$$R_s = \prod_{i=1}^{n} R_i \tag{15.2}$$

Through the use of the above two expressions and further selection of the applied redundancy, the reliability can be determined. The single system redundancy reliability makes direct use of the two expressions. For a system redundancy, a dual redundant subsystem is defined; this consists of two strings, each containing the number of considered subsystems, placed in series. The latter reliability is computed using Equation (15.3).

$$R_{s,p} = 1 - \prod_{i=1}^{n} (1 - R_i) \tag{15.3}$$

where Equations (15.1) and (15.2) are used to describe R_i for each string. These are then used to compute the final reliability. For a partitioned redundancy each of the subsystems is set in a dual redundant system; each pair placed in series. In this configuration, reliability is determined using Equations (15.1) and (15.3) to determine the reliability of each pair; these are then applied to Equation (15.2).

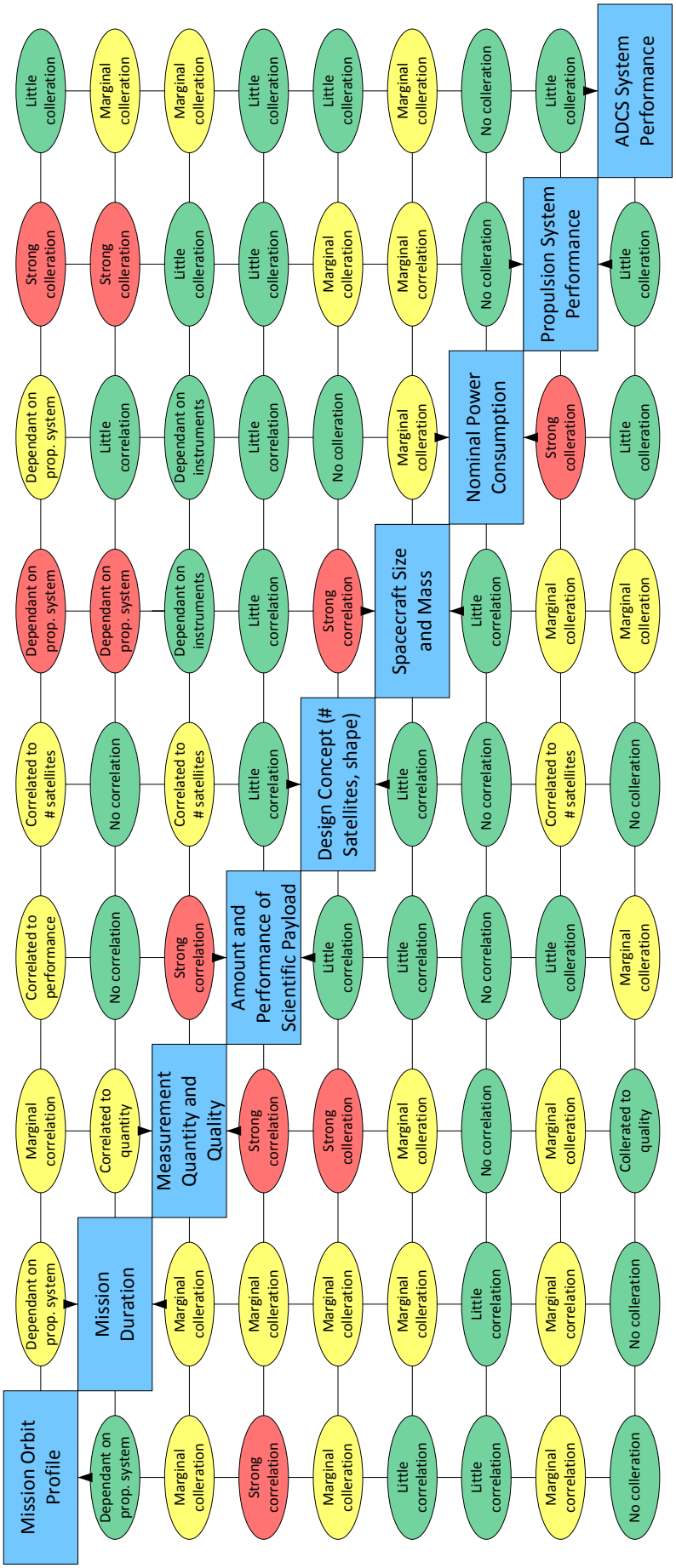

Figure 15.8: Sensitivity analysis displayed in a N^2-chart. The main design parameters are listed diagonally

The most conventional approach that can be taken is that of a single system redundancy, expressed by Equation (15.1) with $\beta = 1$. For this report this will be the selected approach, the lack of detailed information making it unsuitable to carry a more thorough investigation.
A study presented in SMAD presents statistics of spacecraft failures based on known and unknown causes for four different mission lifetimes [18]. Based on Chapter 4, the mission lifetime is estimated to be about 6 years. Within the last couple of decades the percentage of overall spacecraft failures has been oscillating between 4% and 10% [165], yet a trend of improving performance can be distinguished by taking a larger dataset. Assuming a constant failure rate of 5% over a mission lifetime of 6 years results in a spacecraft reliability of 74%, following Equation (15.1), with α being the failure rate. The reliability of each subsystem is based on an estimate of the frequency of spacecraft failures based on subsystem as shown in Section 15.8.1, which is a modified version of table 24-3 found in SMAD [18]. The third column presents the failure rate for the specific mission. The fourth column presents the reliability of each subsystem.

Table 15.2: Estimated frequency of spacecraft failures.

Subsystem	**5 Year Failure Contribution**	**6 Year Failure rate**	**Reliability**
Attitude Control	11%	0.0055	0.967
Thruster/Fuel	16%	0.0080	0.953
Control Processor	4%	0.0020	0.988
Mechanisms/Structures/Thermal	11%	0.0055	0.967
Payload Instrument	3%	0.0015	0.991
Battery/Cell	10%	0.0050	0.970
Electrical Distribution	10%	0.0050	0.970
Solar Array (Deployment and Operating)	12%	0.0060	0.964
Telemetry Tracking and Command	18%	0.0090	0.947
Unknown	5%	0.0025	0.985

15.8.2. Availability

Availability translates to the probability that a certain system will be available when required. Mathematically it is expressed as the ratio between the total uptime and the total time passed. The total time passed is the sum of the uptime and downtime. An example for the downtime concerns the periods of time when the software needs to be updated.
The availability quantity can also be expressed with respect to the failure λand recovery rate μ, if these are assumed to be exponentially distributed. An example is given in Equations (15.4) and (15.5). When considering the availability of an (n-)redundant system, the expression is similar to Equation (15.3).

$$A = \frac{\lambda}{\lambda + \mu} \tag{15.4}$$

$$A_{s,p} = 1 - \prod_{i=1}^{n} (1 - A_i) \tag{15.5}$$

15.8.3. Maintainability

The maintainability describes the ease, accuracy, safety, and economy in the performance of maintenance actions. The maintenance of a spacecraft differs significantly from any other systems. After launch the physical maintenance is limited due to the fact that the system is in orbit. Consequently, carrying out physical maintenance is very unlikely. Although it has occurred for a handful of missions like the Hubble Space Telescope, physical maintenance is rare and far from ideal.
However, other types of maintenance exist that can be performed for the MIRALOS-satellite. Three of these types of maintenance are listed below. For each type a brief description is given.

- **Orbit maintenance** - The satellite has to perform measurements at an initial altitude of 650 km. After orbit insertion, the satellite will lose altitude gradually, mainly due to drag. Solar pressure on the satellite will make the orbit more eccentric, while the drag will make the orbit more circular. The simultaneous effect of these two perturbations result in a cyclical variation of the eccentricity. Making use of the propulsion system, orbit maintenance can effectively be carried out.
- **Software updates** - The final version of the control system and on board computer of the satellite will contain the latest available update of the software. Nonetheless, at the time the satellite is already operating software updates can still be developed and sent to the satellite. In this way the risk of erroneous software decreases, since it can be corrected depending on the mission results. The software updates are non-scheduled maintenance activities. The time at which the software is updated depends on the possible speed of correction and the urgency. For this reason the scheduling of the software updates cannot be done beforehand.
- **Ground operation** - This is a maintenance activity that will be scheduled. It consists of both the maintenance of infrastructure and the communication maintenance. The former type is required to guarantee the availability of the ground control building. Communication maintenance must ensure the functioning of the antennas, the tracking of the satellite, and the

receiving of the scientific data as well as the satellite bus data. It is important to schedule and perform maintenance tasks to avoid erroneous communication between the ground station and the satellite. Parameters describing the maintenance performance are the Mean Time To Repair (MTTR) and the Mean Time To Maintain (MTTM).

15.8.4. Safety

Safety is the absence of unacceptable levels of risk to humans and equipment. In order to list the safety critical functions and show the redundancy philosophy applied, a Failure Modes and Effects Analysis (FMEA) is used. The FMEA is a qualitative analysis in which each component of a system is posited to fail. The effects of that hypothetical failure on the surrounding components and the system level are evaluated [18]. In this section the tool will be used to evaluate the safety aspects of the MIRALOS system design. Using the subsystems as stated in Table 15.2, first the failure modes for each of subsystem have to be considered. Secondly the effect of each of the failure modes on the system operation has to be determined. The different failure modes will be listed in Table 15.3. Thirdly, corrective actions to limit the probability of occurrence of a certain failure mode will be identified. In the first two columns of Table 15.3 the Failure Mode (FM) of each subsystem are shown. The third column contains a short description of the effect on the entire system of a failure in the given failure mode.

Table 15.3: Subsystems, failure modes and corresponding effect on the system

ID	Failure modes	Effect on System
Attitude Control		
FM-01	Sensor failure	No effect if redundant
Control Processor		
FM-02	Overheat	Computer shut down
Propulsion		
FM-03	Explosion	Complete mission failure
FM-04	Ignition failure	No orbit control possible
Structures and Thermal Subsystem		
FM-05	Thermal control failure	Erroneous measurements from affected payload instruments
FM-06	Structural failure	Component failure/Mission failure
FM-07	Mechanism failure	Related component cannot be moved anymore
Payload Operations		
FM-08	Instrument failure	Required system reboot/Mission failure
Power Storage		
FM-09	Wear	Power loss resulting in instruments shut down
Electrical Distribution		
FM-10	Wire misconnection	Misconnected component cannot be used
Power Retrieval		
FM-11	Deployment failure	Partial or full loss of power resulting in instruments shut down
FM-12	Wear	Power loss resulting in instruments shut down
Telemetry, Tracking & Command		
FM-13	Tracking error	Erroneous scientific data
FM-14	Antenna deployment failures	Partial or full communication loss
FM-15	Low signal to noise ratio	Partial or full loss of data and a higher required power
Unknown		

Table 15.4 shows again the failure modes for each satellite subsystem. This table also contains the severity of the failure mode. The severity scale goes from 1 (tolerable) to 5 (catastrophic). The corrective actions to prevent each failure mode from occurring are listed in the third column.

The safety considerations of the spacecraft after it enters an uncontrolled reentry are discussed in the recommendations; it is not yet decided in this phase of the design.

15.9. Market Analysis

A market analysis is performed to ascertain the need of the MIRALOS mission as a compiled scientific experiment. Considering competition within this market, the concept is only applicable when comparing the eagerness of other interested parties to carry their own satellite missions. To them, these may appear to be more valuable to the scientific community compared to another mission. MIRALOS lies in that same market bracket.

Earlier in the exercise, a market analysis was included in the second report of the report series, namely the baseline report [15]. The analysis is shortly summarised and updated in this section. The market for the MIRALOS mission was assessed on eight levels using a method described by D.A. Aaker and D. McLoughlin [166].
With respect to the mission objective, the MIRALOS mission is related to a relatively small market with few to no competitors. The mission is a first of its kind to have rarefied aerodynamic studies placed in a sealed package with atmospheric studies as its

Table 15.4: Failure modes and corresponding correcting actions

ID	Severity	Corrective Action
FM-01	1	Redundant set of sensors
FM-02	3	Accurate thermal control
FM-03	5	Accurate thermal control
FM-04	4	Redundant ignition system
FM-05	5	Thoroughly verify the thermal control system
FM-06	4	Thoroughly verify the satellite structure
FM-07	4	Decrease number of moving parts/test mechanisms
FM-08	4	Thoroughly verify the payload instruments
FM-09	3	Account for wear
FM-10	4	Perform several rounds of checks
FM-11	4	Thoroughly verify the deployment system
FM-12	4	Account for wear
FM-13	3	Use independent tracking devices (GPS, retroreflector)
FM-14	4	Thorough verify the deployment system/redundant antenna
FM-15	4	Accurately estimate power consumption
Other	NA	Identify possible unknown failure modes

main purpose. Since no missions with similar objectives exist, no market exists either from this point of view.
Reconsidering thus the perspective used, by looking at all the different conceptual designs offered to ESA, NASA, and other prominent space agencies for realisation every year, there is harsh competition to get the approval for any design. The market is very diverse, ranging from hobbyists, to research institutes, to official space agencies. The limited budget available to approve missions means only a few can ever be realised. Since the MIRALOS mission has a large financial budget, the mission must be worthwhile to be considered.
In order to structure a market analysis, this process is divided into multiple dimensions, which will be handled in the upcoming subsections. The considered dimensions are:

- Market and sub-market size
- Market and sub-market growth
- Market and sub-market profitability
- Emerging sub-markets
- Trends and developments
- Cost structure
- Distribution systems
- Key success factors

15.9.1. Market and Sub-Market Size

The final product of the MIRALOS project belongs to a large-sized market in terms of competing project proposals. Other missions have already carried measurements on atmospheric properties in LEO, thus the market volume is said to be of medium size and the market potential large. Although satellite missions have been designed to gather data on the Earth's atmosphere, no spacecraft has combined this in-situ data with an investigation of gas-surface interactions. In that sense, MIRALOS lies within a sub-market of its own.

15.9.2. Market and Sub-Market Growth

The market of LEO satellite scientific missions is expanding in direct relation with the number of countries and particulars that become developed enough to consider space applications as a part of their GDP and net balance respectively. Such bodies initially come in contact with well established names in the industry of space science. As a result, they become direct competitors for a chance to be approved. As mentioned in Section 15.9.1, the instrument package of MIRALOS, and corresponding measurements, make it a sole-standing mission. In other words this means that the sub-market of MIRALOS has space to grow, but this growth cannot objectively be predicted. Because the bracket is newly-formed, no extrapolation can be performed, as this will not be of accurate measure. Because MIRALOS is the first mission in its field, no equalisation can be done either, which means that the sub-market is unpredictable.

15.9.3. Market and Sub-Market Profitability

Three factors can be neglected when considering profitability. For the considered sub-market, the threat of new entrants, the threat of substituting products, and rivalry among companies be assumed to be highly improbable. Considering the market of scientific missions in LEO, the two larger factors are the power of the competing bodies (individuals, institutes, space agencies), and the limit of the budget of the presented missions. Available information on the latter two is scarce, however it is undeniable that these will greatly influence the development of the MIRALOS mission.

15.9.4. Emerging Sub-Markets
Information concerning possible emerging sub-markets is limited. MIRALOS is the first mission in its sub-market, but it is hard to know if some other organisation somewhere is considering a similar design with similar mission goals.

15.9.5. Trends and Developments
A trend or development can hardly be identified for the sub-market of MIRALOS. No other products have been designed to fulfil a similar mission, which causes the market trend and development dimension to be negligible in terms of sub-market analysis. Nevertheless, it is fruitful to say that the market of space applications is a developing sector, and multiple trends exist for Earth-observation satellites, communications satellites, other commercial applications, military applications, etc.

15.9.6. Cost Structure
The MIRALOS project is part of the space engineering market, which often has a complex cost structure. Prices defined in this market are relatively high, which causes the cost structure to be an important factor when doing the market analysis. As stated in the requirements, the spacecraft (ground segment and launcher included) for the MIRALOS mission cannot exceed €350,000,000. Such high costs induce a high risk; failure of the project could be disastrous.

15.9.7. Distribution Systems
For this project this specific dimension can be overlooked. There is only one product that will be produced, and this product will not be sold to public customers. Although multiple possible customers still exist at this early stage in the design process, ESA will be used as the default customer, which will use the product to investigate upper atmospheric properties and their effect on the spacecraft surfaces.

15.9.8. Key Success Factors
For a company to achieve its objectives in terms of marketing, a number of important factors have to be defined. These key success factors essentially determine whether a project can meet its goal, when examining the considered market and sub-market.

For the MIRALOS project two key success factors can be defined: the availability of resources, and the reliability of achieved data.

15.9.9. Wrap-up
In the previous section, all eight market dimensions were defined and related to the MIRALOS project. Falling from this, the attractiveness of the particular market that MIRALOS is in is defined and related to customer and competitor analysis. From the covered analysis, it can be said that the 'MIRALOS-submarket' is a small market which has the potential to grow over the upcoming years. It is however hard to predict this growth, as the market is very young, and this mission is the first in its field of application. The future of MIRALOS is and will be greatly affected by the competing bodies. The competition is characterised in terms of attractiveness of design, maximum cost of the mission, and relativity to the current scientific interests of the prominent space agencies to which MIRALOS will be advertised.

15.10. Sustainable Development Strategy
Sustainable development is becoming an increasingly important factor in the space industry. The space industry pollutes the environnement by means of space debris and atmospheric pollution. Space debris forms a major threat to current and future orbiting satellites, disclosing the possible danger to the astronauts residing in the ISS. Atmospheric pollution is also an unwanted side-effect that is induced by rocket launches and disposal by re-entry. The consideration of the space and Earth environment is essential in space design.

15.10.1. International Guidelines
International guidelines have been established to ensure fair usage of the space environment. These are applicable mainly to minimize space debris and maintain usability of frequently used regions in the space surrounding the Earth. There are 17 times more tracked debris in LEO than Medium Earth Orbit (MEO) or Geostationary Earth Orbit (GEO) (approximately 17000 in 2013). Furthermore, the amount of debris that cannot be tracked in LEO is considerably larger. The Space Debris Mitigation Guidelines of the Committee on the Peaceful Uses of Outer Space (COPUOS) dictate the following guidelines regarding space debris mitigation [167]. A concise explanation is given for each guideline.

1. **Limit debris released during normal operations.**
   Space systems should be designed to not release any debris during operations. If this is considered unfeasible, the effect on the space environment should be minimized.
2. **Minimize the potential for break-ups during operational phases.**
   Spacecraft and launch vehicle orbital stages have to be designed to avoid failure modes that might lead to accidental break-ups.

3. **Limit the probability of accidental collision in orbit.**
   During the development of the mission profile the probability of collisions with space objects should be estimated and limited.
4. **Avoid intentional destruction and other harmful activities.**
   In-orbit destruction of space objects should be avoided because of the increased probability of damage to other objects in the same region. If absolutely necessary, the destruction should take place at sufficiently low altitudes to ensure a short orbital decay time of the debris.
5. **Minimize potential for post-mission break-ups resulting from stored energy.**
   If space objects contain unused energy resources, these resources need to be depleted or made safe. If such a hazard is not considered, this poses a threat if hit by debris or in case the system becomes unstable for a reason such as overheating.
6. **Limit the long-term presence of spacecraft and launch vehicle orbital stages in the LEO region after the end of their mission.**
   If the operational lifetime of space objects in LEO have expired, the object should be disposed off as soon as possible, favourably in a controlled manner.

The MIRALOS mission will be designed with these guidelines in mind to minimize the impact of the mission on the long-term space environment.

15.10.2. Considered Factors

A number of factors have been selected that will influence the design of the MIRALOS mission as part of the sustainable development strategy. These factors have been divided in primary and secondary factors. They are presented in this subsection.

Primary Factors

This subsection contains the factors of primary importance.

- **Limitation and elimination of after-life debris:** Spacecraft have a predetermined mission lifetime. Once this lifetime is elapsed, the mission might be continued if possible. Otherwise, a disposal plan is required to limit space debris or to avoid future collisions with operating satellites. In the case of the MIRALOS mission, this is done by manoeuvering the spacecraft to a burn-up orbit or let it decay naturally. This process is described in Section 15.10.3.
- **Limitations of mass:** Limiting the mass of the satellite will decrease the required thrust by the launcher which means less fuel is used. Also less bulk material (such as used stages) is left over from the launcher. Both of these aspects decrease the environmental impact of the launch. The MIRALOS spacecraft will have a mass of around 457.2 kg, which is computed in Section 5.3.1.
- **Usage of flight-proven components:** Using flight-proven components decreases testing and development costs. Testing usually involves mock-up models and other items which have to be disposed of, increasing the use of resources and producing more waste during the design process. In the MIRALOS mission a few flight-proven components will be used such as, for example, the TRSR-2 GPS Receiver.
- **Usage of small/shared launcher:** Launchers use a large amount of fuel and are complex and expensive. It is important to maximise the payload efficiency for each launch. This implies that, in order to limit resources, sharing a launcher with multiple organisations or using a small launcher is favourable, both in cost and waste production. A selection of launchers for the MIRALOS mission is examined in Section 13.4.

Secondary Factors

This subsection contains the factors of secondary importance for sustainable development with respect to the MIRALOS mission.

- **Modest usage of resource requirements:** Keeping in mind the mission objective, the used resources have to be limited to an appropriate amount, making sure that no resource is excessively used. This includes material use, but also labour and monetary use.
- **Limiting fuel use:** The spacecraft at the end of the mission will enter the EOL phase. To dispose of the spacecraft, a defined amount of fuel will be used to place the satellite in a burn-up orbit.
- **Standardisation of test procedures:** By setting proper milestones throughout the design process, MIRALOS-based research satellites and standardised test process allow for a more effective approach to sustainable development.
- **Advancing from educational project to application:** The MIRALOS mission will help to gather experience through an educational medium (e.g. academic projects) and to understand of the basics of rarefied aerodynamics on a fundamental level. Applying the knowledge allows for a better flow to reach results. In comparison, rewarding this mission to a commercial company might deviate the result from a theoretical and practical exercise, to a purely practical one (”one shot mission”). This would go against the notions of sustainable development.
- **Collaboration between institutions:** Collaboration allows, if used properly, a more effective sharing of knowledge, but also subdivision of cost, time, and effort. A joined venture also reduces risks.

- **Sharing know-how and the improvement of global satellite performance:** Sharing the data, findings, and information gathered through MIRALOS will allow a more efficient design for future LEO satellites. This will result in a reduction of fuel required to do similar missions, globally improving satellite performance. In addition, the produced data can be used to improve future atmospheric and orbit calculations.

15.10.3. End-Of-Life Considerations

s The number of LEO objects is increasing, and therefore the chance of impact between these objects increases as well. This in turn creates an ever greater amount of debris, which could eventually lead to a chain reaction. If this trend continues, the LEO region will grow to be unusable. Therefore the EoL of the mission needs to be taken into account.
The requirement by law stipulating that the satellite needs to be out of space by 25 years [167], the implications had to be analysed further. The MIRALOS mission will operate in the $350 - 650$ km region. If no orbit maintenance is at 650 km, the MIRALOS spacecraft will decay and burn up in under half a solar cycle. This result was obtained from the 'GMAT R2013a', a software developed by NASA. This orbital decay time is acceptable, and does not account for the possibility of using the propulsion system to lower the orbit even faster. Independently of the taken approach, it is ensured that the MIRALOS spacecraft will not become long-term space debris and therefore the regulations will be met under any circumstance.

15.11. Compliance Matrix & Feasibility Analysis

This section contains the compliance matrix and the feasibility analysis of the stakeholder requirements as stated in the baseline report [15]. In Table 15.5 all stakeholder requirements are listed again, only now one column is added at the right part of the table. In this column it is stated whether the requirement is met by the current design and which values (if possible) it actually meets. The following colour coding is used: green means that the requirement is met by design, orange that it may be met by design and yellow that it can not be checked whether it is met by design.

Table 15.5: Compliance matrix of the MIRALOS mission (green: sufficient, orange: uncertain, yellow: unknown)

ID	Customer Need	Requirement Met?
MIRALOS-SR-1	The satellite mission should provide in-situ measurements of the energy accommodation coefficient with an accuracy better than 2%.	Related parameters are measured with this accuracy or better, so this requirement should be met.
MIRALOS-SR-2	The satellite mission should provide in-situ measurements of the angular distribution of re-emitted or reflected air particles with a resolution of better than 5° and an accuracy of better than 2%.	Requirement is met when a MCP with $3,240,000$ channels is used, so this requirement should be met.
MIRALOS-SR-3	The satellite mission should provide in-situ measurements of the aerodynamic linear acceleration every 80 km along-track, with a precision better than 1 nm/s^2 and accuracy better than 5%.	Acceleration precision of 10^{-12} m/s^2 can be measured, with an accuracy of 10^{-13}.
MIRALOS-SR-4	The satellite mission should provide information on the dependency of the gas-surface interaction over the full range of incidence angles for a flat panel, between 0° and 90° with a resolution of at least 5°.	Requirement is met when the flat plate is rotated by 5 degrees or less, so this requirement should be met.
MIRALOS-SR-5	The satellite mission should provide information on the dependency of gas-surface interaction for both atomic oxygen and helium dominated atmospheric conditions.	Orbit is designed to meet this requirement.
MIRALOS-SR-6	The satellite mission should provide information for resolving the dependency of gas-surface interactions with atmospheric temperature over a range of at least 300 K.	Orbit is designed to meet this requirement.
MIRALOS-SR-7	The total cost of the mission, including launcher and ground segment, should be below EUR 350 million.	Cost estimation currently on EUR 121 million.
MIRALOS-SR-8	The mission shall launch before 2020.	Can not be checked. Though, the mission is designed to be launched before 2020.

In Table 15.5 it can be seen that one requirement can not be checked: it can not be stated whether the mission will actually be launched before 2020, because the project is only in the design phase. After the design phase a lot of other phases have to be gone through, and depending on the time loss during those phases it can be stated whether the launch deadline will be met.

15.12. Design & Development Planning

Due to limited time and human resources available, only a very preliminary design is provided. Many more steps are to be taken in order to finalise and operate the design. These steps are roughly outlined in Figure 15.9. Furthermore, a schedule is made corresponding to these general remaining activities. This is presented using a Gantt chart, displayed in Figures 15.10 to 15.12 for time slots 2014-2018, 2018-2022 and 2022-2026, respectively.

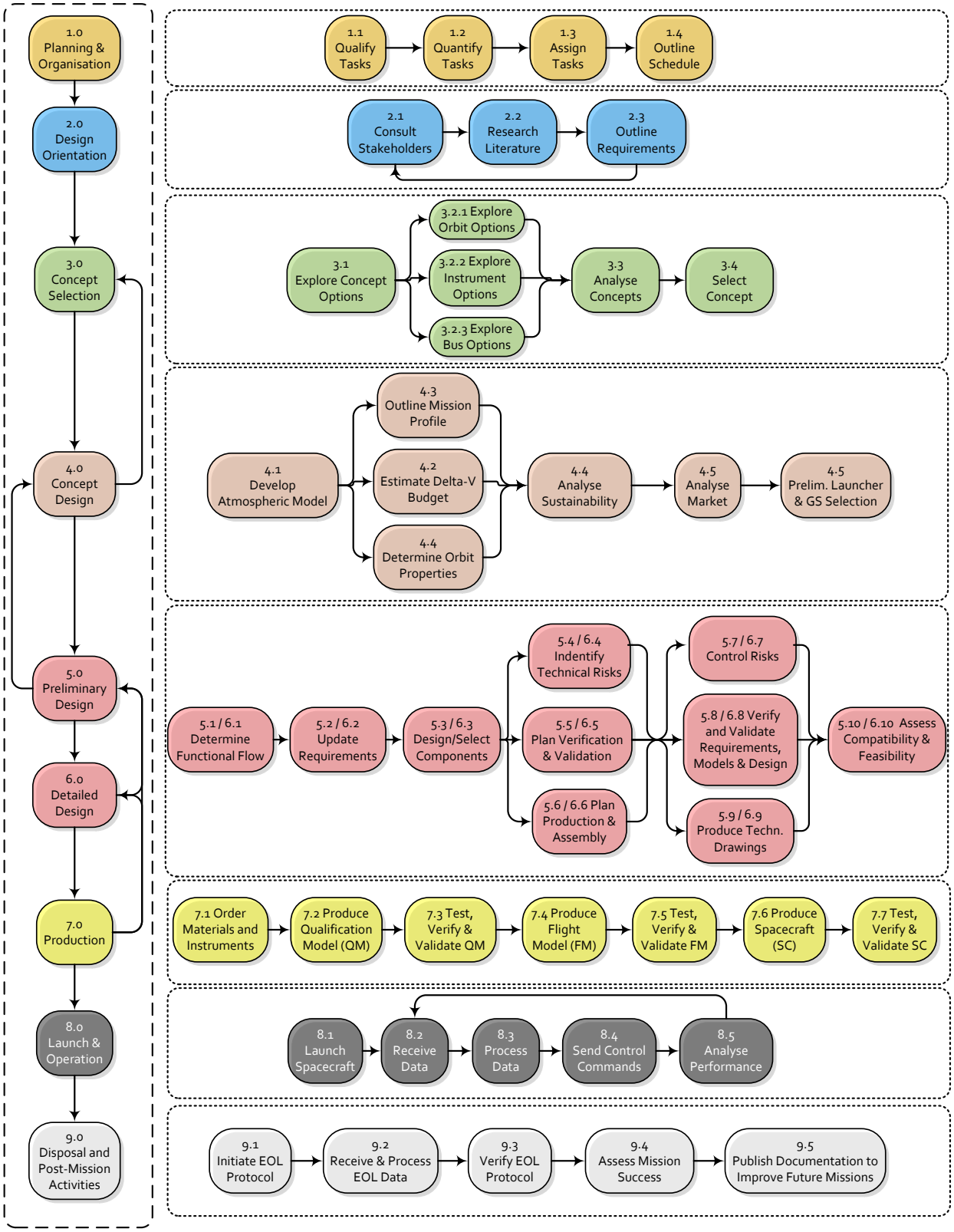

Figure 15.9: Remaining Design & Development Outline

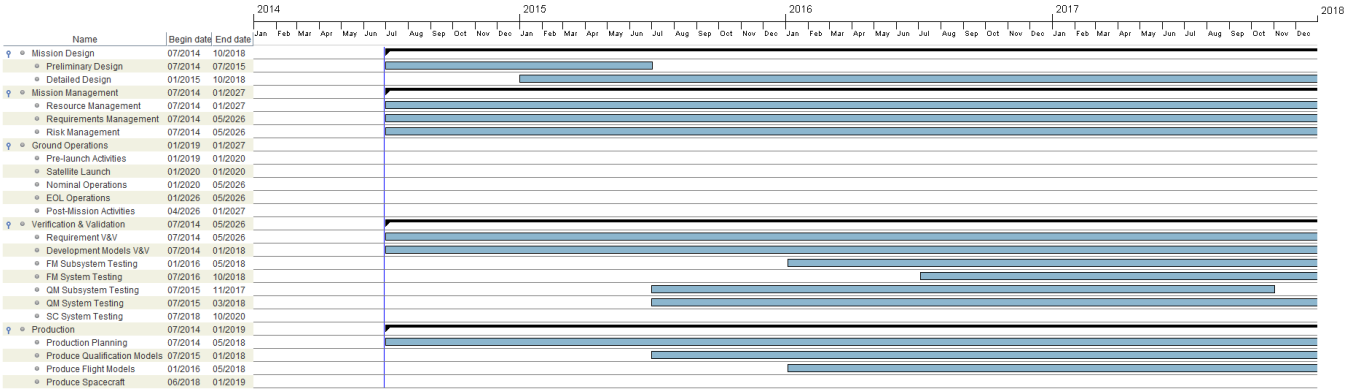

Figure 15.10: Gantt Chart of Remaining Design & Development Activities (2014-2018)

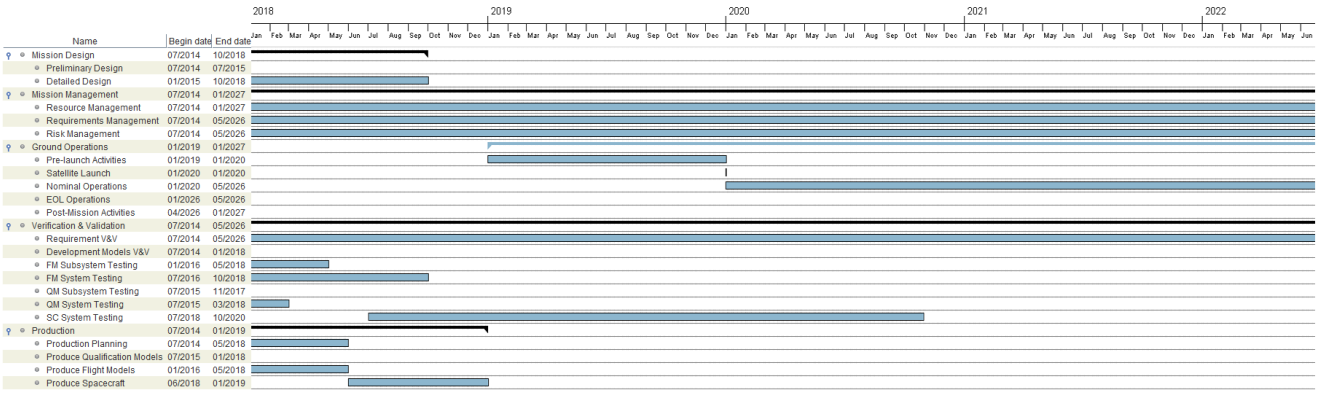

Figure 15.11: Gantt Chart of Remaining Design & Development Activities (2018-2022)

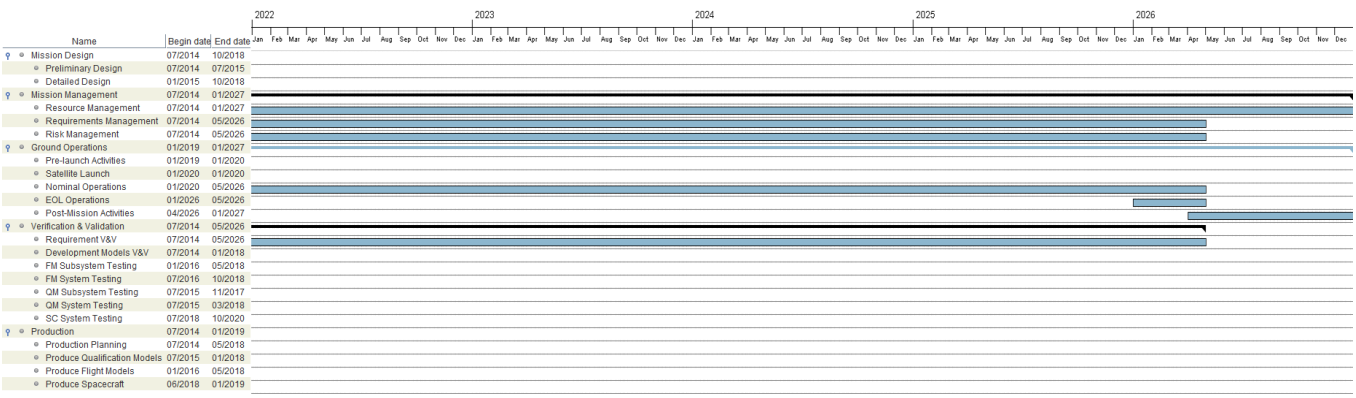

Figure 15.12: Gantt Chart of Remaining Design & Development Activities (2023-2027)

16. Conclusion and Recommendations

The purpose of this report was to describe the design process of the MIRALOS single satellite concept. Each group member was assigned to a particular subsystem. The design of the subsystems and payload instruments has been finalised after several iterations and discussions between the responsible subsystem engineers. Important decisions and selections have been made regarding requirements, orbit selection, payload instruments, and subsystem design.

To accomplish the mission goals, a number of characteristic parameters need to be measured in-situ. These parameters will increase the understanding of particle-surface interactions in LEO, therefore increasing the accuracy of the drag measurements for future LEO missions. The parameters to be measured are:

- Linear and angular accelerations
- Total atmospheric density
- Constituent element particle counts
- Gas temperature
- Spacecraft surface temperature
- Particle incidence angle
- Angular distribution of re-emitted and reflected particles

These parameters are preferably measured over as large a range of altitudes as possible. Therefore a propulsion system has been reconsidered. The orbit analysis was concluded with a nominal mission timeline of six months of observations at each altitude of 600, 500, and 350 km. These observations require a propulsion system able to deliver a total ΔV of 258 m/s in normal solar activity conditions and 279 m/s in high solar activity conditions. The spacecraft shall carry enough propellant to deviate from this mission profile should the conditions encountered during the mission make this necessary.

The orbit profile now defined, the propulsion system could be fully designed. Trading off different propulsion systems resulted in the electrical ion thruster to be the most favorable option, due to its excellent mass performance, high flexibility, and reasonable power consumption. The propulsion system consists of a xenon tank, xenon feed-system assembly, ion propulsion control unit, and an ion thruster with neutraliser.

The spacecraft shape has been mainly designed for a high drag over mass ratio, a simplicity of form to facilitate the drag analysis, and power efficiency in the case of body-mounted solar arrays. These three elements resulted in the selection of an hexagonal shell with a height of 3 m and diameter of 2.2 m (i.e. side lengths of 1.1 m). The location of subsystems within the satellite has been determined by taking into account thermal constraints, instrument pointing requirements, power, and structural requirements. The complete satellite layout is shown in Figure 5.1. The satellite has a total dry mass of 457 kg and carries 13 kg of propellant. It requires 977 W of power and costs EUR 121 million. The mass, power and cost estimation are shown in detail in Section 5.3.

The payload instruments have to a large extent already been selected for the Mid-Term report. Though, there is opted for an accelerometer with a higher accuracy than the SuperSTAR accelerometer which had been selected before. Also, a new instrument is taken onboard the satellite, a UV horizon sounder. This instrument has been selected after consideration of secondary mission objectives. All the instruments are commercially available except for the reflectometer for which a thorough investigation was needed to come to an unexisting design. The payload instruments are listed in Table 5.2.

The ADCS system makes use of a number of sensors and actuators. For the attitude determination, four star sensors, two magnetometers, four sun sensors, and two additional GPS antennae will be used. The attitude control will be performed by the magnetic torque rods operating at 20 and 70 A·m^2. Additionally, twelve cold gas thrusters running on gaseous nitrogen are used for calibration of the mass-trim assembly and in support of the magnetic torque rods.

The EPS provides, stores, regulates, and distributes electrical power to the spacecraft subsystems. A solar photovoltaic-battery system has been selected based on the suitable power range, high specific power, and low specific cost. 17.05 m^2 triple junction gallium arsenide covered interconnected cell solar arrays from Emcore, covering 86.1% of the satellite side area, and three QL075KA lithium-ion batteries from Quallion, resulted from the considered trade-offs. These are capable of providing 975 W to the satellite at all times. The Medium Power PCDU regulates the power between the solar array and batteries, and distributes power to the satellite components.

Thermal requirements were provided to the thermal control engineers from the responsible subsystem engineers. Thermal analysis of the spacecraft delivered important information on what temperatures should be expected on the outer and inner surfaces. An instance of this iteration is the efficiency of the solar cells, which depends on temperature. For the sizing of the

thermal control subsystem, a worst cold, worst hot, and safe mode case have been considered. The thermal control unit will consist of temperature gauges, heaters, MLI thermal blankets, and a control unit.

A direct relation between thermal and structural analysis exists regarding the material used for the satellite structure. Launch loads, vibrations, thermal stability, mass, and ease of manufacturing have been taken into account in the structural design. This resulted in a very conservative structure, using materials such as CFRCE, aluminium, and carbon-carbon having a total mass of 274.8 kg, which comprises 60% of the satellite dry mass value.

The MIRALOS subsystem and payload instruments receive commands from an on-board computer unit, which is part of the C&DH subsystem. The commercially available on-board computer SCS750 with build-in redundancy will be re-equipped with the Motorola PowerPC 603e CPU, seeking optimum clock speed, power, and memory values. In case the SCS750 is overloaded, the RTU 'BU-63705' will take over some of its tasks to offload the on-board computer.

The communications subsystem handles the data flow between satellite and ground station. A transmitter and antenna trade-off revealed that the STC-MS01 transceiver and SSTL patch antenna are the best options in terms of data rate, frequency range, power consumption, and temperature range. The satellite housekeeping and scientific data will be sent to ESTRACK ground stations.

Finally, the launcher selection uncovered the Dnepr-LV to be the most favourable rocket. Its launch is supported by platforms in Baikonur and Yasny in Russia. The Dnepr-LV combines low launch cost, a suitable inclination range, sufficient payload mass, and fairing dimensions.

In general it can be concluded that the MIRALOS mission has been proven to be a feasible, realistic, and scientifically interesting mission. The satellite will contain unprecedented combinations of scientific instruments, both commercially available and newly designed. It provides the scientific community with the opportunity to fill in secondary mission objectives as well. Now, it is up to future MIRALOS engineers and researchers to make the mission a pragmatic prospect to gain insight on satellite drag, atmospheric modelling, and gas-surface interactions.

Recommendations

The conceptual phase of the mission design now complete, some recommendations have to be made for the further stages of the analysis. In this chapter, recommendations for the different subsystems are handled. These require a more developed delineation before the other design phases can be initiated. For the non-technical aspects (the largest part of these described in Chapter 15), only one recommendation can be asserted, which is to regularly update these aspects. For the technical aspects of this mission, covering the subsystem design and integration, several recommendations can be given.

First, the budget analysis has to be iterated in order to keep the design up to date. Changes in the budgets may occur due to changes in instruments or subsystems. Depending on these, design decisions and properties may change, such as the amount of propellant or the size of the magnetic torque rods. Regarding the end of the mission, when the spacecraft will enter an uncontrolled reentry this is to be defined in a later stage of the design phase.

Secondly, recommendations can be made with respect to the spacecraft size. Currently the size is estimated based on outdated launcher information and extrapolation of existing launcher options. A back-of-the-envelope calculation showed that the frontal surface area is sufficient in terms of measurement accuracy. However, the launcher allows for a spacecraft of almost 1.5 times this size, which would yield a much larger frontal surface area, beneficial to measurements. On the other hand, when a more accurate accelerometer is implemented, the spacecraft size can even be reduced. This will reduce the structural weight of the spacecraft, which is also beneficial to the measurements. Furthermore, this would also allow a smaller, cheaper launcher. These options are to be further analysed to determine their feasibility and their impact on all subsystems.

Regarding the subsystems, specific recommendations can be made, described in the following paragraphs.

Payload

This paragraph displays the recommendations of the payload.

- More thorough research on instrument functioning has to be carried out.
- Manufacturers have to be contacted for further instrument and product specifications.
- The design concepts of the reflectometer have to be further worked out, such as the type of vacuum pump used in the ionisation reflectometer.

Propulsion System

This paragraph displays the recommendations of the propulsion system.

- The amount of propellant taken on-board has to be revised and be potentially increased, to increase the flexibility of the second mission objective and the controllability of satellite de-orbiting/re-entry.
- Due to an error that occurred during tank sizing the mass and volume estimate in Section 7.2.1 is not correct. The actual tank dry mass is now 0.5 kg , this should be updated in the mass budget.

- A complete coverage of all LSTs per altitude has to be determined.
- A detailed reliability analysis on all components of the ion propulsion system has to be performed. Based on this it has to be considered whether redundancy is required for some or all components.
- An analysis with respect to the plume of the ion beam and its influence on other spacecraft components such as the solar cells has to be performed.
- The thrust level used to fly all manoeuvres, including orbit maintenance, has to be optimised for burn time, power, and propellant consumption.

ADCS
This paragraph displays the recommendations of the ADCS.

- More information has to be retrieved concerning the mass-trim assembly calibration procedure.
- Further research has to be carried out on available options for attitude sensing and attitude control, both on conceptual and product level.
- The reliability of the μASC and μDDS has to be analysed, both of them not yet space-proven.
- As more electrical components have been pinpointed and electromagnetic interferences is assessed, the internal dipole moment has to be estimated.
- The attitude dynamics and controller have to be determined.
- A more thorough analysis of magnetometers, magnetorquers, and cold gas thrusters has to be performed.
- As in the propulsion subsystem also the sizing of the GN_2 tank contained an error. The updated dry mass is 3.6 kg, this should be updated in the mass budget.

Power System
This paragraph displays the recommendations of the power system.

- Further research on protecting materials surrounding the voered interconnected solar cells has to be performed.
- The effect of plasma interactions with the solar cells has to be investigated.
- Further research on batteries has to be perfoermed to produce a detailed design of the wiring system connection the solar arry via the PRU to the batteries.
- The power distribution of the PRU to the payload instruments and subsystems has to be examined.
- For each of the satellite components, the voltage and current input have to be determined in order to use proper transformers to convert the solar cell voltage to the desired output voltages.

Thermal Control
This paragraph displays the recommendations of the thermal control system:

- For the thermal analysis, the temperature dependence of various material properties has to be taken into account and
- For the thermal analysis, the data on thermal properties of all materials under consideration have to be determined.
- For the thermal analysis, the changes in solar cell efficiency have to be factored in
- For the thermal analysis, the actual heat generation, shape, location and surface properties of each component have to be determined.
- For the thermal analysis, a more suitable program such as ESATAN has to be used.
- For the thermal control system design, the material at the back of the solar cells has to be resolved
- For the thermal control system design, the effect of a highly conductive layer on the temperature distribution of the solar cells has to be investigated.
- For the thermal control system design, the effect of the heat capcity of this layer on the speed at which the solar cells heat up or cool down in eclipse orbits has to be investigated.
- For the thermal control system design, a material with a higher conductivity has to be considered, as this may allow for simpler radiator design.
- For the thermal control system design, the positions of the components have to be re-evaluated.
- For the thermal control system design, investigation into a design which puts the accelerometer on the nadir side of the spacecraft has to be done.

Structural Analysis
This paragraph displays the recommendations of the structural analysis:

- The relative error that was introduced by the honeycomb sandwich panel simplification has to be investigated.
- A number of failure modes, such as skin buckling, detachment of the skin from the core, failure of the honeycomb structure in shear or compression and local failure at the points where the panels are fastened together, that were not considered yet have to be analysed.
- A more thorough structural analysis has to be performed.

- An additional failure mode of shock of detachment has to be examined, not for structural failure but for the case where instruments break during the process.

Command and Data Handling
This paragraph displays the recommendations of the Command and Data Handling subsystem:

- More research has to be done regarding the RTUs in order to produce a more accurate trade-off between different products. Including more RTUs in the trade-off will allow the selection of an even more appropriate unit for the MIRALOS-mission.
- The software language has to be chosen and the code has to be written in such a way that the amount of lines of code is minimised.
- The heat output of the CPU has to be accurately determined in order to use the right insulation and/or active thermal control.
- A more thorough analysis on data storage and housekeeping data transmission has to be performed.
- The interconnection between the components of the OBC system has to be defined.

Communications System and Ground Station Selection
This paragraph displays the recommendations of the communications subsystem and the ground station selection:

- A visibility analysis has to be done in order to define the required data rate more accurately.
- A scientific and housekeeping data rate distribution per subsystem has to be discussed.
- The measurement frequency of each instrument and subsystem has to be defined.
- A thorough uplink budget analysis has to be performed.
- The full design of the omni-directional antenna has to be performed.
- A secondary ground station analysis (for redundancy) has to be done.
- More technical information has to be gathered concerning the Svalbard Ground Station for a third link budget iteration.

Launcher Selection
This paragraph displays the recommendations of the launcher selection

- More technical information has to be gathered concerning the Dnepr-LV launcher for for example vibrational analysis.
- The pre-launch, launch and post-launch procedures have to be set up.
- More research has to be done with respect to the sharing of the launcher with other missions.

The next phases in the design process will also induce new recommendations and even when the process is finished, recommendations can be stated with respect to new projects. However, the above stated recommendations are for a more detailed design and have to be considered before starting the production phase of the spacecraft.

Bibliography

[1] Argyriou Tsikrikonis et al., "MIRALOS Mid-Term Report," 2014.

[2] Jacchia, L. G. and Slowey, J., "Densities And Temperatures From The Atmospheric Drag On Six Artificial Satellites," *Smithsonian Astrophysical Observatory Special Report*, , No. 171, 1965.

[3] Moe, K. and Moe, M., "Gas–surface interactions and satellite drag coefficients," *Planetary and Space Science*, Vol. 53, 2005, pp. 793–801.

[4] Moe, K., Moe, M., and Wallace, S., "Improved Satellite Drag Coefficient Calculations from Orbital Measurements of Energy Accommodation," *Journal of Spacecraft and Rockets*, Vol. 35, No. 3, 1998, pp. 266–272.

[5] Emmert, J. T., Picone, J. M., and Lean, J. L., "Global Change In The Thermosphere: Compelling Evidence Of A Secular Decrease In Density," *Journal of Geophysical Research*, Vol. 109, 2004, doi:10.1029/2003JA010176.

[6] Graziano, B. P., *Computational Modelling of Aerodynamic Disturbances on Spacecraft within a Concurrent Engineering Framework*, Ph.D. thesis, Cranfield University, 2007.

[7] R. Schamberg, "Analytic Representation of Surface Interaction for Free Molecular Flow with Application to Drag of Various Bodies," 1959.

[8] Pilinski, M., Argrow, B., and Palo, S., "Semiempirical Model for Satellite Energy-Accommodation Coefficients," *Journal of Spacecraft and Rockets*, Vol. 47, No. 6, November-December 2010, pp. 951–956.

[9] Doornbos, E. N., *Thermospheric Density and Wind Determination from Satellite Dynamics*, Ph.D. thesis, Delft University of Technology, 2011.

[10] Sentman, L., "Free molecule flow theory and its application to the determination of aerodynamic forces," 1961, LMSC–448514, Lockheed Missiles Space Company.

[11] Koppenwallner, G., "Energy accommodation coefficient and momentum transfer modeling," 2009, HTG–TN–08–11, HTG, Katlenburg Lindau.

[12] J.T. Emmert, J. P. and Lean, J., "Global change in the thermosphere: Compelling evidence of a secular decrease in density," *Journal of Geophysical Research*, Vol. 109, 2004, doi:10.1029/2003JA010176.

[13] NASA, "General Mission Analysis Tool (GMAT)," Website, `http://gmat.gsfc.nasa.gov/` (Accessed: 13-05-2014).

[14] J.H. Waite, J., Lewis, W., and Kasprzak, W., "The Cassini Ion and Neutral Mass Spectrometer (INMS) Investigation," 2004, `http://deepblue.lib.umich.edu/bitstream/handle/2027.42/43764/11214_2004_Article_1408.pdf?sequence=1)` (Accessed: 13-05-2014).

[15] Argyriou Tsikrikonis et al., "MIRALOS Baseline Report," 2014.

[16] O. Montenbruck & R. Kroes, "In-flight performance analysis of the CHAMP BlackJack GPS Receiver," Vol. 7, August 2003, pp. 74–86.

[17] James R. Wertz and Wiley J. Larson, "Space Mission Analysis and Design," 1999.

[18] Wertz, J. R. and Everett, D. F. and Puschell, J. J., *Space Mission Engineering: The New SMAD*, Microcosm Press, 2011.

[19] E. Gill, "Lecture 9 – Concurrent Engineering & Design for Lifecycle," Lecture, 2014.

[20] D. R. Williams, "MAVEN (Mars Atmosphere and Volatile Evolution)," Website, 2002, `http://nssdc.gsfc.nasa.gov/nmc/experimentDisplay.do?id=2002-034A-03` (Accessed: 12-05-2014).

[21] Picone, J., Hedin, A., Drob, D., and Aikin, A., "NRLMSISE-00 empirical model of the atmosphere: Statistical comparisons and scientific issues," *Journal of Geophysical Research*, Vol. 107, No. A12, 2002, doi:10.1029/2002JA009430.

[22] ESA, "ROSINA (Rosetta Orbiter Spectrometer For Ion and Neutral Analysis)," Website, May 2014, `http://sci.esa.int/rosetta/35061-instruments/?fbodylongid=1650`.

[23] University of Kentucky, "Summary of the characteristics of different mass analyzers," Website, 2008, `http://www.research.uky.edu/core/massspec/jeolanalyzers.pdf` (Accessed: 30-06-2014).

[24] Paul Mahaffy, "NGIMS (Neutral Gas and Ion Mass Spectrometer)," Website, 2012, `http://lasp.colorado.edu/home/maven/science/instrument-package/ngims/` (Accessed: 12-05-2014).

[25] Pilinsky, M., "Analysis of a Novel Approach for Determining Atmospheric Density from Satellite Drag," 2008.

[26] Herbert J. Kramer, "SENSE (Space Environmental NanoSatellite Experiment)," Website, 2002, `https://directory.eoportal.org/web/eoportal/satellite-missions/s/sense` (Accessed: 05-06-2014).

[27] EO Sharing Earth Observation Resources, "Swarm (Geomagnetic LEO Constellation)," Website, April 2014, `https://directory.eoportal.org/web/eoportal/satellite-missions/s/swarm` (Accessed: 24-04-2014).

[28] Herbert J. Kramer, "GRACE-FO (Gravity Recovery And Climate Experiment - Follow-on)," Website, 2002, `https://directory.eoportal.org/web/eoportal/satellite-missions/g/grace-fo` (Accessed: 20-06-2014).

[29] Damien Boulanger, Bruno Christophe, et al., "Design update and characteristics improvement of the electrostatic accelerometer for the GRACE Follow-On mission," Website, Powerpoint Presentation by Onera (Accessed: 17-06-2014).

[30] GFZ-Potsdam, "GRACE Payload," Website, October 2000, http://op.gfz-potsdam.de/grace/payload/payload.html (Accessed: 09-05-2014).

[31] He Liao, Benli Wang, Xiaohui Lin, "On-orbit Center of Mass Calibration of Satellite Based on Batch Estimation Theory," 2008.

[32] GRACE Science Team, "GRACE Science Data System Status," Website, 2007, Presentation (Accessed: 10-06-2014).

[33] GFZ-Potsdam, "CHAMP Main Systems," Website, September 2000, http://op.gfz-potsdam.de/champ/systems/main_SYSTEMS.html (Accessed: 09-05-2014).

[34] Earth Observation Portal, "SAC-C (Satélite de Aplicaciones Científicas-C)," Website, May 2014, https://directory.eoportal.org/web/eoportal/satellite-missions/s/sac-c (Accessed: 21-05-2014).

[35] Earth Observation Portal, "Jason-2 / OSTM," Website, May 2014, https://directory.eoportal.org/web/eoportal/satellite-missions/j/jason-2 (Accessed: 21-05-2014).

[36] Earth Observation Portal, "CHAMP (Challenging Minisatellite Payload)," Website, May 2014, https://directory.eoportal.org/web/eoportal/satellite-missions/c-missions/champ (Accessed: 21-05-2014).

[37] Neubert, R., 1.1 GPS/GALILEO Earth Observation, . G., and Remote Sensing, Departments, G. P. D. D. G., "The Retro-Reflector for the CHAMP Satellite: Final Design and Realization," 1998.

[38] Helmholtz-Zentrum Potsdam – Deutsches GeoForschungsZentrum (GFZ), "Laser Reflectors for LEO Satellites," Website, August 2013, http://www.gfz-potsdam.de/en/research/organizational-units/departments/department-1/global-geomonitoring-and-gravity-field/topics/development-operation-and-analysis-of-gravity-field-satellite-\missions/satellite-payload-development-and-integration/laser-reflectors-\for-leo-satellites/ (Accessed: 21-05-2014).

[39] Doornbos, E., "Project Guide Design Synthesis Exercise: Mission To Investigate Rarefied Aerodynamics on Low Orbiting Satellites," https://blackboard.tudelft.nl/bbcswebdav/pid-2222711-dt-content-rid-7538371_2/xid-7538371_2 (Accessed: 22-04-2014).

[40] Gregory, J. and Peters, P., "A Measurement of the Angular Distribution of 5 eV Atomic Oxygen Scattered Off A Solid Surface in Earth Orbit," 1986, pp. 644–656.

[41] Clark, J., "the mass spectrometer - how it works," Website, 2014, http://www.chemguide.co.uk/analysis/masspec/howitworks.html (Accessed: 13-05-14).

[42] Samuel A. Schaaf, P. L. C., "Flow of rarefied gases," , No. 8, 1961.

[43] S. Leoni, "MCP (Microchannel Plate Detector)," pdf, 2007, http://lxmi.mi.infn.it/~sleoni/TEACHING/Nuc-Phys-Det/PDF/papers/MCP.pdf (Accessed: 05-06-2014).

[44] Photonis, "MCP Selection Guide," pdf, 2007, http://www.photonis.com/attachment.php?id_attachment=4 (Accessed: 05-06-2014).

[45] D. C. Humma et al, "Design and performance of the Global Ultraviolet Imager (GUVI)," Tech. rep., The Johns Hopkins University Applied Physics Laboratory, November 1998.

[46] Airbus Defence & Space - Astrium, "Space Propulsion," Website, http://cs.astrium.eads.net/sp/ (Accessed: 16-06-2014).

[47] Aerojet Rocketdyne, "Space Propulsion Systems," Website, https://www.rocket.com/propulsion-systems (Accessed: 16-06-2014).

[48] Martinez-Sanchez, M. and Pollard, J., "Spacecraft Electric Propulsion - An Overview," *Journal of Propulsion and Power*, Vol. 14, No. 5, 1998.

[49] D.M. Goebel and I. Katz, *Fundamentals of Electric Propulsion*, Wiley JPL Space Science and Technology Series , 2008.

[50] O. Räisänen, "A diagram of an electrostatic ion thruster," Online, http://en.wikipedia.org/wiki/File:Electrostatic_ion_thruster-en.svg (Accessed: 17-06-2014).

[51] C.H. Edwards, et al., "The T5 Ion Propulsion Assembly for Drag Compensation on GOCE," Tech. rep., 2010, http://earth.esa.int/workshops/goce04/goce_proceedings/46_edwards.pdf.

[52] Neil Wallace, et al., "The GOCE Ion Propulsion Assembly – Lessons Learnt from the First 22 Months of Flight Operations," *32nd International Electric Propulsion Conference (Wiesbaden, Gernany)*, 2011, IEPC-2011-327.

[53] D.H. Mundy and D.G. Fearn, "Throttling the T5 Ion Engine over a wide Thrust Range," Tech. rep., 1997, http://arc.aiaa.org/doi/pdf/10.2514/6.1997-3196 (Accessed: 19-06-2014).

[54] Fearn, D., "A study of throttling the T5 ion thruster," *32nd Joint Propulsion Conference and Exhibit (Lake Buena Vista, Florida, USA)*, 1996, AIAA 96-3288.

[55] Killinger, R., Bassner, H., Mueller, J., and Kukies, R., "RITA Ion Propulsion for ARTEMIS Lifetime Results," *3rd International Conference on Spacecraft Propulsion, Cannes*, 2000, ESA SP-465.

[56] Ozaki, T., "Development Status of Xenon Ion Engine Subsystem for ETS-VIII," *21st International Communications Satellite Systems Conferebce and Exhibit*, 2003, AIAA 2003-2215.

[57] Honeywell, "Three-Axis Strapdown Magnetometer HMR2300r Datasheet 900232 Rev. B," Website, http://aerospace.honeywell.com/~/media/UWSAero/common/documents/myaerospacecatalog-documents/Missiles-Munitions/HMR2300r.pdf (Accessed: 11-06-2014).

[58] Billingsley Aerospace & Defense, "TFM 100S Spacecraft Attitude Control Triaxial Fluxgate Magnetometer Datasheet," Website, February 2008, http://magnetometer.com/wp-content/uploads/TFM100S-Spec-Sheet-February-2008.pdf (Accessed: 11-06-2014).

[59] SSBV Aerospace & Technology Group, "Earth Horizon Sensor Datasheet (version 1d)," Website, http://www.ssbv.com/ProductDatasheets/page39/page28/index.html (Accessed: 11-06-2014).

[60] EADS SODERN, "STD16 Earth Sensor Datasheet," Website, http://www.sodern.com/sites/docs_wsw/RUB_52/STD16.pdf (Accessed: 11-06-2014).

[61] CubeSatShop.com, "Digital Fine Sun Sensor Product Page," Website, http://www.cubesatshop.com/index.php?page=shop.product_details&flypage=flypage.tpl&product_id=89&category_id=7&option=com_virtuemart&Itemid=69&vmcchk=1&Itemid=69 (Accessed: 11-06-2014).

[62] EADS SODERN, "HYDRA-M CMOS Star Tracker Datasheet," Website, 2013, http://www.sodern.com/sites/docs_wsw/RUB_51/Hydra-M.pdf (Accessed: 11-06-2014).

[63] EADS SODERN, "HYDRA CMOS Star Tracker Datasheet," Website, 2013, http://www.sodern.com/sites/docs_wsw/RUB_51/Hydra.pdf (Accessed: 11-06-2014).

[64] Pietruszewski, A. N., *Prox-1 Attitude Determination and Control*, Geogria Institute of Technology, http://www.ssdl.gatech.edu/papers/mastersProjects/PietruszewskiA-8900.pdf (Accessed: 11-06-2014).

[65] Jena-Optronik, "Autonomous Star Sensor ASTRO APS Active Pixel Sensor datasheet," http://www.jena-optronik.de/de/lageregelungssensoren/sternsensor-astro-aps.html?file=tl_files/pdf/Data%20Sheet%20ASTRO%20APS.pdf (Accessed: 11-06-2014).

[66] Jena-Optronik, "Autonomous Star Sensor ASTRO 15 datasheet," http://www.jena-optronik.de/de/lageregelungssensoren/sternsensor-astro-15.html?file=tl_files/pdf/Data%20Sheet%20ASTRO%2015.pdf (Accessed: 11-06-2014).

[67] Ltd., S. S. T., "Star Tracker: Altair HB+ datasheet," http://www.sstl.co.uk/getattachment/c23c4934-74de-4159-bbec-5635d3cf7eb4/Altair (Accessed: 11-06-2014).

[68] Selex Ex, "A-STR and AA-STR Star Tracker Datasheet," http://www.aiad.it/aiad_res/cms/documents/Startrackers_Selex2013.pdf (Accessed: 11-06-2014).

[69] Terma A/S Space, "Star Tracker HE-5AS Datasheet," http://www.terma.com/media/101677/star_tracker_he-5as.pdf (Accessed: 11-06-2014).

[70] EADS SODERN, "SED26 CCD Star Tracker Datasheet," http://www.sodern.com/sites/docs_wsw/RUB_45/SED26.pdf (Accessed: 11-06-2014).

[71] Ball Aerospace Systems Division, "CT-601 High Accuracy Star Tracker Datasheet," https://engineering.purdue.edu/~bethel/ct601.pdf (Accessed: 11-06-2014).

[72] Surrey Satellite Technology Ltd., "Rigel-L Star Tracker Datasheet," http://www.sst-us.com/getdoc/e8492d28-0e3b-4183-9a9d-6de79823b5aa (Accessed: 11-06-2014).

[73] Jorgensen, J. L., Denver, T., Betto, M., and Jorgensen, P. S., "MicroASC: A Miniature Star Tracker," http://www.dlr.de/Portaldata/49/Resources/dokumente/archiv4/IAA-B4-0706P.pdf (Accessed: 11-06-2014).

[74] Jorgensen, J. L., Denver, T., and Jorgensen, P. S., "MicroASC: A Miniature Star Tracker," http://articles.adsabs.harvard.edu/cgi-bin/nph-iarticle_query?2004ESASP.571E..55J&defaultprint=YES&filetype=.pdf (Accessed: 11-06-2014).

[75] CubeSatShop.com, "MAI-SES Static Earth Sensor Product Page," Website, http://www.cubesatshop.com/index.php?page=shop.product_details&flypage=flypage.tpl&product_id=103&category_id=7&option=com_virtuemart&Itemid=69&vmcchk=1&Itemid=69 (Accessed: 11-06-2014).

[76] Boer, B. D. and Durkut, M., "A low-power and high-precision miniaturized digital sun sensor," Vol. 8876, 2013, http://publications.tno.nl/publication/34606630/oQOZCG/deboer-2013-lowpower.pdf (Accessed: 11-06-2014).

[77] Xie, N. and Theunissen, A. J., "Low-power high-accuracy micro-digital sun sensor by means of a CMOS image sensor," *Journal of Electronic Imaging*, , No. 22.

[78] Yanan, M., Jian, C., Yuan, Z., Ran, C., and Xin, L., "Design and Realization of the Miniature Long-life Integrative Coded Sun Sensor," Proceeding of SPIE.

[79] Montenbruck, O. and Kroes, R., *In-flight performance analysis of the CHAMP BlackJack GPS Receiver*, 2003, doi:10.1007/s10291-003-0055-5.

[80] Adams, J. C., "Robust GPS Attitude Determination for Spacecraft," December 1999.

[81] L-3 Communications: Space & Navigation, "RGA-20 High Performance Gyro Assembly Datasheet," Website, March 2008, http://www2.l-3com.com/spacenav/space_and_nav/space_products/pdfs/SellSheet_RGA_20_Apr11.pdf (Accessed: 11-06-2014).

[82] Fortescue, P., Swinerd, G., and Stark, J., *Spacecraft System Engineering*, John Wiley & Sons, Ltd., 4th ed., 2011.

[83] Bahar, M. N. D., Hassan, M. E. M., Hamzah, N., and Arshad, A. S., "Modular CMOS Horizon Sensor for Small Satellite Attitude Determination and Control Subsystem," *20th Annual AIAA/USU Conference on Small Satellites*, http://digitalcommons.usu.edu/cgi/viewcontent.cgi?article=1592&context=smallsat (Accessed: 12-06-2014).

[84] Maryland Aerospace, Inc., "MAI-SES Static Earth Sensor Product Page," Website, http://www.miniadacs.com/miniadacs_013.htm (Accessed: 12-06-2014).

[85] L. E. Marchese et al, "A Compact Lightweight Earth Horizon Sensor using an Uncooled Infrared Bolometer," Vol. 6796, http://spiedigitallibrary.org/data/Conferences/SPIEP/21089/679629_1.pdf (Accessed: 12-06-2014).

[86] Servo Corporation of America, "MiDES Datasheet," https://wiki.umn.edu/pub/AEM_Air_Launch_Team/ComponentList/minihorizonsensor.pdf (Accessed: 12-06-2014).

[87] Herbert J. Kramer, "GRACE (Gravity Recovery And Climate Experiment)," Website, 2002, https://directory.eoportal.org/web/eoportal/satellite-missions/g/grace (Accessed: 09-05-2014).

[88] Earth Observation Portal, "GOCE (Gravity field and steady-state Ocean Circulation Explorer)," Website, May 2014, https://directory.eoportal.org/web/eoportal/satellite-missions/g/goce (Accessed: 09-05-2014).

[89] Ley, W., Wittmann, K., and Hallmann, W., *Handbook of Space Technology*, John Wiley & Sons, Ltd., 2009, ISBN: 978-0-470-69739-9.

[90] KVH Industries, Inc., "DSP-4000 High-Performance Dual-Axis Fiber Optic Gyro Datasheet," Website, 2011, http://www.kvh.com/ViewAttachment.aspx?guidID={5F2CDBA5-81D8-4944-964F-EB78235FD957} (Accessed: 12-06-2014).

[91] KVH Industries, Inc., "DSP-1750 Worlds Smallest High-Performance Fiber Optic Gyro Datasheet," Website, 2011, http://www.kvh.com/ViewAttachment.aspx?guidID={F9A02687-184D-4445-B979-AB726666CBE2} (Accessed: 12-06-2014).

[92] IMAR-Navigation, "iNAV-RQT-1003 RLG Based Inertial Navigation System for Advanced Applications Datasheet," Website, 2011, http://www.imar-navigation.de/downloads/NAV_RQT_1003_en.pdf (Accessed: 12-06-2014).

[93] Kearfott Corporation: Guidance & Navigation Division, "KI-4903 Monolithic Ring Laser Gyro Inertial Navigation Unit Datasheet," Website, 2011, http://www.kearfott.com/images/stories/pdf/DATASHEETS_KGN_NJ/IMU/ki-4903_high_performance_inu_kit.pdf (Accessed: 12-06-2014).

[94] Herbert J. Kramer, "PROBA-2 (Project for On-Board Autonomy-2)," Website, 2014, https://directory.eoportal.org/web/eoportal/satellite-missions/p/proba-2 (Accessed: 12-06-2014).

[95] Ball Aerospace, "HAST High Accuracy Star Tracker Datasheet," http://www.ballaerospace.com/file/media/D1503%20HAST%2001_09_loRes.pdf (Accessed: 12-06-2014).

[96] Usbeck, T., Wohlfart, J., and Schelkle, M., "A Flexible Cold Gas Propulsion System Concept for Different Space Applications," 2004, http://articles.adsabs.harvard.edu/cgi-bin/nph-iarticle_query?2004ESASP.555E..76U&defaultprint=YES&filetype=.pdf (Accessed: 13-06-2014).

[97] Christian Siemes, "ESA Working Paper EWP-2384: GOCE gradiometer calibration and Level 1b data processing," pdf.

[98] MOOG Bradford Engineering B.V., "Thruster Control Valve Datasheet," Website, http://bradford-space.com/userfiles/BE%20Datasheet%20-%20Thruster%20Control%20Valve%20-%202012.pdf (Accessed: 22-05-2014).

[99] Marotta, "Cold Gas Microthruster Datasheet," Website, http://www.marotta.com/files/Datasheets/cgmt_ds.pdf (Accessed: 17-06-2014).

[100] Zandbergen, B., "Cold Gas Systems," Website, 2014, http://www.lr.tudelft.nl/en/organisation/departments/space-engineering/space-systems-engineering/expertise-areas/space-propulsion/propulsion-options/chemical-rockets/cold-gas/ (Accessed: 16-06-2014).

[101] ZARM Technik, "Magnetic Torquers for Spacecraft Attitude Control," Website, June 2005, http://www.smad.com/analysis/torquers.pdf (Accessed: 13-06-2014).

[102] M. R. Patel, *Spacecraft Power Systems*, CRC Press, 2005.

[103] Emcore, "Space Solar Cells," Website, 2014, http://www.emcore.com/space-photovoltaics/space-solar-cells/ (Accessed: 12-06-14).

[104] Spectrolab, "Photovoltaics," Website, 2014, http://www.spectrolab.com/solarcells.htm (Accessed: 12-06-14).

[105] Azurspace, "Space Solar Cells," Website, 2014, http://www.azurspace.com/index.php/en/products/products-space/space-solar-cells (Accessed: 09-06-14).

[106] Semiconductor Today, "Sharp claims record 37.7% efficiency for non-concentrator solar cell," Website, 2014, http://www.semiconductor-today.com/news_items/2012/DEC/SHARP_101212.html (Accessed: 10-06-14).

[107] Clyde Space, "Spacecraft Batteries," Website, 2014, http://www.clyde-space.com/products/spacecraft_batteries (Accessed: 09-06-14).

[108] Quallion, "Battery Product Specifications," Website, 2014, http://www.quallion.com/sub-sp-main.asp (Accessed: 09-06-14).

[109] Willson, R. and Hudson, H., "The Sun's luminosity over a complete solar cycle," *Nature*, , No. 351, 1991, pp. 42–44, doi:10.1038/351042a0.

[110] NASA, "Earth Orbit Environmental Heating," PDF, http://oce.jpl.nasa.gov/practices/2301.pdf (Accessed: 30-06-2014).

[111] Quallion, "QL075KA," Website, 2014, http://www.quallion.com/new-pdf/QL075KA_75Ah%20Satellite%20Cell.pdf (Accessed: 09-06-14).

[112] Emcore, "ZTJ Photovoltaic Cell," Website, 2014, http://www.emcore.com/wp-content/uploads/ZTJ-Cell.pdf (Accessed: 12-06-14).

[113] Stern, T. and DeLapp, S., "Techniques for Magnetic Cleanliness on Spacecraft Solar Arrays," *2nd International Energy Conversion Engineering Conference*, 2004.

[114] Airbus Defence & Space, "Medium Power PCDU," Website, 2014, http://www.astrium.eads.net/en/equipment/medium-power-pcdu.html (Accessed: 12-06-14).

[115] David G. Gilmore, *Spacecraft Thermal Control Handbook, Volume I: Fundamental Technologies*, The Aerospace Corporation, 2002.

[116] Haynes, W. M., *CRC Handbook of Chemistry and Physics*, CRC Press, Boca Raton, Florida, 92nd ed., 2011.

[117] Granta Design Ltd., "CES EduPack," databse, 2013.

[118] Duffie, J. A. and Beckman, W. A., *Solar Engineering of Thermal Processes*, John Wiley & Sons, Inc., Hoboken, New Jersey, 2013.

[119] ASTM International, "ASTM E490-00a (2014)," Standard, 2014, http://enterprise.astm.org/filtrexx40.cgi?+REDLINE_PAGES/E490.htm.

[120] Rickman, S. L., "A Simplified, Closed-Form Method for Screening Spacecraft Orbital Heating Variations," Tech. rep., NASA Johnson Space Center, https://tfaws.nasa.gov/TFAWS02/Data/Thermal/Rickman.pdf (Accessed: 29-05-14).

[121] CubeSat Project, U. o. L., "The Technology of Solar Cells," Website, 2008, http://cubesat.wikidot.com/the-technology-of-solar-cells (Accessed: 20-06-2014).

[122] Barry Zandbergen, "AE1201: Aerospace Design & Systems Engineering Elements I, Part: Spacecraft (bus) design and sizing," Internal.

[123] Garzon, M. M., "Development and Analysis of the Thermal Design for the OSIRIS-3U Cubesat," Tech. rep., Pennsylvania State University, 2012.

[124] et Al., J. B., "Mechanical, Power and Thermal Subsystem Design for a CubeSat Mission," Tech. rep., Worcester Polytechnic Institute, 2012, https://www.wpi.edu/Pubs/E-project/Available/E-project-031212-121649/unrestricted/Mechanical,_Power,_and_Thermal_Subsystem_Design_for_a_CubeSat.pdf (Accessed: 25-05-14).

[125] Pont, D., "Summary of Properties for Kapton Polyimide Films," PDF, http://www2.dupont.com/Kapton/en_US/assets/downloads/pdf/summaryofprop.pdf (Accessed: 23-06-2014).

[126] Design1st, "Emmissivity values," PDF, http://www.design1st.com/Design-Resource-Library/engineering_data/ThermalEmissivityValues.pdf (Accessed: 23-06-2014).

[127] ISC Kosmotras, "Space Launch System Dnepr User Guide," Tech. Rep. Issue 2, November 2001.

[128] ESA, "On Board Computer," Website, http://www.esa.int/Our_Activities/Space_Engineering/Onboard_Computer_and_Data_Handling/Onboard_Computers (Accessed: 11-06-2014).

[129] Maxwell Technologies, "SCS750 single board computer," Website, http://www.maxwell.com/products/microelectronics/products/space-sbc (Accessed: 11-06-2014).

[130] Herbert J. Kramer, "Glory," Website, 2002, https://directory.eoportal.org/web/eoportal/satellite-missions/g/glory (Accessed: 12-06-2014).

[131] Herbert J. Kramer, "KazEOSat-2 (Medium Resolution Earth Observation Satellite), Kazakhstan," Website, 2002, https://directory.eoportal.org/web/eoportal/satellite-missions/k/kazeosat-2 (Accessed: 12-06-2014).

[132] Herbert J. Kramer, "SPOT-6 and SPOT-7 Commercial Imaging Constellation," Website, 2002, https://directory.eoportal.org/web/eoportal/satellite-missions/s/spot-6-7 (Accessed: 12-06-2014).

[133] Herbert J. Kramer, "SEOSat/Ingenio - Imaging mission of Spain," Website, 2002, https://directory.eoportal.org/web/eoportal/satellite-missions/s/seosat (Accessed: 12-06-2014).

[134] Charles Dunn, Willy Bertiger, Garth Franklin, Ian Harris, Gerhard Kruizinga, Tom Meehan, Sumita Nandi, Don Nguyen, Tim Rogstad, J. Brooks Thomas, Jeff Tien, "The Instrument on NASA's GRACE Mission: Augmentation of GPS to Achieve Unprecedented Gravity Field Measurements," Tech. rep., 2014.

[135] Steve Chien, Rob Sherwood, and Richard Doyle, "The TechSat-21 Autonomous Sciencecraft Experiment," Tech. rep., 2000.

[136] CPUshack, "Welcome Back Rosetta: The Dynex MAS31750 Awakens," Website, 2014, http://www.cpushack.com/2014/01/20/welcome-back-rosetta-the-dynex-mas31750-awakens/ (Accessed: 13-06-2014).

[137] Tom Flatley, "Advanced Hybrid On-Board Science Data Processor - SpaceCube 2.0," Tech. rep., 2011.

[138] Leon W. Couch II, *Digital and Analog Communication Systems*, Pearson, 2013.
[139] Surrey Satellite Technology Ltd., "S-Band Transmitter," Website, 2014, http://www.sstl.co.uk/Products/Subsystems/Communication/Receivers/Transmitter/S-Band-Transmitter (Accessed: 10-06-14).
[140] Clyde Space, "CubeSat S-Band Transmitter," Website, 2014, http://www.clyde-space.com/cubesat_shop/communication_systems/301_cubesat-s-band-transmitter (Accessed: 10-06-14).
[141] ISIS Space, "ISIS – TXS Small Satellite S-Band Transmitter," Website, 2014, http://www.isispace.nl/brochures/ISIS_TXS_Brochure_v.12.4.pdf (Accessed: 11-06-14).
[142] L-3 Cincinnati Electronics, "T-711 Transmitter," Website, 2005, http://www.cinele.com/images/space_datasheets/t-711.pdf (Accessed: 11-06-14).
[143] COM DEV Europe, "S-Band TT&C Transceiver STC-MS01," Website, 2010, http://www.comdevintl.com/docs/TTC%20Data%20sheet%20V2-10.pdf (Accessed: 11-06-14).
[144] ESA, "ESTRACK Tracking Stations," Website, January 2013, http://www.esa.int/Our_Activities/Operations/Estrack_tracking_stations (Accessed: 12-06-2014).
[145] J.A. King, "AMSAT/IARU Annotated Link Model System," Website, 2008, http://www.amsatuk.me.uk/iaru/spreadsheet.htm (Accessed: 05-05-14).
[146] K. Poling, *Goldeneye Link Budget Summary*, University of Minnesota.
[147] Louis J. Ippolito Jr., *Radiowave Propagation in Satellite Communications*, Van Nostrand-Reinhold, 1986.
[148] ESA, *ESA Tracking Stations (ESTRACK) Facilities Manual (EFM)*, European Space Operations Centre, 2008.
[149] Surrey Satellite Technology Ltd., "S-Band Quadrifilar Helix Antenna," Website, 2014, http://www.sstl.co.uk/Products/Subsystems/Communication/Antennas/S-Band-Quadrifilar-Helix-antenna (Accessed: 10-06-2014).
[150] Antcom Corp., "L, S, C, X, and Ku-Band Antennas," Website, 2014, http://www.antcom.com/documents/catalogs/LSC-BandAntennas2.pdf (slide 8) (Accessed: 10-06-2014).
[151] Surrey Satellite Technology Ltd., "S-Band Patch Antenna," Website, 2014, http://www.sstl.co.uk/Products/Subsystems/Communication/Antennas/S-Band-Patch-Antenna (Accessed: 10-06-2014).
[152] Clyde Space, "S-Band Patch Antenna," Website, 2014, http://www.clyde-space.com/cubesat_shop/communication_systems/302_s-band-patch-antenna (Accessed: 10-06-2014.
[153] Poynting Antennas, "High Gain S-band Sector Antenna," Website, 2012, http://www.poyntingdefence.com/upload/brochure_files/Poynting%20SECT-A0022%20Brochure.pdf (Accessed: 10-06-14).
[154] Poynting Antennas, "High Gain Wideband Dish," Website, 2012, http://www.poyntingdefence.com/upload/brochure_files/Poynting%20GRID-A0006%20Brochure.pdf (Accessed: 10-06-14).
[155] Directive Systems, "2.28-2.35 GHz Loop Yagi Model 1321LYRM," Website, 2013, http://www.directivesystems.com/PDF/1321LYRM.PDF (Accessed: 10-06-14).
[156] L & M Technologies, "Logistics Operations Services," Website, 2014, http://www.lmtechnologies.com/what-we-do/services/ (Accessed: 12-05-2014).
[157] National Aeronautics and Space Administration (NASA), "OIA - Logistics Division," Website, 2014, http://ld.hq.nasa.gov/ (Accessed: 12-05-2014).
[158] ESA, "Launch Vehicle Catalogue," December 2004, ESA contract no. 8152/88/F/BL.
[159] ISC Kosmotras, "Space Head Modules of Dnepr LV," Febuary 2014.
[160] NASA, "Small Wind and Temperature Spectrometer," Website, http://www.nasa.gov/mission_pages/station/research/experiments/205.html (Accessed: 16-05-2014).
[161] Spencer, N., Niemann, H., and Carignan, G., "The Neutral-Atmosphere Temperature Instrument," *Radio Science*, Vol. 8, No. 4, April 1973, pp. 287–296.
[162] ESA, "Calibration/GOCE/Earth Explorers/The Living Planet Programme/Observing the Earth/Our Activities/ESA," Website, http://www.esa.int/Our_Activities/Observing_the_Earth/The_Living_Planet_Programme/Earth_Explorers/GOCE/Calibration (Accessed: 13-05-2014).
[163] Pedley, M., "High Precision Calibration of a Three-Axis Accelerometer," Website, January 2013, http://cache.freescale.com/files/sensors/doc/app_note/AN4399.pdf (Accessed: 13-05-2014).
[164] Thomas Immel, "TIMED (Thermosphere-Ionosphere-Mesosphere Energetics and Dynamics)," Website, 2001, http://nssdc.gsfc.nasa.gov/nmc/spacecraftDisplay.do?id=2001-055B (Accessed: 04-06-2014).
[165] Lafleur, C., "The Spacecraft Encyclopedia," Website, http://claudelafleur.qc.ca/Spacecrafts-index.html (Accessed: 13-05-2014).
[166] Aaker, D. A., *Strategic Market Management – Global Perspectives*, Wiley Pages, 2009.
[167] United Nations Office for Outer Space Affairs, "Space Debris Mitigation Guidelines of the Committee on the Peaceful Uses of Outer Space," 2010, http://asi-sdmmt2014.isro.gov.in/sites/default/files/space_debris_mitigation_guidelines_copuos.pdf (Accessed: 15-05-2014).

A. List of Technical Requirements

The system requirements for the mission, spacecraft, and subsystems are listed in Table A.1. The abbreviations used are: Technical (T), Constraint (C), General (GN), Subsystem (SUB), PL, Propulsion (PROP), ADCS, EPS, Thermal (THM), Structural (STRC), CDH, Communication (COM), Ground Station (GS), Launcher (LN), System Integration (INTG) and Sustainability (SUST).

Table A.1: Mission Requirements

ID (MIRALOS-SYS-)	Requirement
T-GN-1	The mission shall allow the study of LEO gas-surface interactions, including the modelling of aerodynamic forces and torques.
T-GN-1-1	The orbit shall include both a helium and an oxygen dominated atmosphere.
T-GN-2	For critical design components, redundancy shall be implemented.
T-GN-3	All components shall have a minimum design lifetime of 6 years in LEO.
T-GN-4	The spacecraft shall be manufacturable.
T-SUB-PL-1	The payload shall have a mass of at most 61.5 kg.
T-SUB-PL-2	The payload shall have a maximum power consumption of 45 W
T-SUB-PL-3	The payload shall have a maximum data rate of 23.3 kbit/s.
T-SUB-PL-4	The centre of mass of the spacecraft shall coincide with that of the accelerometer to an accuracy of 50 µm RMS.
T-SUB-PL-5	The accelerometer shall measure 3-axis linear accelerations with a precision of at least 1 nm/s².
T-SUB-PL-6	The accelerometer shall measure 3-axis linear accelerations with an accuracy of at least 5%.
T-SUB-PL-7	The accelerometer shall measure 3-axis linear accelerations within a range of $10^{-9} - 10^{-4}$ m/s² at EOL.
T-SUB-PL-8	The accelerometer shall measure 3-axis angular accelerations with an accuracy of at least 2%.
T-SUB-PL-9	The mission shall measure the energy accommodation coefficient with an accuracy better than 2%.
T-SUB-PL-10	The accelerometer shall measure 3-axis angular accelerations with an accuracy better than 2%.
T-SUB-PL-11	The GPS receiver shall receive data from at least four GPS satellites.
T-SUB-PL-12	The reflectometer shall provide information on the dependency of the gas-surface interaction over the full range of incidence angles for a flat panel, between 0° and 90° with a resolution of at least 5°.
T-SUB-PL-13	The reflectometer shall provide measurements of the angular distribution of re-emitted or reflected air particles with a resolution of better than 5 degrees and an accuracy of better than 2 %.
T-SUB-PL-14	All instruments shall perform measurements at least once every 80 km along-track.
T-SUB-PL-15	The mission shall provide information for resolving the dependency of gas-surface interactions with atmospheric temperature over a range of at least 300 K.
T-SUB-PL-16	All instruments shall be able to withstand vibrational loads experienced during launch.
T-SUB-PROP-1	The propulsion system shall be capable of providing a ΔV of 500m/s.
T-SUB-PROP-2	The propulsion system shall perform all orbit changes in less than one month.
T-SUB-PROP-3	The propulsion system shall consume less then 780W of power.
T-SUB-PROP-4	The propulsion system shall be capable of at least twenty cycles.
T-SUB-PROP-5	The propulsion system shall wiegh less than 150kg.
T-SUB-ADCS	The ADCS shall provide attitude knowledge and control of the spacecraft.
T-SUB-ADCS-1	The ADCS shall provide coarse 3-axis attitude knowledge with an accuracy better than half the field of view of the fine sensor.
T-SUB-ADCS-2	The ADCS shall provide fine 3-axis attitude knowledge with an accuracy of at least $25''$ (RMS 3σ).
T-SUB-ADCS-3	The ADCS shall be able to maintain a slew rate between 0.0011 and 0.0012 rad/s, with an average angular acceleration of $1.71 \cdot 10^{-8}$ rad/s².
T-SUB-ADCS-4	The ADCS shall provide attitude knowledge with a minimum frequency of 0.1 Hz.
T-SUB-ADCS-5	The ADCS shall not make use of parts that rely on the motion of mechanical components for attitude sensing.
T-SUB-ADCS-6	The ADCS shall provide coarse 3-axis attitude control with an accuracy of at least $5°$ (RMS, 3σ).
T-SUB-ADCS-7	The ADCS shall provide fine 3-axis attitude control with an accuracy of at least $8'$ (1σ).
T-SUB-ADCS-8	The ADCS shall not make use of parts that rely on the motion of mechanical components for attitude control.
T-SUB-ADCS-9	The ADCS shall have a maximum dry mass of 36.6 kg, including 20% redundancy.

Continued on next page...

Table A.1: Mission Requirements

ID (MIRALOS-SYS-)	Requirement
T-SUB-ADCS-10	The ADCS shall have a maximum power consumption of 32 W.
T-SUB-ADCS-11	The ADCS shall be able to perform a modding manoeuvre at least every two months, consisting of pseudo-random millinewton-meter torques throughout 24 hours.
T-SUB-EPS	The EPS shall control the power retrieval and distribution within the spacecraft.
T-SUB-EPS-1	The EPS shall generate an EOL power output of 975 W.
T-SUB-EPS-2	The solar cells shall generate power up to a temperature of at least 400 K.
T-SUB-EPS-3	The EPS batteries shall be able to store at least 2.24 MJ of energy in total.
T-SUB-EPS-4	The EPS shall have a mass of at most 38.99 kg.
T-SUB-EPS-4-1	The solar array shall have a mass of at most 14.32 kg.
T-SUB-EPS-4-2	The combined battery mass shall be at most 18.17 kg.
T-SUB-EPS-4-3	The PRU mass shall have a mass of at most 6.5 kg.
T-SUB-EPS-5	The combined solar array area shall be most 17.02 m^2.
T-SUB-EPS-6	The PRU shall be able to distribute the generated power to all power requiring satellite components.
T-SUB-EPS-7	The three QL075KA batteries shall be fully charged before launch.
T-SUB-THM-1	The thermal control system shall keep the spacecraft components within their operating temperature range during normal operating modes.
T-SUB-THM-2	The thermal control system shall keep the spacecraft components within their survival temperature range during safe-mode operations.
T-SUB-THM-3	The thermal control system shall provide a temperature stability of 10 mK per 200 s for the accelerometer during normal operations.
T-SUB-THM-4	The thermal control system shall not consume more than 150 W of power.
T-SUB-THM-5	The thermal control system shall have a mass of at most 4.21 kg.
T-SUB-STRC-1	The lowest eigenfrequency of the spacecraft in the longitudinal direction shall be in excess of 40 Hz.
T-SUB-STRC-2	The lowest eigenfrequency of the spacecraft in the lateral direction shall be in excess of 20 Hz.
T-SUB-STRC-3	The spacecraft shall withstand launch loads of 8 g in the longitudinal direction and 1 g in the lateral direction.
T-SUB-CDH-1	The CDH shall control each of the spacecraft subsystems and the spacecraft payload instruments.
T-SUB-CDH-2	The CDH required power shall be at most 9.5 W.
T-SUB-CDH-2-1	The OBC required power shall be at most 7.5 W.
T-SUB-CDH-2-2	The RTU required power shall be at most 2 W.
T-SUB-CDH-3	The CDH shall have a mass of at most 1.55 kg.
T-SUB-CDH-3-1	The RTU shall have a mass of at most 1.5 kg.
T-SUB-CDH-3-2	The RTU shall have a mass of at most 0.050 kg.
T-SUB-CDH-4	The CDH shall be able to store all necessary data received from the subsystems and payload instruments.
T-SUB-CDH-5	The CDH should detects faults by other spacecraft components.
T-SUB-COM	The communications subsystem shall provide transmission of data retrieved on the spacecraft and receival of data sent from the ground station.
T-SUB-COM-1	The uplink and downlink carrier frequency shall comply to the ESTRACK standards.
T-SUB-COM-2	The satellite shall have contact with the ground station at least twice a day.
T-SUB-COM-3	The satellite shall be able to send all retrieved data between to contact periods to the ground station in one contact period.
T-SUB-COM-4	The link margin shall be at least 3 dB.
T-SUB-COM-5	Both up- and downlink antenna shall be usable simultaneously.
T-SUB-COM-6	The communications subsystem shall have a maximum mass of 1.4 kg.
T-SUB-COM-7	The communications subsystem shall have a maximum power consumption of 38.0 W
T-SUB-COM-8	The communications subsystem shall receive a maximum instrument data rate of 36.0 kbit/s.
T-SUB-COM-9	Redundancy shall be present in the form of an omni-directional antenna.
T-SUB-GS	The ground station shall provide receival, storage and processing of the transmitted data and transmission of commands and software updates.
T-SUB-GS-1	The ground station shall receive, process and store all data that are downlinked from the spacecraft.
T-SUB-GS-2	The ground station shall transmit commands and software updates to the spracecraft.
T-SUB-GS-3	The ground station shall connect with the spacecraft at every possibility.
T-SUB-LN	The launcher shall provide transportation to the orbit
T-SUB-LN-1	The launcher shall provide sufficient fairing dimensions for the spacecraft.
T-SUB-LN-2	The launcher shall provide orbit injection at 650 km altitude.
T-SUB-LN-3	The launcher shall comply to legislations.

Continued on next page...

Table A.1: Mission Requirements

ID (MIRALOS-SYS-)	**Requirement**
C	The design shall meet the stakeholder requirements with the specified resources.
C-GN-1	The total cost of the mission shall be no more than €350,000,000.
C-GN-2	The mission shall launch before 2020.
C-GN-3	The mission shall be conform to (inter)national laws and regulations.
C-SUST	The mission shall be sustainable.
C-SUST-1-1	The physical design shall be sustainable.
C-SUST-1-2	The design process shall be sustainable.
C-SUST-2	The mission shall incorporate an end-of-life protocol.
C-SUST-2-1	The satellite shall burn up in the atmosphere at the end of the mission.
C-SUST-3	Data retrieved from the mission shall be released for public use.
T-SUB-INTG-1	All components shall be inter-compatible.
T-SUB-INTG-2	The centre of pressure and centre of mass shall have a maximum RMS separation of 5.0 mm.
T-SUB-INTG-3	The magnetometer shall be isolated from the spacecraft's internal electromagnetic interferences.

B. Technical Drawings

This chapter contains the technical drawings for the chosen design option. Of the following drafts, the reflectometer is a complete new design instrument (Figure B.2). The MIRALOS draft shows the outer dimensions of the hexagonal shape of the bus Figure B.1. MIRALOS is also a new design.

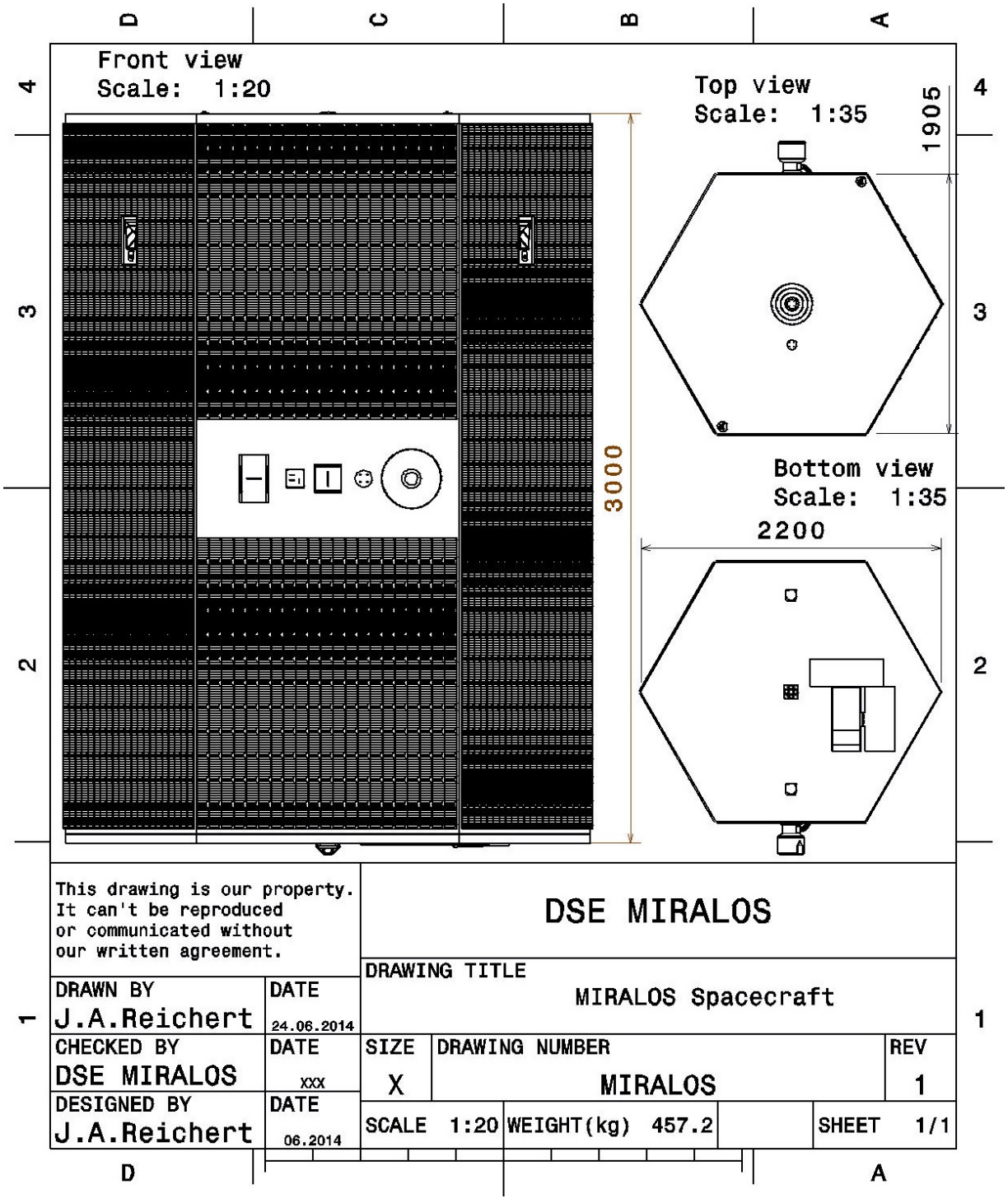

Figure B.1: MIRALOS Draft

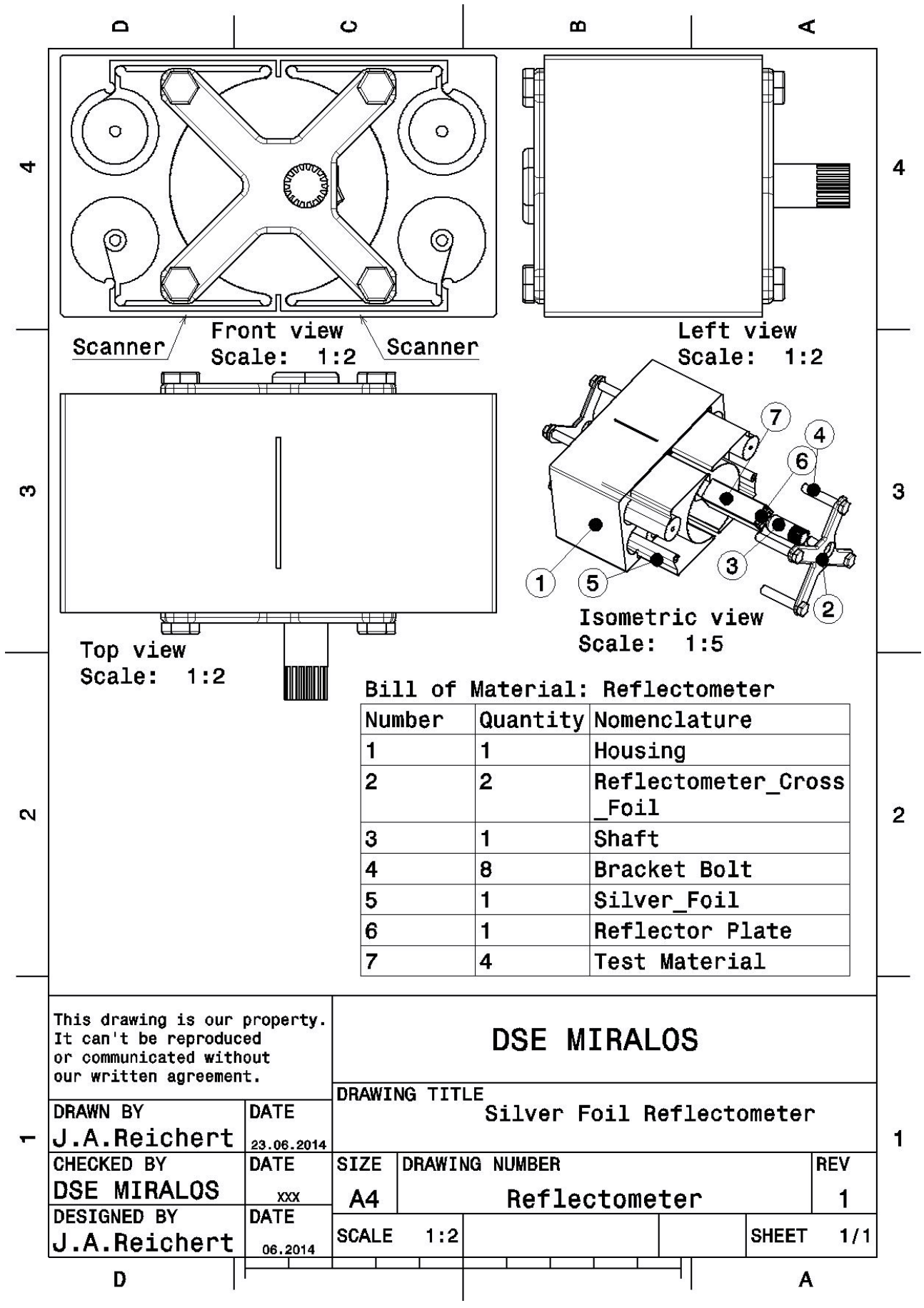

Bill of Material: Reflectometer

Number	Quantity	Nomenclature
1	1	Housing
2	2	Reflectometer_Cross_Foil
3	1	Shaft
4	8	Bracket Bolt
5	1	Silver_Foil
6	1	Reflector Plate
7	4	Test Material

DSE MIRALOS

DRAWING TITLE: Silver Foil Reflectometer

DRAWN BY: J.A.Reichert	DATE: 23.06.2014	SIZE: A4	DRAWING NUMBER: Reflectometer	REV: 1
CHECKED BY: DSE MIRALOS	DATE: XXX			
DESIGNED BY: J.A.Reichert	DATE: 06.2014	SCALE: 1:2		SHEET: 1/1

Figure B.2: Reflectometer Draft

C. Technical Risk Assessment

This appendix is a living document in which risks have been identified, assessed and eliminated. The risks are displayed in Table C.1. These originate from the very early design phases down to the subsystem designs. Previously identified but eliminated risks are omitted from the table, which explains the irregular list of IDs.

Table C.1: Risk Quantification and Mitigation

Risk (ID)	**Probability - Severity**	**Quantification and Mitigation**
Ground Station Problems (M01)	Very low - Negligible	Problems may occur with ground station operations, such as data retrieval or command uplink. The satellite is designed to be compatible with multiple ground stations.
Data Link Blockage (M02)	Very low - Negligible	Any obstructions caused by design will be found during the planned verification and validation activities. The only obstructions may be external, with a minimal probability. No mitigation is planned.
Environmental Issues (M03)	Very low - Negligible	A polluted space environment (space debris) may interfere with the mission success. No mitigation is planned.
Power System Failure (M04)	Low - Catastrophic	Complete or part power system failure may result in decreased performance or even preliminarily failure within several orbits. Redundancy is present for the individual EPS components. The power system has been sized for maximum power usage during orbit change manoeuvres at EOL, and thereby will perform more efficiently throughout most of the mission. Verification and validation procedures are planned.
Power Storage Failure (M04-1)	Low - Marginal	As described in Chapter 9, 2.23 QL075KA batteries are required for the power storage. Three of these batteries are included in the EPS design. Therefore, if one battery fails, the spacecraft is still able to operate normally during most of the mission profile. Only in the extreme case of consecutive eclipses at 350 km altitude with activated propulsion, the spacecraft will encounter a shortage in power which will force it to go into a less power consuming mode. It can be concluded that this risk is mitigated by the battery redundancy and the general application of a safety factor of 10%.
Solar Cell Failure (M04-2)	Low - Marginal	The failure of a single or multiple solar cell will have a rather low impact on the total power since the solar array will consist of solar cells in total. This risk is mitigated by taking into account a contingency factor of 10% and solar cell degradation factors. However failing solar cells can introduce thermal risks since part of the solar energy will not be converted into electric energy anymore.
PRU Failure (M04-3)	Very low - Critical	The PRU distributes the generated power to the batteries, subsystems and payload. A failure of this component has catastrophic consequences for the mission as several or all instruments will not receive the power they require. Therefore, proper mitigation of this risk is of critically importance. The Medium Power PCDU has a very high reliability and contains build in redundancy.
Thermal System Failure (M05)	Low - Critical	Thermal system failure may cause components to go outside their operational and survival temperature limits. Other thermal requirements may also not be met. This implies that some components may not perform as desired, or not even perform at all. Redundancy has to be built in for the active part of the thermal control system to ensure functioning throughout the spacecraft lifetime. Verification and validation procedures are planned.
C&DH Failure (M06)	Low - Critical	An OBC failure has critical consequences for the satellite in the sense that the OBC commands every subsystem. Fortunately, the failure has a low probability of occurrence due to the redundancy of CPUs. The SCS750 on board computer contains build in redundancy. Also, in case of overloading of the SCS750 , the RTU can take over some of the processes of the SCS750. Verification and validation procedures are planned for this subsystem.
Structural Failure (M07)	Low - Critical	A safety factor of 2 has been used in the design of the structural components. Component level tests will be performed, and vibration and load responses of the integrated spacecraft can be tested on the ground. Verification and validation procedures are planned for this subsystem.

Continued on next page...

Table C.1: Risk Quantification and Mitigation

Risk (ID)	Probability - Severity	Quantification and Mitigation
Payload Instrument Failure (M08)	Low - Critical	A payload selection is made and designed to meet the set requirements. Considering redundancy, a second mass spectrometer is taken on-board. This also applies to the reflectometer. Although the two reflectometers included in the design are configured differently, both are able to give accurate results. The GPS is internally redundant. A smaller patch antenna of lower accuracy is also used to provide redundancy. No redundancy is incorperated in the design for the laser retro-reflector, as the failure probability is extremely low. The accelerometer has electronic and thermal control redundancy. For the Ultraviolet Imager, redundancy is implemented with respect to the detector used (by implementing one more detector). It is assumed that the mirror will be manufacture in such way as to give the defined measurements prior to launch. Verification and validation procedures are planned for this subsystem.
Instrument Operation Deficiency (M08-1)	Very Low - Critical	Flight-proven and newly designed instruments are used for the scientific operations. It is clear what data these instruments collect and in what way. All required quantities to be measured will be done so in-situ. Pre-existing models will solely be used for validation of the data. By tests, verification, and validation, this risk will be minimised.
Instrument Accuracy Deficiency (M08-2)	Low - Critical	The instruments are to provide measurements with a certain accuracy. As the drag force on the spacecraft is on a nm/s^2 scale, very accurate equipment is required. The instruments are both flight-proven and newly designed, and both meet the accuracy requirements of the mission. Verification and validation are planned.
Instr. Calib. Failure (M08-3)	Low - Critical	Instrument calibration is required for accurate measurements. The most significant application of this is for the accelerometer instrument. To calibrate the accelerometer six mass-trim assemblies are used on three sides of the spacecraft (two on the bottom, two on the top, two on the side). The mitigation plan for this risk corresponds to the plan of (M08-2).
Instrument Operation Failure (M08-4)	Medium - Critical	Not all instruments are flight-proven and therefore there is a chance that instruments will fail prematurely. For this reason, redundancy is implemented for the mass spectrometer and reflectometer. The redundancy is achieved by adding a second instrument for each of the latter.
ADCS Failure (M09)	Low - Critical	The ADCS is aimed to have no single-point failures. Verification and validation procedures are planned.
Lack of Propellant (M09-1)	High - Critical	Propellant is required for calibration of the mass-trim assembly. The amount of fuel is sized on an extreme case and includes a 50% contingency factor. However, the fuel usage for calibration on the GOCE mission was more than twice as high for a 2 year mission [96]. Without fuel, the satellite can no longer be calibrated and the data becomes less accurate. Hence, more research is done towards this topic.
Excess Spinning (M09-2)	Low - Marginal	If the spacecraft is spinning at very high rates (due to orbit deployment or transfers), it may be difficult to determine the spacecraft's orientation. By applying the different sensors and by a trial-and-error method using the magnetorquers, the satellite can be stabilised to a coarse level.
Component Failure (M09-3)	Very Low - Catastrophic	Redundancy has been implemented for each coarse and fine sensor, and for the actuators. Additionally, all components are designed for a mission of at least 6 years, but preferably more. Verification and validation procedures are planned.
Internal Magnetic Interference (M09-4)	Medium - Critical	The magnetometer and magnetic torque rods rely on magnetic fields for attitude sensing and control. However, the spacecraft itself also produces an internal magnetic field. This may introduce uncertainty in results of the magnetometer. Also, the effective torques applied by the magnetic torque rods may differ from what is desired. Depending on the magnitude of interference, attitude sensing and control using the Earth's magnetic field may not be possible. This will severely complicate measurements and attitude control. Sensor redundancy is implemented, and verification and validation procedures are planned.
Component Unavailability (M09-5)	Medium - Marginal	As state-of-the-art sensors are selected, these may not be available for implementation yet. In this case, new sensors will have to be selected. To quantify this risk, the developers are contacted.
PL Deployment Obstruction (M10)	Very low - Catastrophic	During the initiation phase, problems may occur with respect to instruments. Verification and validation procedures are planned.

Continued on next page...

Table C.1: Risk Quantification and Mitigation

Risk (ID)	**Probability - Severity**	**Quantification and Mitigation**
Communication System Failure (M11)	Medium - Critical	Multiple antennas are implemented for up- and downlink, including redundancy. Redundancy for the transceiver is also included. Verification and validation procedures are planned.
Transmission Failure (M11-1)	Medium - Critical	In case the signal that is constructed by the transmitter of the spacecraft is incorrect, incorrect data will be sent to the ground station. This means that incorrect data will be used for analysis, thus causing an incorrect analysis.
Receiver Failure (M11-2)	Medium - Critical	The receiver on the spacecraft is used for the receival of commands or software updates from the ground station. When commands can not be received by the spacecraft it can not be controlled from the ground if necessary, which causes a high risk.
Antenna Failure (M11-3)	Medium - Marginal	For both up- and downlink antennas will be incorporated in the spacecraft design. Next to that an omni-directional antenna is included for redundancy (and for when the spacecraft has an attitude misalignment). Failure of more than one antenna will however have a critical severity, as the uplink and downlink can not be done simultaneously anymore.
Launch Failure (M12)	Low - Catastrophic	A launcher has been selected for the mission. No mitigation is planned.
Launch Site Incompatibility (M12-1)	Low - Catastrophic	The launch site is selected and compatible with the launch requirements. The regulations and legislation for different launch sites are investigated. The launch site is consulted to ensure no other restrictions exist.
Launch Deployment Failure (M12-2)	Very Low - Marginal	After launch, it is possible that the launcher does not insert the spacecraft in the correct orbit. Due to the presence of thrusters, the severity of this failure depends on the altitude and orbit the satellite ends up in. No mitigation is planned.
Spacecraft Collision (M13)	Very Low - Catastrophic	The satellite may collide with other crafts or debris. Damage of the spacecraft ranges from no damage to complete system failure. No mitigation is planned.
Oxygen-surface Influences (M14)	Low - Critical	There is a risk that atomic oxygen will stick on the spacecraft and thereby influence measurements in the helium dominated region. This will hinder measurements and thereby limit what is analysed in oxygen dominated conditions. A request upon the scientific community is done to provide more insight in this risk.
Exceeding Mass Budget (M15)	Very Low - Catastrophic	The total mass cannot exceed its budget for launch and instrument operations. A high mass lowers accuracy of drag measurements and puts requirements on a larger, more expensive launcher. The mass budget is constantly updated, reflected upon and managed using a contingency plan.
Exceeding Power Budget (M16)	High - Marginal	If the power budget is exceeded, the power subsystem is to be adjusted or alternatively it should be decided to operate the spacecraft with less power or only for a part of each orbit. This will impact data frequency and quality. The power budget is constantly updated, reflected upon and managed using a contingency plan.
Exceeding Cost Budget (M17)	Low - Critical	See (M15) and (M16).
Propulsion System and ODCS Failure (M18)	Medium - Critical	As Ion propulsion is a rather new technology failures (mostly temporary) are not uncommon. More detail on this matter can be found in Section 7.2.1.
System Integration Failure (M19)	Low - Critical	The different system components should be compatible and in support of each other. Risk areas are thermal, electromagnetical and vibrational. By faulty integration, interference between components (i.e. electromagnetically) might impact the performance of the magnetometer, magnetorquers and payload. Verification and validation procedures are planned.